



2016

BEHAVIOR OF RC BEAMS STRENGTHENED IN FLEXURE WITH SPLICED CFRP ROD PANELS

Akram Rasheed Jawdhari

University of Kentucky, akram.hassan@uky.edu

Digital Object Identifier: <http://dx.doi.org/10.13023/ETD.2016.113>

[Click here to let us know how access to this document benefits you.](#)

Recommended Citation

Jawdhari, Akram Rasheed, "BEHAVIOR OF RC BEAMS STRENGTHENED IN FLEXURE WITH SPLICED CFRP ROD PANELS" (2016). *Theses and Dissertations--Civil Engineering*. 37.
https://uknowledge.uky.edu/ce_etds/37

This Doctoral Dissertation is brought to you for free and open access by the Civil Engineering at UKnowledge. It has been accepted for inclusion in Theses and Dissertations--Civil Engineering by an authorized administrator of UKnowledge. For more information, please contact UKnowledge@lsv.uky.edu.

STUDENT AGREEMENT:

I represent that my thesis or dissertation and abstract are my original work. Proper attribution has been given to all outside sources. I understand that I am solely responsible for obtaining any needed copyright permissions. I have obtained needed written permission statement(s) from the owner(s) of each third-party copyrighted matter to be included in my work, allowing electronic distribution (if such use is not permitted by the fair use doctrine) which will be submitted to UKnowledge as Additional File.

I hereby grant to The University of Kentucky and its agents the irrevocable, non-exclusive, and royalty-free license to archive and make accessible my work in whole or in part in all forms of media, now or hereafter known. I agree that the document mentioned above may be made available immediately for worldwide access unless an embargo applies.

I retain all other ownership rights to the copyright of my work. I also retain the right to use in future works (such as articles or books) all or part of my work. I understand that I am free to register the copyright to my work.

REVIEW, APPROVAL AND ACCEPTANCE

The document mentioned above has been reviewed and accepted by the student's advisor, on behalf of the advisory committee, and by the Director of Graduate Studies (DGS), on behalf of the program; we verify that this is the final, approved version of the student's thesis including all changes required by the advisory committee. The undersigned agree to abide by the statements above.

Akram Rasheed Jawdhari, Student

Dr. Issam E. Harik, Major Professor

Dr. Yi-Tin Wang, Director of Graduate Studies

BEHAVIOR OF RC BEAMS STRENGTHENED IN FLEXURE WITH SPLICED
CFRP ROD PANELS

DISSERTATION

A dissertation submitted in partial fulfillment of the requirements for the degree of
Doctor of Philosophy in the College of Engineering
at the University of Kentucky

By

Akram Rasheed Jawdhari

Lexington, Kentucky

Director: Dr. Issam Elias Harik, Professor of Civil Engineering
Lexington, Kentucky 2016

Copyright© Akram Rasheed Jawdhari 2016

ABSTRACT OF DISSERTATION

BEHAVIOR OF RC BEAMS STRENGTHENED IN FLEXURE WITH SPLICED CFRP ROD PANELS

FRP laminates and fabrics, used as an externally bonded reinforcement (EBR) to strengthen or repair concrete members, have proven to be an economical retrofitting method. However, when used to strengthen long-span members or members with limited access, the labor and equipment demands may negate the benefits of using continuous EBR FRP. Recently, CFRP rod panels (CRPs) have been developed and deployed to overcome the aforementioned limitations. Each CRP is made of several small diameter CFRP rods placed at discrete spacing. To fulfill the strengthening length, CRP's are spliced together and made continuous by means of overlaps (or finger joints).

In this doctoral dissertation, the effectiveness of spliced CRPs as flexural strengthening reinforcement for RC members was investigated by experimental, analytical and numerical methods. The experimental research includes laboratory tests on (1) RC beams under four-point bending and (2) double-lap shear concrete specimens. The first set of tests examines the behavior of concrete members strengthened with spliced CRPs. Several beams were fabricated and tested, including: (a) unstrengthened, (b) strengthened with spliced CRPs, (c) strengthened with full-length CRPs, and (d) strengthened with full-length and spliced CFRP laminates. The double-lap shear tests serve to characterize the development length and bond strength of two commonly used CRPs. Several small-scale CRPs, with variable bond lengths, were tested to arrive to an accurate estimation of development length and

bond strength. Several other specimens were additionally tested to preliminarily examine the effects of bond width and rod spacing.

A 3D nonlinear finite element simulation was utilized to further study the response of CRP strengthened RC beams, by extracting essential data, that couldn't be measured in the experimental tests. Additionally, analytical tools were added to investigate the behavior of tested bond and beam specimens. The first tool complements the double-lap shear tests, and provides mathematical terms for important characteristics of the CRP/concrete bond interface. The second tool investigates concrete cover separation failure, which was observed in the beam testing, for RC beams strengthened with full-length and spliced CRPs.

KEYWORDS: Spliced CFRP rod panels (CRPs), RC beam, double-lap shear, 3D F.E models, CZM debonding models, concrete cover separation.

Akram Jawdhari
Student's Signature

04/21/2016
Date

BEHAVIOR OF RC BEAMS STRENGTHENED IN FLEXURE WITH SPLICED
CFRP ROD PANELS

By

Akram Rasheed Jawdhari

Dr. Issam E. Harik
Director of Dissertation

Dr. Yi-Tin Wang
Director of Graduate Studies

04/21/2016
Date

To my parents, wife, brothers and sisters, I dedicate this work.

ACKNOWLEDGEMENTS

First and foremost, I would like to thank Almighty God (Allah), whose many blessings have made me who I am today. I would like to express my deepest gratitude and appreciation to my supervisor Dr. Issam Harik, who has played an important role in my academic and personal life. I would like to thank you for showing me the right way to become a researcher, and academician and for your patience when I screw up. I would also like to thank my committee members, Dr. Hans Gesund, Dr. Brad Davis, and Dr. Tingwen Wu for serving as my committee members and for providing me with invaluable advices, comments, and suggestions. I would especially like to thank Dr. Abeetha Peiris for his enormous help during all stages of the research. I would like to thank students who helped me with the experimental tests, including Micheal Crossley, Cody Cousins, Brice Benifield, Ethan Russel, and Harry Donagy. Thanks are extended to staff in the Civil Engineering Department, University of Kentucky, especially to Ms. Sheila Williams, and Ms. Suzanna Wampler.

A special thanks to my family. Words cannot express how grateful I am to my father, my mother, and my siblings for all of the sacrifices that you've made on my behalf. At the end I would like express appreciation to my beloved wife Zainab Al-Bujasim who spent sleepless nights with and was always at my support.

Finally, I would like to thank my sponsor the Higher Committee for Education Development (HCED) for their financial support of my PhD journey.

TABLE OF CONTENTS

ACKNOWLEDGEMENTS.....	iii
TABLE OF CONTENTS.....	iv
LIST OF TABLES	x
LIST OF FIGURES	xi
CHAPTER 1: INTRODUCTION.....	1
1.1 Problem Background (The Need for Retrofit)	1
1.2 Lap-Spliced FRP Plates (Laminates)	3
1.3 CFRP Rod Panels (CRP Strengthening System)	5
1.4 Research Objective.....	8
1.5 Research Significance	8
1.6 Dissertation Layout	9
CHAPTER 2: LITERATURE REVIEW	15
2.1 Conventional Strengthening Methods.....	15
2.2 Adhesively Bonded Plates.....	16
2.2.1 <i>Adhesively Bonded Steel Plates</i>	17
2.3 Strengthening of Concrete Members with FRP	20
2.3.1 <i>Adhesively Bonded FRP Plates (Laminates, Strips)</i>	21
2.3.2 <i>Adhesively Bonded FRP Fabrics (Sheets)</i>	23
2.3.3 <i>Near Surface Mounted (NSM) Technique</i>	26

2.3.4 <i>Pre-stressed FRP's</i>	29
2.4.5 <i>Other Novel Techniques</i>	32
CHAPTER 3: BOND STUDY ON CFRP ROD PANELS EXTERNALLY ADHERED TO CONCRETE	37
3.1 Synopsis.....	37
3.2 Introduction.....	38
3.3 Experimental Program.....	39
3.3.1 <i>Specimen Description and Strengthening Schemes</i>	39
3.3.2 <i>Specimen Preparation</i>	40
3.3.2.1 <i>Concrete Blocks</i>	40
3.3.2.2 <i>CFRP Rods and CRP's</i>	41
3.3.2.3 <i>Adhesive</i>	41
3.3.3 <i>Surface Preparation and CRP Installation</i>	42
3.3.4 <i>Test Setup and Instrumentation</i>	42
3.4 Test Results.....	43
3.4.1 <i>Development Length</i>	44
3.4.2 <i>Average Bond Strength</i>	46
3.4.3 <i>Load Transfer Mechanism along CRP Bond Length</i>	47
3.4.4 <i>Shear Stress Distribution along CRP Bond Length</i>	48
3.4.5 <i>Shear Stress- Slip Relation</i>	50
3.4.6 <i>Effect of Bond (Panel) Width</i>	52

3.5	Conclusions.....	53
CHAPTER 4: FLEXURAL STUDY ON RC BEAMS STRENGTHENED WITH CFRP ROD PANELS AND CFRP LAMINATES.....		
4.1	Synopsis	79
4.2	Introduction	80
4.3	Experimental Program.....	83
4.3.1	<i>Dimensions of RC Beams</i>	83
4.3.2	<i>Specimen Description and Strengthening Schemes</i>	83
4.3.3	<i>Materials</i>	85
4.3.4	<i>Surface Preparation and CFRP Installation</i>	86
4.3.5	<i>Test Setup and Instrumentation</i>	88
4.4	Results and Discussions	89
4.4.1	<i>Modes of Failure</i>	89
4.4.2	<i>Maximum Loads and Capacity Increase</i>	91
4.4.3	<i>Load Mid-Span Behavior</i>	93
4.4.4	<i>Cracking Patterns</i>	94
4.4.5	<i>Strain Profile along Depth, at Mid-Span</i>	95
4.4.6	<i>Strain Behavior across the CRP width</i>	95
4.4.7	<i>Strain and shear stress along the CRP and /CFRP laminate</i>	96
4.5	Conclusions	99

CHAPTER 5: FINTE ELEMENT ANALYSIS OF RC BEAMS BONDED TO CFRP ROD PANELS AND CFRP LAMINATES	137
5.1 Synopsis	137
5.2 Introduction.....	138
5.3 Experimental Program	139
5.4 FE Analysis.....	141
5.4.1 <i>Modeling of Materials</i>	141
5.4.1.1 <i>Concrete Material modeling</i>	141
5.4.1.2 <i>Steel Reinforcement</i>	144
5.4.1.3 <i>CFRP Material (Rods, Laminates, and Fabrics), and Adhesives</i>	144
5.4.2 <i>Geometrical Representation</i>	144
5.4.3 <i>Element Types</i>	145
5.4.4 <i>Loading Scheme and Boundary conditions</i>	146
5.4.5 <i>FE Meshing</i>	147
5.4.6 <i>Nonlinear Solution</i>	147
5.4.7 <i>Modeling of Debonding</i>	148
5.4.7.1 <i>CZM Model for Debonding of CRP</i>	149
5.4.7.2 <i>CZM Model for Debonding of CFRP fabric and laminates</i>	151
5.5 Results and Discussions.....	152
5.5.1 <i>Load-Deflection Response</i>	152
5.5.2 <i>Simulation of Concrete Cover Separation</i>	153

5.5.3 Simulation of Debonding and Concrete Crushing Failures	154
5.5.4 Load versus Strain in CFRP at Mid-Span.....	154
5.5.5 Strain Profile along CRP and CFRP Laminate Length.....	156
5.5.6 Load versus Concrete Strain at Mid-Span	156
5.5.7 Tensile Stress Distribution in CRP and CFRP laminate.....	157
5.5.8 Maximum Tensile Stress in CRP and CFRP laminate	158
5.5.9 Interfacial Shear Stress distribution along CFRP Length	159
5.6 Conclusions.....	160
CHAPTER 6: ANALYTICAL INVESTIGATION OF CFRP ROD PANELS	
BONDED TO CONCRETE MEMBERS	208
6.1 Synopsis.....	208
6.2 Introduction.....	209
6.3 Analysis of Double-Lap Shear Tests	210
6.3.1 Slip Modulus, k	214
6.3.2 Model Verification.....	215
6.3.3 Parametric Study.....	216
6.3.3.1 Development Length	216
6.3.3.2 CRP Width Effects.....	217
6.4 Analysis of concrete Cover Separation	218
6.4.1 Analytical models	218
6.4.1.1 Shear Capacity Based Models	219

6.4.1.2 Concrete Tooth Models.....	220
6. 4.2 Application of Analytical Models to RC Beams Strengthened with CRPs.....	221
6.4.2.1 Analytical model No. 2.....	221
6.4.2.2 Analytical model No. 3.....	224
6.4.3 Results of analytical models no.2, and no.3.....	226
6.5 Conclusions.....	228
CHAPTER 7: CONCLUSIONS AND RECOMMENDATIONS.....	244
7.1 Summary and Conclusions.....	244
7.1.1 Conclusions of Chapter 3 (Double-Lap Shear Tests).....	244
7.1.2 Conclusions of Chapter 4 (Four-Point Bending Beam Tests).....	246
7.1.3 Conclusions of Chapter 5 (Finite Element Analysis).....	249
7.1.4 Conclusions of Chapter 6 (Analytical Models).....	251
7.2 Study Limitations and Future Recommendations.....	252
7.2.1 Effects of Rod Spacing.....	255
APPEDIX A.....	260
APPEDIX B.....	268
APPEDIX C.....	276
REFERENCES.....	290
VITA.....	306

LIST OF TABLES

Table 3.1. (a) Series I of double-lap shear test matrix.....	55
Table 3.1. (b) Series II of double-lap shear test matrix.	56
Table 3.1. (c) Series III of double -lap shear test matrix.	57
Table 3.2 (a). Failure loads and modes of failure for Series I and II specimens.	58
Table 3.2 (b). Failure loads and modes of failure for Series III specimens.	59
Table 4.1. CRPs used in the experimental program.....	101
Table 4.2. Beam test matrix	102
Table 4.3. Concrete cylinder compressive strength.....	103
Table 4.4. Maximum load and mode of failure for beams in table 4.2.....	104
Table. 4.5 (a) Load vs. deflection curves, and ductility [SI units].....	105
Table. 4.5 (b) Load vs. deflection curves and ductility [US units].....	106
Table 5.1 Numerical parameters for CZM model of CFRP fabric and laminates.	163
Table 5.2 (a) Comparisons between FE and experimental results, SI.	164
Table 5.2 (b) Comparisons between F.E and experimental results, US.	165
Table 5.3 Stress at maximum, and stress ratio for CFRP strengthening.....	166
Table 5.4 FE predicted interfacial shear and peeling stresses, at maximum load	167
Table 5.5 FE predicted locations of maximum shear and peeling stresses.....	168
Table 6.1. (a) Results of analytical investigation of CCS, SI system.	230
Table 6.1. (b) Results of analytical investigation of CCS, US customary system.....	231

LIST OF FIGURES

Fig. 1.1 Lap-spliced FRP plates on concrete bridge (after Stallings et al 2000).	12
Fig. 1.2 CRP strengthening technique (actual panels).	13
Fig. 1.3 CRP strengthening technique (schematics).	14
Fig. 2.1 Methods used in the past to repair or upgrade concrete structures.	35
Fig. 2.2 NSM strengthening system, (a) NSM rods, (b) NSM strips.	36
Figure. 3.1. Double-lap shear specimen.	60
Fig. 3.2 Small-scale CRP's used in the bond testing program.	61
Fig. 3.3 Double lap test specimen fabrication.	62
Fig. 3.4 Double-lap shear specimen in testing machine.	63
Fig. 3.5 Strain gage layout for a specimen with bond length of 150 mm.	64
Fig. 3.6. Concrete block failure mode.	65
Fig. 3.7. Rod peel-off failure mode.	66
Fig. 3.8. Concrete shear-off failure mode of CRP-070.	67
Fig. 3.9. Concrete shear-off failure mode of CRP-195.	68
Fig. 3.10. Failure load vs. bond length, l_b	69
Fig. 3.11. Adhesive bond strength, τ_b , vs. bond length, l_b , for CRP-070 and CRP-195. ..	70
Fig. 3.12 Strain variation along the bond length, for CRP-070.	71
Fig. 3.13 Measured transfer length vs. relative load level, for CRP-070.	72
Fig. 3.14 Strain variation along bond length, for CRP-195.	73
Fig. 3.15 Measured transfer length vs. relative load level, for CRP-070.	74
Fig. 3.16 Shear stress vs. relative load level for CRP-070 and CRP-195.	75
Fig. 3.17 Shear stress vs. slip model for CRP-070 and CRP-195.	76

Fig. 3.18 Comparison of failure loads for specimens with different bond widths.....	77
Fig. 3.19 Strain variation along bond length.....	78
Fig. 4.1 Geometry of RC beams and CRP strengthening	107
Fig. 4.1 (continued) Geometry of RC beams and CRP strengthening.....	108
Fig. 4.2 Geometry of RC beams and CFRP laminate strengthening layout	109
Fig. 4.3 Installation of CRPs.....	110
Fig. 4.4 Installation of CFRP fabric at CRP ends.	111
Figure 4.5 Installation of CFRP laminate.	112
Fig. 4.6 Schematics of beam test setup.....	113
Fig. 4.7 CSSC2 Beam placed in the test frame.....	114
Fig. 4.8 Strain gage layout (dimensions are in mm).	115
Fig. 4.8 (continued) Strain gage layout (dimensions are in mm).....	116
Fig. 4.9 Failure mode of control beam.....	117
Fig. 4.10 Failure due to concrete cover separation	118
Fig. 4.10 (continued) Failure due to concrete cover separation.....	119
Fig. 4.11 Intermediate crack induced debonding failure	120
Fig. 4.12 CFRP Laminate debonding failure.....	121
Fig. 4.13 Capacity increase percentage (over control beam) of CRP-070, CFRP laminate, and CRP-195 strengthening systems.	122
Fig. 4.14 Load mid-span deflection for CRP strengthened beams.	123
Fig. 4.15 Load mid-span deflection for CFRP laminate strengthened beams.	124
Fig. 4.16 Load mid-span deflection for CRP-070 and CRP-195.....	125

Fig. 4.17 Load mid-span deflection for the control beam and beams strengthened with CRP-070 and CFRP laminate.	126
Fig. 4.18 Crack patterns in RC beams	127
Fig. 4.18 (continued) Crack patterns in RC beams.....	128
Fig. 4.19 Strain profile along depth, at mid-span, CS70 and CS195 beams.....	129
Fig. 4.19 (continued) Strain profile along depth, at mid-span, CSSC2 beam.....	130
Fig. 4.20 Load level, P/P_{max} vs. strain along CRP width.....	131
Fig. 4.20 (continued) Load level, P/P_{max} vs. strain along CRP width	132
Fig. 4.21 Tensile strain and shear stress distribution along CRP length, beam SS70 (spliced CRP-070).....	133
Fig. 4.22 Tensile strain and shear stress distribution along CRP length, beam SSW70 (spliced and anchored CRP-070).	134
Fig. 4.23 Tensile strain and shear stress distribution along CFRP laminate length, beam CSSC2 (full-length CFRP laminate).....	135
Fig. 4.24 Tensile strain and shear stress distribution along CFRP laminate length, beam SSSC2 (spliced CFRP laminate system).....	136
Figure 5.1 (a) Geometry of experimental RC beams, CRP strengthening technique.	169
Figure 5.1 (a) (continued) Geometry of experimental RC beams, CRP strengthening technique, dimensions in mm	170
Figure 5.2 Geometry of experimental RC beams, CFRP laminate strengthening	171
Figure 5.3 concrete constitutive material models.	172
Figure 5.4 Steel constitutive material model.	173
Figure 5.5 Uniaxial stress-strain response of CFRP components and adhesives.	174

Figure 5.6 Boundary conditions and loading scheme of FE models.	175
Figure 5.7 FE mesh of RC beams strengthened with CRPs or CFRP laminates.	176
Figure 5.8 FE mesh of RC beams strengthened with CRPs, showing FE model of CFRP rods at overlap and CRP end locations.	177
Figure 5.9 FE mesh of RC beams strengthened with spliced CRPs, and anchored at CRP ends with CFRP fabrics.	178
Figure 5.10 FE mesh of RC beams strengthened with full-length CFRP laminate.	179
Figure 5.11 FE mesh of RC beams strengthened with spliced CFRP laminate system..	180
Figure 5.12 Geometry of INTER 205 element (after ANSYS 2012).	181
Figure 5.13 FE simulation of debonding at various interfaces by INTER 205 element.	182
Figure 5.14 Bilinear CZM model.....	183
Figure 5.15 Load-mid span deflection comparisons, between experiment and FE, for Control beam (specimen CB2).....	184
Figure 5.16 Load-mid span deflection comparisons, between experiment and FE, for beams strengthened with CRP-070.....	185
Figure 5.16 (continued) Load-mid span deflection comparisons, between experiment and FE, for beams strengthened with CRP-070.....	186
Figure 5.17 Load-mid span deflection comparisons, between experiment and FE, for beams strengthened with CFRP laminates.....	187
Figure 5.18 Normal stress distribution of section A-A.....	188
Figure 5.19 FE simulation of concrete crushing failure of control beam (beam CB2) ..	189
Figure 5.20 FE simulation for debonding of the beam strengthened with two spliced CRP-070, and anchored with CFRP fabric (beam SSW70).	190

Figure 5.21 FE simulation for debonding of the beam strengthened with two spliced CRP-195, and anchored with CFRP fabric (beam SSW195).	191
Figure 5.22 FE simulation for debonding and concrete crushing failures of the beam strengthened with full-length CFRP laminate (beam CSSC2)	192
Figure 5.23 FE simulation for debonding and concrete crushing failures of beam strengthened with spliced CFRP laminate system (beam SSSC2)	193
Figure 5.24 Load vs. strain in CRP-070, at mid-span.....	194
Figure 5.25 Load vs. strain in CRP-070, at mid-span.....	195
Figure 5.26 Strain distribution along CRP-070 surface, for loads up to 18 kN.....	196
Figure 5.26 (cont.) Strain distribution along CRP-070 surface, for loads up to 18 kN..	197
Figure 5.27 Strain distribution along CFRP laminate surface, for loads up to 18 kN	198
Figure 5.27 (cont.) Strain distribution along CFRP laminate surface.....	199
Figure 5.28 Load vs. strain at concrete’s outermost compressive and tensile surfaces..	200
Figure 5.28 (continued) Load vs. strain at concrete’s outermost compressive and tensile surfaces	201
Figure 5.29 Tensile stress distribution in CRP-070 and CFRP laminate, at constant moment region, $P = 18$ kN (4 kip).....	202
Figure 5.30 Tensile stress distribution in CRP-195, at constant moment region, $P = 18$ kN (4 kip).....	203
Figure 5.31 FE shear distribution along CRP/concrete interface, for CRP-070, at maximum load	204
Figure 5.31 (continued) FE shear distribution along CRP/concrete interface, for CRP-070, at maximum load.....	205

Figure 5.32 FE shear stress distribution along laminate/concrete interface, for CFRP full-length laminate (beam CSSC2), at maximum load.....	206
Figure 5.33 FE shear stress distribution along laminate/concrete interface, for spliced CFRP laminate system (beam SSSC2), at maximum load	207
Fig. 6.1. (a) Concrete block bonded to CRP, (b) finite segment of bonded CRP, showing the bond interface and acting forces	232
Fig. 6.2. Experimental and analytical (model no.1) strain-displacement comparisons for double-lap shear tests	233
Fig. 6.2. (continued) Experimental and analytical (model no.1) strain-displacement comparisons for double-lap shear tests	234
Fig. 6.2. (continued) Experimental and analytical (model no.1) strain-displacement comparisons for double-lap shear tests	235
Fig. 6.3. Transfer length vs. bond length relation, obtained from model no.1	236
Fig. 6.4. Transfer length vs CRP width relation, obtained from model no.1	237
Fig. 6.5. Concept of concrete tooth models (after Zhang et al 1995).	238
Fig. 6.6. First concrete tooth with proper forces, (a) three-dimensional section, (b) two-dimensional section.....	239
Fig. 6.7. CRP strengthened RC beam, calculations of bending moment (M_{B-B}).....	240
Fig. 6.8. (a) Equivalent plate concept, (b) tested beam, showing shear force and bending moment at panel's end and applied loads.	241
Fig. 6.9. Analytical/experimental failure load ratios for analytical models no.2, 3.....	242
Fig. 6.10. Prediction of model no.3, as a percentage of experimental load, with and without bending moment.	243

Fig. 7.1. Concrete shear-off failure in specimen with rod spacing 257

Fig. 7.2. Rod peel-off failure in a specimen with rod spacing..... 258

Fig. 7.3 Stress ratio in CFRP rods of specimens with different rod spacing. 259

CHAPTER 1: INTRODUCTION

1.1 Problem Background (The Need for Retrofit)

Reinforced and prestressed concrete structures will need performance modification and improvement at one point in their lifetime (Allawi 2006, Al-Mahmoud et al. 2009, and Obaidat 2010). The need for structural repair or replacement is attributed to many reasons, including but not limited to: deterioration as a result of aging, severe environmental exposure, natural events, vehicular impacts, errors in the design and/or in the construction, inferior materials used in the building, changes in function, and updates to the design codes. When a structure becomes deteriorated and/or unable to withstand the applied loads, there are two possible solutions: replace the structure, or repair the current one. However, full structure replacement has become an unfavorable choice due to the tight budgets and low resources of most local, state, and federal agencies. Also, full structure replacement imposes other disadvantages due to the disruption of construction, such as: the need for detours and traffic problems. From this it can be concluded that when the opportunity of a cost-effective and easy to implement repair is available, structural engineers, owners, and operators will opt to repair or upgrade the structure rather than replace it.

The Federal Highway Administration (FHA) publishes a status report every few years to assess the ongoing condition of all U.S bridges. In (FHA 2013) report, it was estimated that of the 607,751 bridges in the U.S, 24% of them are listed as either “Structurally Deficient” or “Functionally Obsolete”. Structurally deficient refers to bridges in which major structural elements have deteriorated and lost a large component of their internal resistance.

Although the term structurally deficient does not designate these bridges to be completely unsafe for usage; it does indicate that in such bridges, the load-carrying capacity of major structural members has decreased to less than the designed value. Therefore, major repair, load adjustment, or replacement procedures should be carried out in order for the bridge to remain in service and function as intended. On the other hand, the term functionally obsolete describes bridges that have been designed and constructed according to earlier standards; and since the standards have been updated, these bridges have failed under the new standards. Unlike the structurally deficient category, the functionally obsolete category does not involve structural deficiencies such as deterioration, corrosion, or damage, but rather it includes geometrical inadequacies such as insufficient deck width or road approach, or low under bridge clearance (FHA 2010).

Furthermore, according to (FHA 2010) study, the percentage of bridges that are 25-50 years old is 37.7 %. In addition, 20.7 % of the bridges are more than 50 years old. In addition, FHA study specifies the typical life of a standard bridge to be 50 years. Therefore, by comparing the above data, it's evident that there is a large portion of highway bridges, providing necessary services to millions of Americans, are either in immediate need for rehabilitation or replacement procedures, or soon will be.

The information above on the deficiencies and aging issues of our nation's bridges, and the call for immediate corrective actions is just one example describing the importance that structural engineers must seek out efficient, cost-effective, and easy-to-install rehabilitation techniques for our nation's infrastructure.

1.2 Lap-Spliced FRP Plates (Laminates)

Externally bonded reinforcement (EBR) consisting of fiber reinforced polymer (FRP) composites has been successfully deployed worldwide for strengthening existing concrete structures. It is generally more economical and convenient than other repair systems (Attari et al 2012, Vasudevan and Kothandaraman 2014). Numerous experimental and field applications have shown that EBR FRP can efficiently increase the flexural strength of a concrete member (Bonacci and Maalej 2001, Lee et al 2005, Chansawat et al 2009, Si-Larbi et al 2012, Ren et al 2015).

One of the drawbacks of the EBR FRP method is the man power needed to attach continuous laminate along the entire length of the member. The difficulty is more evident when the concrete member is too long or inaccessible (e.g., bridge over waterway or multi-lane expressway). Construction of scaffolding along the length of a member can be time consuming and costly (Peiris 2011). Although splicing FRP laminates is an option, it is not commonly used in practice. Much of the research investigating lap-splicing FRP plates/sheets has focused on steel substrate. For example, Yang and Nanni 2002 investigated the lap-splice length and fatigue performance of lap-spliced CFRP laminates through double lap-shear steel coupon tests. It was found that 38.1 mm (1.5 in.) lap-splice length is sufficient to provide continuity for the lap-splice system, under static loads. Fatigue tests were performed on 101.6 mm (4 in.) lap-spliced specimens. The study reported that the provided lap-splice length can resist more than 2.0 million load cycles with no effects on residual strength, providing that the maximum applied stress does not exceed 40% of the ultimate static strength.

Dawood and Rizkalla 2006 conducted an experimental study on steel beams and double-lap shear steel specimens to investigate the effectiveness of lap-spliced CFRP laminates, using different splice configurations. The study indicated that controlling failure mode is debonding of the splice from the primary laminates due to high shear stresses at splice ends. The study also showed that implementing reverse taper at the splice ends results in reduction of the end shear stresses, and could increase the structure load capacity. Dawood et al 2007 extended the above study to include the effects of various taper configurations, the effects of increasing splice length, and the effects of using mechanical anchorage near the splice ends. The study reported that using reverse taper at both (1) the butt-joint of primary laminates, and at (2) at splice ends results in increasing the splice capacity to twice as the splice without reverse taper. While increasing the splice length or providing additional mechanical anchorage have minimum influence.

The research on lap-spliced CFRP plates bonded to concrete substrate was pioneered in late 90's by Alabama Department of Transportation (ALDOT), [Tedesco et al 1996, and 1998, Stallings et al 2000]. In that research, the CFRP lap-splicing technique was implemented in the field to rehabilitate an existing concrete bridge in Alabama. The retrofit procedure consisted of strengthening the all girders at bottom face by bonding three CFRP primary plates, that are equal in length and disconnected at one third-of-length locations to form two joints (called "butt-joints"), and CFRP splices over the butt-joints (figure 1.1). Along the sides of three girders, CFRP primary plates and splices of similar configuration to the attachment at bottom, were used. Field load testes, using a commercial truck with known weight and axle positions, were performed before and after implementing the rehabilitation procedure. Strain measurement of tensile steel rebars and along the surface

of primary and splice plates, as well as deflections, have shown that the rehabilitation system was effective in reducing rebar tensile stresses, and bridge deflections.

Stalling and Porter 2003 performed laboratory tests on large-scale RC beams strengthened with lap-spliced CFRP plates. Splices of 610 mm (24 in.) and 915 mm (36 in.) lengths were investigated. The effects of splice location were explored by attaching the splice at (1) one splice at maximum bending moment (mid-span), and (2) two splices at shear span. The study showed that the predominant failure mode is debonding of splice by high shear stresses at splice ends, due to the difference in strains between primary plate and splice.

The study also included small-scale tension tests consisting of CFRP primary plates connected by splices. Both the beam tests and tension tests indicated that there was a uniform strain at the threshold of debonding. For design purposes, the study devised to limit the strain at the end of splice to 1682 micorstrain, in order to prevent debonding of the splice. The study also concluded that in order for the splices to be fully functional, and to avoid shear failure in the splice, the average shear stress should be kept below 15% of the shear strength of the adhesive. This implies that relatively very long splices are required. To our best knowledge, there has not been other recent researches on lap-spliced CFRP plates, bonded to concrete structures.

1.3 CFRP Rod Panels (CRP Strengthening System)

Carbon fiber reinforced polymer (CFRP) rod panels (CRP's) have recently been developed and deployed in the field to overcome the above limitations of FRP laminates (Harik and Peiris 2014). CRP's are externally bonded to the concrete substrate in a manner similar to other externally bonded reinforcement (EBR). However, CRPs are made from small

diameter CFRP rods. The group of rods are placed side by side at discrete spacing to form a panel [figures 1.2 (a), 1.3 (a)]. The rods are then mounted to a fiberglass backing to facilitate the handling of the panel and to keep the rod spacing consistent. This change in orientation from FRP laminates to CRPs, in turn changes the area of the CFRP. The area of CRPs becomes the product of the individual rod area by the number of rods provided. Therefore, the total area can be adjusted by either varying rod diameter, rod spacing or both. Nominally, CRPs are usually given the term CRP- X^3 ($X^3=XXX=070, 145, 195, \text{etc.}$), which indicates that CRP can resist XXX kips of force per 1-ft wide section. Each panel is approximately 1.2 m (4 ft.) long.

CRPs are attached to the structural member as externally bonded reinforcement (EBR). Attachment of CRP onto a structural substrate can be summarized as such: (1) a uniform layer of adhesive is applied onto the substrate. (2) CRP is then brought to its correct position and pressed gently, forcing the adhesive to flow around the rods and fill completely between the rods. (3) Finally, CRP is covered with a second adhesive coat.

In this attachment configuration, CRP will be centered and embedded inside the adhesive, [figure 1.3 (c)]. Adhesive thickness will approximately be 2-to-3 millimeters greater than rod diameter. Neighboring panels are brought together and made continuous by overlapping “finger joint” methods, [figures 1.3 (c, d)]. The overlap length, conservatively selected based on preliminary double-lap shear tests conducted by Harik and Peiris (2014), is 150 mm (6 in.). Each alternate panel is produced with an extra rod to provide symmetry on both sides of the overlap region.

Potential advantages of using CRP technique are:

1- CRP technique is suitable for rehabilitation/strengthening of members with long span or limited access (e.g. bridges over waterways and freeways). Under such circumstances, application of externally bonded FRP laminates (plates) would be interfered by the need for large equipment and manpower, required for attaching continuous laminates. Splicing FRP laminates is still uncommon practice. Few studies have reported on the viability of lap splicing FRP plates for concrete members (Yang and Nanni 2002; Stalling and Porter 2003). However, within spliced (overlapped) CRPs, the retrofit program can easily be carried out by few workers with relatively simple equipment, therefore leading to a significant reduction in the repair cost and time.

2- Within CRP technique, the bond width (w_f) can be increased by adjusting rod spacing and rod diameter, for a constant CFRP area. Several researches have shown through experimental and analytical studies that increasing bond width results in delaying or complete prevention of pre-mature debonding failures for FRP plated concrete and steel members (Chen and Teng 2001, Kamel et al 2003, Obaidat 2011). This capability is unavailable with CFRP laminates, due to their solid geometry and limited available thickness.

3- Since the rods are embedded inside the adhesive layer, adhesive will provide a degree of protection against chemical and environmental attacks.

1.4 Research Objective

The main objective of this doctoral dissertation is to investigate, experimentally, analytically and numerically, the effectiveness of spliced CRPs used as external reinforcement for strengthening concrete structures.

1.5 Research Significance

FRP composites have been widely used in the last few decades as an alternative reinforcement to conventional materials, such as steel. FRPs can be used in new constructions to complement or completely replace steel rebars and grids, or as an additional reinforcement to strengthen or repair deficient structures. As this system continues to develop, new ideas and techniques emerge to overcome the limitations and flaws encountered within early developed FRP systems.

The current proposed research is anticipated to provide an insight on one of the new FRP techniques used in strengthening concrete members. CFRP Rod panels are developed to reduce labor and equipment costs by means of using short panels jointed together by overlapping. The technique is used in lieu of other forms (i.e plates, fabrics) when the to-be repaired structure has limited access (e.g. bridge over busy roadway). Although, there have been some laboratory tests that investigate the behavior of concrete members bonded to CRPs, as well as some field applications utilizing CRPs for bridge repair (Harik and Peiris 2014). This proposed research serves as the first in-depth study to evaluate the flexural and bond responses of CRPs, when they are bonded to concrete substrate. The experimental, numerical and analytical outcomes of this proposed research study will be

significantly important in support of the developed technique; in order to gain reliability on the system and introduce it into the market.

1.6 Dissertation Layout

This dissertation is organized in seven chapters. The main body of the work, which includes experimental, numerical, and analytical investigations of the effectiveness of spliced CRPs to strengthen concrete members, is presented in chapters 3, 4, 5, and 6. An outline of the contents of the following chapters is explained as follows:

Chapter 2: Literature Review

This chapter provides a state-of-the-art literature survey on past and current methods used to repair or upgrade concrete members. Current strengthening methods that utilize FRP forms material, including (1) externally bonded FRP plates (laminates) and sheets, (2) near surface mounted (NSM) FRP rods and strips, and (3) externally bonded pre-stressed FRP plates, are examined. Each of the above strengthening techniques is reviewed in terms of its characteristics, method of application onto the concrete substrate, advantages and limitations, while also listing laboratory studies and field applications, that investigate the applicability of these techniques onto the retrofit of concrete structures.

Chapter 3:

The development length and bond strength, along with other factors, expected to effect the bond behavior of CRP/concrete joint, are studied experimentally through laboratory tests

on double-lap shear specimens. Results are presented for two CRPs, with two rod diameters and two rod spacing.

Chapter 4:

The flexural behavior of overlapped CRPs is experimentally studied by testing laboratory-size, RC beams under four-point bending. In order to measure the effectiveness of overlapped CRPs, and to compare the results with the other widely used strengthening methods, the beam testing program includes: (1) control (un-strengthened) specimen, (2) specimens strengthened with full-length CRPs, and (3) specimens bonded to full-length and spliced CFRP laminates, in addition to specimens bonded to overlapped CRPs.

Chapter 5:

3D nonlinear finite element (F.E) analysis of the specimens tested in chapter 4 is performed. The steps followed to create the finite element analysis are presented. Also, the simulation results are compared with the findings of the experimental testing. The validated F.E models are further used to extract essential data that can't be produced from the experiments. And finally, to study in detail the performance of CRPs in strengthening RC beams.

Chapter 6:

Presents two analytical tools to investigate the behavior of CRPs when used to strengthen or retrofit concrete members. The first tool complements the double-lap shear tests in chapter 3, and provides mathematical terms for important characteristics of the CRP/concrete interface; such as adhesive shear stress, relative slip between concrete and CRP, and tensile strains in CRP. The second tool investigates concrete cover separation failure, which was observed in the beam testing for RC beams strengthened with full-length and overlapped CRPs.

Chapter 7:

Concludes the major findings of the dissertation and summarizes recommendations for future work. Also this chapter lists the limited factors and case studies undertaken in the current investigation and provides suggestions about how to further examine other potential parameters.

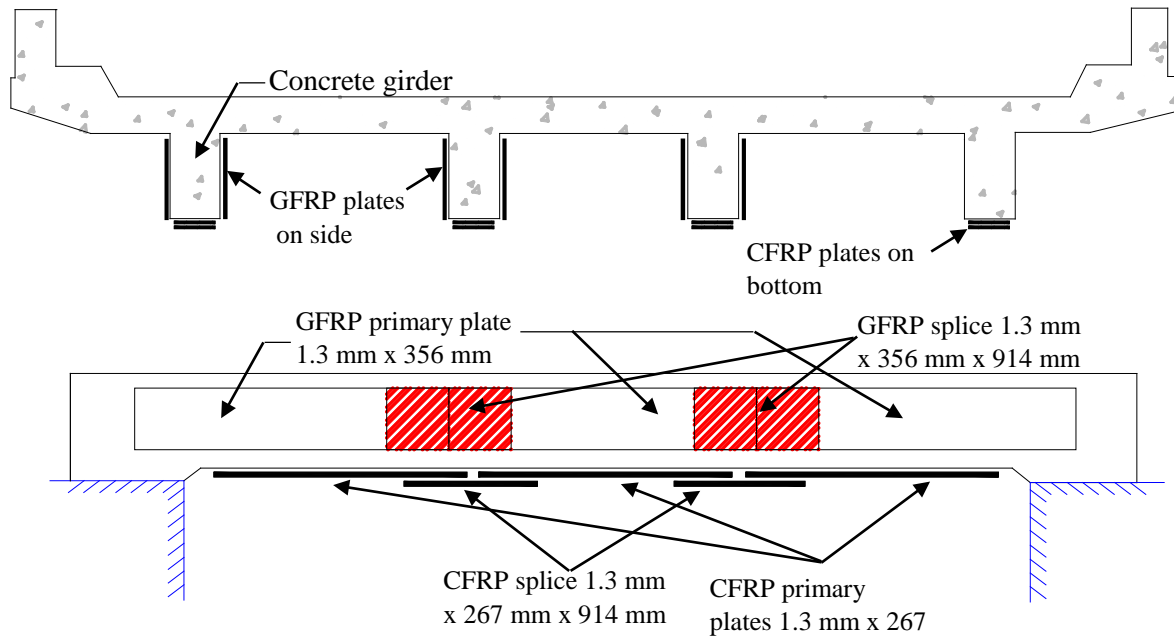
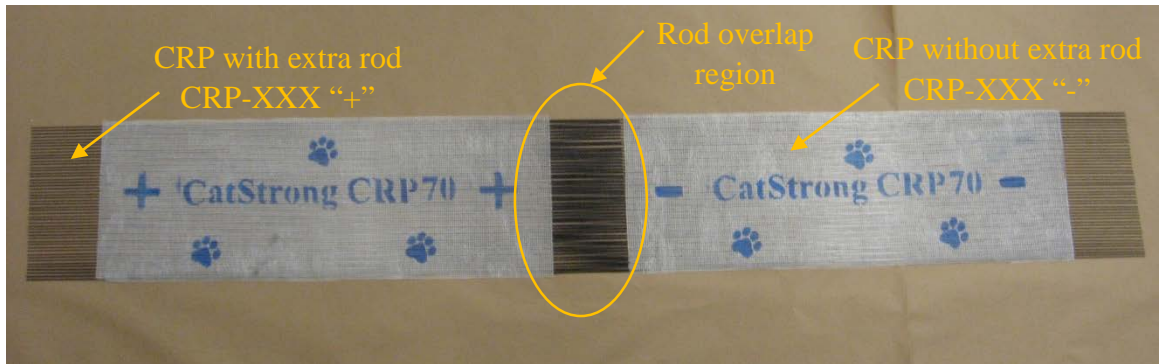


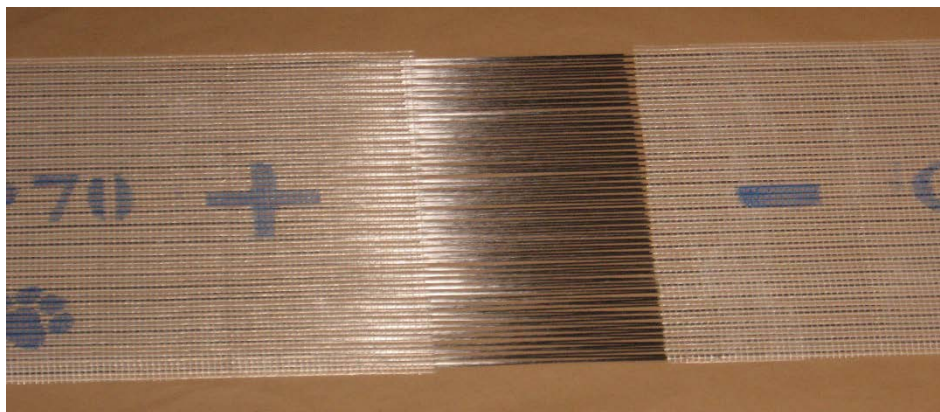
Fig. 1.1 Lap-spliced FRP plates on concrete bridge (after Stallings et al 2000).



(a) Individual CRP (pictured CRP-195)

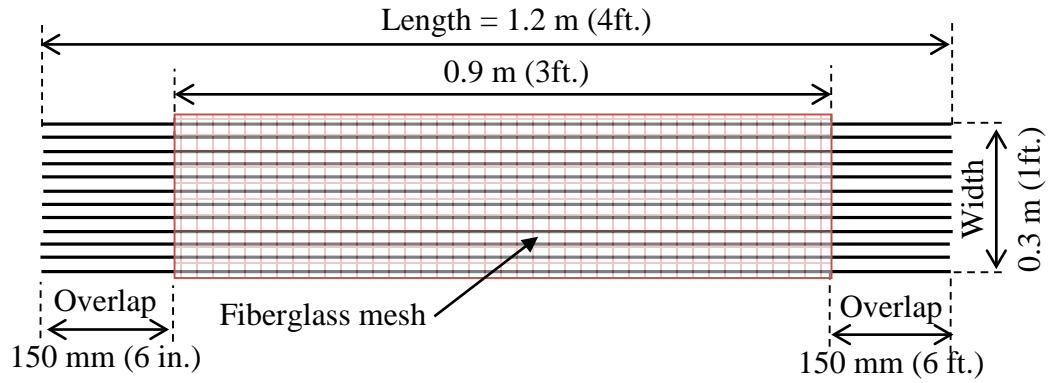


(b) Two panels, arranged in overlapping layout (pictured CRP-070)

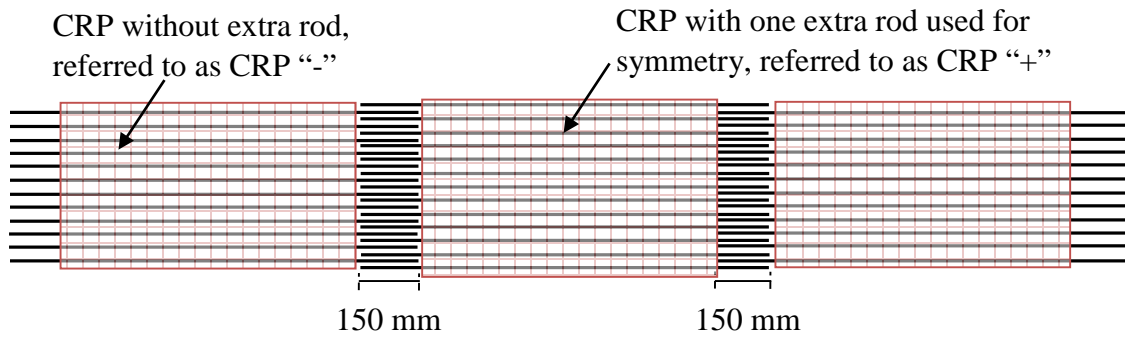


(c) Close-up of rod overlap region (pictured CRP-070)

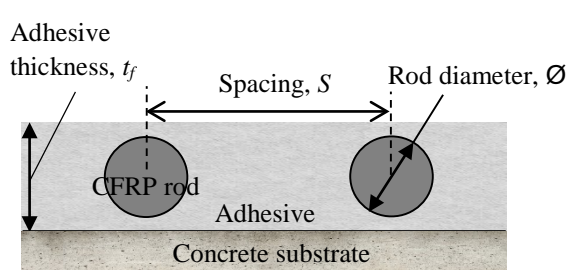
Fig. 1.2 CRP strengthening technique (actual panels).



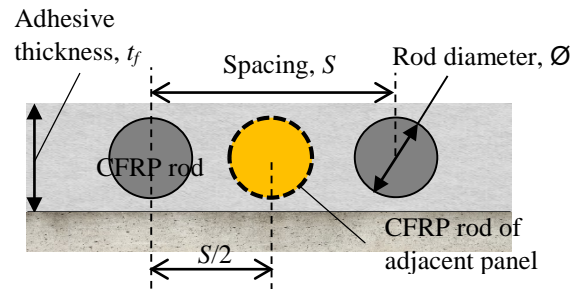
(a) One CRP panel, enlarged to show details



(b) Three CRP's made continuous by means of overlap



(c) CRP placement on concrete, section outside overlap region



(d) CRP placement on concrete, section inside overlap region

Fig. 1.3 CRP strengthening technique (schematics).

CHAPTER 2: LITERATURE REVIEW

2.1 Conventional Strengthening Methods

In civil engineering applications, the repair and strengthening of concrete and steel infrastructure is as important as the design, analysis and construction aspects. The following are a number of conventional techniques used for repair before the development of strong structural adhesives and plate bonding techniques:

- 1- Introduction of additional supports intended to reduce the member's span, and hence decrease forces and deformations in the member, [figure 2.1 (a)], (Wipf et al 1987, Al-Jelawy 2013).
- 2- Increasing dimensions of the section, by stapling additional reinforcement and casting new concrete, to enlarge the section's capacity, [figure 2.1 (b)], (Hollaway and Leeming 2000).
- 3- Replacing non load-bearing sections with load-bearing ones; or using lighter partitions and coverings, to reduce dead weight (Jones et al 1982).
- 4- Using external prestressing technique, in which the pestressing strands act as an additional tensile reinforcement, to increase or supplement the internal reinforcement, [figure 2.3 (c)] (Wipf et al 1987, Al-Jelawy 2013).

Although these conventional methods can suffice in restoring or increasing a member's capacity, they have a number of disadvantages. Conventional methods require extensive labor and time, they cause disruption to the structure functionality, and sometimes, demand evacuation of the buildings inhabitants or closure if necessary (Jones et al 1982).

2.2 Adhesively Bonded Plates

In the last few decades, the development of strong bonding agents, in conjunction with a better understanding of the mathematical concepts governing how composite parts interact and behave when they are bonded together, and the development of numerical and analytical tools (e.g. finite element method, advanced closed-form equations) used in predicting the behavior and failure mechanism of different engineering materials, have all guided structural engineers and researchers toward the development of new repair techniques that are cost-effective, and easy-to-install. Plate bonding technique is one of those great repair methods. It involves attaching a steel or FRP plate onto the structural substrate (e.g. concrete, steel, masonry, timber, etc.) with the help of bonding agent, oftentimes, epoxy adhesives.

Since concrete has a relatively low tensile strength, therefore it cracks in tension at low load levels, and given that other parameters such as moisture, freeze-thaw cycles, chemical attacks, etc., could cause significant corrosion of the steel reinforcement and lead to a reduction in the member's load capacity, external plates could be bonded to the concrete soffit as a supplementary reinforcement to restore the lost tensile force due to cracking and/or steel corrosion in repair projects. Likewise, in strengthening projects, bonded plates could be glued to the uncracked, un-corroded concrete member to increase the member's load capacity to certain limits when such capacity needs to be increased due to: change of structure's function, adaptation of new, more rigorous design codes, or increase in operational loads.

2.2.1 Adhesively Bonded Steel Plates

During 1960s, the use of steel plates as an externally bonded reinforcement for strengthening, repair, and retrofit of structural elements, is believed to have first initiated in South Africa and France (Chajes et al 1994, Norris et al. 1997, Toutanji et al. 2006). The technique was attractive at first because it offered many advantages including cost-effectiveness compared to other conventional methods, small to negligible changes in the member's geometry, tangible increase in strength and stiffness, and reduction in deflections and cracks (Macdonald and Calder 1982, Jones et al. 1982, and Narayan et al. 1996). Furthermore, steel plates have isotropic properties, are ductile, and possess a relatively long fatigue life (Jumaat and Alam 2008).

Large numbers of laboratory studies have shown that RC beams or slabs bonded in tension with steel plates could achieve a substantial increase of strength and stiffness, within both service and ultimate-load stages; while also achieving a decrease in cracks and deformations (Macdonald 1978, and 1982, Van Germet 1980, Jones et al 1988, Swamy et al 1989). For Example, Oehler's 1992 tests of grouped RC beams, with a focus on flexural and shear peeling failures, were in fact strengthened with steel plates. During these tests, various variables were changed such as: concrete compressive strength, shear reinforcement amount, shear span, and distance between supports and plate ends, this allowed for the arrival at a design model capable of preventing debonding induced by flexure and/or shear forces. In addition, in Barnes et al. 2001, steel plates joined by means of bolting or adhesive bonding, were attached to the sides of 2330 mm (91 in.) long RC beams, proving to enhance the shear capacity. Furthermore, the fatigue life of beams bonded to steel plates was studied in Hwan et al 2003. The study found that strengthened

beams had a better fatigue resistance at the same load level than their un-plated counterparts. Finally, the bearing capacity of RC beams, was also significantly enhanced due to the presence of adhesively bonded steel plates, as studied by Lei Dong et al. 2012.

Further studies also showed that RC slabs could also be strengthened with steel plates. In Ebead and Marzouk 2002, two-way RC slabs with a square side of 1900 mm and a built-in column at the center were showed to have strengthened with steel plates of 1.5 mm thick. The plates were located at the central region near the column, in which, punching shear force is high. Static (central point load, and moment) and cyclic loads were considered. For strengthened specimens subjected to point loads, the ultimate load increased by 54 and 36.5%, for internal reinforcement ratios of 1%, and 0.5%, respectively. Specimens subjected to combination of point load and moment had an increase of at least 88% in ultimate capacity.

Zhang et al. 2001 carried out an experimental program on square, two-way, simply-supported, RC slabs strengthened with steel plates. The results of the testing revealed that steel plates were able of enhancing cracking and ultimate load behavior as well as reducing cracks and deflections. No debonding failure was observed in the strengthened specimens, and the authors assumed that debonding is unlikely to occur in plated two-way RC slab. One-way RC slabs, having a length 1500 mm, a width of 600 mm, and a thickness of 60 mm, were strengthened in flexure with steel plates bonded at the bottom, (Rasheed and Al-Azawi 2013). According to the authors, bonded plates were effective in increasing the crack load by at least 60%, and ultimate load by at least 85%. Debonding at plate ends was the predominant failure mode.

In field applications, steel plates were successfully applied to strengthen or repair RC buildings, bridges or other types of structures. (Mander 1981, Van Germert and Maesschalck 1983, Sims 1985). Plates have also been applied to the sides of concrete members to repair or strengthen structures with inadequate shear reinforcement (Swamy et al 1989, Taljstan 1994, Barnes and Mays 2001).

However, steel plate bonding technique has some disadvantages that limit its full utilization within structural repair/strengthening projects. Those disadvantages may include: (1) corrosion: since steel plates are bonded to the external surface of the member, they are generally un-protected against corrosion, in which, steel material is highly susceptible to; and due to the reduction of the plate's sectional-area, corrosion could result in deterioration of the bond strength (Hollaway and Leeming 2000, Obaidat 2010). (2) Difficulty of transportation: especially with long sections, due to the high density of steel. Furthermore, due to the lack of flexibility, it is hard to use the technique within complex shape members. (3) High labor costs: since steel plates are heavy, handling and installing them is a cumbersome task, most times, requiring the use of massive false-works and clamping systems to hold the plates in place while adhesive is in the process of curing. Consequently, both the project's cost and time would be increased (Jumaat and Alam 2008). (4) Cracking and debonding: In practice, the delivery lengths of the plates are limited, therefore when long sections need to be strengthened, jointed plates or lap-spliced are used to achieve the strengthening length. Those jointed plates would then, be connected by the use of welding and/or bolting, which both are observed to cause several issues such as cracks within concrete as in the case of bolting, large normal and shear stresses at the bond interface, and debonding failures (Norris et al. 1997, Toutanji et al. 2006).

2.3 Strengthening of Concrete Members with FRP

In the last two decades, there has been an extensive increase in the use of fiber reinforced polymer (FRP) composites for structural engineering projects, (Alaee and Karihaloo 2003, Aram et al 2008). Due to the composites' excellent attributes of high strength and stiffness, low density, and immunity to corrosion, FRP's have made their way into the zenith of structural applications. Despite that FRP sections are more expensive than other conventional structural materials, like concrete and steel, the project's total cost is generally competitive due to the cost savings received from labor, equipment, and time. Since FRPs are lightweight, and easy to install, the need for labor and equipment is reduced. (ACI 440.2R-2008).

Furthermore, FRP's have various configurations, enabling them to be used in a host of assignments. Rectangular sections, angles, channels, tubes, bars, tendons, rods, etc., are just some examples of the shapes available in the market. Within the civil engineering field, FRP's can be employed in two ways: internal and external reinforcement. In the construction of reinforced and pre-stressed concrete members (e.g. beams, columns, and slabs), FRPs can be used as an internal reinforcement to replace or supplement steel rebars, tendons, or grids, particularly in corrosive environments (Micelli and Nanni 2004, Nour et al 2007, De Luca et al 2010, Triantafillou and Matthys 2013). On the other hand, most utilizations of FRP involve applying the advance material as an external reinforcement to repair or strengthen structures that are weak in flexure, shear, torsion, etc. (Arduini and Nanni 1997, Blanksvard et al 2009, El-Maaddawy and El-Dieb 2011).

2.3.1 Adhesively Bonded FRP Plates (Laminates, Strips)

Pultruded FRP plates (also called laminates or strips), of high tensile strength, are glued to the soffit of concrete members to increase the flexural capacity. The plate must be glued to the tensile face of the member in a way that ensures the fibers are aligned with the member's longitudinal axis. Additional resistance moment, resulting from the plate's tensile force and its distance from neutral axis, would be added to the section nominal moment capacity. Improvements in load-carrying resistance, post-cracking stiffness, reductions in crack widths and deflections at service are abundantly reported in the literature for FRP plated concrete members (Meier 1987, Bonacci and Maalej 2001, Eshwar et al 2005, El Maaddawy and Soudki 2008, and Florut et al 2014). Other studies geared toward the long-term behavior, fatigue performance, environmental exposure, and time-dependent (dynamic) applications of FRP bonded concrete are also abundant (Plevris and Triantafillou 1994, Ferrier and Hamelin 2002, Savoia et al 2005, Kesavan et al 2013, Rabinovitch 2014).

In a study of strengthening by FRP plating by Meier and his colleagues (Meier et al. 1992), presented a four-point, static testing program on 60 small-scale RC beams, strengthened by soffit CFRP laminate, 0.3 mm (0.012 in) thick and 200 mm (8 in.) wide. The flexural capacity of strengthened specimens was reported to be over 100% more than control beam, the deflection to be 50% less, and cracks were smaller in width and spaced closely. Further, in another study by Ritchi (1991), Glass and carbon (FRP) plates were adhesively bonded to the soffit of 2.74 m (9 ft.) long RC beams, and tested to failure in flexure. The study found that when comparing with un-plated control specimens, the FRP bonded beams, achieved 17 to 99 % increase of the at-service stiffness, and 40-97% increase of ultimate

strength. Also, in a study by Jumaat and Alam 2008, 2300 mm long, RC beams with a cross section of 125 x 250 mm, for width, and depth, respectively, were bonded to CFRP plates and tested in four-point bending,. The testing revealed that FRP bonded beams were able to achieve 54% increase in failure loads over the control specimen for un-anchored FRP plates, and 96% for end-anchored FRP plates.

To mimic practical field applications, in which most bridge or building repair projects are under some loading levels, pre-loaded concrete beams (to 85% of capacity) were strengthened with FRP plates, and tested in flexure, Alfarabi et al 1994. Pre-loading to the suggested levels didn't influence the flexural behavior of tested strengthened specimens when compared to un-loaded strengthened reference beam. At the University of Arizona, full-scale concrete rectangular and flanged beams were repaired in flexure by GFRP plates and tested under four-point setting, Saadatmanesh and Ehsani 1991. The experimental program is believed to be the first testing performed on large scale FRP repaired members in the US. Considerable improvements in strength and stiffness, and reduction in stress levels of internal steel, were observed.

Besides experiments, in some places, experimental repair programs have been a huge success. In Delaware, several RC bridges comprised of prestressed box beams were in a bad structural shape due to severe cracking at the beams' tensile faces. The bridges were scheduled for replacement, but later on the replacement was canceled since their capacity was successfully restored by bonding FRP plates to the tensile side of each beam, Chajes et al 1993. Another example of a successful FRP plating is the concrete deck slab of the two-span, composite bridge over Deerfoot trail in Calgary, Canada. The bridge was in need for strengthening to carry out the current design live loading, Hutchinson et al 2003.

CFRP strips, 100 mm (4 in.) wide and 1.2 mm (0.048 in.) thick, spacing 500 mm (20 in.) apart, were added to the tension face of the slab at negative moment locations.

The feasibility of attaching FRP plates to retrofit concrete members against blast loading was examined through experimental testing and analytical modeling by Wu et al 2009. FRP plating was found to be an appropriate technique for retrofitting blast damaged concrete elements, and effective in increasing the energy absorption at such loading event. As part of a larger program concerning the long-term durability, fatigue endurance, low temperature, and dynamic loading effects on FRPs, Lopez et al 2003 tested four RC concrete beams glued to FRP laminates. The study concluded that temperature as low as -29°C (-20.2°F) didn't have an impact on the interfacial bond between concrete and FRP, nor on the ultimate load performance. In another test to evaluate the effects of using bonded composite reinforcement, Ebead and Marzouk (2004) studied two-way concrete slabs that were bonded in the soffit with carbon FRP strips and glass FRP laminates. The study found that flexural capacity was increased by in average by 35.5%, with a similar increase in initial stiffness.

2.3.2 Adhesively Bonded FRP Fabrics (Sheets)

Although FRP plates are best known for use with flexural applications and FRP fabrics for shear repair or column confinement, fabrics can be also used to enhance bending capacity. Fabrics are very flexible and can follow the outline of an un-even surface and bend at right angles. Since the production of bonded fabrics involve impregnating dry or pre-preg fibers with a saturating resin at site, the cost of the fabric system is generally less than for factory manufactured plates. Numerous number of research studies, concerning bonding FRP

fabrics (sheets) to strengthen or repair concrete members in bending, have been found. Various types of FRP fabrics, including E-glass, aramid, and graphite CFRP fibers, were bonded with two-part epoxy to the bottom of RC beams, and tested in flexural setting, Chajes et al 1994. The composite reinforcement contribute to an increase in the flexural capacity by 36-57%, depending on the type of FRP reinforcement, while the post-cracking stiffness enhanced by 45-53%. E-glass and graphite fiber FRP strengthened specimens failed by fabric tensile rupture in the constant-moment region, while specimens bonded to aramid fabrics, failed by compressive concrete crushing.

The effects of strengthening pre-cracked members and changing the orientation of fibers were examined experimentally in Norris et al 1997. CFRP sheets with fibers oriented either parallel to beam's length (0^0), diagonal to length ($\pm 45^0$), or perpendicular to length (90^0) were bonded to concrete beams, which were tested under flexural conditions. As for pre-cracking effects, the study concluded that pre-cracked strengthened specimens performed similar to their un-cracked peers. The fiber orientation, however, has a great deal of influence. Fibers with longitudinal orientation presented the largest increase in strength and decrease in deflection, but the beams failed in brittle matter by end-peeling. Beams bonded with perpendicularly oriented fibers presented strength increase, 20% less than of unidirectional fibers, and showed greater ductility increase. $\pm 45^0$ oriented fibers provided the highest ductility increase.

Twelve simply supported concrete beams, spanning 4.5 m (14. 76 ft.), were bonded with unidirectional CFRP sheets or fabrics having different layouts and anchoring types and tested in flexural setting, to investigate the feasibility of CFRP bonding, Alagusundaramoorthy et al 2002. The flexural strength of the beams was increased by 49%

for bonded CFRP sheets, by 58% for bonded and anchored CFRP sheets, and by 40% for bonded CFRP fabrics. Carbon FRP sheets were bonded to RC beams with dimensions of 2000 mm for length, 150 mm for width, and 200 mm for height, Esfahani et al 2007. Four-point flexural testing of the strengthened beams indicated that the flexural capacity, and stiffness of the beams were significantly enhanced when bonding CFRP sheets. The study also found that ACI 440 and Canadian ISSS code equations, overestimate the flexural capacity of RC beams glued to CFRP sheets, and the overestimation increases when small internal reinforcement ratios are used. CFRP sheets were also applied to enhance the resistance of RC slabs with openings, Enochsson et al 2007. As concluded by the study, the flexural resistance of concrete slabs with an opening can be increased by attaching CFRP reinforcement.

An experimental study by Gharachorlou and Ramezaniapur 2010 investigated the effects of chloride ions penetration and other harsh environmental conditions on concrete elements bonded with GFRP and CFRP sheets. Complete wrapping of the specimens with sheets resulted in 70% reduction in chloride ions penetration. Only 13.6% degradation of flexural capacity, when specimens strengthened with FRP sheets and immersed in salt water, at higher temperature, was observed; while specimens that were fully confined with the sheets achieved an increase in ultimate strength by 8.1%.

Furthermore, FRP sheets have also been attached to masonry walls and elements, and have been proved to be very effective for in-plane or out-of-plane strength enhancement (Myers et al 2004, Schnerch 2007). The flexural behavior of unreinforced masonry walls, strengthened with GFRP sheets, was examined by Ehsani and Saadatmanesh 1996. Walls, measuring 215 mm wide, 100 mm thick, and 1450 mm long, were adhesively bonded to

GFRP sheets and tested in four-point bending. A remarkable enhancement of flexural capacity of 24 times the capacity of control specimen was reported in the study. GFRP sheets of different layouts were bonded to 10 full-scale infill masonry walls and tested, under uniform pressure in the out-of-plane direction, Lunn et al 2011. Several key factors were studied including: aspect ratio of the wall, FRP coverage ratio, number of masonry wythes, and FRP anchorage. The GFRP sheets were successful in strengthening the wall and increasing the out-of-plane load resistance, with a proper anchorage method. Foster et al 2005 recorded an increase in strength, pseudo-ductility, and energy dissipation for masonry walls strengthened with GFRP wet lay-up sheets, when the specimens were tested under combination of gravity loads and cyclic lateral pressure.

2.3.3 Near Surface Mounted (NSM) Technique

NSM technique is a novel method of strengthening/repairing concrete members in flexure and/or shear and is used in lieu of externally bonded (EB) FRP plates or fabrics, to overcome some of the limitations and shortcomings associated with EB technique. Its [NSM method] simply consists of inserting FRP rods or plates (strips) inside pre-cut grooves or slits within the concrete cover. Adhesives or other types of bonding agents are then used to fill the grooves/slits and bond the composite material onto the concrete substrate, (figure 2.2). In some cases, using NSM technique instead of externally bonded plates or fabrics can be more beneficial and yet necessary. Advantages of using NSM technique with respect to externally bonded FRP (EBR) are: reasonable protection of the FRP material against environmental attacks, fire, and vandalism since the composite material would be embedded inside the concrete cover; preparation of concrete surface to

provide a strong bond with the composite reinforcement is un-needed within NSM method, and that in turn, would reduce both cost and time of the repair project; no reduction of floor height or bridge clearance due to the installation of the strengthening material is associated with NSM; the method becomes particularly attractive for flexural strengthening in the negative moment regions of slabs and decks, in which, external reinforcement would be subjected to mechanical and environmental damage and would require a protective cover, which could interfere with the presence of floor finishes (De Lorenzis and Nanni 2002, Hassan and Rizkalla 2003, EL-Hacha and rizkalla 2004, Badawi and Soudki 2009, Al-Mahmoud et al. 2010, Capozucca 2014).

Laboratory applications and experimental testing have showed that NSM rods/strips can be successively applied in strengthening or upgrading RC members in flexure. Badawi 2007 conducted an experimental program on 22 RC beams to investigate the monotonic and fatigue behavior of NSM strengthened concrete members. Un-prestressed and prestressed (to 40% or 60% of the rod's tensile strength) CFRP rods were both used. Generally, both the monotonic and fatigue strength of the strengthened beams were enhanced due to the presence of the rods. For un-prestressed rods, the monotonic yield and ultimate loads were increased by 26% and 50%, respectively, as referenced to the control specimen. Another increase of 16% was registered for the flexural stiffness. The prestressed rods contributed further, and an increase of up to 91%, 79%, and 52.6% were reported for yield load, ultimate load, and flexural stiffness, respectively, when prestressed rods (40% or 60%) were used. Foret and Limam 2008 carried out an investigation on RC two-way slabs strengthened with NSM FRP rods. The load bearing capacity, as revealed by testing, was enhanced when NSM rods are bonded to the slabs. 14 wallets of hollow

clay masonry units, measuring 60 x 120 x 19 cm, four masonry beams, measuring 90 x 12.5 x 9 cm, and three walls of void-concrete blocks, measuring 60 x 60 x 9 cm, were strengthened with NSM GFRP rods of 6 and 10 mm in diameter and tested experimentally, Tinazzi et al. 2000. Flexural and shear testing revealed that the additional NSM reinforcement was able to maximize the shear and flexural performance. For the concrete block walls, an increase in the flexural strength as referenced to the control specimen, of 7 times to 15.7 times, depending on the number of rods attached, was observed. The masonry units also received an appreciable increase of strength due to the presence of the rods. When the units were subjected to cyclic loading, good energy dissipation of the strengthened units was recorded over the un-strengthened specimen. Also in shear tests, all the strengthened masonry units, achieved substantial increase in shear capacity.

Tumialan et al 2001 presented an experimental program on un-reinforced masonry (URM) walls strengthened with GFRP rods, embedded in grooves inside horizontal and/or vertical joint locations. Shear testing was carried out through a diagonal loading set-up. The shear strength of the strengthened units was about two times the capacity of the analogous un-strengthened sample. A modified epoxy adhesive, reinforced by short glass fibers, was suggested to be used as an adhesive for bonding NSM GFRP rods to URM walls, Bajpai and Duthinh 2003. The new epoxy formulation was implemented to improve the development behavior of the rods. Flexural testing of GFRP rod strengthened walls, using four-point bending, indicated that the epoxy was active in providing full anchorage for the rods, and failure was therefore, due to tensile rod rupture.

2.3.4 Pre-stressed FRP's

FRP plating technique is most recognized in increasing the ultimate load capacity, while its effects on serviceability state are limited due to pre-mature debonding failures taking place within service loading conditions. In most practical applications, the ultimate state design will never control the failure of the member. Rather, cracks widths and sizes, deflections, and other serviceability requirements would govern the behavior of concrete members. This being said, an innovative idea of pre-stressing the composite material before applying it to the substrate of the member, could fulfil the serviceability needs, prove more cost-effective, while also increasing the ultimate loads. The idea of pre-stressing the soffit plate was initiated with steel plates bonded structures during 1960s (Hollway and Leeming 2000), and it was expended to FRP material in the 1990s (Franca 2007).

Several laboratory studies and field cases, dealing with bonding prestressed FRP material onto concrete, have taken place and been recorded in the literature (Triantafillou et al 1992, Luke et al 1998, El-Hatcha et al 2003, Nordin and Tajsten 2006, El-Hatcha et al 2013). The effects of prestressing CFRP sheets were experimentally investigated in Wight et al 2001. Through flexural testing of RC beams bonded with pre-stressed CFRP sheets, the study concluded that the pre-stressing assisted in improving serviceability by reducing cracks widths and delaying their onsets, decreasing deflections, and at the same time, increasing ultimate capacity. Huang et al 2000, 2005 carried out an experimental program on 2.0 m (6.56 ft.) long T-section RC beams to examine the phenomenon of debonding failure that takes place at the plate-ends, when the prestress force is released. The study concluded that using glass FRP plates could mitigate the debonding, since GFRP composite has a modulus of elasticity comparable to that of concrete, and therefore, the adhered components would

transfer forces in a compatible way. While carbon FRP plates, which have a modulus in the range of seven times greater than concrete, were not recommended.

Badawi and Soudki 2009 presented a similar experimental program on RC beams strengthened with prestressed NSM CFRP rods. Prestressing values of 40% and 60% in the rods, resulted in 90% increase in the yielding load, and 79% increase in the ultimate load, over the control sample. Peng et al 2014 compared the effectiveness of using pre-stressed NSM CFRP strips as replacement to non-prestressed strips through a flexural testing procedure on rectangular RC beams. The study found that prestressed NSM strips improved the load-carrying capacity better than non-prestressed strips. Hajihashemi et al 2011 reported an increase in cracking load, and ultimate capacity when prestressed, rather than un-prestressed, NSM CFRP laminates are bonded to RC beams. Several rectangular, simply supported RC beams were bonded to prestressed CFRP laminates and tested under central point load, Sakar and Tanarlan 2014. The study investigated a new, easy-to-implement in the field, device for applying the prestress force, and carried out the experimental program to assess the outcomes of the method. Specimens attached to prestressed laminates failed by FRP rupture, while specimens bonded to un-prestressed laminates failed by FRP debonding. At least twice the increase in ultimate load that was recorded for un-prestressed laminates was registered for pre-stressed ones, when both are compared to control beam.

Kotynia et al 2014 carried out an experimental program consisting of RC slabs strengthened with prestressed CFRP laminates. The main objective was to study the effectiveness of prestressed FRP material in enhancing the behavior of preloaded concrete slabs. The strengthening method was deemed promising in improving the ultimate limits

and serviceability state. The range of increase in the flexural load capacity was between 64-119%. Several slabs, made of Granite stones, were reinforced with prestressed NSM CFRP bars and tested in monotonic flexural setting, Guo and Chai 2014. Prestressing the composite bars resulted in a higher efficiency than non-prestressed bars, in terms of flexural stiffness and strength. An increase of 60% in the cracking load was recorded, when the bars were stressed to 30% of their guaranteed strength. Smaller spacing and width for cracks, was also noticed, when using prestressed bars.

Other research into the same subject has proven the feasibility of prestressed FRP rods, sheets, and plates in improving service conditions and strength of concrete beams, girders, slabs, and masonry units---both in laboratory testings and field applications (Kim et al 2008, Choi et al 2011, Kotynia et al 2011, Michels et al 2013, Wu et al 2014). However, the method has not yet completely matured, and most recent studies are concentrating on practical challenges that need to be tackled before the method becomes a mainstream. For example, considerable amount of research has focused on the device that applies the prestressing force, and researchers are trying to find an easy to use devices (Monti and Liotta 2006, Franca and Costa 2007); on the stress limit that can be applied to the FRP material and results in optimum utilization of the reinforcement, while reducing the risks of release-debonding (Berset 2002); on anchorage systems to hold the reinforcement in place while the stress is released, their types and effects (Andra et al 2001, Wu et al 2006).

2.4.5 Other Novel Techniques

When introduced into the civil engineering community, FRPs were a breakthrough innovation that helped in solving issues related to heavy weight and corrosion of steel plates and rebars, and helped in making retrofit of our aging infrastructure become a favorable choice. However, no material is 100% perfect, and FRP abides to that rule of nature. Some limitations inherited within the composite nature or interaction (bond) with the structure, have pushed researchers and engineers to further improve FRPs intrinsic composition or the bonding method to give superior characteristics for specific applications. Ongoing innovations of different composite systems are difficult to count, and therefore, the following paragraphs provide only a review on some of the innovative methods available in the literature.

Several ways have been employed to bond the advance reinforcement onto the substrate of a structural member in addition to adhesive bonding method. A relatively recent method consisting of mechanical bonding through the use of high strength bolts has been developed (Lamanna et al 2001, 2004, Martin and Lamanna 2008). The method eliminates the need for some procedures encountered in adhesively bonded applications. For example, mechanical fastening requires no surface preparation and curing for adhesives, therefore the structure can be put into service immediately after completion of fastening, and the cost required for those procedures can be cut down. Lamana 2002 carried out an extensive program to validate the viability of mechanical fastening through experimental testing of both small-scale and large-scale rectangular RC beams. Several parameters were considered such as fastener spacing and number of rows, predrilled holes, edge distance between last fastener and plate end, and fastener connection strength. Small-scale

specimens strengthened with mechanically fastened CFRP strips showed 34.2% and 24.8% increase of yield and ultimate moment capacity, respectively, over the un-strengthened specimen. Similarly, the large-scale beams gave 21.6% and 20.1% increase of yield and ultimate moments, respectively. Furthermore, the study concluded that failure mode of the mechanically attached strips was gradual, and attachment of strips took less time than adhesively bonded strips.

In El Maaddawy and Soudki 2008, FRP reinforcement was attached to the bottom of RC two-way slabs by means of mechanical anchorage- to investigate the potential of using mechanically anchored FRP plates, throughout the entire bonded length, in lieu of adhesive bonded plates, un-anchored or anchored at ends. A quasi-static testing, using four-bending loading scheme, was performed to validate the feasibility of the suggested technique. The new method granted similar increases of flexural strength as compared to adhesively bonded reinforcement, while deflections at failure stage were higher than from bonded plates, and only 15% lower than from the control specimen, indicating a good enhancement in the ductility of concrete members. Elsayed et al 2009 carried out a similar study, in which mechanically fastened FRP plates were added to the soffit of concrete slabs with or without central opening. The flexural capacity of the strengthened slabs was about 30-70% greater than the for un-strengthened (control) slabs.

Another novel technique, comprised of FRP fabrics, grids, and networks embedded in an in-organic cementitious matrix, has been recently developed, Taljsten et al 2006, Tommaso and Focacci 2008, Nanni 2012, Loreto et al 2014. The technique is named fabric-reinforced cementitious-matrix composites (FRCM) and is bonded to the structural member as an external reinforcement. Other techniques, similar to FRCM, are also developed, and they

all are based on the idea of selecting various types for reinforcement and/or matrix to produce specific characteristics. To name few, textile reinforced concrete (TRC), consists of multi-axial textile fabrics as the reinforcement and fine-grained, high strength concrete as matrix; textile reinforced mortar (TRM), made of textile fabrics and polymeric matrix; and mineral based composite (MBC), having fiber composite grid embedded in cementitious binder (Ombres 2012). The biggest benefits of using FRCM instead of FRP material are: better behavior in elevated temperatures and during fire events, applicability in wet surfaces, enhanced resistance to ultra-violet light, and perhaps the most important advantage is that, FRCM bonded members maintain higher ductility than FRP bonded ones due to the gradual failure type as a result of slippage at the fiber/cementitious matrix interface (Ombres 2011).

Ombres 2012 reported an increase of 30% in flexural strength for FRCM bonded concrete beams over un-strengthened sample. In their experimental study, Ambrisi and Focacci 2011, found analogous increase in flexural capacity of FRCM strengthened concrete beams, as compared to FRP bonded beams, with FRCM beams performing better in term of ductility retention. Taljsten and Blanksvard 2007 presented a flexural pilot study of RC one-way slabs strengthened with FRCM technique. CFRP grids were used as reinforcing fibers with cementitious mortar as binding agent, and the composite was called mineral based composite. The behavior of slabs bonded to the new composite was comparable to FRP bonded peer slabs. Nanni 2012 reported several field applications of deteriorated structural projects, repaired with FRCM technique. Those projects included plain concrete vault, a bridge RC pier, a concrete trestle pedestals, a RC tunnel, and a masonry chimney.

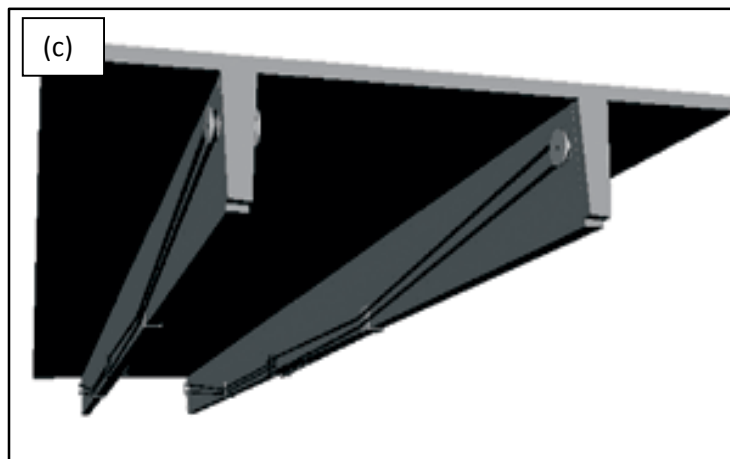


Fig. 2.1 Methods used in the past to repair or upgrade concrete structures, (a) extra supporting (Alkhadraji 2004), (b) section enlargement (Alkhadraji and Thomas 2009), and (c) external prestressing technique (Alkhadraji 2004).

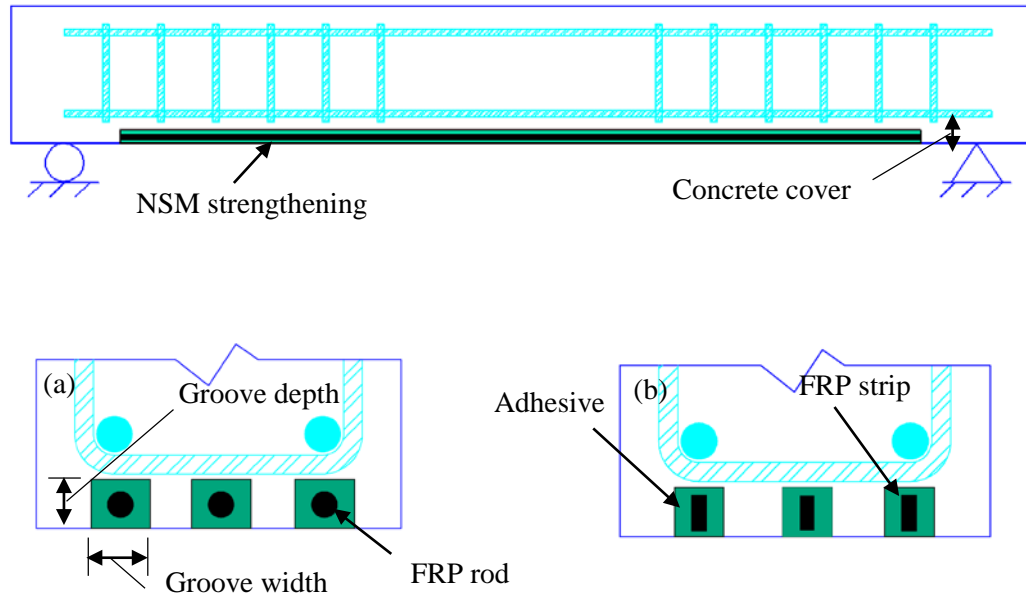


Fig. 2.2 NSM strengthening system, (a) NSM rods, (b) NSM strips.

CHAPTER 3: BOND STUDY ON CFRP ROD PANELS EXTERNALLY ADHERED TO CONCRETE

3.1 Synopsis

Fiber reinforced polymer (FRP) laminates (plates, strips) and fabrics (sheets) used as externally bonded reinforcement (EBR) to strengthen or repair concrete structural members have proven to be an economical retrofit alternative. However, when strengthening long-span members with limited access (e.g. bridges over waterways and freeways), labor and equipment demands may hinder the use of continuous EBR FRP. Recently, carbon FRP (CFRP) rod panels (CRP's) have been developed and deployed to overcome the aforementioned limitations. Each CRP is made of several small diameter CFRP rods placed at discrete spacing. Several CRP's are brought together and made continuous, to fulfill the strengthening length, by means of a lap-splice (or finger joint). In this chapter, the bond behavior between CRP and concrete was experimentally investigated. Twenty-five double-lap shear specimens were tested under pull-off loading to evaluate the bond strength, development length, transfer mechanism, shear stress-slip relation, and effects of other variables expected to influence the bond behavior. The bond strength and development length were established for two CRPs, CRP-070 (generated with rods of 2.00 mm (0.08 in.) in diameter, spaced at 6.25 mm (0.25 in.), and CRP-195 (generated with rods of 4.00 mm (0.16 in) in diameter, spaced at 9.35 mm (0.38 in.)). The development length was estimated to be 100 mm (4.00 in.), and 125 mm (5 in.), for CRP-070, and CRP-195, respectively. The bond strength for one-unit (e.g. one meter) wide CRP was determined to be 563 kN/m (38.5 kip/ft.) for CRP-070 and 712 kN/m (48.8 kip/ft.) for CRP-195.

3.2 Introduction

Numerous experimental and field applications have shown that EBR FRP can efficiently increase the flexural strength of a concrete member (Bonacci and Maalej 2001, Lee et al 2005, Chansawat et al 2009, Si-Larbi et al 2012, Ren et al 2015). One of the drawbacks of the EBR FRP method is the man power needed to attach continuous laminate along the entire length of the member. The difficulty is more evident when the concrete member is too long or inaccessible (e.g., bridge over waterway or multi-lane expressway). Construction of scaffolding along the length of a member can be time consuming and costly (Peiris 2011). Although splicing FRP laminates is an option, it is not commonly used in practice. Research on the applicability of lap-splicing FRP plates/sheets has been carried out for steel substrate (Yang and Nanni 2002, Dawood and Rizkalla, and Dawood et al 2007).

Carbon fiber reinforced polymer (CFRP) rod panels (CRP's) have recently been developed and deployed in the field. CRPs are externally bonded to the concrete substrate in a manner similar to other externally bonded reinforcement (EBR). Each panel is 1.2 m (4 ft) long and is made of a number of small diameter rods that are attached to a glass mesh intended to facilitate handling of the panels and to retain a uniform spacing between rods. In the field, the panels are connected through a finger joint "lap-splice" to form a continuous EBR and fulfil the strengthening length. Within CRP's, splicing of short-length panels can provide an economical alternative, where individual workers can carry out the strengthening process using a boom truck or simple scaffolding, thus reducing labor and equipment costs.

3.3 Experimental Program

Each double-lap shear specimen was constructed using two concrete blocks as the inner adherends [figure 3.1 (a)]. Each block is 300 mm (12 in.) in length and has a square cross-section of 100 x 100 mm (4 x 4 in.). A deformed steel rebar with a diameter of 25 mm (1 in.) was embedded in the center of each block and used to attach the specimen onto the testing machine. The CRP was attached on two opposite sides of the blocks, as per double-lap shear test. The dimensions of double-lap concrete specimen were selected based on the recommendations of JSCE-E 543 (2000), and the specimen is shown in figure 3.1.

3.3.1 Specimen Description and Strengthening Schemes

The bond test matrix, comprising 25 specimens, was selected according to the objective of the chapter, which is to (1) to establish the development length for, CRP-070, and CRP-195, and (2) to measure effects of parameters expected to influence the bond behavior and ultimate load capacity of CRPs. The two panels have a 150 mm (6 in.) overlap, intended to provide continuity between spliced panels. A wide range of bond lengths was tested for each panel in order to accurately establish the development length. This range was chosen based on previous studies performed on CFRP rods (Harik and Peiris 2014). The bond test matrix is presented in table 3.1. According to the above parameters, the test matrix is divided into three major groups of specimens, as follows:

Series I: specimens in this series were prepared to determine the development length for a CRP-070, fabricated with CFRP rods of 2 mm (0.078 in.) diameter, spaced at 6.35 mm (0.25 in.).

Series II: this series was intended to evaluate the effects of varying CRP bond width (or CRP /concrete width ratio) and rod spacing on the bond behavior and ultimate load capacity of CRP-070.

Series III: specimens in this series were prepared to determine the development length for a CRP--195, fabricated with CFRP rods of 4 mm (0.156 in.) diameter, spaced at 9.5 mm (0.375 in.).

The specimen identification is designated by a combination of five components: series number (I, II,), CFRP rod diameter (2 mm or 4 mm), rod spacing (6.35, 9.5 mm), and bond width (in mm), and bond length (also in mm). The A and B letters that appear at the end of occasional codes indicate specimen repetition. Some specimens failed due to concrete cracking outside the bond area; therefore, another specimen with the same bond length was fabricated and tested. However, for specimen I-2-6-50-25, the testing was repeated due to doubts that the first fabricated specimen could have had geometric or loading faults.

3.3.2 Specimen Preparation

3.3.2.1 Concrete Blocks

The concrete blocks, used in this experiment as the inner adherends, were made from mix-ready concrete having a targeted concrete compressive strength of 34.5 MPa (5000 psi). The concrete components, with added water, were mixed for about three minutes. Immediately before being filled with the mixed concrete, the wooden block forms were anointed with a release agent, and the steel rebar was placed and centered in the forms. The concrete was applied in three layers per block and compacted with rounded-end tampering rod, similar to the procedure used in making concrete cylinders for compressive strength tests, following ASTM C31/C31M-09 (2009) standards. The compressive strength of the

cured concrete was confirmed by rebound hammer tests, following ASTM C805-08 (2008) standards. The average rebound hammer compressive strength of concrete was 32 MPa (4650 psi) for 40 rebound measurements obtained from all specimens, each specimen being tested on its four faces.

3.3.2.2 CFRP Rods and CRP's

CFRP rods were used to generate CRP-070 and CRP-195, used in this experiment. The rods were produced by Diversified Structural Composites (2016) and the manufacturer's guaranteed tensile modulus of elasticity is 134 GPa (19,500 ksi) and tensile strength is 2,340 MPa (320 ksi). For double-lap shear tests, small-scale CRP's were fabricated with the number of rods, rod spacing, and panel width defined according to the bond test matrix in table 1. Each panel had a total length consisting of a control length of 213 mm (8.5 in.), including 12.5 mm (0.5 in.) gap between the two concrete blocks, and a variable bond length [figure 3.2 (a)]. On the control length side, the CRP was mounted on a fiberglass backing to keep the rods accurately aligned according to the specified spacing. The fiberglass mesh was not used on the bond length side, as it was assumed that any presence of the backing would cause discontinuity within the tested bond length. Figure 3.2 shows one of the panels used in the bond testing program.

3.3.2.3 Adhesive

The adhesive used to adhere the CRPs to the concrete blocks is Sikadur 30 high modulus (2014). It is a high strength structural epoxy paste with a manufacturer's specified tensile

modulus of elasticity of 4,482 MPa (6.5 x 10⁵ psi) and tensile strength of 24.8 MPa (3,600 psi).

3.3.3 Surface Preparation and CRP Installation

The block faces, on which CRP panels are to be bonded to, were ground using an electric grinder to remove any dust and laitance, and to provide a rough bonding surface profile [figure 3 (a)]. The concrete and CRP faces were then wiped clean with acetone. The two-part epoxy adhesive was then applied onto the concrete surface with a profile to a nominal epoxy thickness of 2 mm (0.078 in.) as shown in figure 3 (b). This process was carried out on both sides of the specimen, as per double-lap shear configuration. The CRP was then placed in position and gently pressed, forcing the epoxy to flow around the rods and fill completely between the rods [figure 3 (c)]. Finally, the panel was covered with more epoxy, [figure 3 (d)], and the specimens were left to cure for at least 10 days.

3.3.4 Test Setup and Instrumentation

A 1335 kN (300 kip) universal load testing machine, with a displacement controlled rate of 1.25 mm/min (0.05 in./min), was used to perform the double-lap shear tests. Figure 4 shows the testing machine being loaded with a typical bond specimen. Each specimen was loaded until failure, which was defined as either one or a combination of the following criteria: (1) debonding of CRP, and (2) concrete block cracking failure. Before application of CRPs onto the concrete blocks, the two blocks comprising the double-lap configuration were placed inside a steel casing, [figure 3.3 (b, c, d)]. The casing was meant to keep the specimen aligned in the longitudinal direction, and minimize twisting or bending moments.

The blocks were allowed to slide freely inside the casing, by lubricating the points of attach between the block and the casing with a WD-40 lubricant, and providing a sufficient clamping space.

The structural behavior of the CRP/concrete bonded interface was examined by using strain gages mounted on the surface of the adhesive, along the center line of the bond's length. Specimens with bond lengths 62.5 mm (2.5 in.) or longer, were instrumented with 3.20 mm (0.125 in.) foil-type electric resistance strain gages. The gages were mounted on the concrete block that contained the bond length. On one side of the bond length, as per double-lap configuration, the entire length was equipped with gages spaced at 25 mm (1 in.) apart, and that side was referred to as the "monitored side". On the other side of the bond length, one gage was placed near the gap between the two blocks on several specimens to evaluate the load transfer and balance between the two sides of double-lap configuration. This side was referred to as the "un-monitored side".

Figure 3.5 shows the strain gage layout for a specimen with a bond length of 150 mm (6 in.). Since the rods are of very small diameters [2 mm (0.08 in.) for CRP-070 and 4 mm (0.16 in.) for CRP-195], it was difficult to mount strain gages on the surface of the rods. The strains were measured at the surface of adhesive above the rods and were assumed to correspond to the ones in the rods unless any debonding or other signs of distress at the rod/adhesive interface were identified.

3.4 Test Results

Table 3.2 summarizes the bond test results for CRP-070 and CRP-195, presenting the values of recorded failure loads and observed modes of failure. The failure mode for four of the specimens was by concrete block failure outside the CRP-concrete bond region (figure 3.6). Since the

failure did not relate to CRP-concrete bonded region, and was caused by either: misalignment of the concrete blocks in longitudinal direction, accidental twisting forces or a combination of the two, these specimens were discarded. Other two specimens failed by rod-peel off from the embedding adhesive, combined with cracks in the adhesive near the gap between the two blocks (figure 3.7).

For the remaining eighteen specimens, nine in Series I for the CRP-070 and nine in Series II for CRP- 195, the mode of failure was a concrete shear-off failure beneath the adhesive layer. A thin concrete layer, having an average thickness of 1 mm to 6 mm was attached to the debonded CRP-adhesive system after failure. Figure 3.8, and figure 3.9 show the failure mode of typical CRP-070 and CRP-195 specimens, respectively. The failure initiated on one side of the specimen. Ideally, the failure should initiate simultaneously on both sides of the specimen, due to the size of the specimen and the setup in the test machine, it is very difficult to insure perfect symmetry during the fabrication and testing process.

3.4.1 Development Length

There has been a general understanding between researchers that there exists a minimum length, necessary to attain a failure within the reinforcement (Miller and Nanni 1999). This length is called the development length (also referred to as effective bond length). Within the development length, most of the force transfer is expected to occur. That means, providing a bond length, larger than the development length, would not result in an increase in bond strength. However, failure of members with short bond lengths is generally brittle and sudden, while members having longer bond lengths tend to fail in a gradual, ductile manner.

Fig. 3.10 presents the failure load, P_f , and the corresponding bond length, l_b , for the specimens in Series I and II (tables 3.1 and 3.2). As the bond length was increased, the failure load increased initially and leveled off for longer bond lengths. A development length, l_d , can be estimated as the distance up to the leveling off point. l_d is estimated to be 100 mm (4 in.) for CRP-070 and 125 mm (5 in.) for CRP-195. The bond strength, estimated as the load at the leveling-off line, for 1-m (0.30 ft.) wide CRP-070 and CRP-195, was determined to be 563 kN/m (38.5 kip/ft), and 712 kN/m (48.8 kip/ft), respectively. Based on the results of current investigation, a simple analytical model, for predicting the failure load (only for concrete shear-off failure) of 1 m (3.28 ft.) wide CRP-070 and CRP-195 bonded to concrete, can be written as follows:

(a) For CRP-070.

$$P_u = 5.63 \times l_b \quad (\text{kN/m}) \quad \text{for } l_b \leq 100 \text{ mm} \quad (3.1a)$$

$$P_u = 9.625 \times l_b \quad (\text{kip/ft}) \quad \text{for } l_b \leq 4 \text{ in.} \quad (3.1b)$$

$$P_u = 563 \quad (\text{kN/m}) \quad \text{for } l_b > 100 \text{ mm} \quad (3.2a)$$

$$P_u = 38.5 \quad (\text{kip/ft}) \quad \text{for } l_b > 4 \text{ in.} \quad (3.2b)$$

(b) For CRP-195.

$$P_u = 5.70 \times l_b \quad (\text{kN/m}) \quad \text{for } l_b \leq 125 \text{ mm} \quad (3.3a)$$

$$P_u = 9.76 \times l_b \quad (\text{kip/ft}) \quad \text{for } l_b \leq 5 \text{ in.} \quad (3.3b)$$

$$P_u = 712 \text{ (kN/m)} \quad \text{for } l_b > 125 \text{ mm (4.75 in.)} \quad (3.4a)$$

$$P_u = 48.8 \text{ (kip/ft)} \quad \text{for } l_b > 5 \text{ in.} \quad (3.4b)$$

Where: P_u = ultimate load of CRP in kN/m (kip/ft), l_b = bond length in mm (in.).

3.4.2 Average Bond Strength

The average bond strength of CRP-070 and CRP-195 can be calculated by dividing the failure load of each test specimen by the bond area. This factor, bond strength, is of great value when establishing a design procedure for the strengthening program, in which the FRP quantity and dimensions can be determined so that debonding failure can be avoided, providing that local bond stresses are lower than the bond strength. The bond strength of FRP/concrete interface is influenced mainly by concrete surface preparation method, concrete strength, and geometry of the FRP reinforcement (Bizindavyi and Neale 1999). The authors also reported that the bond strength observed in experimental tests documented in the literature vary between 2.5-15.32 MPa (0.36-2.22 ksi).

The adhesive average bond stress at failure (or average bond strength), τ_b , is plotted against the bond length, l_b , in figure 3.11 for CRP-070 and CRP-195, and is expressed as follows:

$$\tau_b = \frac{P_f}{2 \cdot l_b \cdot w_f} \quad (3.5)$$

In which, P_f is the load at failure for the double lap shear specimen, and w_f is the width of CRP. The average bond strength of specimens having bond lengths shorter than the established development length, fluctuated between 5-7.5 MPa (0.72-1.01 ksi) for CRP-070 specimens and between 4-7.5 MPa (0.58-1.01 ksi) for CRP-195 specimens. This fluctuation, while being in an accepted range, might be attributed to inevitable geometrical and loading imperfections. More importantly, as can be seen in figure 3.11, and for bond

lengths exceeding the development length, τ_b decreases linearly and will approach zero for large bond lengths. For the current study, adhesive bond strength is deduced from specimens that have a bond length equal to the development length, l_d , and is found to be 5.5 MPa (0.8 ksi) for both CRP-070 and CRP-195.

3.4.3 Load Transfer Mechanism along CRP Bond Length

As mentioned before, specimens with bond lengths larger than development length (l_d) fail in a ductile manner, while specimens with lengths shorter than l_d display a brittle failure. This trend was also seen in the current investigation as will be illustrated in the following paragraphs. The distribution of strain along the CRP bond length at various loads, are presented in figure 3.12 (for a typical CRP-070 bonded specimen) and figure 3.14 (for a typical CRP-195 bonded specimen). For both specimens, the bond length is 150 mm (6 in.). As can be seen from these figures, at low loads, strain gages located close to the gap between the two concrete blocks register large strains, while strain gages located far from the gap, register negligible strains.

Bizindaviyi and Neale 1999 defines the portion of bond length bounded by the gap and the location where the strain reading diminishes as the “transfer length”. When loading increases to values causing the shear stress in the region bounded by the transfer length to exceed the average bond strength, local debonding occurs in that section, and the transfer length moves toward the rest of bond length. If the provided bond length is sufficiently larger than the development length, this shift of transfer length and multiple occurrence of local debonding can take place several times, indicating a ductile failure type.

Figures 3.13 and 3.15 depict the evolution of transfer length over different load levels, for CRP-070 and CRP-195 bonded specimens, respectively. Both specimens are of bond lengths equal to 150 mm (6 in.) which are larger than the determined developments lengths for both panels. Figure 3.13 and figure 3.15 show that there is a shift in the transfer length as the load level increases, indicating the possibility of local debonding. The first local debonding and transfer length shift can be of great importance since it will define the threshold of the debonding process. For CRP-070, the first local debonding, calculated from this experiment, is approximated to occur at a stress level of 33% of rod guaranteed strength. While for CRP-195, the first local debonding is estimated to exist at a stress level of 20% of rod ultimate strength. . Strain variation along bond length and transfer length vs. relative load level results for the rest of tested specimens are given in appendix (A).

3.4.4 Shear Stress Distribution along CRP Bond Length

The adhesive local shear stress (τ_a) at the concrete-adhesive interface along CRP bond length can be calculated from strain gage data and force equilibrium of the panel section bonded to concrete block. The equilibrium considers shear stresses at the concrete-adhesive interface and tensile forces of CFRP rods. However, it neglects the tensile forces contributed by the adhesive, since the adhesive elastic modulus is small when compared to the CFRP rod modulus. Other assumptions used in the analysis are: (1) a uniform shear stress between two known strain gage locations, (2) the strain readings at the adhesive surface are corresponding to CFRP rod strains, and (3) CFRP rod material is linear elastic until failure. The adhesive shear stress of a typical segment bounded by two strain gage locations, x_i and x_{i-1} , is calculated as follows:

$$\tau_a \cdot (x_i - x_{i-1}) \cdot w_f = E_f \cdot A_f \cdot (\varepsilon_{f(x_i)} - \varepsilon_{f(x_{i-1})}) \quad (3.6)$$

or,

$$\tau_a = \frac{\varepsilon_{f(x_i)} - \varepsilon_{f(x_{i-1})}}{x_i - x_{i-1}} \cdot E_f \cdot \frac{A_f}{w_f} \quad (3.7)$$

Where:

x_i, x_{i-1} = locations of strain gages measured from the gap between concrete blocks, mm (in.), E_f = CFRP rod tensile modulus, MPa (psi), $\varepsilon_{f(x_i)}, -\varepsilon_{f(x_{i-1})}$ = measured strains at locations x_i, x_{i-1} , respectively, mm/mm (in./in.), A_f = cross-sectional area of CRP (i.e. area of a single rod multiplied by number of rods), mm² (in²), and w_f = width of CRP, mm (in.).

Proceeding with the above calculations for all strain gages mounted on the bond length, the shear stress distribution along the entire bond length can be deduced, provided that the distance between strain gages is small. Figure 16 shows the distribution of shear stresses at various portions of the bond length as a function of the load level for two specimens, one from CRP-070, and the other from CRP-195. In both specimens, the bond length is 150 mm (6 in.). At each load level, the shear stress calculated from equation 3.7 was determined for each region delimited by the two adjacent gages, and shear stress vs. load level curve was constructed for the entire bond length.

As can be seen from the figures; at low load levels, only regions close to the gap between the two concrete blocks carry large shear stresses, while shear stresses at regions located far from the gap are very small. This trend also indicates the existence of development length/initial transfer length within which force transfer takes place. Furthermore, figure 3.16 shows that when the shear stress at the region with highest stresses reaches a peak

value, the shear stress then tends to decrease, while at the same time, the shear stress in the next region increases. This observed trend are explained by lines 1, 2, and 3. The reduction in shear stress in a region indicates that local debonding is taking place, while the build-up of shear stress in the following region infers that the load transfer mechanism has shifted toward new region. Other researchers have found similar behavior for FRP laminates and fabrics bonded to concrete substrate (Bizindavyi and Neale 1999, Kamel et al. 2003).

3.4.5 Shear Stress- Slip Relation

From strain gage readings, the local shear stress vs. slip (τ - s) model can be obtained, provided that many strain gages are used and positioned at small intervals along the bond length. The τ - s relationship is extremely important when defining analytical models for different joint properties like: development length, bond strength, and ultimate load capacity, since the area under that curve defines the interfacial fracture energy of the bonded joint, G_f . Furthermore, to accurately capture the debonding initiation and progression of bonded concrete-CRP joints in numerical analysis simulations (e.g. finite element), the shear stress vs. slip model becomes highly beneficial.

To accurately define the shear vs. slip model from discrete strain gage data, the bond length has to be long enough to decently capture all the joint slips and to validate the assumption of zero slip at bond length ends. For the current study, the τ - s model for both panels, was obtained from specimens having at least 125 mm (5 in.) long bond lengths. Furthermore, only specimens that failed by debonding at concrete-epoxy interface, and hadn't developed any visible concrete cracks, were used to obtain the model. The slip is

defined as the relative displacement between the reinforcement (CRP in this study) and a parent material (concrete), and is calculated from strain data as follows:

$$\frac{ds(x)}{dx} = \varepsilon_f - \varepsilon_c \quad (3.8)$$

$$\varepsilon_f = \frac{du_f}{dx} \quad \text{and} \quad \varepsilon_c = \frac{du_c}{dx}, \quad (3.9)$$

Where $s(x)$ is the slip in mm (in.) at location x , measured from the gap between the two concrete blocks. u_f and u_c are the displacement of CRP and of concrete, respectively. ε_c is concrete strain, and ε_f is CRP strain (assuming strain in CFRP rods is equivalent to strain at adhesive surface). Concrete strain can be neglected when compared to CRP strain.

Therefore:

$$\frac{ds(x)}{dx} \approx \varepsilon_f \quad (3.10)$$

And,

$$s(x) = s(x=0) + \int_0^x \varepsilon_f \cdot dx \quad (3.11)$$

For discrete strain data, and assuming the slip at the bond length end [$s(x=l_b)$] can be neglected prior to debonding, equation 7 becomes:

$$s(x_i) = \frac{1}{2} \cdot \sum_{j=1}^i \{ \varepsilon_f(x_j) - \varepsilon_f(x_{j-1}) \} \cdot \{ x_j - x_{j-1} \} \quad (3.12)$$

At any load level, slip for the entire bond length [at the gap between concrete blocks, ($x = 0$)], $s(x = 0)$, can be obtained from equation 3.12. Then, $s(x = 0)$ is calculated for all load levels, prior to first local debonding, and combined with shear stress [at $x = 0$, $\tau_a(x = 0)$] to produce, the shear stress vs. slip model. To accurately define the shear vs. slip model from discrete strain gage data, the bond length has to be long enough to decently capture all the joint slips and to validate the assumption of zero slip at $x = l_b$. For the current study, the τ - s models for CRP-070 and CRP-195 were deducted from specimens that have bond lengths of 150 mm (6 in.), and hadn't developed any visible concrete cracks. Figure 3.17 plots the τ - s model for both CRP-070 and CRP-195, at load level corresponding to first local debonding.

3.4.6 Effect of Bond (Panel) Width

The effects that the bond (panel) width, w_f , has on the bond strength and ultimate load capacity of CRP's were studied using the results of double-lap shear specimens bonded to CRP-070. Two specimens from the current study, specimens I-2-6-50-150 and I-2-6-25-150, in addition to a third specimen obtained from a previous study on bond behavior of CRP's, conducted by Harik and Peiris 2014, were used to make the observations. All three specimens had similar properties (e.g. bond length, rod diameter, rod spacing, etc.), with only one varied parameter, w_f . The bond length of all specimens is 150 mm (6 in.), and the rod diameter 2 mm (0.078 in.), while the rod spacing 6.35 mm (0.25 in.). To facilitate proper comparison between specimens with different bond widths (and, in turn, different CFRP areas), each specimen's failure load was divided by the number of rods used in the specimen.

Figure 3.18 plots the failure load per number of rods against the bond width for the three aforementioned specimens. It can be seen the failure load per number of rods was comparable for all three specimens, indicating that bond width had negligible effects on the bond strength of the concrete-CRP joint. Also, the failure mode for all the three specimens was identical, concrete shear-off, suggesting also that bond width did not influence the mode of failure. Furthermore, Figure 3.19 depicts the strain distribution along bond length for the two specimens conducted in the current study, at a load of 17.80 kN (4 kip). The figure shows that the transfer length for both specimens is within similar value, and strains within the transfer length region, for specimen with $w_f=25$ mm (1 in.) are almost double the strains in specimen with $w_f=50$ mm (2 in.).

3.5 Conclusions

This chapter presented 25 double-lap shear experiments to estimate the development length, bond strength, and other properties related to bond between CRP and concrete substrate. CRP is a panel made of small diameter CFRP rods, with spacing, between individual rods, greater than the rod diameter. Each panel is mounted on a fiberglass backing to facilitate handling, and connected with other panels by “finger joint” or “lap-splice” method. Two CRP’s were evaluated in this chapter, namely: CRP-070 (fabricated with 2 mm diameter CFRP rods, spaced at 6.35 mm, and CRP-195 (fabricated with 4 mm diameter CFRP rods, spaced at 9.5 mm). The following conclusions can be drawn: (1) the development length was found to be 100 mm (4 in.) for CRP-070 and 125 mm (5 in.) for CRP-195; (2) the bond strength for 1-m wide panel was estimated to be 563 kN/m (38.5

kip/ft) for CRP-070 and 712 kN/m (48.8 kip/ft) for CRP-195; and (3) the adhesive average bond strength was estimated to be 5.5 MPa (0.85 ksi) for both panels.

While this chapter provided a means to establish the basic characteristics of the bond behavior between two commonly used CRPs and concrete substrate, such as development length, and bond strength, there are other equally important factors need to be investigated. Those factors include the behavior at the finger joint between spliced CRPs, effects of long term effects such as creep, freeze-thaw cycles, UV exposure, temperature, etc.

Table 3.1. (a) Series I of double-lap shear test matrix.

Specimen Identification	Bond length		Specimen Identification	Bond length	
	mm	in.		mm	in.
I-2-6-50-25 A	25.0	1.0	I-2-6-50-75 B	75.0	3.0
I-2-6-50-25 B	25.0	1.0	I-2-6-50-100	100.0	4.0
I-2-6-50-37	37.5	1.5	I-2-6-50-125 A	125.0	5.0
I-2-6-50-50	50.0	2.0	I-2-6-50-125 B	125.0	5.0
I-2-6-50-62	62.5	2.5	I-2-6-50-150	150.0	6.0
I-2-6-50-75 A	75.0	3.0	I-2-6-50-175	175.0	7.0

- Rod diameter = 2 mm (0.078 in.)

- Rod spacing = 6.35 mm (0.25 in.)

- CRP panel (bond) width = 50 mm (2 in.)

- Number of rods = 8

- A_{fp} (CRP area, for one side of double specimen) = 23.7 mm² (0.04 in.²)

Table 3.1. (b) Series II of double-lap shear test matrix.

Specimen code	Rod spacing		Bond width	
	mm	in.	mm	in.
II-2-6-25-150	6.35	0.25	25.0	1.0
II-2-9-37-150	9.50	0.38	37.5	1.5
II-2-12-50-150	12.50	0.50	50.0	2.0

- Bond length 150 mm (6 in.)

- Rod diameter = 2 mm (0.078 in.)

- Number of rods= 4

- A_{frp} (CRP area, for one side of double specimen) = 11.9mm² (0.02 in.²)

Table 3.1. (c) Series III of double -lap shear test matrix.

Specimen code	Bond length		Specimen code	Bond length	
	mm	in.		mm	in.
III-4-9-19-25	25.0	1.0	III-4-9-19-100	100.0	4.0
III-4-9-19-37	37.5	1.5	III-4-9-19-125	125.0	5.0
III-4-9-19-50	50.0	2.0	III-4-9-19-150	150.0	6.0
III-4-9-19-62	62.5	2.5	III-4-9-19-175A	175.0	7.0
III-4-9-19-75	75.0	3.0	III-4-9-19-175B	175.0	7.0

- Rod diameter = 4 mm (0.156 in.)

- Rod spacing = 9.5 mm (0.375 in.)

- CRP panel (bond) width = 19 mm (0.75 in.)

- Number of rods = 2

- A_{fcp} (CRP area, for one side of double specimen) = 23.7 mm² (0.04 in.²)

Table 3.2 (a). Failure loads and modes of failure for Series I and II specimens.

Specimen code	Bond length		Failure load		Failure mode
	mm	in.	kN	kip	
I-2-6-50-25A	25	1	12.703	2.856	Concrete shear-off ^a
I-2-6-50-25B	25	1	12.828	2.884	Concrete shear-off ^a
I-2-6-50-37	37.5	1.5	27.058	6.083	Concrete shear-off ^a
I-2-6-50-50	50	2	34.723	7.806	Concrete shear-off ^a
I-2-6-50-62	62.5	2.5	30.639	6.888	Concrete block failure ^b
I-2-6-50-75A	75	3	30.510	6.859	Concrete block failure ^b
I-2-6-50-75B	75	3	39.776	8.942	Concrete shear-off ^a
I-2-6-50-100	100	4	53.343	11.992	Concrete shear-off ^a
I-2-6-50-125A	125	5	40.367	9.075	Concrete block failure ^b
I-2-6-50-125B	125	5	53.988	12.137	Concrete shear-off ^a
I-2-6-50-150	150	6	63.676	14.315	Concrete shear-off ^a
I-2-6-50-175	175	7	47.164	10.603	Concrete shear-off ^a
II-2-6-25-150	150	6	31.840	7.158	Concrete shear-off ^a
II-2-9-37-150	150	6	47.195	10.561	Rod peel-off
II-2-12-50-150	150	6	49.322	11.088	Rod peel-off

^a Concrete shear-off failure refers to debonding at concrete-epoxy interface through shearing-off concrete, in which, a layer of concrete would be attached to the detached CRP panel.

^b Concrete block failure by cracking outside the bond region. Specimens failed in this manner were disregarded in any calculations related to the bond behavior (e.g. bond strength, development length, shear stress-slip relation).

Note: A_{frp} (area of CRP for one side of the double-lap configuration) is 23.7 mm² (0.04 in²) for specimens in series I and III, and it is 11.9 mm² (0.02 in²) for specimens in series I.

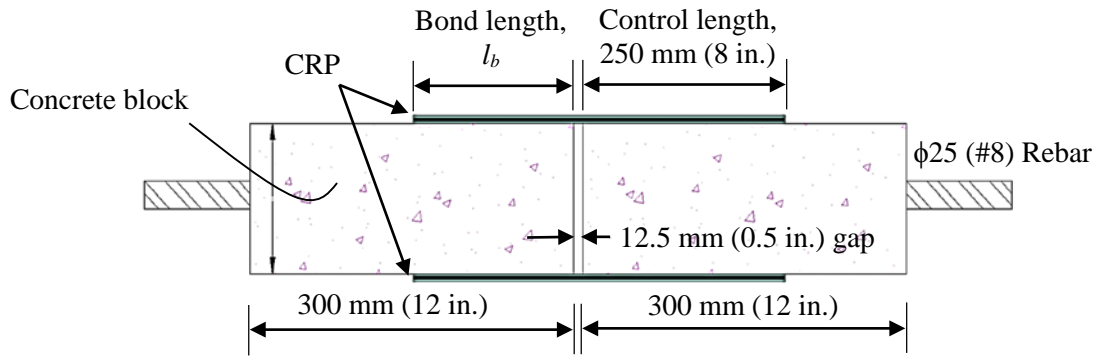
Table 3.2 (b). Failure loads and modes of failure for Series III specimens.

Specimen Identification	Bond length		Failure load		Failure mode
	mm	in.	kN	kip	
III-4-9-19-25	25	1	5.306	1.193	Concrete shear-off ^a
III-4-9-19-37	37.5	1.5	5.711	1.284	Concrete shear-off ^a
III-4-9-19-50	50	2	8.980	2.019	Concrete shear-off ^a
III-4-9-19-62	62.5	2.5	14.158	3.183	Concrete shear-off ^a
III-4-9-19-75	75	3	20.400	4.586	Concrete shear-off ^a
III-4-9-19-100	100	4	21.565	4.848	Concrete shear-off ^a
III-4-9-19-125	125	5	26.089	5.865	Concrete shear-off ^a
III-4-9-19-150	150	6	26.471	5.951	Concrete shear-off ^a
III-4-9-19-175A	175	7	33.246	7.474	Rod/adhesive interface ^b
III-4-9-19-175B	175	7	29.340	6.596	Concrete shear-off ^a

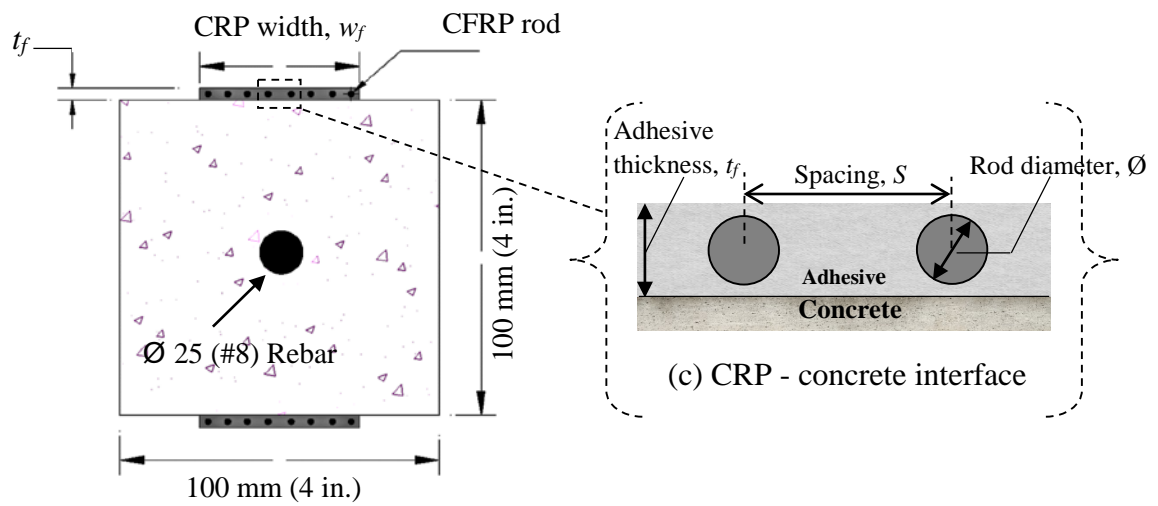
^a Concrete shear-off failure refers to debonding at concrete-epoxy interface through shearing-off concrete, in which, a layer of concrete would be attached to the detached CRP panel.

^b In specimen III-4-9-175A, the rod debonded from the embedding adhesive. After observation of the failed specimen, it was found that the rod was not properly covered in adhesive. This specimen was disregarded from calculations related to bond behavior.

Note: A_{frp} (area of CRP for one side of the double-lap configuration) is 23.7 mm² (0.04 in²) for specimens in series I and III, and it is 11.9 mm² (0.02 in²) for specimens in series I.



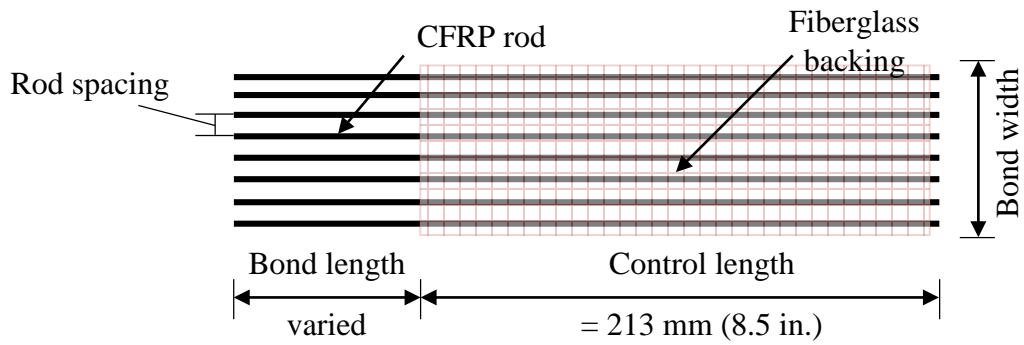
(a) Side view



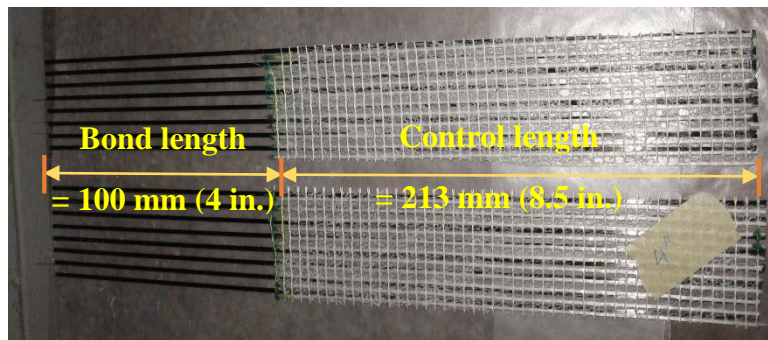
(b) Cross-section

(c) CRP - concrete interface

Figure. 3.1. Double-lap shear specimen.



(a) Small-scale CRP used in the double-lap tests



(b) Small-scale CRP-070, with a bond length of 100 mm (4 in.)

Fig. 3.2 Small-scale CRP's used in the bond testing program.



Fig. 3.3 Double lap test specimen fabrication: (a) concrete surface preparation, (b) adhesive application, (c) CRP placement, (d) application of second layer of adhesive.



Fig. 3.4 Double-lap shear specimen in testing machine.

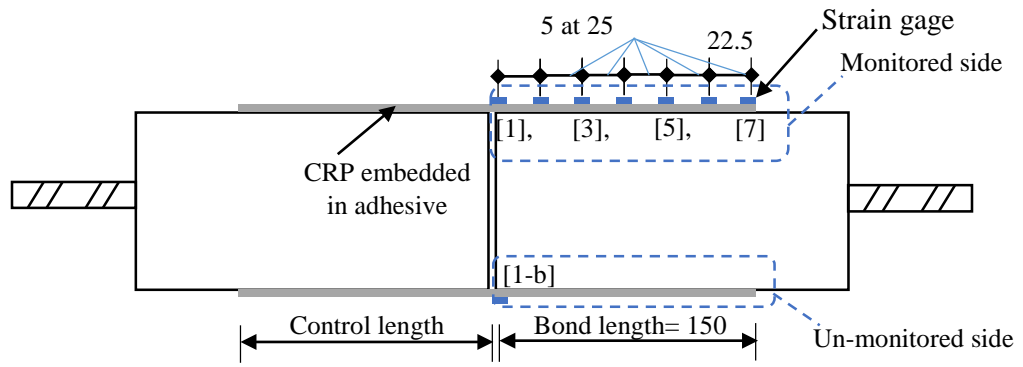
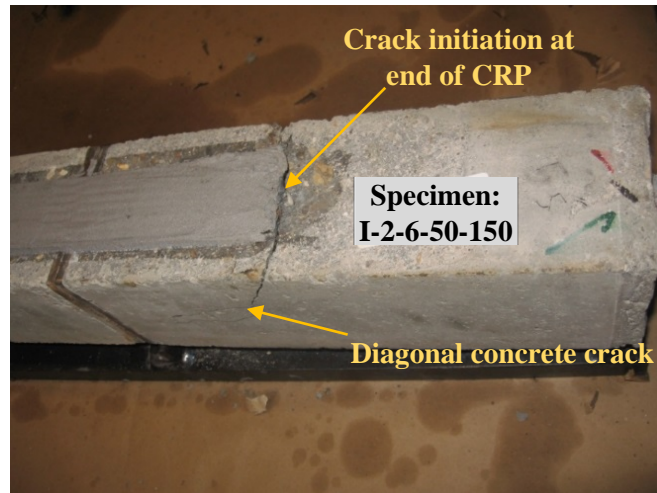
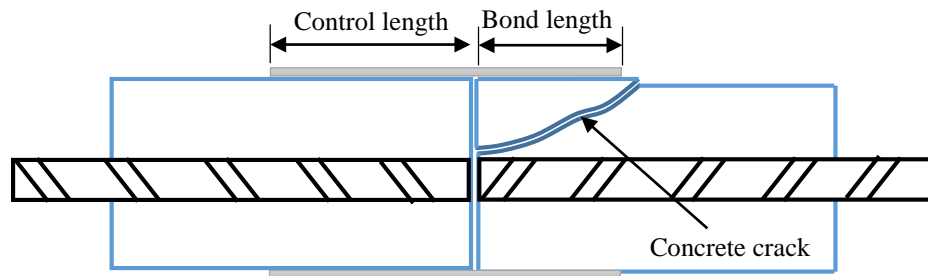


Fig. 3.5 Strain gage layout for a specimen with bond length of 150 mm (6 in.), all dimensions are in mm (25 mm =1 in.).

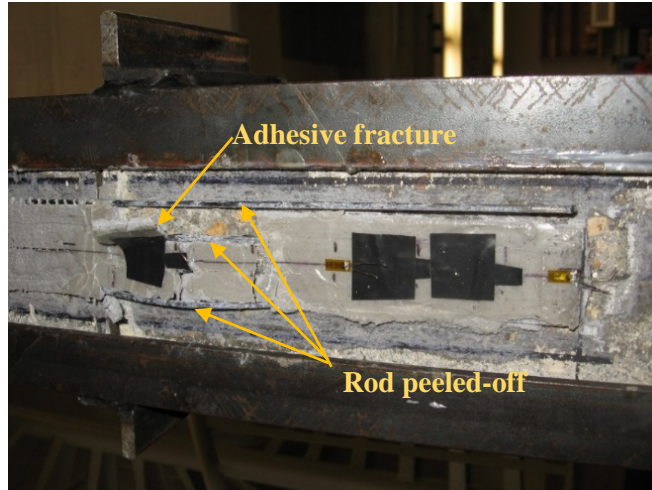


(a) Cracks location in the concrete block failure mode

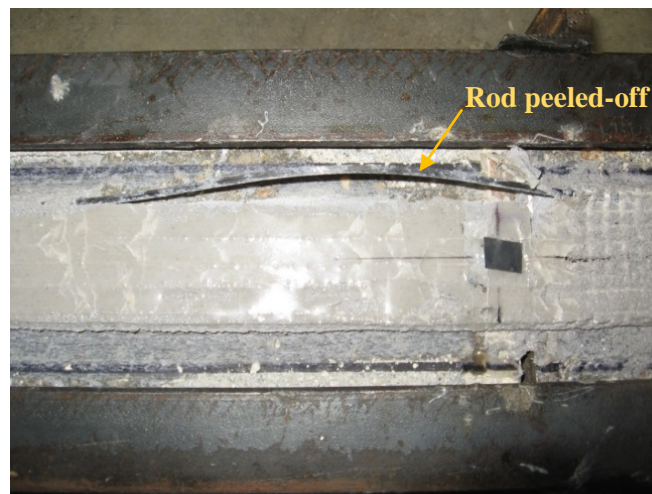


(b) Schematics of the concrete block failure

Fig. 3.6. Concrete block failure mode.

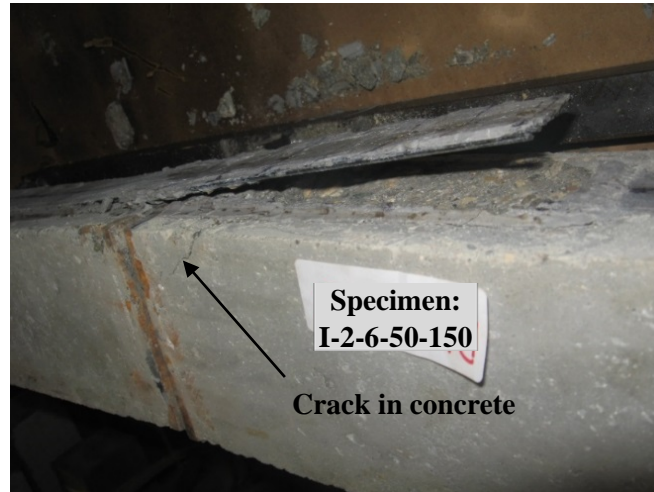


(a) Monitored side, specimen (II-2-9-37-150)

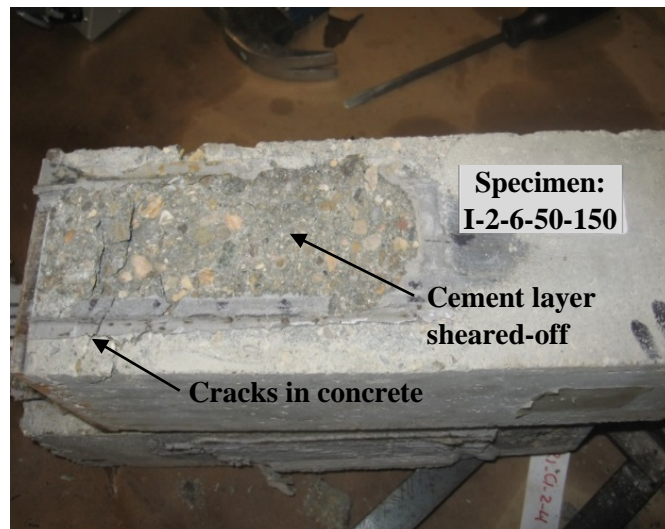


(b) Un-monitored side, specimen (II-2-9-37-150)

Fig. 3.7. Rod peel-off failure mode.

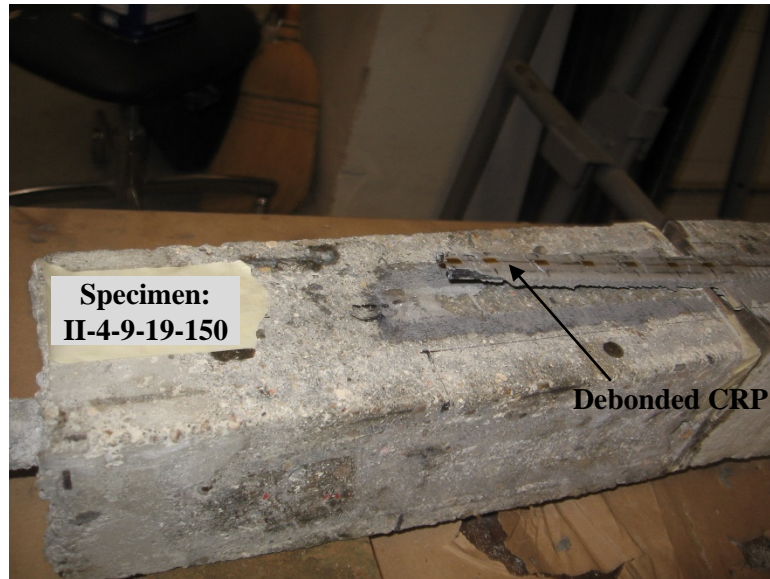


(a) Typical shear-off failure in the double-lap specimens

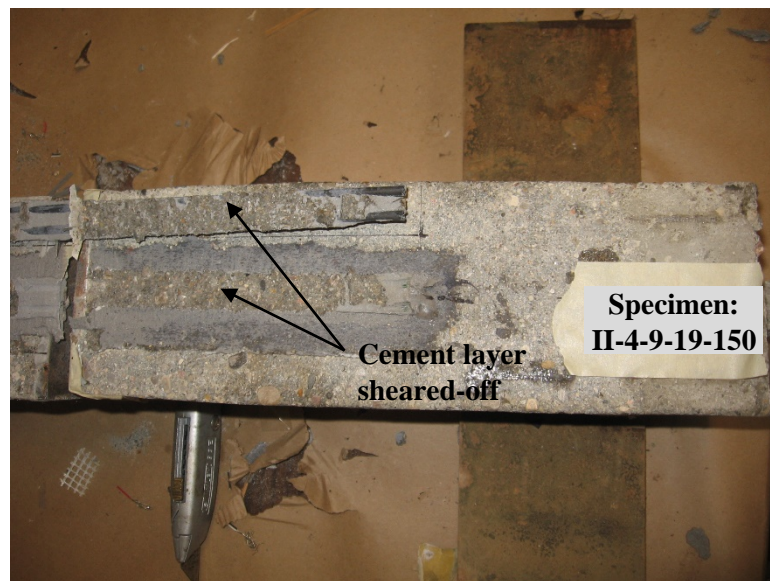


(b) Concrete surface after removing the CRP

Fig. 3.8. Concrete shear-off failure mode of CRP-070 ($l_b=150$ mm).

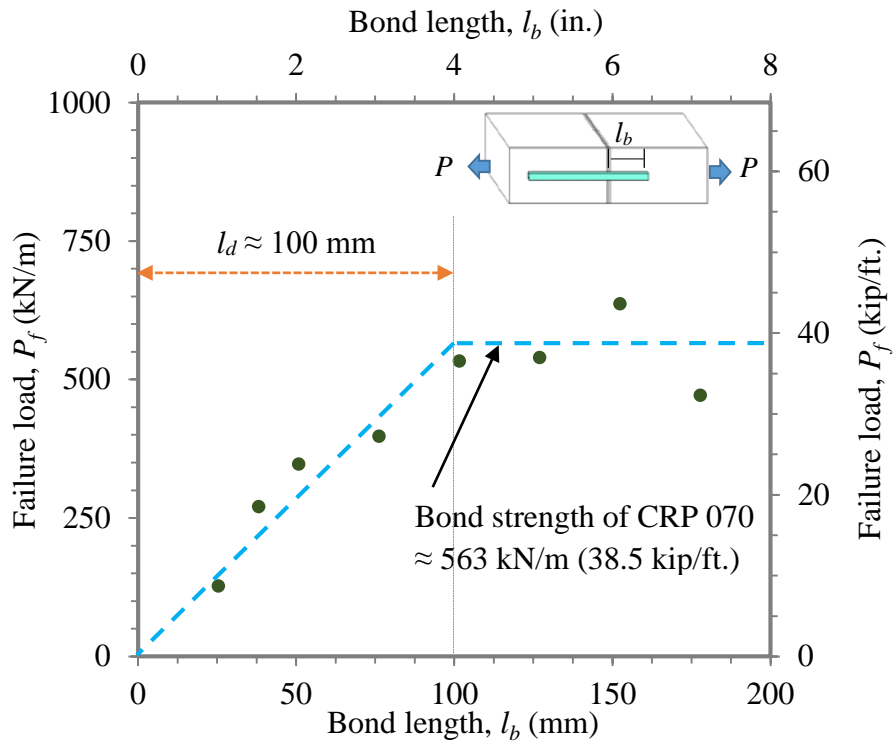


(a) Typical shear-off failure in the double-lap specimens

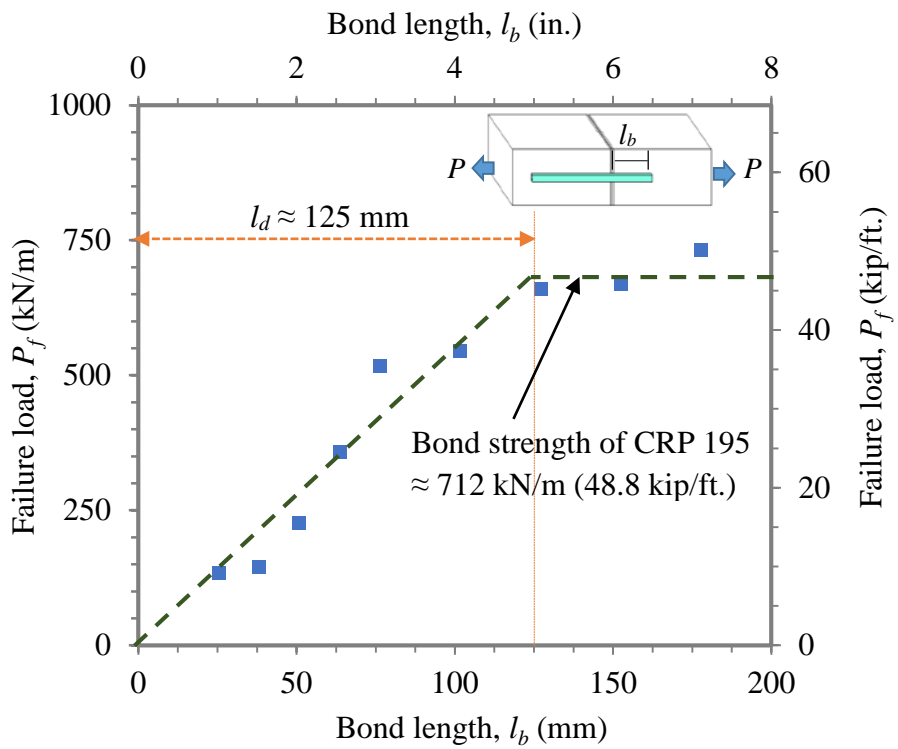


(b) Concrete surface after removing the CRP

Fig. 3.9. Concrete shear-off failure mode of CRP-195 ($l_b=150$ mm).

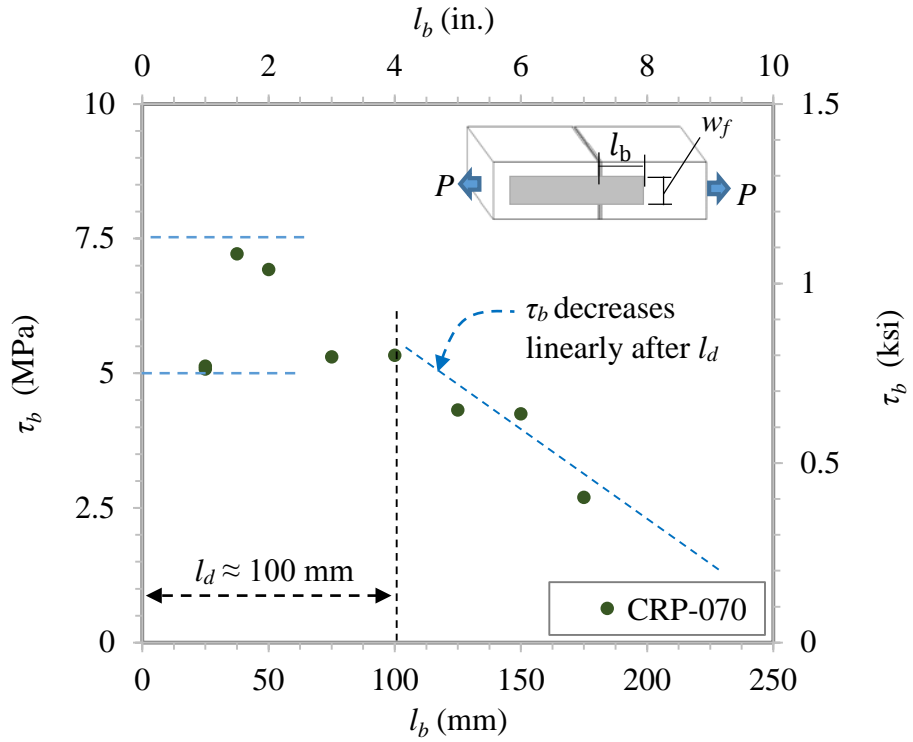


(a) CRP070

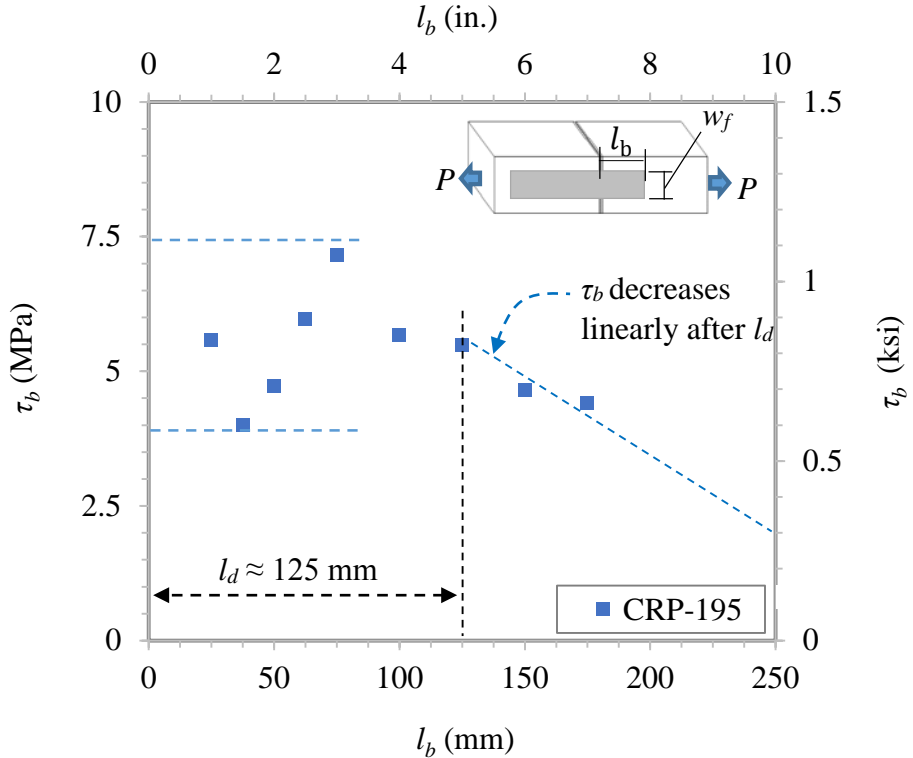


(b) CRP 195

Fig. 3.10. Failure load vs. bond length, l_b .



(a) CRP-070



(b) CRP-195

Fig. 3.11. Adhesive bond strength, τ_b , vs. bond length, l_b , for CRP-070 and CRP-195.

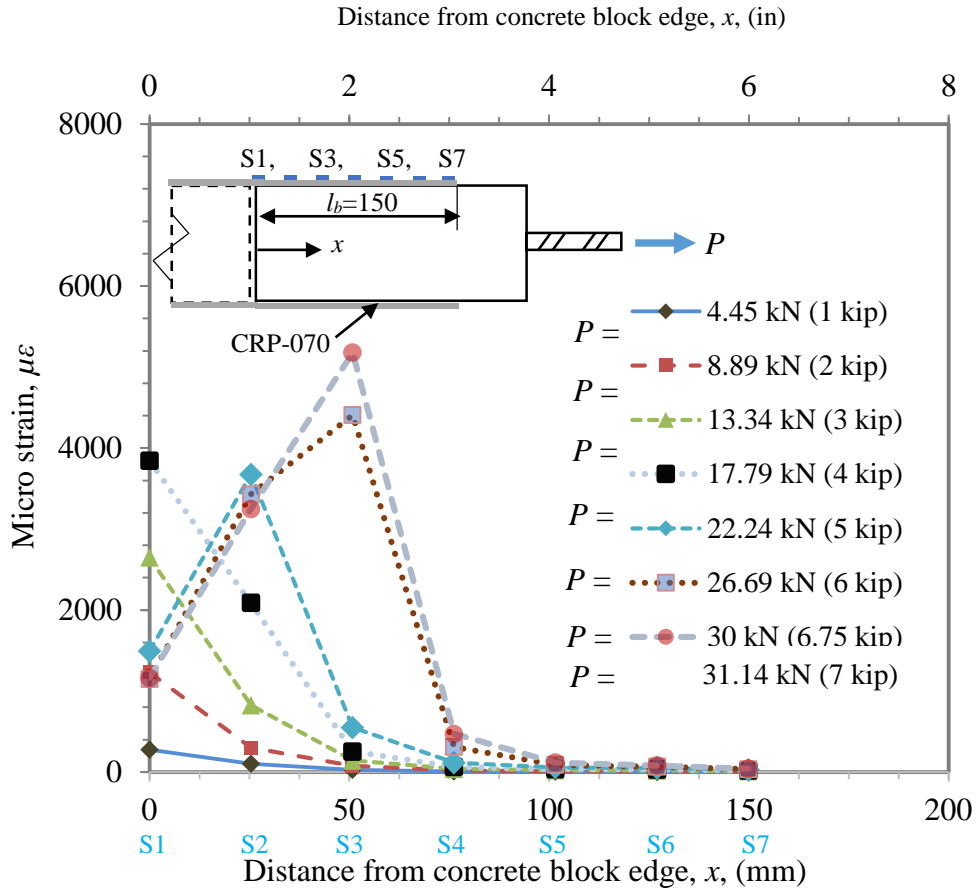


Fig. 3.12 Strain variation along the bond length, for CRP-070 with $l_b = 150$ mm (6 in.) and different load levels, P .

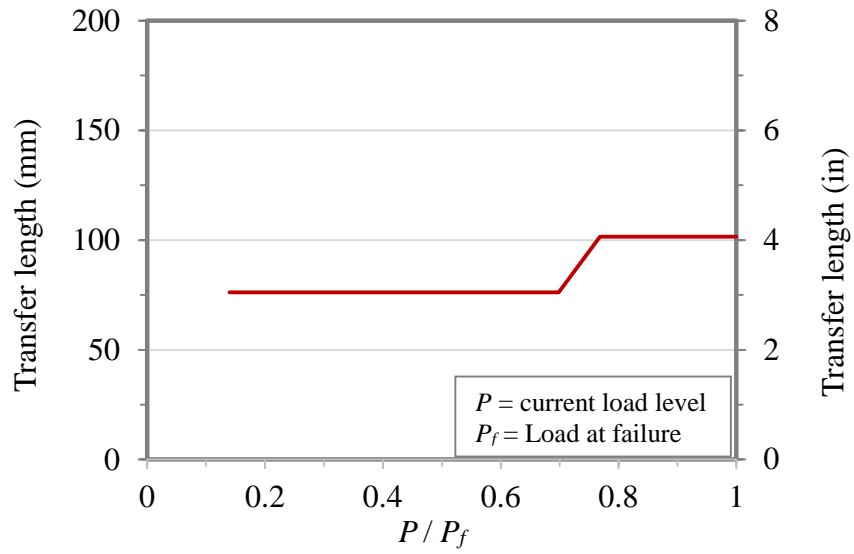


Fig. 3.13 Measured transfer length vs. relative load level, for CRP-070 with $l_b = 150$ mm and different load levels, P , up to failure.

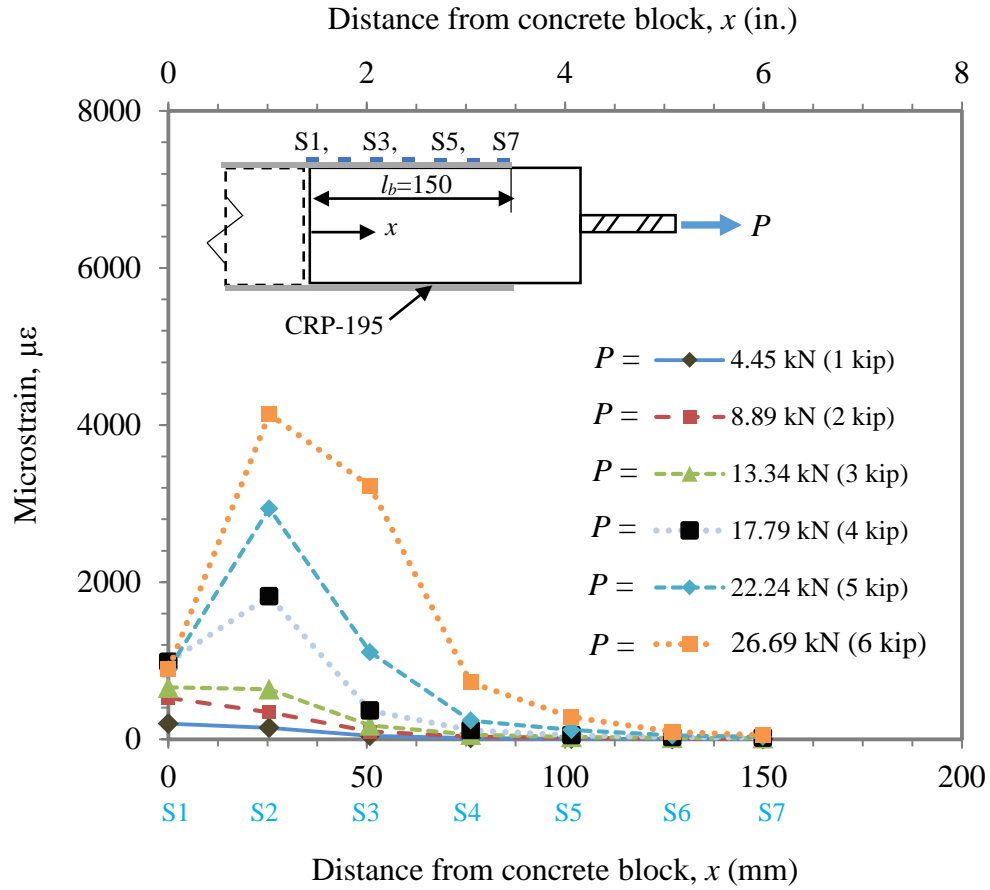


Fig. 3.14 Strain variation along bond length, for CRP-195 with $l_b = 150$ mm (6 in.) and different load levels, P .

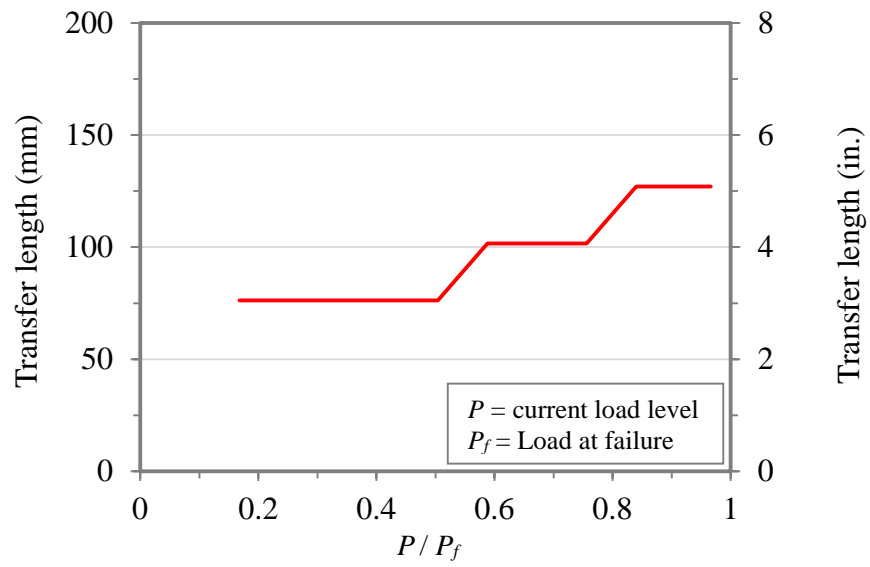
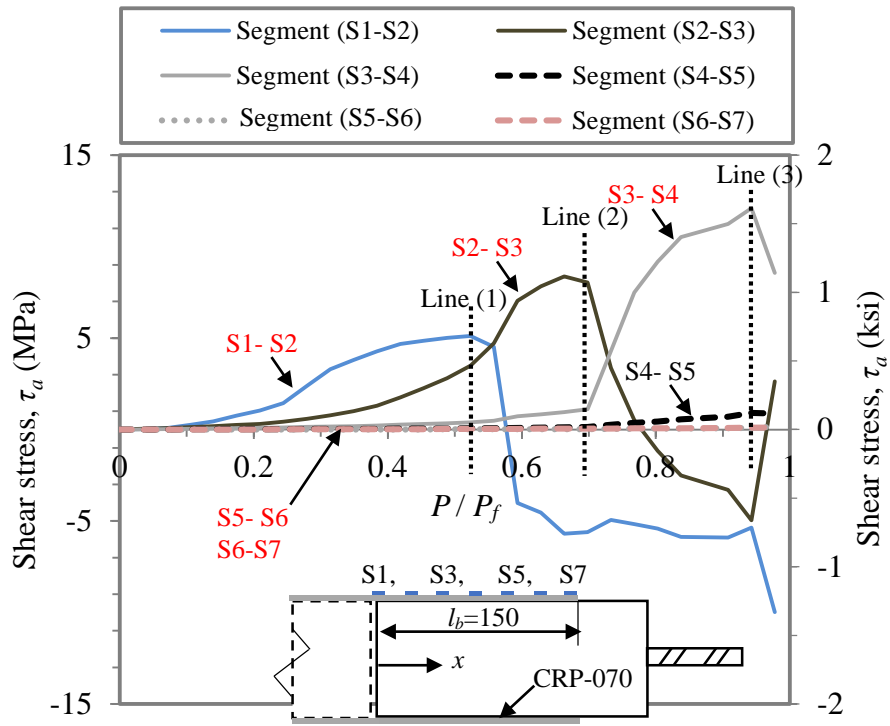
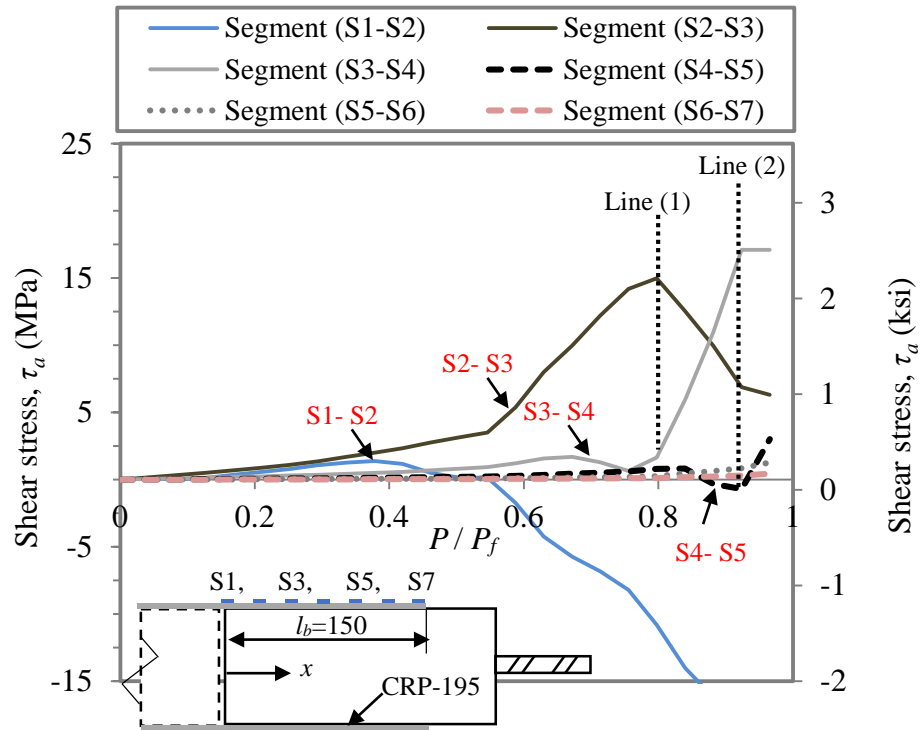


Fig. 3.15 Measured transfer length vs. relative load level, for CRP-070 with $l_b = 150$ mm and different load levels, P , up to failure.



(a) CRP-070, specimen (I-2-6-25-150), (l_b) = 150 mm (6 in.)



(b) CRP-195, specimen (III-4-9-19-150), (l_b) = 150 mm (6 in.)

Fig. 3.16 Shear stress vs. relative load level for CRP-070 and CRP-195.

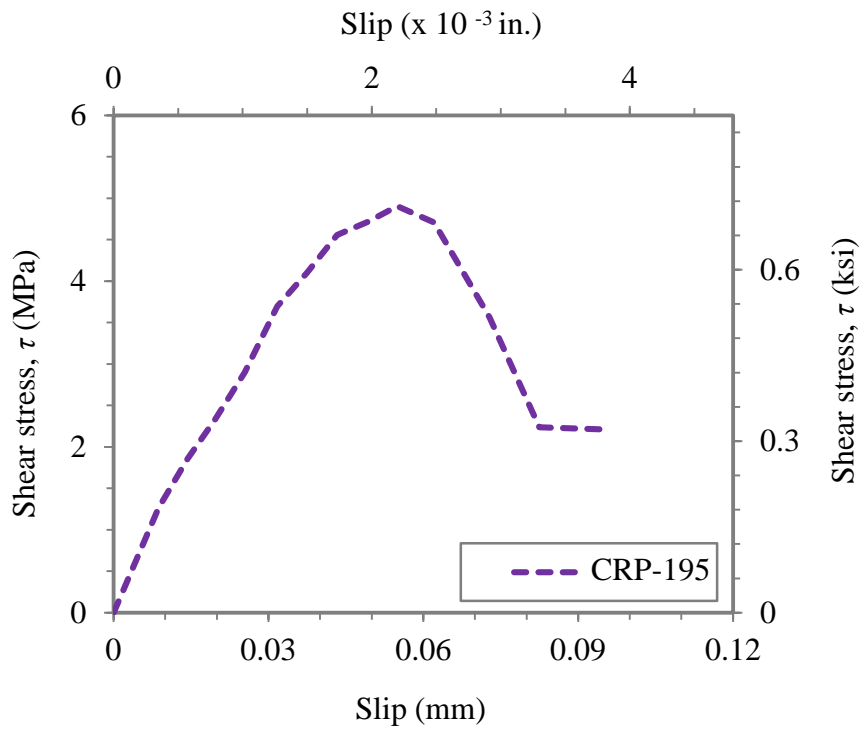
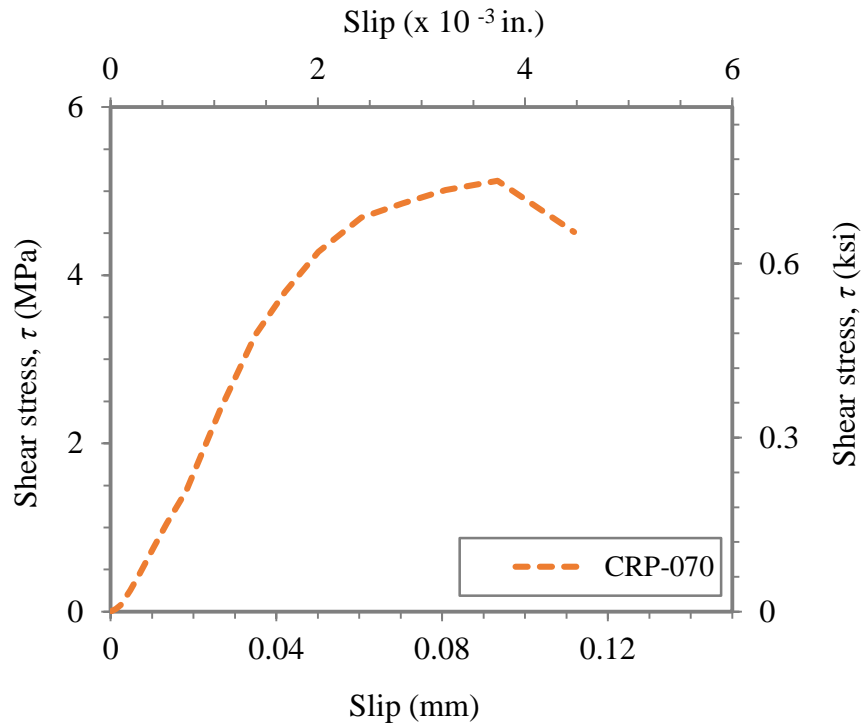


Fig. 3.17 Shear stress vs. slip model for CRP-070 and CRP-195.

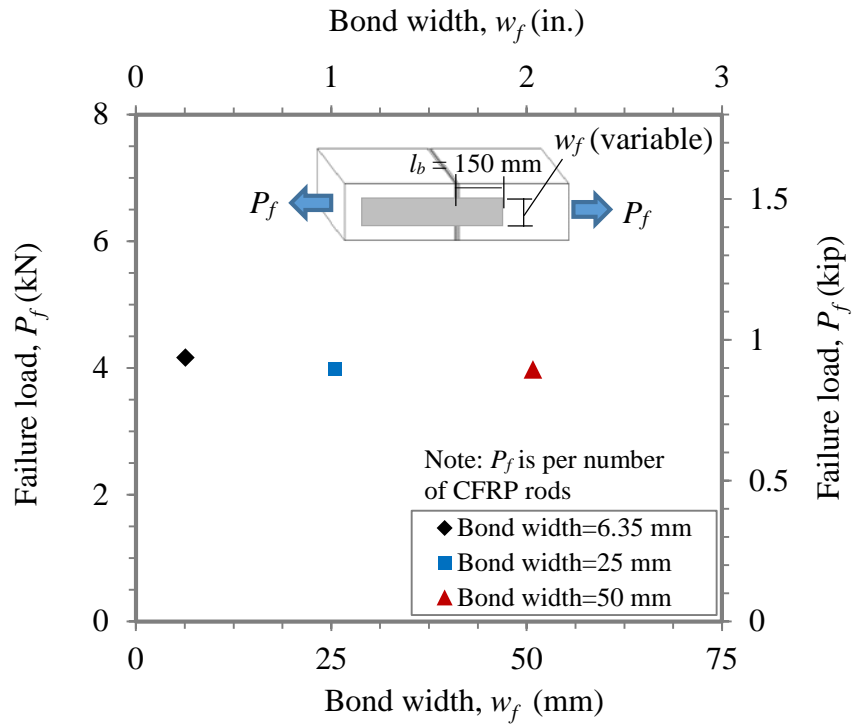


Fig. 3.18 Comparison of failure loads for specimens with different bond widths.

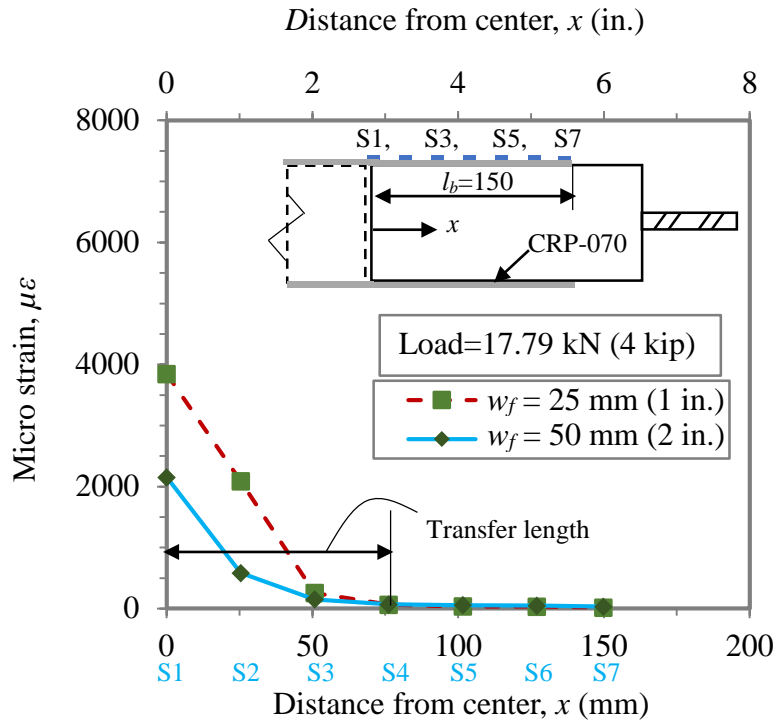


Fig. 3.19 Strain variation along bond length, for specimens (I-2-6-50-150) and (II-2-6-25-150).

CHAPTER 4: FLEXURAL STUDY ON RC BEAMS STRENGTHENED WITH CFRP ROD PANELS AND CFRP LAMINATES

4.1 Synopsis

Recently, carbon FRP (CFRP) rod panels (CRPs) have been developed and deployed to overcome some of the limitations accompanying current methods of repair with CFRP laminates. CRPs are externally bonded to a concrete substrate in a manner similar to other externally bonded reinforcement (EBR). Each panel is 1.2 m (4 ft) long and is made of a number of small diameter rods that are attached to a glass FRP mesh. In the field, the panels are connected through a finger joint to form a continuous EBR.

In this chapter, the effectiveness of using spliced CRP's in strengthening RC beams was evaluated by conducting four-point flexural tests on nine beam specimens. The experimental program consists of: (1) control (or unstrengthened) beam; (2) two beams strengthened with a continuous (full-length) CRP; (3) two beams strengthened with two spliced CRPs; (4) two beams strengthened with two spliced CRPs, and anchored at ends with U-shaped CFRP fabric; (5) one beam strengthened with a continuous CFRP laminate; and (7) one beam strengthened with spliced CFRP laminates. For beams in (2), (3), and (4), one beam was strengthened with CRP-070 (fabricated with rods of $\text{Ø}=2$ mm, spaced at 6.35 mm), while the other beam was strengthened with CRP-195 (fabricated with rods of $\text{Ø}=4$ mm, spaced at 9.5 mm). The CFRP area (A_f) of CRP-070 and CFRP laminate are equal to 64 mm^2 ($100 \times 10^{-3} \text{ in}^2$), while A_f of CRP-195 is 173 mm^2 ($268 \times 10^{-3} \text{ in}^2$). The following sections report the experimental program that was carried out.

4.2 Introduction

In the last few decades, the development of strong bonding agents, in conjunction with a better understanding of the behavior of composite parts, and the development of robust numerical and analytical tools, have guided structural engineers and researchers to find new repair techniques that are cost-effective, and easy-to-install. The plate bonding technique is one of the repair methods. It involves attaching a steel or FRP plate onto the structural substrate (e.g. concrete, steel, masonry, timber, etc.) with the help of a bonding agent, oftentimes, epoxy adhesives. FRP plates (laminates) have become an ideal choice for plate bonding technique due to the excellent attributes of FRP material, such as high strength and stiffness, immunity to corrosion, ease of handling and installation, minimum added weight and minor increase in the member size [Adhikary and Mutsuyoshi (2002), Ahn et al. (2006), De Lorenzis et al. (2010), Guenaneche et al. (2014)].

When strengthening long-span beams with limited access (e.g. bridges over waterways and freeways), labor and equipment demands may hinder the use of continuous EBR FRP. Splicing of FRP laminates is still an uncommon practice. Several laboratory and field studies have investigated the viability of lap-splicing FRP laminates for steel members [Yang and Nanni (2002), Dawood and Rizkalla (2006), Dawood et al (2007)]. Peiris (2011) presented a technique consisting of ultra-high modulus CFRP plate strip panels as an alternative for lap-spliced FRP laminates. Each panel is 1.2 m (4 ft.) long and consists of 5 mm (0.2 in.) or 10 mm (0.4 in.) wide ultra-high modulus CFRP strips. To fulfil the total strengthening length, several panels are brought together and jointed by means of 150 mm (6 in.) overlap “finger joint”. Experimental tests and finite element analysis on small-scale wide flange steel beams have validated the viability of the technique, and results

shown that overlapped panels are better alternative than regular lap-spliced laminates, when comparing ultimate load-capacity of the joint, Peiris (2011).

Several other studies were also performed on concrete members [Tedesco et al (1996), and (1998), Stallings et al (2000)]. Stalling and Porter (2003) performed laboratory tests on large-scale RC beams strengthened with lap-spliced CFRP plates. Splices of 610 mm (24 in.) and 915 mm (36 in.) lengths were investigated. The effects of splice location were explored by attaching (1) one splice at maximum bending moment (mid-span), and (2) two splices at shear span. The study showed that the predominant failure mode is debonding of splice due to high shear stresses at splice ends resulting from the difference in strains between primary plate and splice. The study also included small-scale tension tests consisting of CFRP primary plates connected by splices. Both the beam tests and tension tests indicated that there was a uniform strain at the threshold of debonding. For design purposes, the study devised to limit the strain at the end of splice to 1682 microstrain in order to prevent debonding of the splice. The study also concluded that in order for the splices to be fully functional, and to avoid shear failure in the splice, the average shear stress at the splice end should be kept below 15% of the shear strength of the adhesive. This implies that relatively very long splices are required.

Carbon fiber reinforced polymer (CFRP) rod panels (CRPs) have recently been developed and deployed in the field to provide a substitute for lap-spliced FRP plates, and provide an economical retrofit for concrete and steel bridges. CRPs are made from small diameter CFRP rods that are placed side by side at discrete spacing to form a panel. The rods are then mounted to a fiberglass backing to facilitate the handling of the panel and to keep the rod spacing consistent. Spacing between rods is selected so that rods in the overlap region

can easily be inserted in the field. Neighboring panels are brought together and made continuous by an overlapping “finger joint” method. The overlap length, conservatively selected based on preliminary double-lap shear tests conducted by Harik and Peiris (2014), is 150 mm (6 in.).

Each alternate panel is produced with an extra rod to provide symmetry on both sides of the overlap region. CRPs are externally bonded to the concrete substrate in a manner similar to other externally bonded reinforcement (EBR). The CFRP area of CRPs is the product of the individual rod area by the number of rods provided. Therefore, either varying rod diameter, rod spacing or both can adjust the total area. Nominally, CRPs are usually given the term CRP-X3 (X3=XXX=070, 145, 195, etc.), which indicates that the CRP can resist XXX kips of force per 1-ft wide section. Each panel is 1.2 m (4 ft.) long.

The objective of this chapter is to experimentally investigate the effectiveness of overlapped CRPs for strengthening of RC members. Nine RC beams are tested to quantify the effectiveness of CRP strengthening by comparing the flexural behavior and ultimate load with an un-strengthened beam (or control beam), and with beams bonded to conventional CFRP laminates.

4.3 Experimental Program

4.3.1 Dimensions of RC Beams

The dimensions of RC beams were selected to ensure that the specimens are strong in shear and weak in flexure. The flexural and shear reinforcements were determined following the ACI 318-11 (2011) specifications. Furthermore, the shear reinforcement was doubled at load-points and support. The flexural and shear behavior of CFRP strengthened RC beams was examined for potential shear failure following ACI 318-11 and ACI 440.2R-08 (2008) specifications.

The RC beams are 3000 mm (120 in.) long and have a square cross-section of 150 x 150 mm (6 x 6 in.). The flexural reinforcement consists of two \emptyset -10 mm (0.375 in.) deformed steel rebars located at the beam's tension face. The shear reinforcement consists of \emptyset -3 mm (0.125 in.) steel stirrups located at shear span. The stirrups were spaced at 150 mm (6 in.) for most parts of shear span, while for locations at supports and load-points, the stirrups were spaced at 75 mm (3 in.). Furthermore, to facilitate the attachment and vertical alignment of shear stirrups, two \emptyset -10 mm deformed steel rebars located at the beam's compression face were added, [figure 4.1 (a), and 4.2 (a)].

4.3.2 Specimen Description and Strengthening Schemes

Nine RC beams selected for the experimental program, including: (1) one control (or un-strengthened) beam; (2) one beam strengthened with a continuous (full-length) CRP-070; (3) one beam strengthened with a spliced CRP-070 [two CRP-070 made continuous at mid-span by 150 mm (6 in) overlap]; (4) one beam strengthened with two spliced CRP-070 and anchored at panel's ends with U-shaped CFRP fabrics; (5) one beam strengthened with a

continuous CRP-195; (6) one beam strengthened with two spliced CRP-195 [two CRP-195 made continuous at mid-span by 150 mm (6 in) overlap]; (7) one beam strengthened with two spliced CRP-195 and anchored at panel's ends with U-shaped CFRP fabrics; (8) one beam strengthened with a continuous CFRP laminate; and (9) one beam strengthened with spliced CFRP laminate system. The strengthening length for all CFRP strengthened beams is 2286 mm (90 in.). CFRP laminate and CRP-070 have an equal cross-sectional area (A_f) of 64 mm^2 ($100 \times 10^{-3} \text{ in}^2$), while for CRP-195, A_f is 173 mm^2 ($268 \times 10^{-3} \text{ in}^2$). Both CRP-070 and CRP-195 were set to have a width, w_f , that covers the entire beam's underside. While CRP-070 and CFRP laminate had an equal cross-sectional area to compare the performance of the two strengthening systems, CRP-195 was included in the program to investigate its performance when it's used to strengthen a concrete member.

The control beam was used as a reference specimen to provide comparative data on different characteristics, such as strength, stiffness, ductility, cracks and deflections, for beams strengthened with CRPs as well as CFRP laminates. Specimens in (2), (5), were tested to compare the behavior of spliced CRPs and the effectiveness of the 150 mm (6 in.) overlap in maintaining continuity between spliced panels, with un-spliced (full-length) counterpart panels.

Specimens in (4), (7), were added to measure the effectiveness of CFRP end anchorage in preventing pre-mature failures (e.g. end peeling, concrete cover separation), expected to occur at end locations. The fabric used in this testing was SikaWrap Hex 103C, and its dimensions were designed according to ACI 440.2R-08 (2008) standards. The design yielded one ply, U-shaped fabric, with a thickness of 1 mm (0.04 in.) and width of 300

mm. A second ply was added on top of the first one to further control the failure location. The fabric fibers were oriented perpendicular to the beam's longitudinal axis. Beams in (8), (9) were cast to compare CRP strengthening technique, both un-spliced and spliced panels, with commonly used externally bonded laminates. The spliced laminate system consists of two main laminates, having a length of 1143 mm (45 in.) each, and a splice, having a length of 1220 mm (48 in.). The splice length, 1220 mm (48 in.), was selected based on a study by Stallings and Porter (2003). Table 4.1 provides essential information on the properties of CRP-070 and CRP-195. Table 4.2 lists the test matrix and gives information about strengthening parts, while figures 4.1 and 4.2 show the dimensions of RC beams and strengthening parts.

4.3.3 Materials

High strength concrete was used in the fabrication of the RC beams. For each individual beam, three concrete cylinders [with dimensions of 150 mm (6 in.) for the diameter and 300 mm (12 in.) for the height] were cast and tested on the same day of beam testing. Testing was conducted in accordance with ASTM C31/C31M-09 (2009) standards of making and curing concrete specimens, and ASTM C39/C39M-09 (2009) standards of test method for compressive strength of concrete cylinders. The average compressive strength of all nine specimens is 64.7 MPa (9384 psi). Compressive strengths of individual beam and cylinders, as well as average values, are listed in table 4.2. The concrete modulus, E_c , was determined by attaching strain gages onto several concrete cylinders and plotting the stress-strain curve while the specimens were in compression, following ASTM C469/C469M-10 (2010) standards. The modulus was found to be 4.068×10^4 MPa (5.90×10^6 psi).

Grade 60 steel rebars were used for both the longitudinal (tensile and compressive) and shear reinforcements. The mechanical properties of the steel were verified by performing tensile tests on several specimens, prepared from the actual rebars used in the experimental program, according to ASTM A370-09 (2009) standards.

CFRP rods were used to generate the CRP-070 and CRP-195. The manufacturer's [Diversified Structural Composites (2015)] guaranteed tensile modulus of elasticity is 134 GPa (19,500 ksi) and the tensile strength is 2,340 MPa (320 ksi). CFRP laminates were normal modulus Sika CarboDur S1012 and had a tensile strength of 2800 MPa (406 ksi) and a modulus of elasticity of 160 GPa (23200 ksi), according to the manufacturer's specifications [Sika CarboDur plates, (2011)].

CFRP fabrics were SikaWrap Hex 103C type and had a tensile strength of 960 MPa (139 ksi) and a modulus of elasticity of 73 GPa (10600 ksi) [SikaWrap Hex 103C, (2014)]. Two types of adhesive were used in the experiment: (1) Sikadur 30 (epoxy adhesive), which was used as the adhesive for bonding CRP and CFRP laminates to the beam's bottom face, and (2) Sikadur 300 (impregnating resin), used to impregnate and bond CFRP fabric to the beam's side face and to the bottom of CRP. The material properties for Sikadur 30 are: 24.8 MPa (3.6 ksi) for tensile strength and 4482 MPa (650 ksi) for modulus of elasticity [Sikadur 30 (2014)], and for Sikadur 300: 55 MPa (8 ksi) for tensile strength and 1724 MPa (250 ksi) for modulus of elasticity [Sikadur 300 (2014)].

4.3.4 Surface Preparation and CFRP Installation

Proper bond between concrete substrate and FRP material plays an extraordinary role in executing a successful and effective strengthening or rehabilitation project. An adequate bond allows for strong transfer and distribution of forces between the two adhered

materials, and a sound surface preparation is part of the process to achieve a high-quality retrofit. The beam's tensile face, where the strengthening material will be applied, was ground using an electric grinder to remove any dust, laitance, foreign particles, and to abrade an aggregate rich layer that provides a rough surface profile for CFRP bonding. Prior to the application of the adhesive, both the beam's tensile face and the CFRP surface were wiped clean with acetone.

CRPs were applied onto the beam's tensile face in the following sequence: (1) the concrete face was coated with a uniform layer of approximately 2 mm (0.078 in.) thick SikaDur 30 epoxy adhesive [figure 4.3 (a)]; (2) CRP was placed into position and pressed gently, forcing the epoxy to flow around the rods and fill the gap between the rods [figure. 4. 3 (b, c)]; and (3) an additional coat of adhesive was placed to completely embed CFRP rods [figure 4.3 (d)]. The beams were left to cure, with the first beam test performed 51 days after the placement of CFRP systems (CRP and CFRP laminate).

When CFRP fabric is applied, the above steps are first carried out, followed by the surface preparation in the region where the fabric will be bonded (i.e hand grinding and wiping clean with acetone). The prepared surface was later wetted with SikaDur 300 adhesive using a hand-brush. At the same time, the fabric was saturated with SikaDur 300. Next, the saturated fabric was placed onto the wet concrete and CRP surfaces and smoothed out by hand to prevent formation of folds and wrinkles. Plastic rollers were used to remove any air entrapped under the fabric and further impregnate the fabric with resin [figure 4.4]. A second fabric ply was applied on top of the first one. The beams were left to cure for an additional 21 days after the placement of CFRP fabric.

The CFRP laminates were applied according to the manufacturer's guidelines [Sika CarboDur plates, (2011)]. SikaDur 30 adhesive was applied to the concrete surface with a profile to a nominal epoxy thickness of 1.5 mm (0.06 in.). At the same time, the same adhesive was also applied to the laminate bonding surface with a roof-shaped profile to a nominal thickness of 1.5 mm (0.06 in.). Next, the laminate was placed onto the concrete surface at its designated location and pressed with a plastic roller until the adhesive was forced out on both sides of the laminate. The excessive adhesive was then removed and pressure was applied on the laminate for 24 hours, [figure 4.5]. For the application of the spliced CFRP laminate system, main laminates were firstly applied onto the concrete, according to the above procedure, followed immediately by attaching the splice on the surface of main laminates.

4.3.5 Test Setup and Instrumentation

All nine beams were tested in four-point bending with simple support conditions at the ends. The clear span between supports was 2743 mm (108 in.), while the span between load points was 762 mm (30 in.), as shown in figure 4.6. A hydraulic actuator, with 890 kN (200 kip) load capacity, was used to apply the force. A load cell placed above the actuator head was used to record the load increments. Two cable extension type displacement sensors were attached to the bottom of the beam at mid-span and quarter-span. In addition, at mid-span, two linear variable displacement transducers (LVDTs) were attached to accurately measure the mid-span deflection, observe any twisting or differential deflection, and provide extra safety measurement if the displacement sensors malfunction. A third displacement sensor was attached to the reaction frame to measure any movement

of the reaction frame during loading. A data acquisition system connected to a laptop computer was used to digitally record and collect the test data, load cell readings, displacement sensor readings, and strain-gauge readings. Figure 4.7 shows a beam under testing.

All beams were instrumented with foil type electrical resistance strain gauges. On the concrete surface along the beam depth at mid-span (all beams) and along the length at bottom face (control beam), 50 mm (2 in.) long gages were attached. For CFRP strengthened beams, 3 mm (0.125 in) long gages were used along the length of the CRP or CFRP laminate. It was not possible to attach gages directly on the surface of CFRP rods due to their small diameter. Alternatively, gages were attached to the surface of adhesive. The strain at the surface of adhesive is assumed to correspond to the strain in rods, considering the following conditions: (1) distance from the surface of adhesive to the rod centroid is negligible, (2) no debonding or other signs of distress at the rod/adhesive interface, and (3) no slip between rods and adhesive.

4.4 Results and Discussions

4.4.1 Modes of Failure

The control beam (CB2, table 4.2) failed in the conventional way for under-reinforced concrete members, by yielding of tensile steel reinforcement, followed by crushing of compressive concrete in the mid-span region, figure 4.9. Beams strengthened with full-length and spliced CRP-070 and CRP-195 (CS70, SS70, CS195 and SS195, table 4.2) failed by concrete cover separation (CCS), at one of panel ends. The failure started by formation of a diagonal crack, few millimeters outside the panel's end. At the level of

tensile steel reinforcement, the crack propagated horizontally, resulting in separation of concrete cover from the beam section. In some instances, shear or flexural-shear cracks, near load points, are present, and may be coupled with CCS failure, figure 4.10.

The failure was sudden and the load dropped immediately after the cover separation was visible. Beams strengthened with spliced and anchored CRP-070 and CRP-195 (SSW70, and SSW195, table 4.2) failed by intermediate crack-induced debonding (ICID), figure 4.11. The failure initiated in the vicinity of flexural or flexural-shear crack on the beam's tension side as a result of differential vertical movement at the ends of the crack. At failure of specimens SSW70 and SSW195, the CRP debonded from the concrete substrate, at the concrete adhesive interface, with a thin layer of concrete attached to the adhesive. In SSW70 beam, ICID was also coupled with delamination of the concrete cover at mid-span region, figure 4.11 (a). Additionally, for both SSW70 and SSW195, the CFRP fabric debonded from the beam's side, possibly due to the push-out forces generated from debonding of CRP by ICID.

Beams strengthened with CFRP laminates (CSSC2, and SSSC2, table 4.2) failed by laminate debonding initiated at the end of the laminate. For the beam strengthened with a full-length laminate (CSSC2, table 4.2), the failure initiated at one of the laminate's ends and propagated toward mid-span. Debonding was along laminate/adhesive interface (i.e adhesive remained attached to the concrete soffit), as can be seen in figure. 4.12 (a). The beam strengthened with spliced laminate system (SSSC2, table 4.2), failed by debonding of the splice from the laminate system. Debonding initiated at one end of the splice, and progressed toward the butt-joint between main laminates, figure. 4.12 (b). For both beams,

after debonding of CFRP laminates, loading was continued until failure by concrete crushing, figure. 4.12.

4.4.2 Maximum Loads and Capacity Increase

The recorded maximum loads, defined as the peak load within the load-mid span deflection curve, and failure modes for the nine beams, are presented in table 4.4. The maximum loads at failure for the strengthened beams and the corresponding percentage increase in load capacity relative to the control beam are as follows: 38.98 kN (8.76 k) or 112% increase for the full-length CRP-070; 37.94 kN (8.53 k) or 106% increase for the spliced CRP-070; 47.43 kN (10.66 k) or 158% increase for the spliced/anchored CRP-070; 27.3 kN (6.15 k) or 49% increase for the full-length laminate; and 24.2 kN (5.45 k) or 31.8% increase for the spliced laminate.

The results presented in Table 4.4 and figure 4.13(a) show that, relative to the beams strengthened with CFRP laminates, the beams strengthened with CRPs achieved more than double the capacity increase. This is due to the different modes of failure. The CFRP laminates failed by debonding at laminate or splice ends, while debonding was not observed within CRP-070. This is primarily due the geometrical properties of CRP and CFRP laminate. The CRP is made of several rods at discrete spacing that permit the resin cover the entire surface area of each rod while, for the laminate, the resin covers the bottom face (or ~ 50% of the surface area). In order to provide the same cross sectional area of CFRP, the bond width $w_f = 150$ mm (6 in.) CRP-070 [(figure 4.1 (e))] compared to $w_f = 50$ mm (2 in.) for the laminate [(figure 4.2 (d))]. Experimental and analytical studies have

shown that increasing w_f results in delaying or preventing the end-debonding failure (Chen and Teng 2001, Kamel et al 2004, Obaidat 2010).

The maximum loads and percentage increase in load capacity for beams strengthened with CRP-195 (CS195, SS195, and SSW195, table 4.2), are as follows: 37.42 kN (8.41 k) or 104% increase for the full-length CRP-195; 35.80 kN (8.05 k) or 95% increase for the spliced CRP-195; 54.17 kN (12.18 k) or 195% increase for the spliced and fabric anchored CRP-195. Beams strengthened with full-length or spliced CRP-070 and CRP-195, despite that CFRP area, A_f of CRP-195 is 2.7 times that of CRP-070, failed at similar maximum loads figure 4.13 (b). This is due to the fact that CCS failure was predominant. The failure is primarily affected by the concrete strength. Since the beams were made of one concrete batch, A_f is not expected to increase the maximum load. On the other hand, CFRP end anchorage was very effective in preventing CCS failure and further increasing the load capacity of beams strengthened with spliced CRPs, as can be seen in table 4.4, for SSW70 and SSW195 beams. Since CCS was prevented, SSW195 beam, with $A_f = 173 \text{ mm}^2$ ($268 \times 10^{-3} \text{ in}^2$), has achieved higher load capacity increase than SSW70 beam, with $A_f = 64 \text{ mm}^2$ ($100 \times 10^{-3} \text{ in}^2$), figure 4.13 (b).

The objective of this testing was to investigate the effectiveness of spliced CRPs, and to examine if the proposed 150 mm (6 in.) overlap is sufficient in transferring forces between spliced panels and maintaining composite action throughout loading stages. Notably, specimens strengthened with spliced CRPs behaved in a similar manner when compared to respective full-length CRPs, and both failed at comparable maximum loads and identical failure modes. No signs of debonding or distress were observed at the rod overlap region for all four beams strengthened with spliced CRPs. In contrast, the beam with a CFRP

laminated splice (figure 4.2), in which the splice length was designed following recommendations by Stallings and Porter (2003), failed due to debonding of the splice from the laminate system.

4.4.3 Load Mid-Span Behavior

Table 4.5 lists the cracking, yielding, and maximum loads, and their respective deflections, as observed in the experimental program. Also shown in the table, the percentage increase in cracking, yielding and maximum loads, as compared to the control beam. The ductility, defined by the ratio of the deflection at maximum load divided by the deflection at yielding of tension steel, is also presented in table 4.5. At cracking and yielding stages, both CRP and CFRP laminate strengthened beams showed comparable increase of loads and deflections over the control beam. The ductility for the control beam and beams strengthened with CFRP laminates range between (6.25 and 7.03). Beams bonded to CRP-070 yielded a ductility of 2.91 (for full-length CRP-070), 2.11 (for spliced CRP-070), and 2.65 (for spliced and fabric anchored CRP-070). Ductility of CRP-195 bonded beams was 1.32 (for full-length CRP-195), and 1.31 (for spliced and fabric anchored CRP-070), while ductility of the beam bonded to spliced CRP-195 was not presented, since the specimen failed before reaching yielding load.

Figures 4.14 and 4.15 show the load mid-span deflection response of beams strengthened with CRP-070, CRP-195, and CFRP laminates, respectively. After cracking, all strengthened beams showed an increase in the stiffness when compared with control beam. Figure 4.14 (a) shows that the load deflection response of beams strengthened with spliced CRP-070 (SS70, SSW70, table 4.2) were similar to the beam bonded to full-length CRP-

070 (CS70, table 4.2) prior to yielding stage. Figure 4. 14 (b) shows that the load deflection response of spliced CRP-195 (SS195, SSW195, table 4.2) were identical to the full-length CRP-195 (CS195, table 4.2).

Figure 4.16 presents the load mid-span deflection response for the CRP-070 and CRP-195 strengthened beams, and the control beam. The post-cracking stiffness of CRP-195 beams is larger than that of the CRP-070 beams. This is expected since the CFRP area, A_f , of CRP-195 is larger than of CRP-070 (173 mm^2 vs. 64 mm^2).

Figure 4.17 presents the load mid-span deflection response for the CRP strengthened beams, CFRP Laminate strengthened beam, and the control beam. The response of the strengthened beams is similar prior to debonding of the laminates.

4.4.4 Cracking Patterns

Figure 4.18 presents the visually observed cracking patterns on the beams. To permit crack observations, each specimen was painted white and grids of 25x25 mm (1x1 in.) were drawn at both sides of the beam. During testing, two persons, one on each side of the specimen, were positioned to document the load at which each crack develop and to trace the crack path. The first crack was observed at loads of 8.9 kN (2 kip) for the control beam, 15.7 kN (3.5 kip) for beams strengthened with CRP-070, 23.7 kN (5.3 kip) for beams strengthened with CRP-195, and 13.3 kN (3 kip) for beams strengthened with CFRP laminates.

4.4.5 Strain Profile along Depth, at Mid-Span

Strain distributions along the beam's depth at mid-span were generated using strain data obtained from the three concrete strain gages, S1, S2, and S3 mounted on the beam side at different depths [figure 4.8 (a)]. These distributions were generated at several load levels prior to and after yielding of tension steel. Strain data for the control beam are not presented herein, due to strain gage malfunction.

Strain profiles for beams strengthened with full-length CRP-070, CRP-195 and CFRP laminate, for several load levels [(P/P_{max}) , where P is current load, and P_{max} is maximum load] up to failure, are shown in figure 4.19. For other strengthened beams, similar plots are given in figures B.1 through B.3 (in appendix B). The neutral axis (N.A), defined as the ordinate where strains are zero, is approximately at mid-height for loads below cracking. After cracking, the N.A moves up toward the beam's compressive face. The N.A then approaches a constant value for loads exceeding the load at yielding of tension steel. The measured post-yielding N.A, obtained from figures 4.19, and B.1 to B.4 in Appendix B, is approximately 37.5 mm (1.5 in.) for CRP-070 strengthened beams, 50 mm (2 in.) for CRP-195 strengthened beams, and 40 mm (1.6 in.) for CFRP laminate strengthened beams.

4.4.6 Strain Behavior across the CRP width

In several specimens, strengthened with CRPs, an additional strain gage was placed at mid-span, 38 mm (1.5 in.) from the longitudinal center line, to examine the behavior of CRP in the transverse direction. Figure 4.20 shows the load levels (P/P_{max}) vs. strain curve, for the central gage and side gage, in four CRP strengthened beams. As can be seen in, the load-strain behavior at center of CRP and at 38 mm from center are in good agreement.

4.4.7 Strain and shear stress along the CRP and /CFRP laminate

Tensile strain and shear stress variations along the CFRP reinforcement length were generated from the readings of strain gages mounted on the surface of the strengthening material, for several load levels up to ultimate. For each specimen, the load levels were normalized by dividing the selected load value by the specimen maximum load. Shear stress is the adhesive local shear stress, τ_a , at the concrete-adhesive interface along the CRP or CFRP laminate length, and is calculated by considering the equilibrium of the CFRP reinforcement section bonded to concrete, as follows:

(a) For CRP bonded beams.

$$\tau_a = \frac{\varepsilon_f(x_i) - \varepsilon_f(x_{i-1})}{(x_i - x_{i-1})} \cdot E_f \cdot \frac{A_f}{w_f} \quad (4.1)$$

(b) For CFRP laminate bonded beams.

$$\tau_a = \frac{\varepsilon_f(x_i) - \varepsilon_f(x_{i-1})}{(x_i - x_{i-1})} \cdot E_f \cdot t_f \quad (4.2)$$

Where;

x_i, x_{i-1} are the locations of any two consecutive gages, measured from a reference point, E_f is CFRP tensile modulus, MPa (psi), $\varepsilon_f(x_i), \varepsilon_f(x_{i-1})$ are strains at locations x_i, x_{i-1} respectively, A_f is the cross-sectional area of CRP [figure 4.1], w_f is width of CRP [figure 4.1 (a)], and t_f is thickness of CFRP laminate [figure 4.2].

Figures 4.21 to 4.24 present the, tensile strains and shear stress variations between the support and the beam's mid-span. The results for four of the beams are presented in this chapter and rest are presented appendix B in figures B.4 to B.7. The maximum shear stress, τ_a , for beams bonded to full-length or spliced CRP-070 or CRP-195 [figure 4.20, and

figures B.4 to B.6], is approximately 3 MPa (0.445 ksi) compared to the average adhesive bond stress of 5.50 MPa (0.80 ksi) derived from the double-lap shear tests (section 3.4.3 in chapter 3). It should be noted that none of the full-length or spliced CRP strengthened beams failed by debonding.

As previously mentioned in section 4.4.1, the two beams strengthened with spliced and anchored CRP-070 and CRP-195 failed by interfacial crack induced debonding (ICID), which is known to initiate at flexural or flexural-shear cracks (Teng et al 2003). Figures 4.22, and B.5 in Appendix B, show large tensile strain values near the loading-point, along with maximum shear stress of 5.0 to 7.5 MPa (0.72 to 1.09 ksi) at the same location. This shear stress range exceeds the adhesive average bond stress of 5.50 MPa (0.80 ksi), indicating that debonding may have initiated near load-point and propagated elsewhere. Furthermore, ACI 440.2R-08 (2008) guide for design and construction of externally bonded FRP systems places an upper limit on the FRP strain, to prevent ICID failure [equation 10-2 in ACI 440.2R-08 (2008)]

$$\varepsilon_{fd} = 0.083 \sqrt{\frac{f'_c}{nE_f t_f}} \leq 0.9\varepsilon_{fu} \quad (4.3)$$

Where; ε_{fd} is FRP effective strain (upper limit to prevent ICID failure); f'_c is concrete's compressive strength, MPa; n is number of FRP plies; ε_{fu} is the rupture strain of CFRP rods; and other variables were previously defined in this section. If the properties of the beam [(f'_c) , table 4.4] and CFRP rods [(E_f) , section 4.3.3] are inputted in equation 4.3, while assuming that t_f can be approximated for a virtual FRP plate, having A_f and w_f of CRP, [$t_f = A_f / w_f$], ε_{fd} can be determined for the two beams strengthened with spliced and

anchored CRP-070 and CRP-195. Figure 4.22 (a), shows that for the beam bonded to spliced and anchored CRP-070 (SSW70, table 4.2) the strain at the surface of CRP, near the loading point have exceeded the ACI strain limit, ϵ_{fd} . Figure B.7 (appendix. B) shows similar trend where the strain near loading point of the beam bonded to spliced and anchored CRP-195 (SSW195, table 4.2) is almost equal to ϵ_{fd} .

For the beam bonded to the full-length CFRP laminate, figure 4.23 shows that, at a load level (P/P_{max}) of approximately 0.75 a peak shear stress (debonding stress) of 4.25 MPa (0.62 ksi) was reached at roughly 150 mm (6 in.) from the laminate end. In the subsequent load levels, the shear stress at the above location dropped, and other peak stresses were registered at other locations indicating the initiation and propagation of the debonding process.

For the beam strengthened with spliced CFRP laminate system, figure 4.24 shows the strain and shear stress variations along the length of the laminate system. It should be noted that the strain variations are plotted for half beam, from the end of main laminate to the mid-span section, while shear stress variations are plotted for the splice laminate only, from end of splice to mid-span. Figure 4.24 shows that, approximately, at a load level of 0.375, a peak shear stress (debonding stress) of 2 MPa (0.29 ksi), was registered at splice ends. As the load increased, the shear stress at splice end decreased, while other locations inside the splice, picked up significant increase in shear stress. This indicates that the debonding started at the splice ends and progressed toward the splice center, as was observed in the experiment.

4.5 Conclusions

The primary goal of this chapter was to investigate experimentally the behavior and effectiveness of using overlapped (spliced) CFRP rod panels (CRPs) to rehabilitate or strengthen concrete members in lieu of other FRP strengthening techniques. To study such effects, several variables that examine the applicability and optimum use of overlapped CRPs were investigated. First, the behavior of the proposed 150 mm (6 in.) overlap length and its effectiveness in providing continuity for the overlapped CRPs, and in turn, their behavior in comparison to full length panels was studied.

The flexural testing was completed by performing static, four-point bending tests on small scale RC beams that were strengthened in tension with CRPs or CFRP laminates. Six specimens were strengthened in tension with CRPs, using both spliced and un-spliced panels, as well as spliced panels that had CFRP fabrics on their ends. To measure quantitatively the effectiveness of the suggested CRP system, three other specimens were fabricated and tested:--one control specimen that was an un-strengthened RC beam, and two beams strengthened with spliced and full-length CFRP laminates.

Testing concluded the following: (1) the proposed 150 mm (6 in.) overlap seems to be sufficient in transferring forces between spliced panels and maintaining composite action throughout loading stages. Notably, specimens strengthened with spliced CRPs or full-length CRPs, both failed at comparable maximum loads and identical failure modes. No signs of debonding or distress were seen at the rod overlap region in all of the four beams strengthened with spliced CRPs. In contrast, spliced CFRP laminates debonded from the laminate system. (2) Comparing CRPs to CFRP laminates, both full-length and spliced counterparts, it was found that CRPs achieved larger capacity increase. This is due to the

different type of failure experienced in the CRP technique. CFRP laminates failed prematurely by debonding at laminate or splice ends, while debonding was not observed with CRP-070.

(3) Beams strengthened with full-length or spliced CRP-070 and CRP-195, failed at similar maximum loads; despite that the CFRP area, A_f , of CRP-195 is 2.7 times that of CRP-070. A_f was not effective in enhancing the flexural capacity due to the nature of failure in full-length or spliced CRP strengthened beams. Since the failure mode is initiated at concrete cover (concrete cover separation, CCS). (4) Beams strengthened with spliced and anchored CRPs failed by intermediate crack-induced debonding (ICID). (5) CFRP end anchorage was very effective in preventing CCS failure and further increasing the load capacity of beams strengthened with spliced CRPs.

Table 4.1. CRPs used in the experimental program.

Panel	Rod diameter		Rod spacing		Rods per 1-ft wide panel	Strength of 1-ft wide panel ^{(a), (b)}	
	mm	in.	mm	in.		kN	kip
CRP-070	2.00	0.08	6.35	0.25	48	326.66	73.44
CRP-195	4.00	0.16	9.50	0.38	32	871.10	195.84

^(a)The guaranteed tensile stress of CFRP rods is 2.34 GPa (320 ksi), Diversified Structural composites (2015).

^(b)The strength of 1-ft wide CRP is calculated by multiplying the strength of one rod by number of rods per 1-ft panel. Strength of individual rods, determined from the rod's guaranteed strength and rod area, is 6.8 kN (1.53 kip) for 2 mm (0.078 in.) diameter rods, and 27.2 kN (6.12 kip) for 4 mm (0.156 in.) diameter rods.

Table 4.2. Beam test matrix.

Beam specimen	CFRP strengthening scheme	Area of CFRP	
		mm²	x 10⁻³ in²
CB2	Control beam	NA	NA
CS70	One full length CRP-070.	64	100
SS70	Two spliced CRP-070.	64	100
SSW70	Two spliced CRP-070, anchored with CFRP fabric at the beam ends.	64	100
CSSC2	One full length CFRP laminate.	64	100
SSSC2	Spliced CFRP laminate system.	64	100
CS195	One full length CRP-195.	173	268
SS195	Two spliced CRP-195.	173	268
SSW195	two spliced CRP-195, anchored with CFRP fabric at the beam ends.	173	268

Table 4.3. Concrete cylinder compressive strength [150 mm x 300 mm (6 in. x 12 in.) cylinders].

Beam specimen	Cylinder compressive strength		Avg. compressive Strength	
	MPa	psi	MPa	psi
CB2	68.44	9927	68.83	9983
	68.80	9980		
	69.25	10044		
CS70	69.44	10072	68.02	9866
	68.69	9963		
	65.93	9563		
SS70	68.79	9977	64.41	9342
	65.30	9471		
	59.15	8580		
CSSC2	65.74	9535	66.89	9702
	66.93	9708		
	68.00	9864		
SSSC2	68.85	9987	67.67	9816
	66.10	9588		
	68.07	9874		
SSW70	65.25	9464	66.43	9636
	64.03	9287		
	67.96	9857		
CS195	59.06	8566	58.30	8456
	58.59	8498		
	57.25	8304		
SS195	55.06	7986	59.50	8630
	60.96	8842		
	62.49	9064		
SSW195	63.74	9245	62.23	9026
	65.93	9563		
	57.03	8272		

Table 4.4. Maximum load and mode of failure for beams in table 4.2.

Beam specimen	Max. load		Failure mode
	kN	kip	
CB2	18.38	4.13	Yielding of tension followed by crushing of concrete
CS70	38.98	8.76	Concrete cover separation (CCS)
SS70	37.94	8.53	Concrete cover separation (CCS)
SSW70	47.43	10.66	Intermediate crack-induced interfacial debonding (ICID)
CSSC2	27.34	6.15	Laminate end debonding
SSSC2	24.23	5.45	Splice debonding from main laminates
CS195	37.42	8.41	Concrete cover separation (CCS)
SS195	35.80	8.05	Concrete cover separation (CCS)
SSW195	54.17	12.18	Intermediate crack-induced debonding (ICID)

Table. 4.5 (a) Load and deflection at cracking, yielding of steel, and at maximum, and ductility [SI units].

Beam specimen	P_{cr} (kN)	% increase ⁽¹⁾	Δ_{cr} (mm)	P_y (kN)	% increase ⁽²⁾	Δ_y (mm)	P_{max} (kN)	% increase ⁽³⁾	Δ_{max} (mm)	Ductility ⁽⁴⁾
CB2	5.20	NA	1.67	13.49	NA	18.45	18.38	NA	129.80	7.03
CS70	7.93	52.50	2.85	20.75	53.8	19.77	38.98	112.0	57.62	2.91
SS70	7.45	43.3	2.07	24.68	82.9	22.12	37.94	106.4	46.67	2.11
SSW70	7.50	44.2	2.60	28.01	107.6	26.94	47.43	158.0	71.53	2.65
CSSC2	6.97	34.0	2.68	18.45	36.8	15.97	27.34	48.7	99.85	6.25
SSSC2	8.0	53.8	2.08	19.5	44.4	13.98	24.23	31.8	90.05	6.44
CS195	7.41	42.5	2.37	30.23	124.1	18.66	37.42	103.6	24.68	1.32
SS195	7.19	38.2	2.35	— ⁽⁵⁾	— ⁽⁵⁾	— ⁽⁵⁾	35.79	94.7	23.90	— ⁽⁵⁾
SSW195	7.92	52.3	2.60	45.50	237.2	30.30	54.17	194.7	39.78	1.31

(1) = $\frac{P_{cr}-P_{cr}(CB2)}{P_{cr}(CB2)}$ %, (2) = $\frac{P_y-P_y(CB2)}{P_y(CB2)}$ %, (3) = $\frac{P_{max}-P_{max}(CB2)}{P_{max}(CB2)}$ %, (4) = $\frac{\Delta_{max}}{\Delta_y}$ %, (5) = yielding was not observed for beam (SS195)

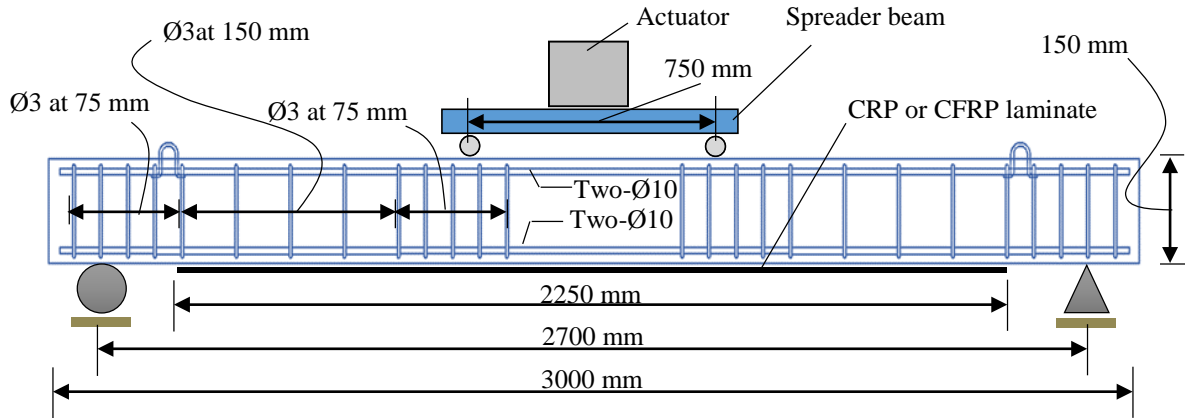
Where: P_{cr} is the load at cracking, P_y is the load at yielding of tension steel, and P_{max} is the maximum load. Δ_{cr} is the deflection at cracking, Δ_y is the deflection at yielding of tension steel, and Δ_{max} is the deflection at maximum load.

Table. 4.5 (b) Load and deflection at cracking, yielding of steel, and at maximum, and ductility [US units].

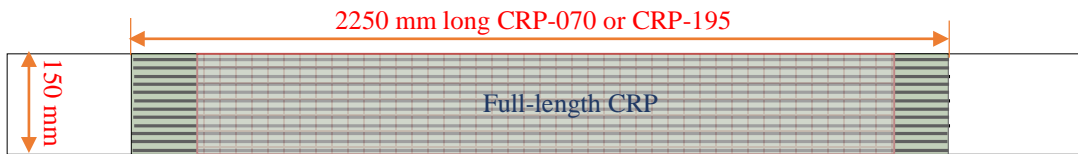
Beam specimen	P_{cr} (kN)	% increase ⁽¹⁾	Δ_{cr} (mm)	P_y (kN)	% increase ⁽²⁾	Δ_y (mm)	P_{max} (kN)	% increase ⁽³⁾	Δ_{max} (mm)	Ductility ⁽⁴⁾
CB2	1.17	NA	0.07	3.03	NA	0.73	4.13	NA	5.11	7.03
CS70	1.78	52.5	0.11	4.66	53.8	0.78	8.76	112.0	2.27	2.91
SS70	1.67	43.3	0.08	5.55	82.9	0.87	8.53	106.4	1.84	2.11
SSW70	1.69	44.2	0.10	6.30	107.6	1.06	10.66	158.0	2.82	2.65
CSSC2	1.57	34.0	0.10	4.15	36.8	0.63	6.15	48.7	3.93	6.25
SSSC2	1.80	53.8	0.08	4.38	44.4	0.55	5.45	31.8	3.54	6.44
CS195	1.67	42.5	0.09	6.80	124.1	0.73	8.41	103.6	0.97	1.32
SS195	1.62	38.2	0.09	— ⁽⁵⁾	— ⁽⁵⁾	— ⁽⁵⁾	8.05	94.7	0.94	— ⁽⁵⁾
SSW195	1.78	52.3	0.10	10.23	237.2	1.19	12.18	194.7	1.57	1.31

⁽¹⁾ = $\frac{P_{cr} - P_{cr}(CB2)}{P_{cr}(CB2)}$ %, ⁽²⁾ = $\frac{P_y - P_y(CB2)}{P_y(CB2)}$ %, ⁽³⁾ = $\frac{P_{max} - P_{max}(CB2)}{P_{max}(CB2)}$ %, ⁽⁴⁾ = $\frac{\Delta_{max}}{\Delta_y}$ %, ⁽⁵⁾ = No yielding could be observed for beam (SS195)

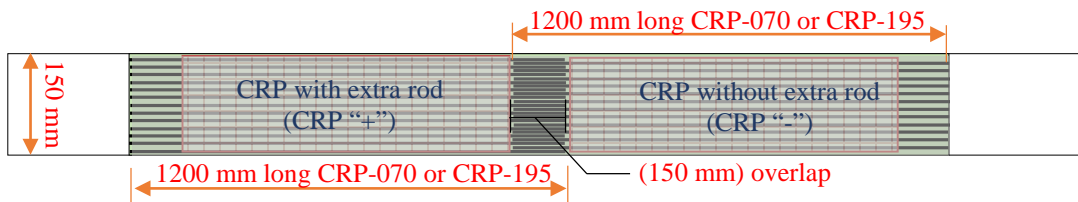
Where: P_{cr} is cracking load, P_y is yielding load, and P_{max} is maximum load. Δ_{cr} is cracking deflection, Δ_y is yielding deflection, and Δ_{max} is deflection at maximum load.



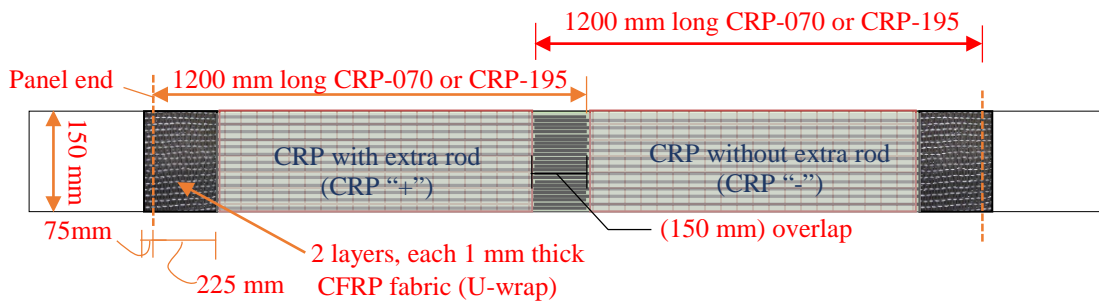
(a) RC beam details



(b) Bottom face of RC beam strengthened with full-length CRP (CRP-070, CRP-195)



(c) Bottom face of RC beam strengthened with spliced CRP (CRP-070, CRP-195)



(d) Bottom face of RC beam strengthened with spliced CRP (CRP-070, CRP-195) and anchored at panel's ends with CFRP fabrics

Fig. 4.1 Geometry of RC beams and CRP strengthening.

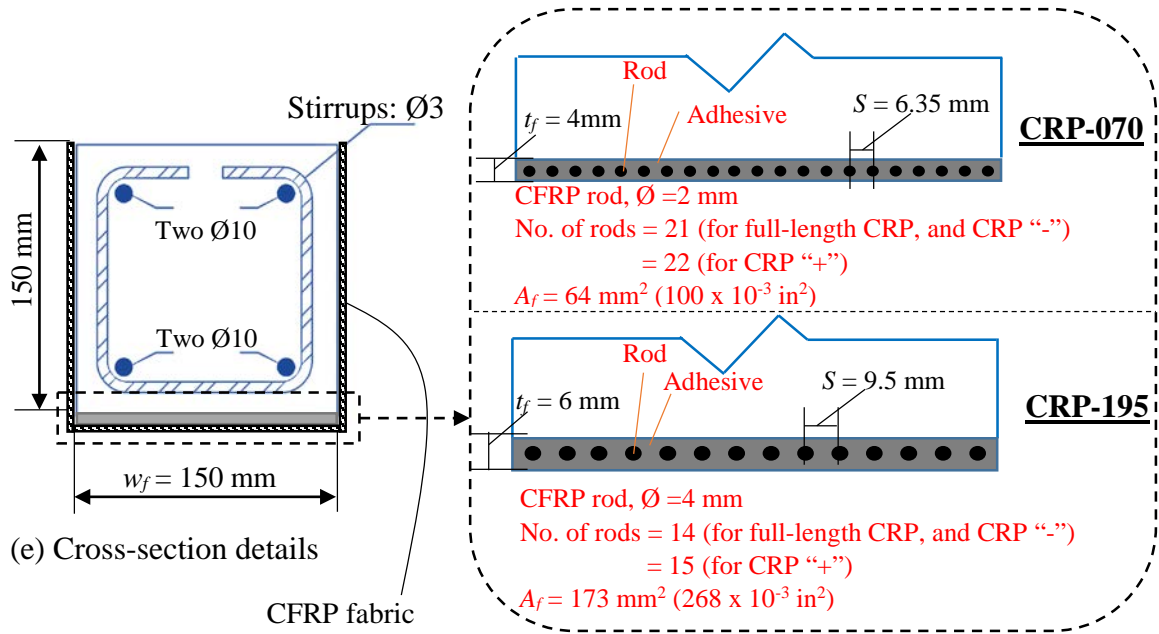


Fig. 4.1 (continued) Geometry of RC beams and CRP strengthening.

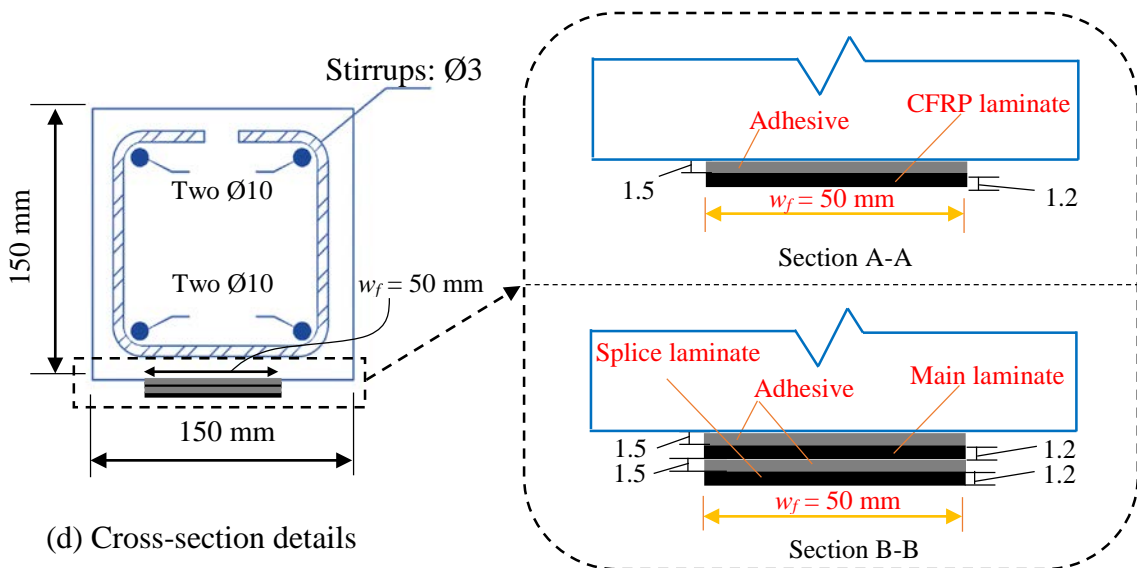
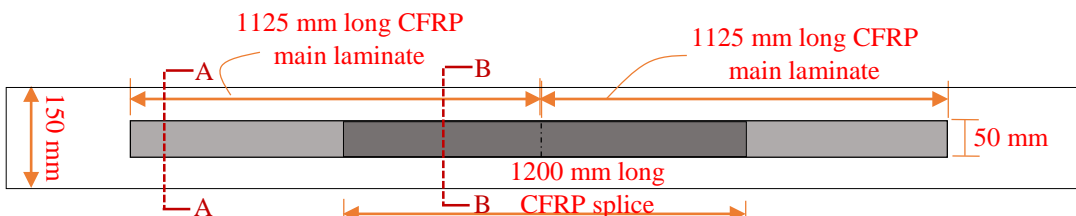
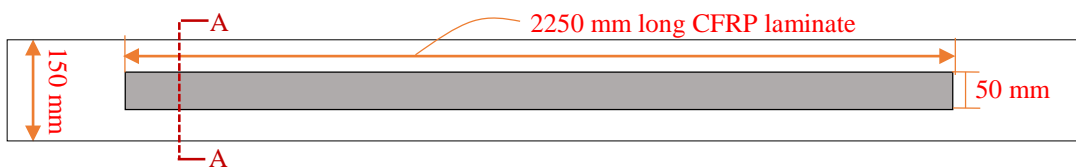
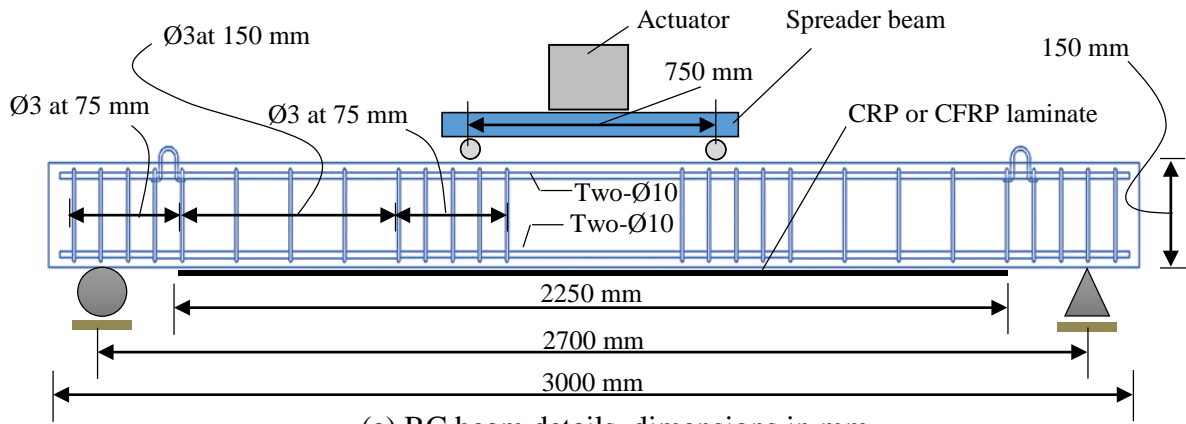


Fig. 4.2 Geometry of RC beams and CFRP laminate strengthening layout (dimensions in mm).

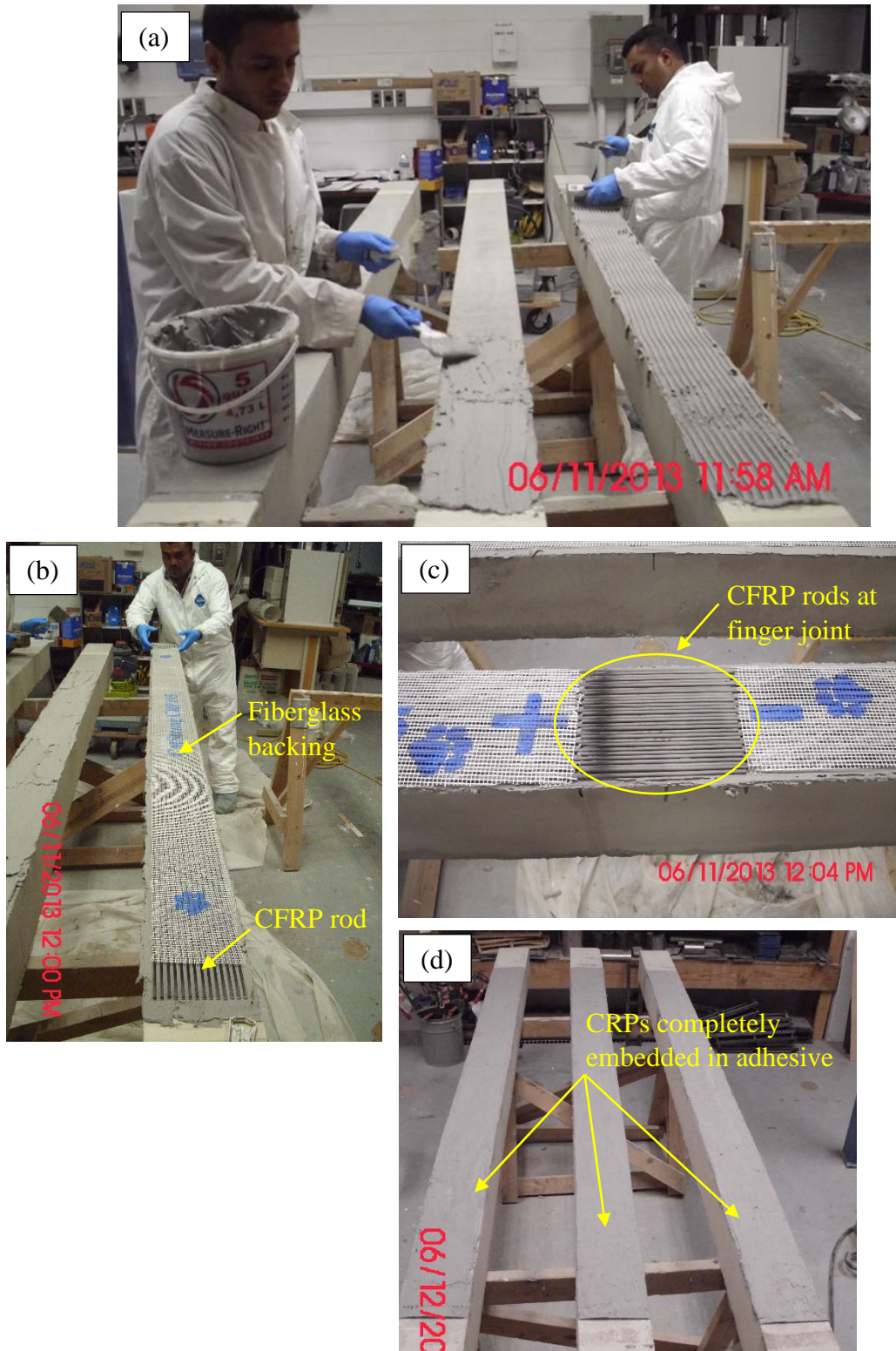


Fig. 4.3 Installation of CRPs: (a) application of first adhesive layer, (b) placement of CRP, (c) placement of CRPs at finger joint, (d) CRPs embedded in adhesive.



Fig. 4.4 Installation of CFRP fabric at CRP ends.



Figure 4.5 Installation of CFRP laminate.

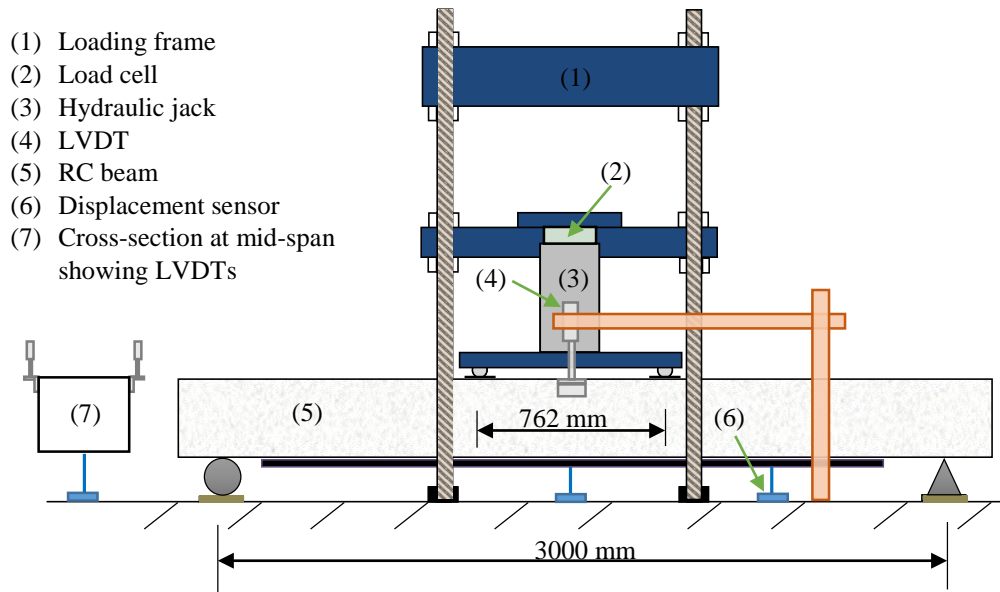
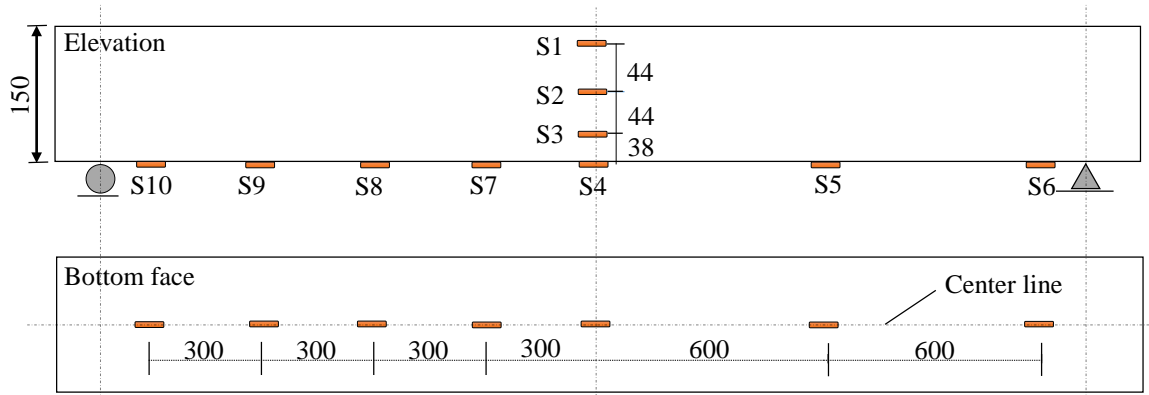


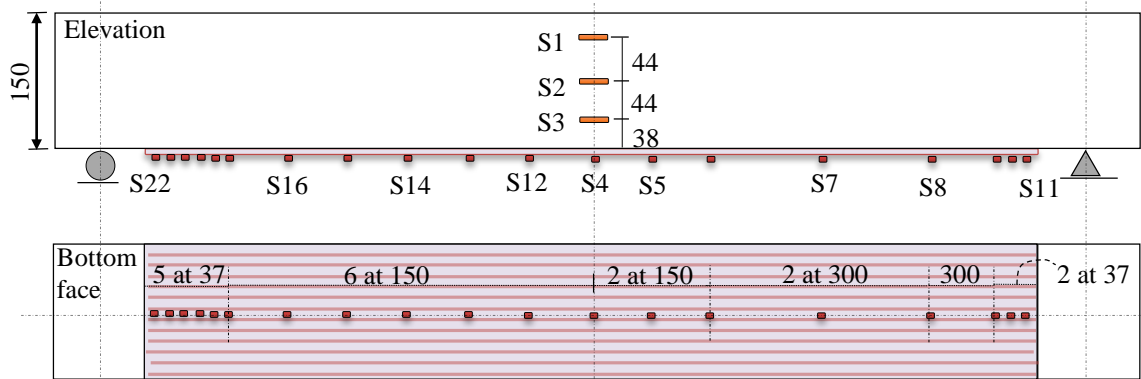
Fig. 4.6 Schematics of beam test setup.



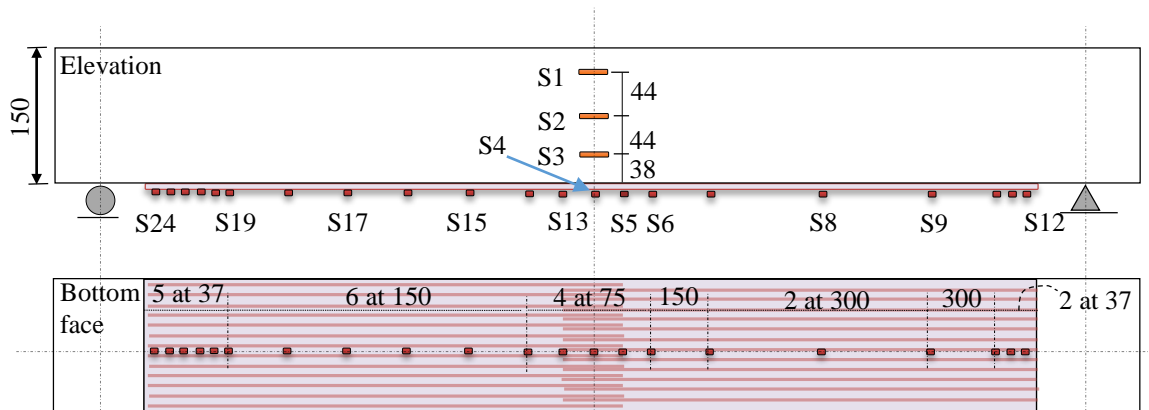
Fig. 4.7 CSSC2 Beam placed in the test frame.



(a) CB2 beam (control)

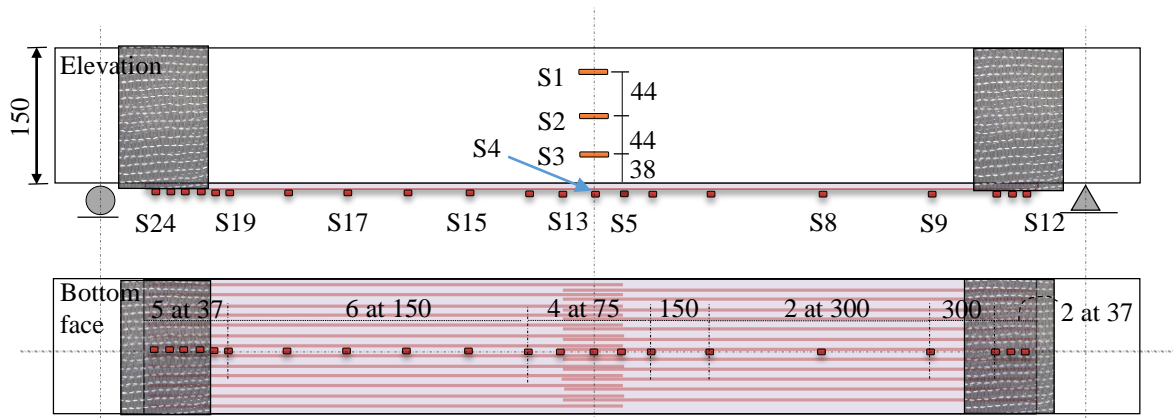


(b) CS70, and CS195 beams (strengthened with one-full length CRPs)

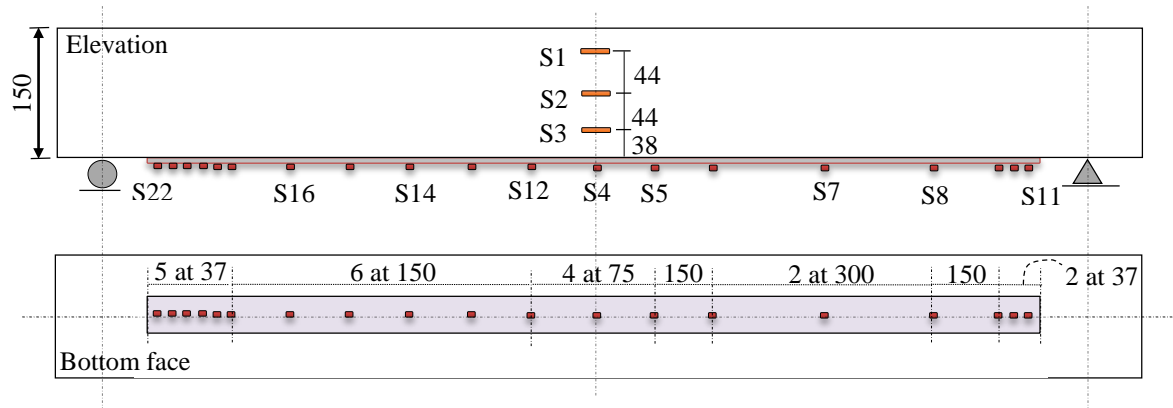


(c) SS70, and SS195 beams (strengthened with spliced CRPs)

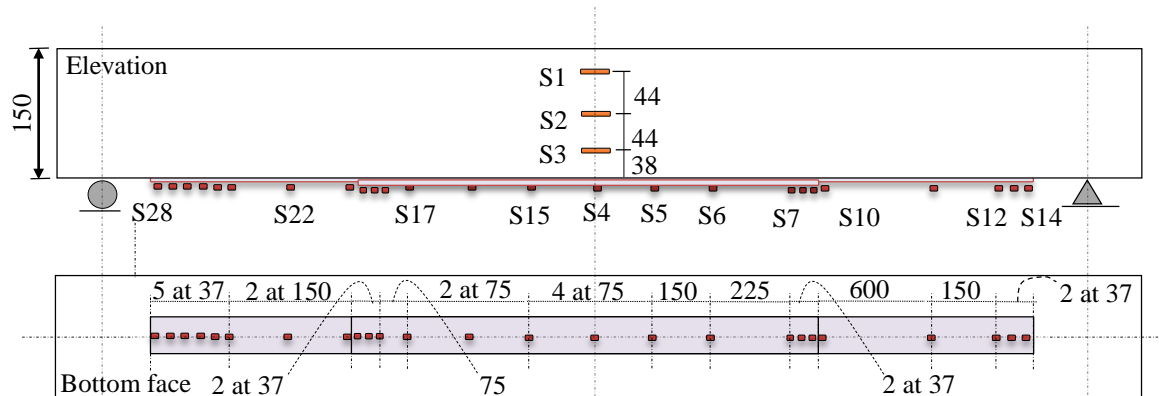
Fig. 4.8 Strain gage layout (dimensions are in mm).



(d) SSW70, and SSW195 beams (strengthened with spliced and anchored CRPs)



(f) CSSC2 beam (strengthened with one full length CFRP laminate)



(g) SSSC2 beam (strengthened with spliced CFRP laminate system)

Fig. 4.8 (continued) Strain gage layout (dimensions are in mm).

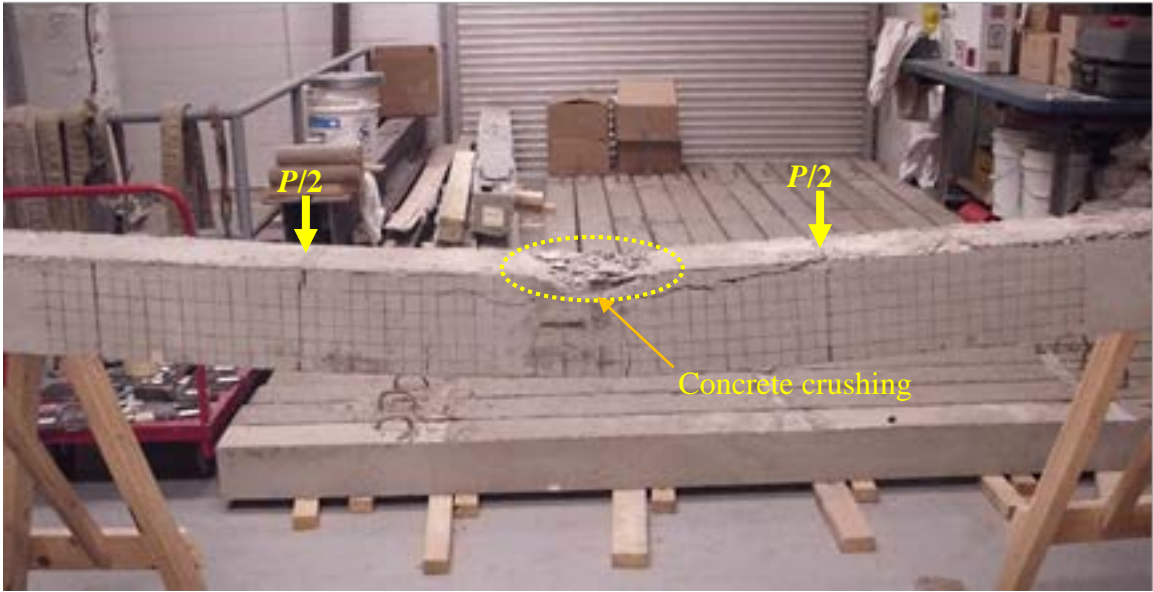


Fig. 4.9 Failure mode of control beam.

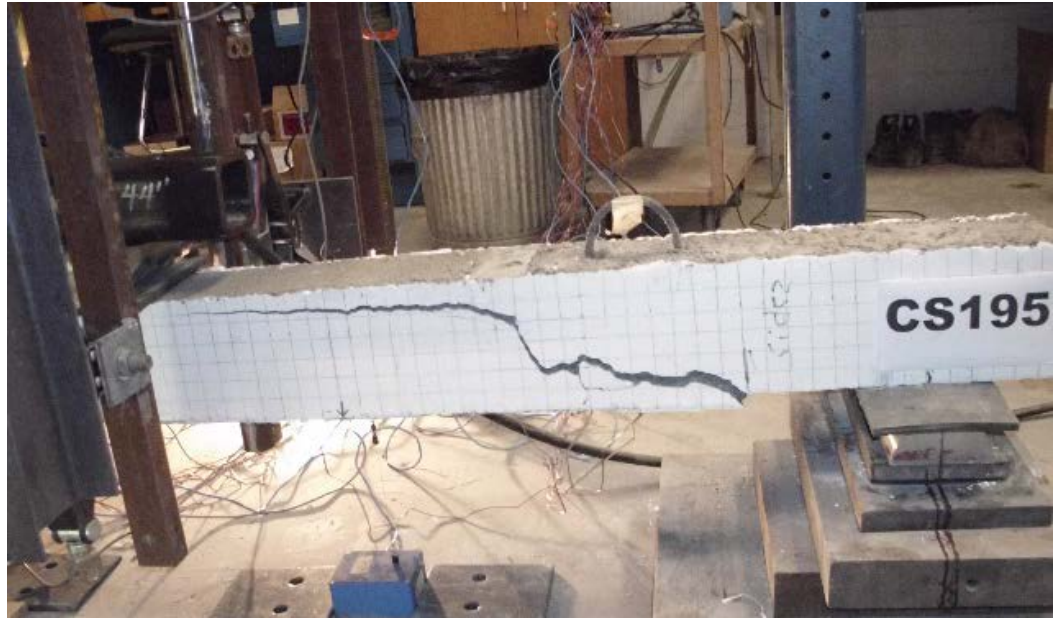


(a) CS70 beam



(b) SS70 beam

Fig. 4.10 Failure due to concrete cover separation.



(c) CS195

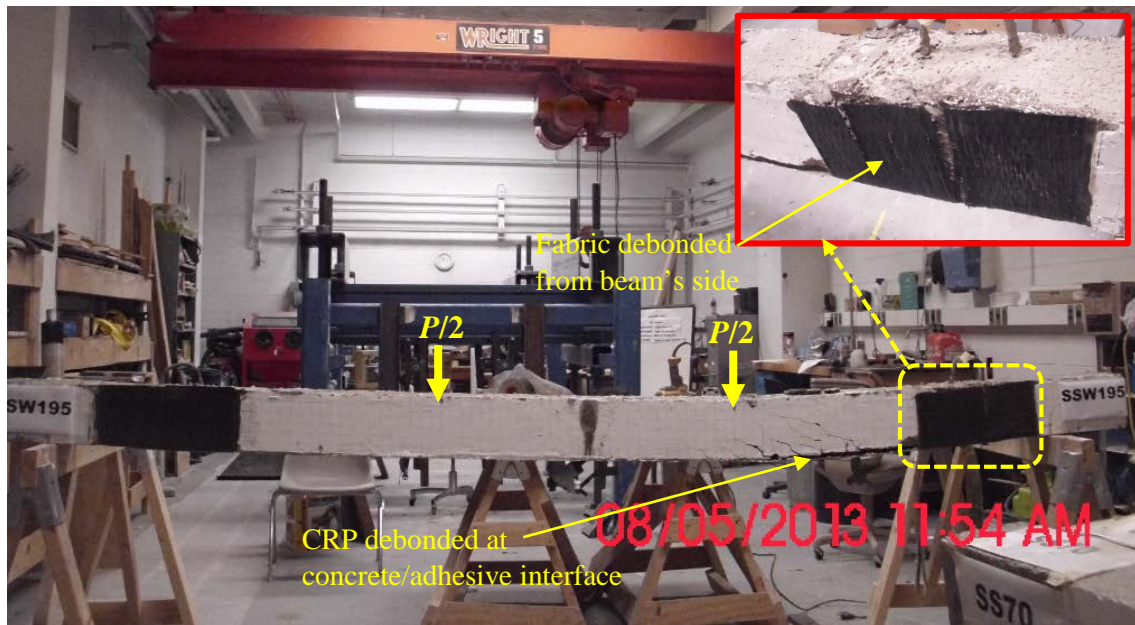


(d) SS195

Fig. 4.10 (continued) Failure due to concrete cover separation.

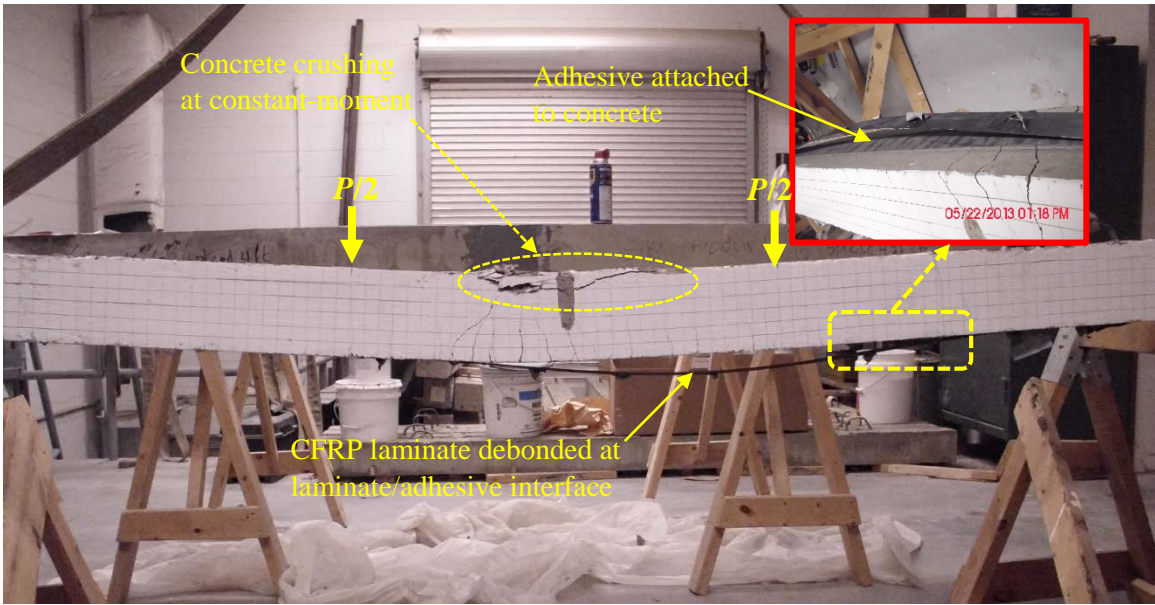


(a) SSW70

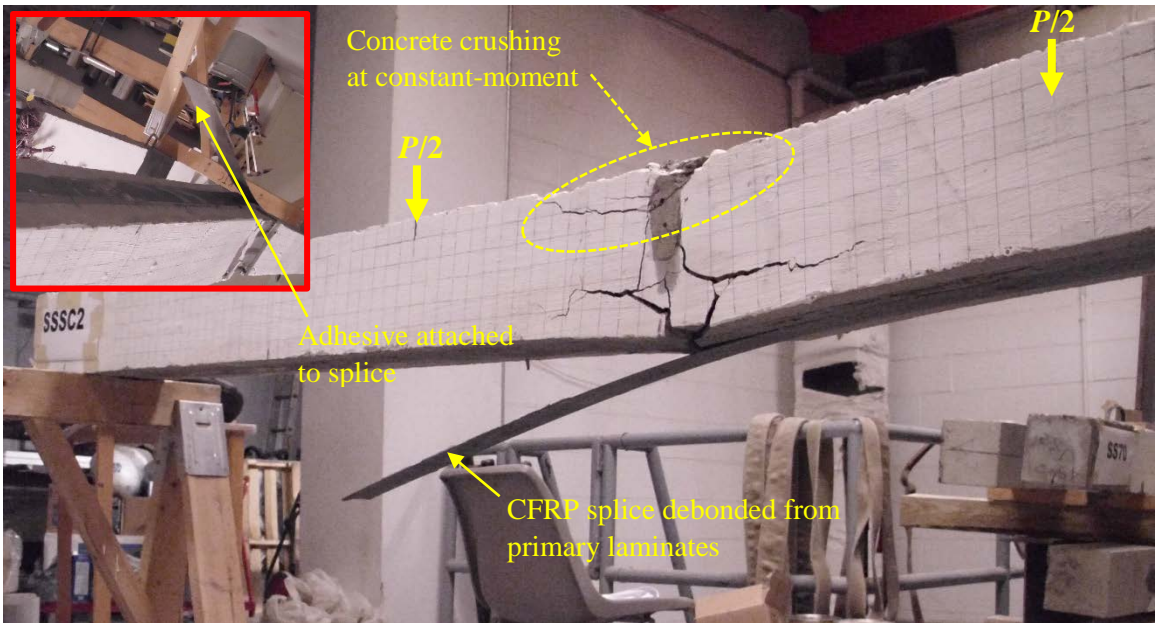


(b) SSW195

Fig. 4.11 Intermediate crack induced debonding failure.



(a) CSSC2



(b) SSSC2

Fig. 4.12 CFRP Laminate debonding failure.

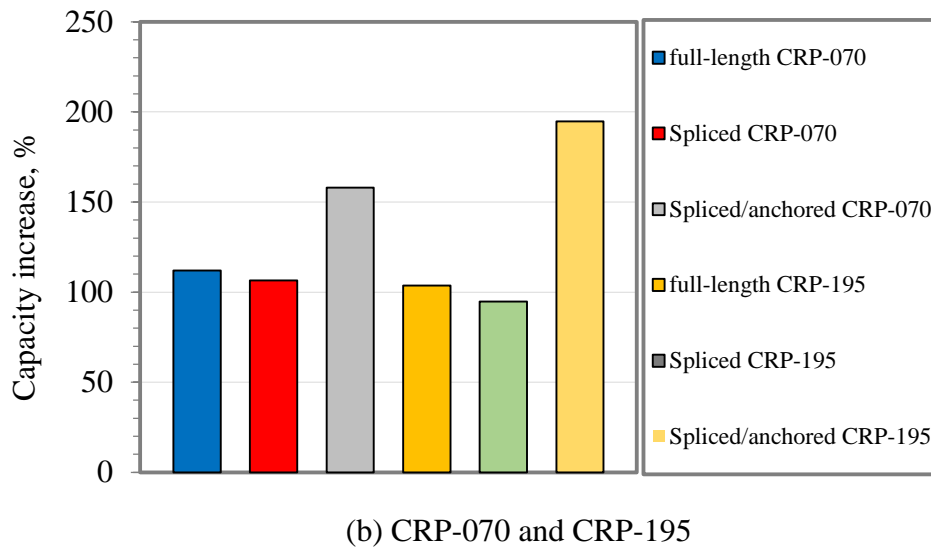
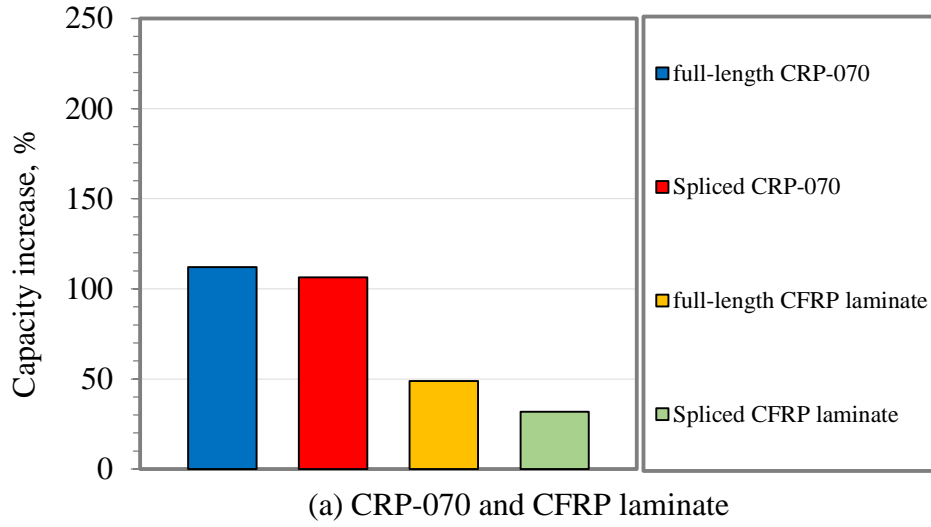
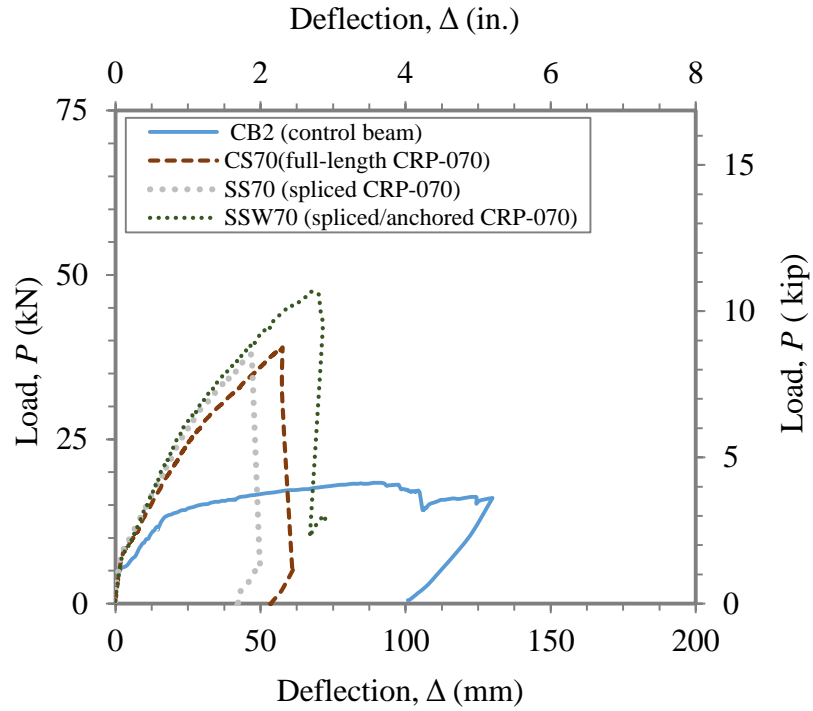
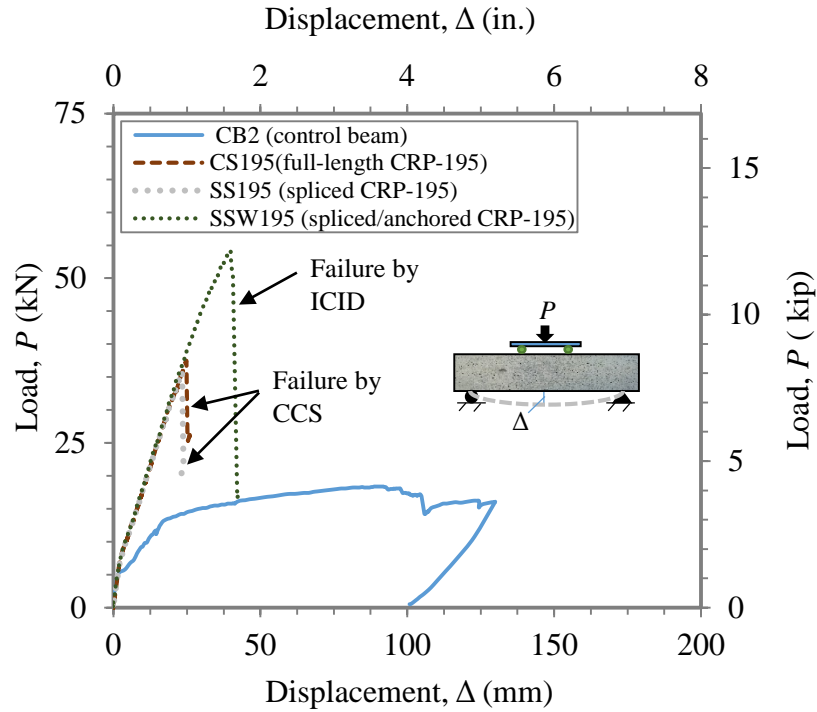


Fig. 4.13 Capacity increase percentage (over control beam) of CRP-070, CFRP laminate, and CRP-195 strengthening systems.



(a) CRP-070 strengthened beams



(b) CRP-195 strengthened beam

Fig. 4.14 Load mid-span deflection for CRP strengthened beams.

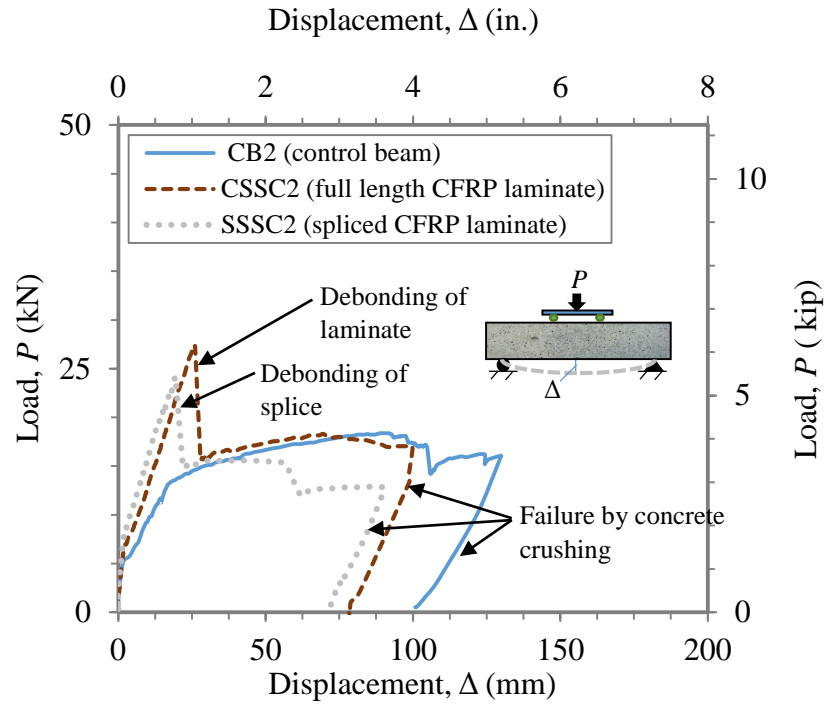


Fig. 4.15 Load mid-span deflection for CFRP laminate strengthened beams.

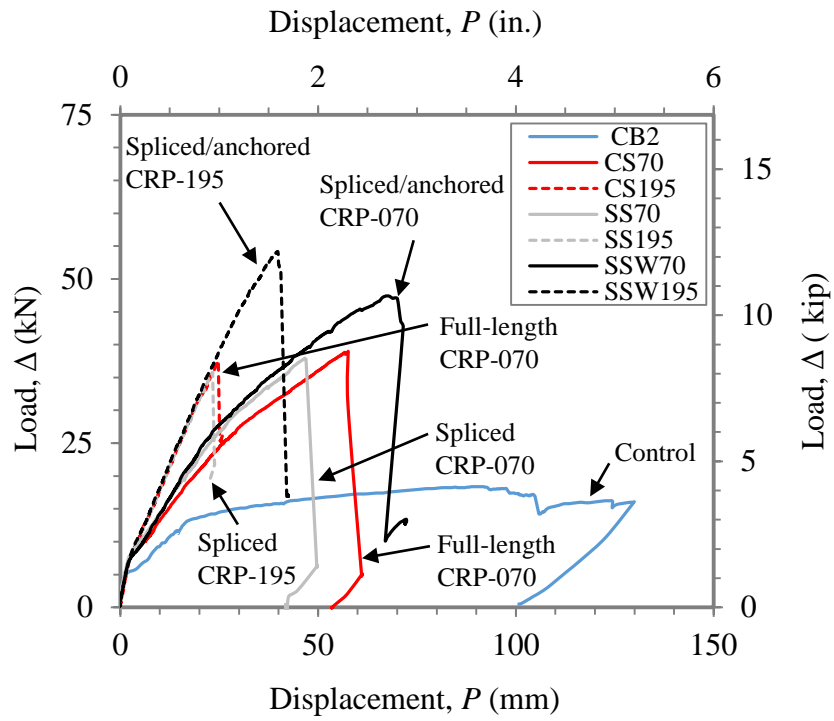


Fig. 4.16 Load mid-span deflection for CRP-070 and CRP-195.

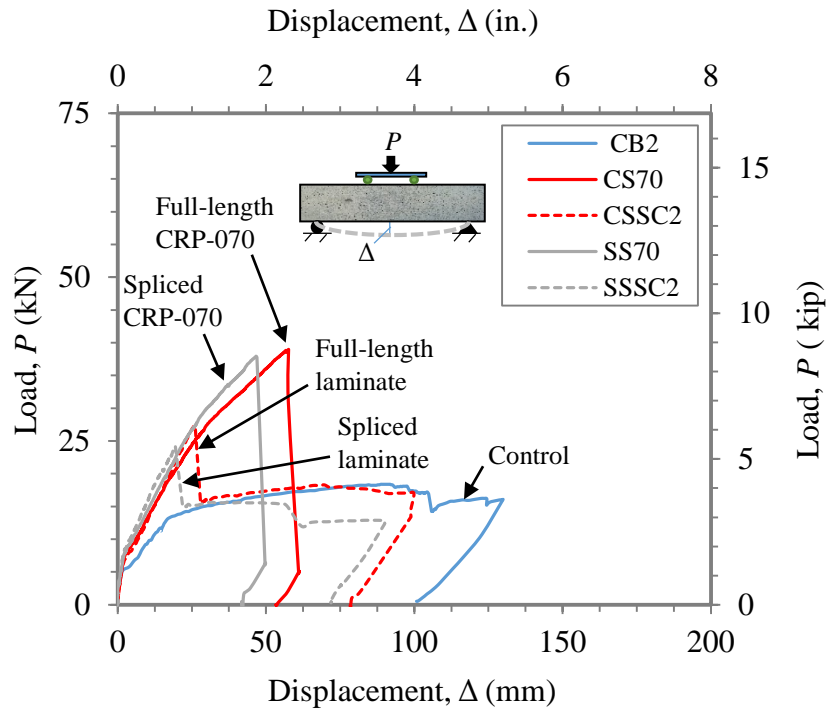


Fig. 4.17 Load mid-span deflection for the control beam and beams strengthened with CRP-070 and CFRP laminate.

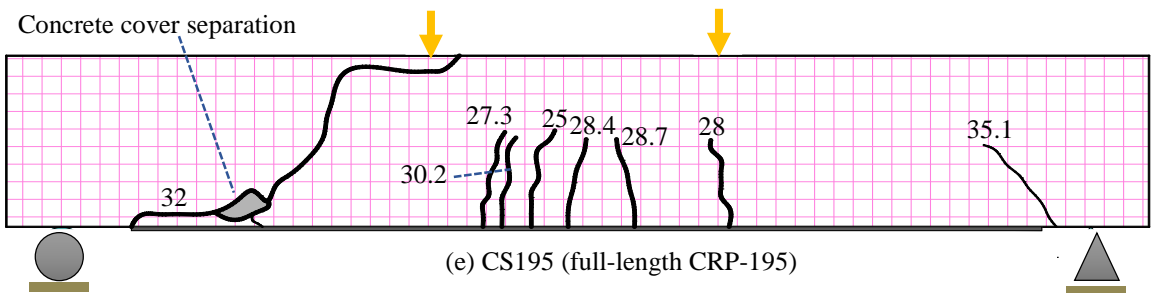
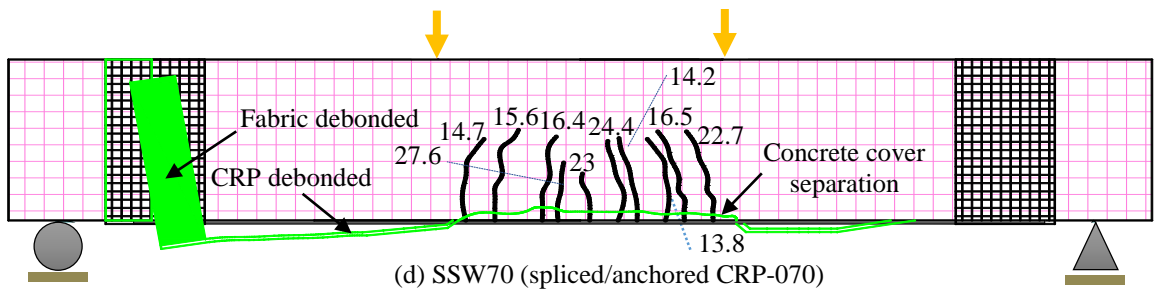
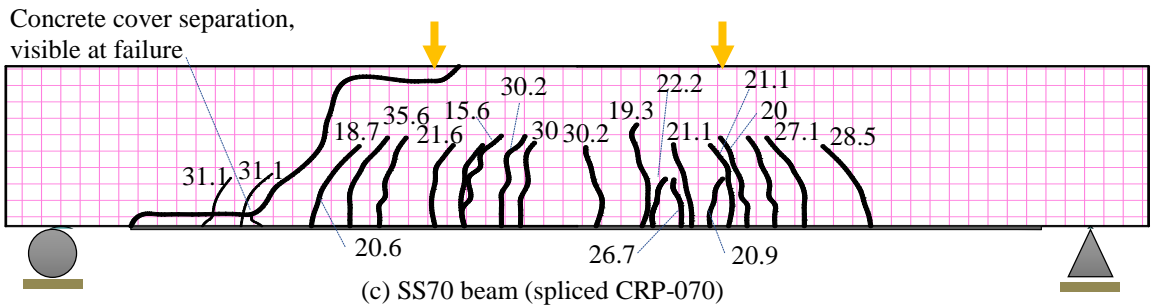
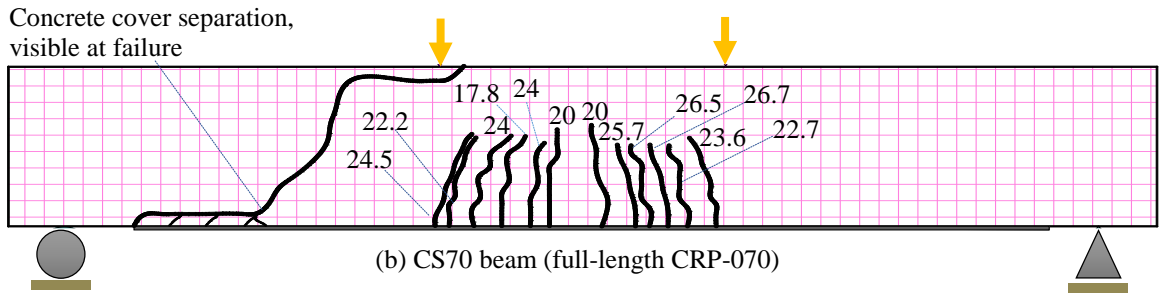
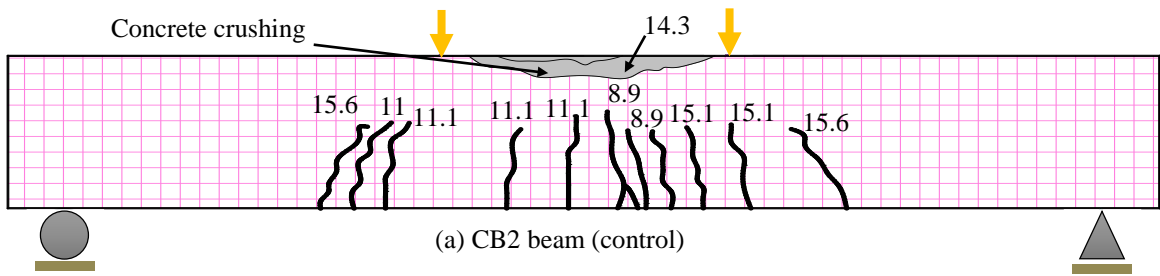


Fig. 4.18 Crack patterns in beams (numbers next to the cracks are loads, in kN, at which the crack was visible. Note 1 kN = 0.225 kip).

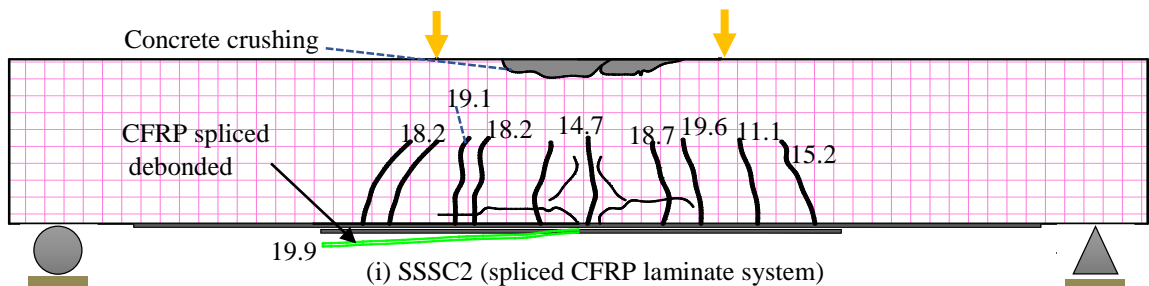
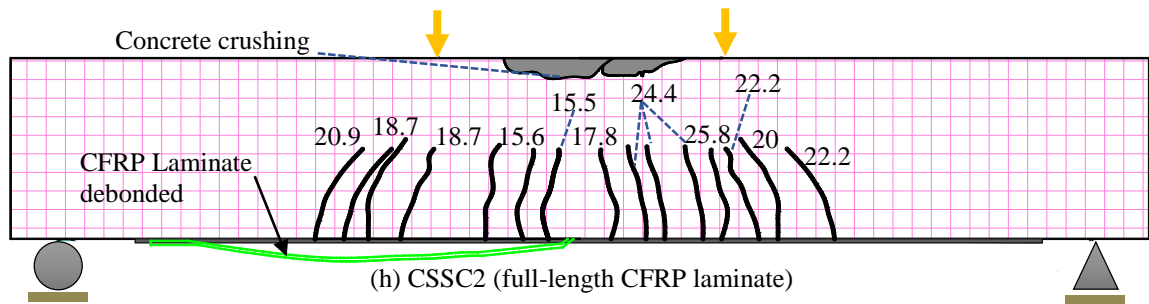
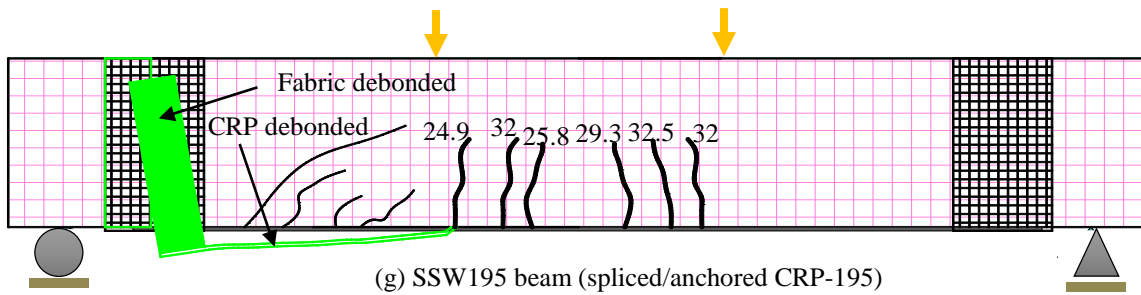
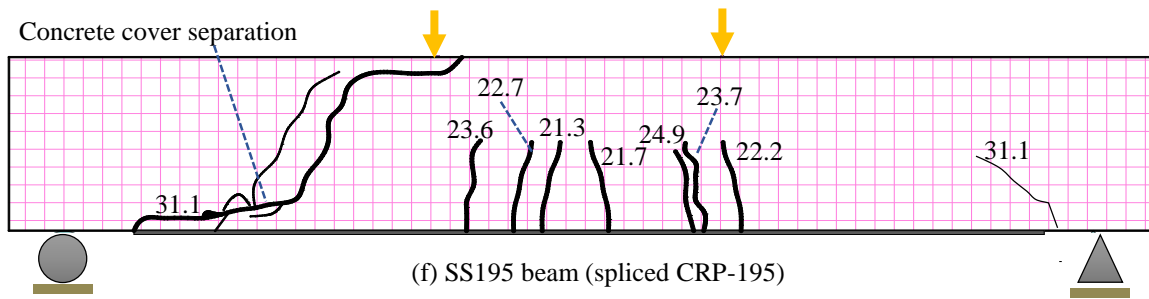
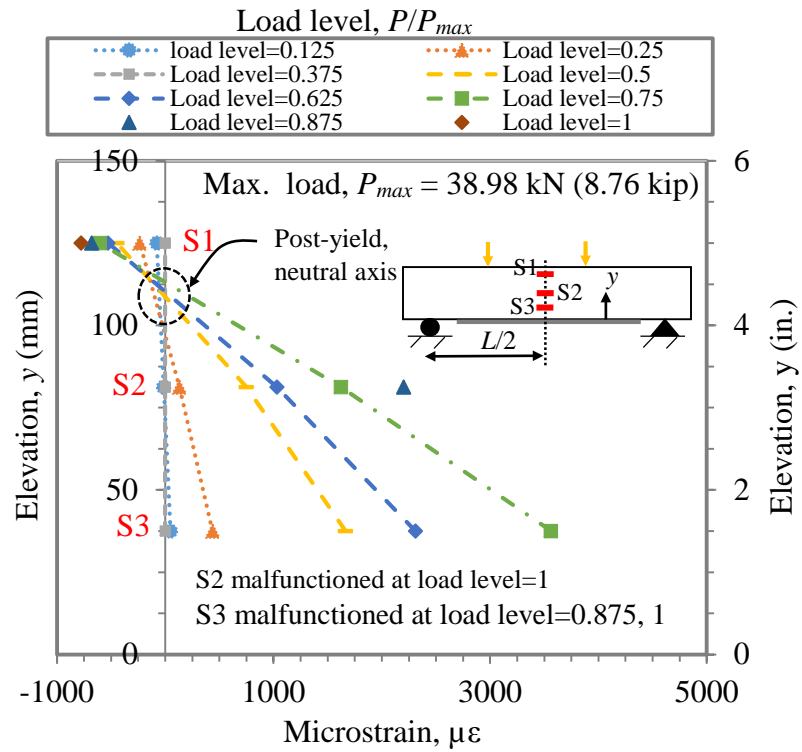
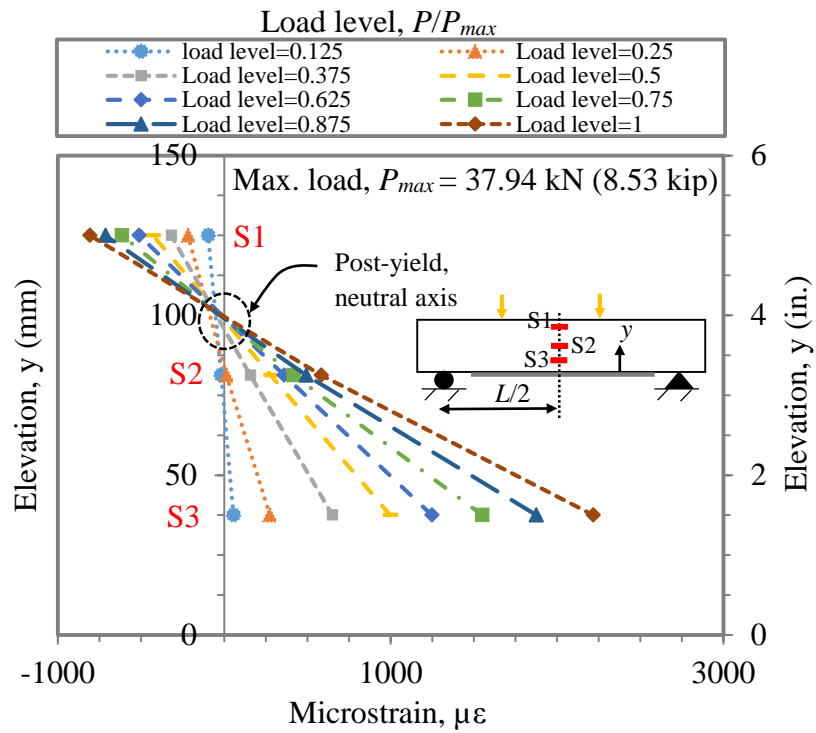


Fig. 4.18 (continued) Crack patterns in beams, (numbers next to the cracks are loads, in kN, at which the crack was visible. Note 1 kN = 0.225 kip).

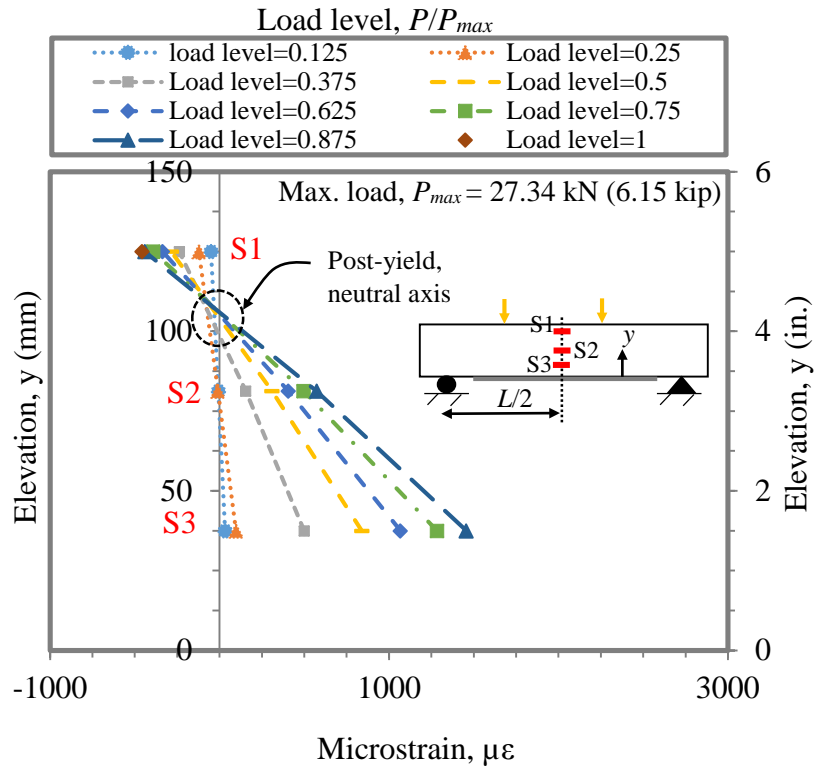


(a) CS70 beam (full-length CRP-070)



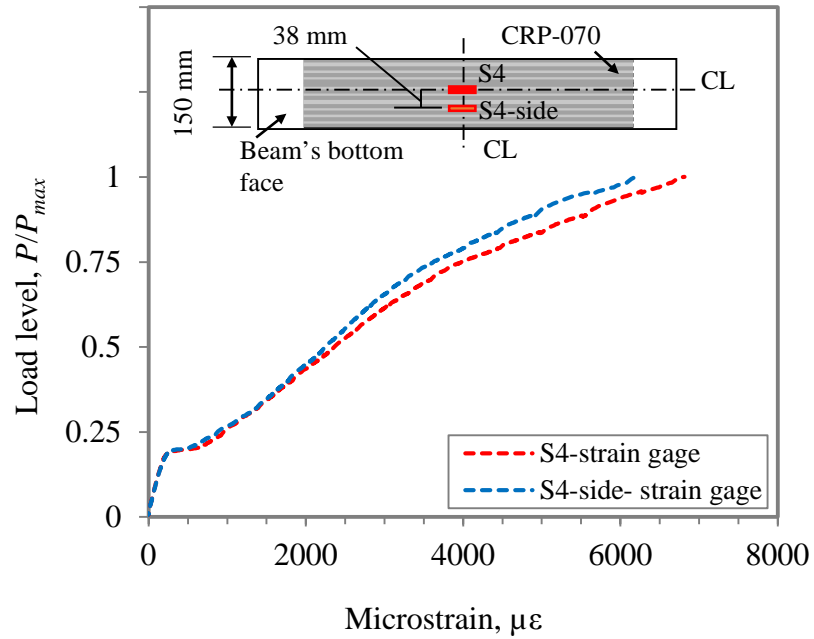
(a) CS195 beam (full-length CRP-195)

Fig. 4.19 Strain profile along depth, at mid-span, CS70 and CS195 beams.

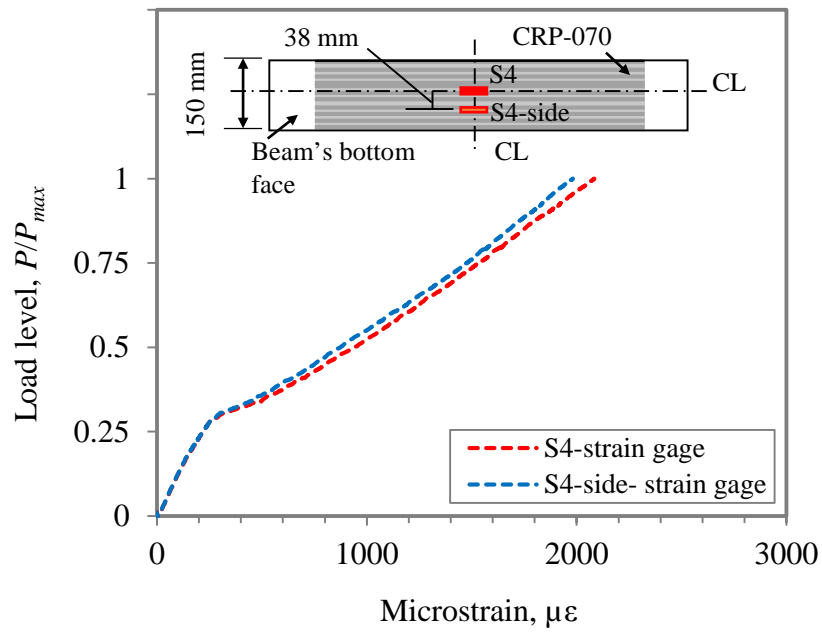


(c) CSSC2 beam (full-length CFRP laminate)

Fig. 4.19 (continued) Strain profile along depth, at mid-span, CSSC2 beam.

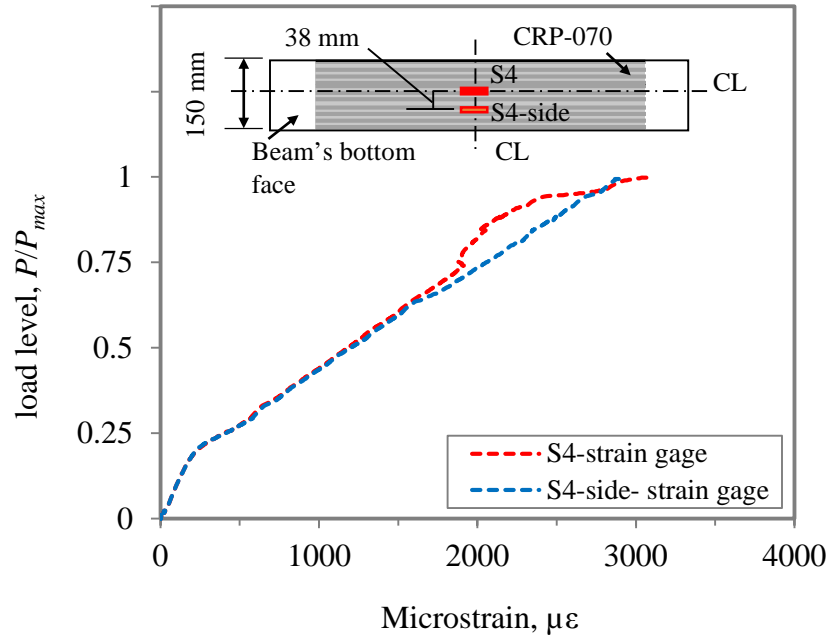


(a) SSW70 beam (spliced/anchored CRP-070)

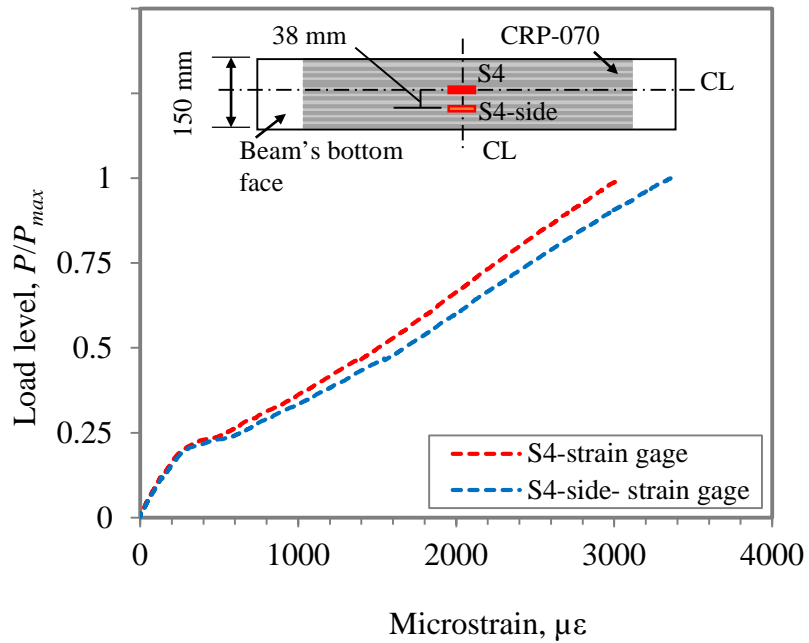


(b) CS195 beam (full-length CRP-195)

Fig. 4.20 Load level, P/P_{max} vs. strain along CRP width.

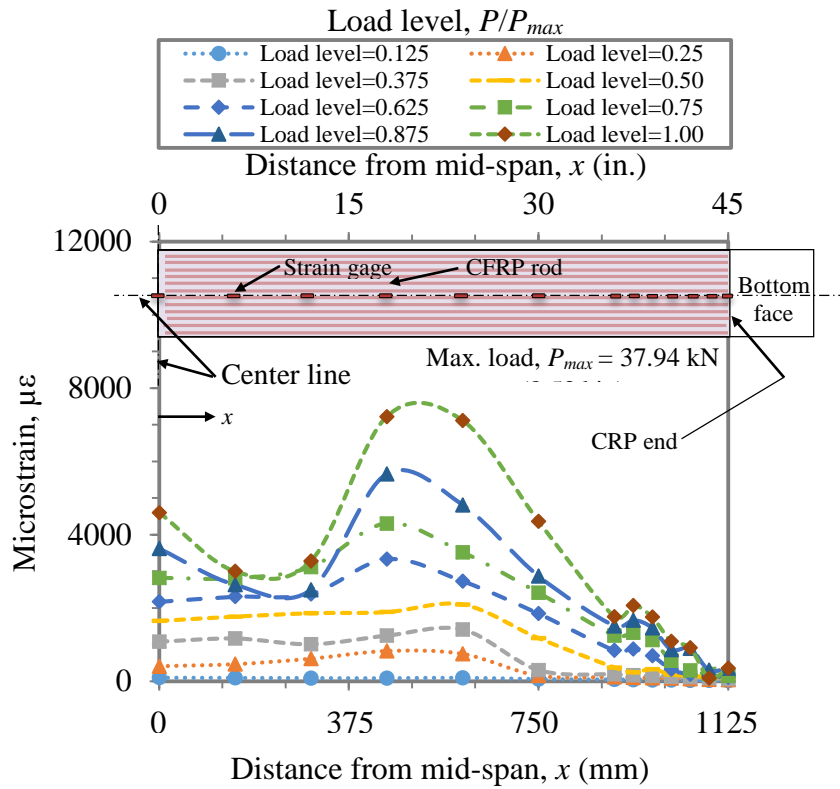


(c) SS195 beam (spliced CRP-195)

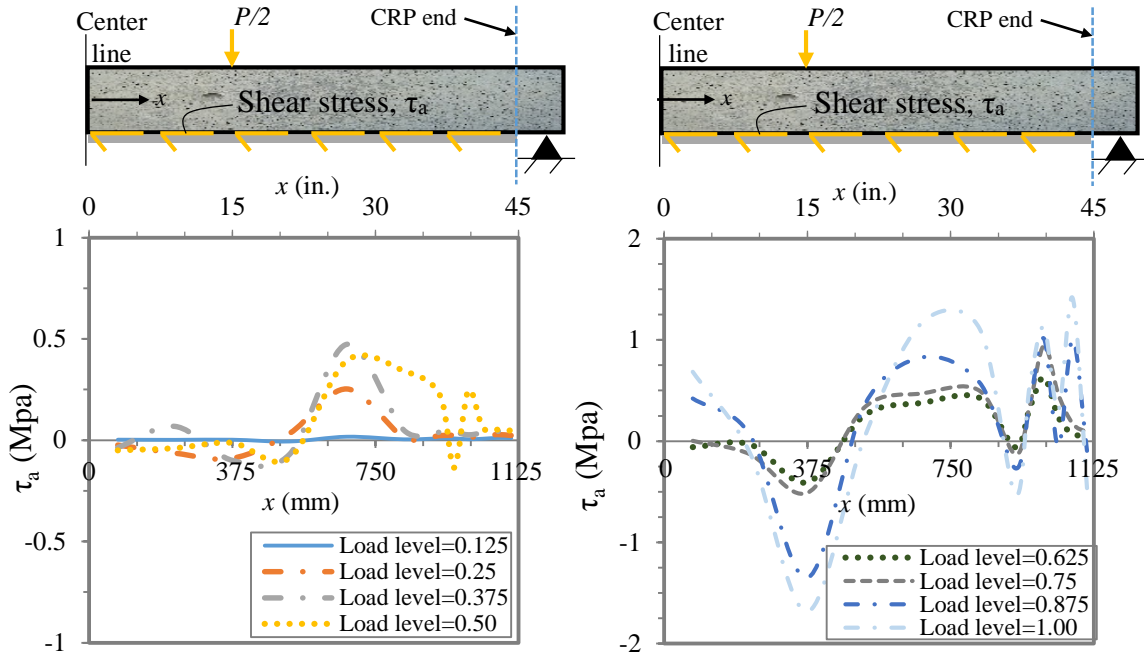


(d) SSW195 beam (spliced and anchored CRP-195)

Fig. 4.20 (continued) Load level, P/P_{max} vs. strain along CRP width.

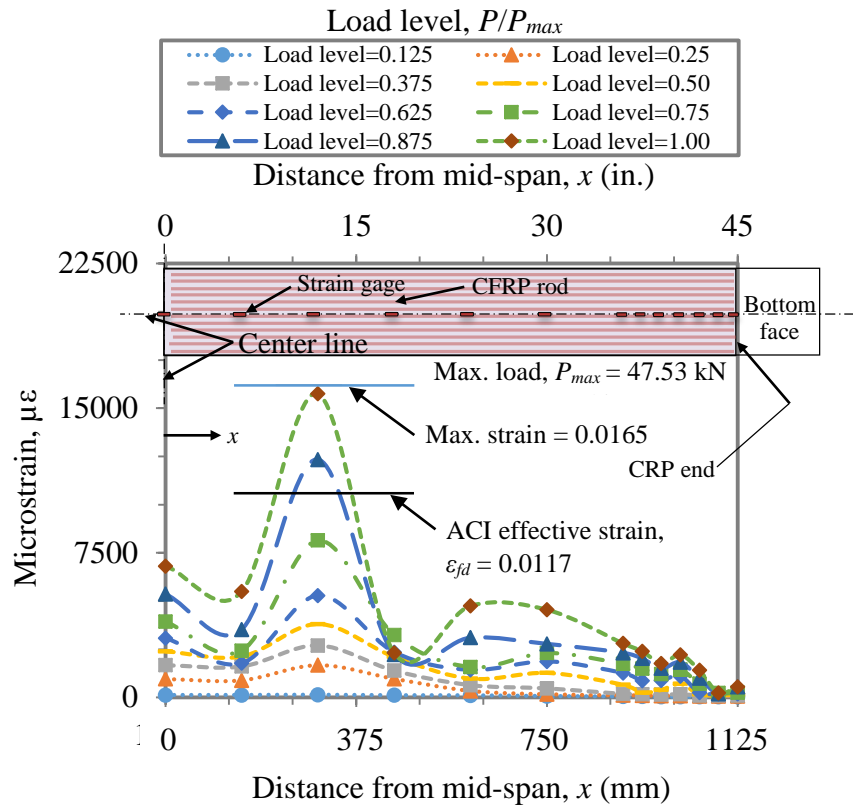


(a) Tensile strains

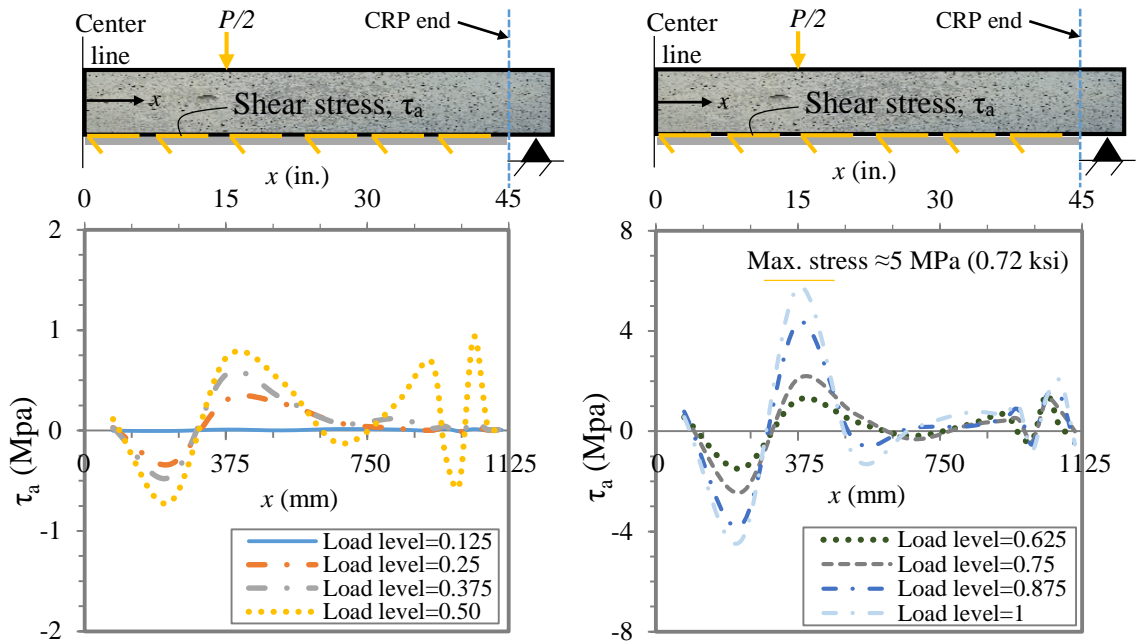


(b) Shear stresses

Fig. 4.21 Tensile strain and shear stress distribution along CRP length, beam SS70 (spliced CRP-070).

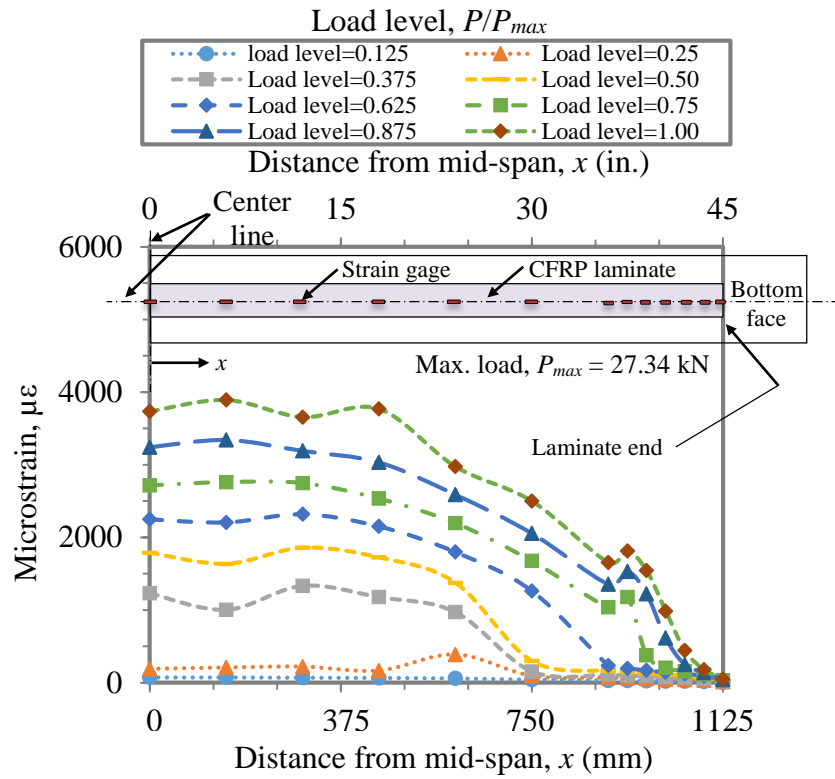


(a) Tensile strains

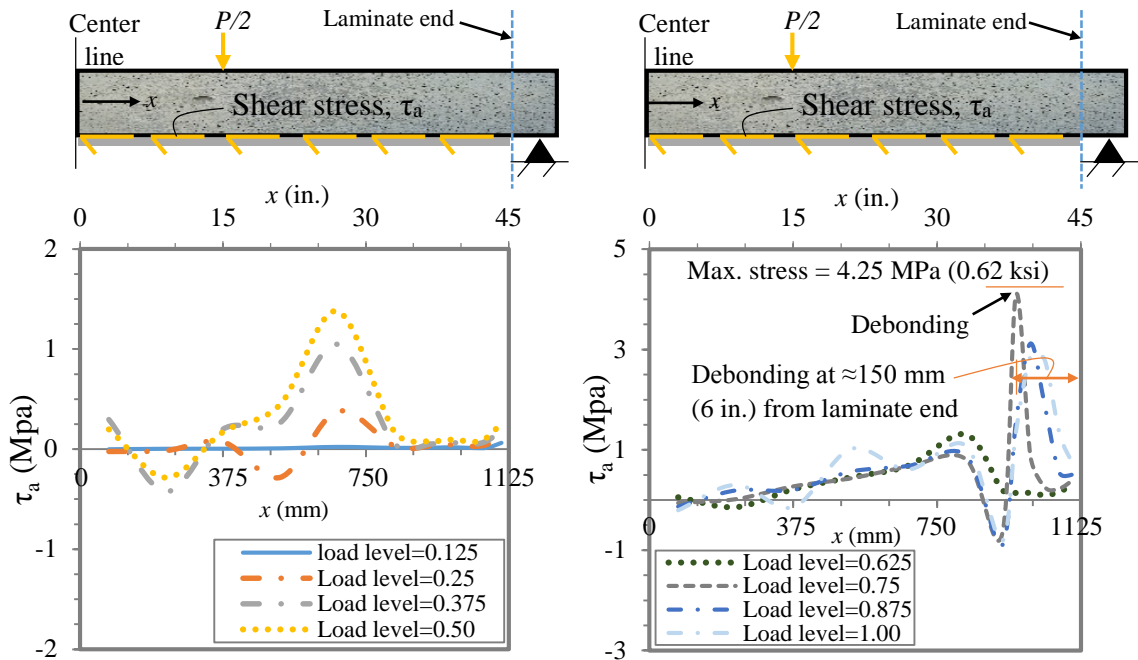


(b) Shear stresses

Fig. 4.22 Tensile strain and shear stress distribution along CRP length, beam SSW70 (spliced and anchored CRP-070).

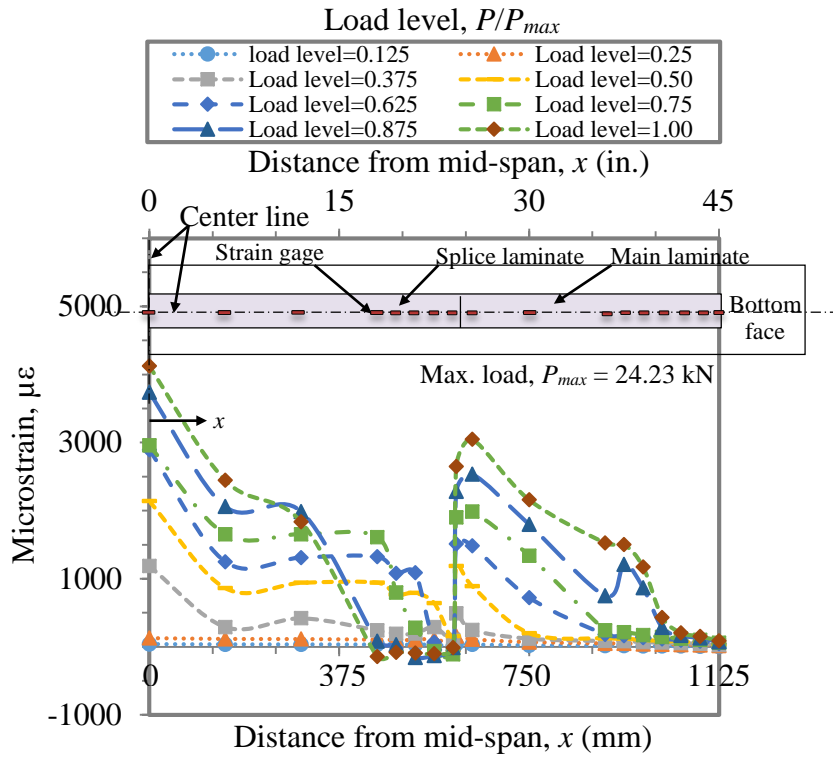


(a) Tensile strains

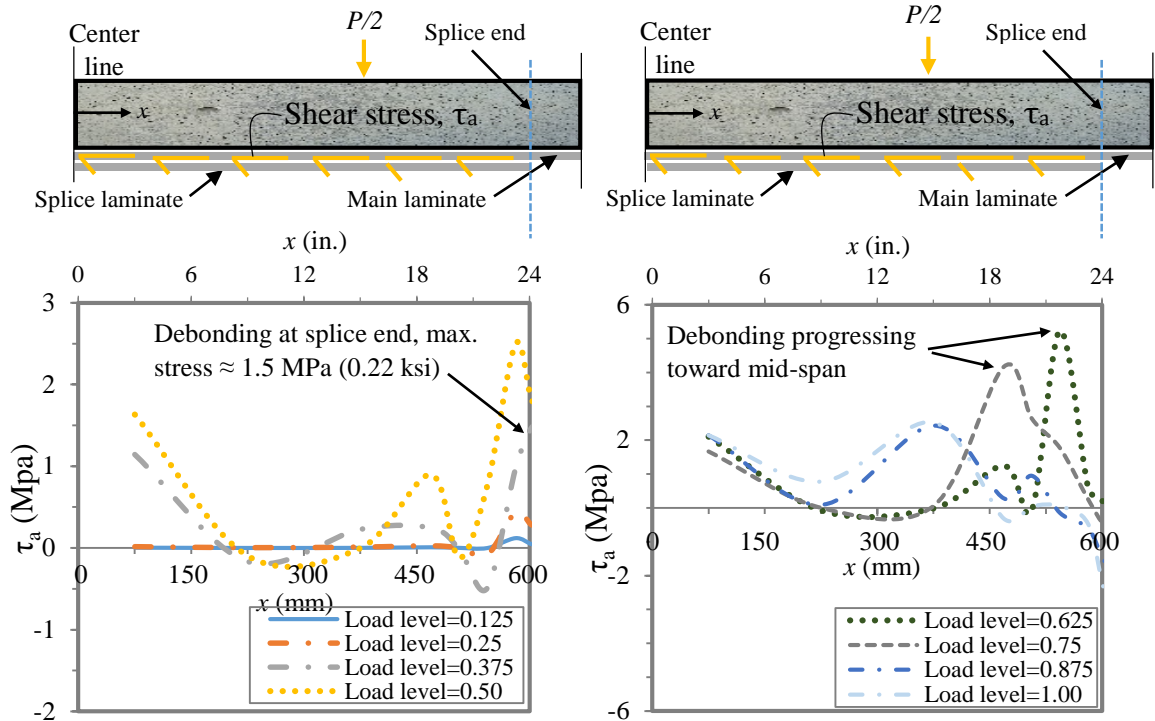


(b) Shear stresses

Fig. 4.23 Tensile strain and shear stress distribution along CFRP laminate length, beam CSSC2 (full-length CFRP laminate).



(a) Tensile strains



(b) Shear stresses

Fig. 4.24 Tensile strain and shear stress distribution along CFRP laminate length, beam SSSC2 (spliced CFRP laminate system).

CHAPTER 5: FINITE ELEMENT ANALYSIS OF RC BEAMS BONDED TO CFRP ROD PANELS AND CFRP LAMINATES

5.1 Synopsis

In this chapter, comprehensive three dimensional (3D) finite element (FE) models of RC beams, flexurally strengthened with CFRP rod panels (CRP's) and CFRP laminates, were developed. The models consider the nonlinearity of concrete material, including: concrete nonlinear stress-strain behavior in compression, cracking, crushing, stress softening behavior in tension, and effects of confinement on concrete compressive stress-strain relation. The structural behavior of CRP's, especially the overlap region, was explicitly captured by modeling CFRP rods as discrete reinforcement embedded inside the adhesive layer. Debonding phenomenon, observed in some specimens bonded to CRP's and CFRP laminates, was fully implemented using proper cohesive zone models (CZM), and interface elements. The results show that the FE models were able to capture the debonding load and location, and simulate the load mid-span deflection response with reasonable correlation to the experiments. Due to implementing a displacement-controlled loading scheme, the FE response was able to capture the drops in load that were seen in some specimens due to debonding or concrete crushing failures. Concrete cover separation failure, which occurred in several specimens strengthened with CRP, was predicted in the FE analysis, with percentage difference between FE and experimental maximum load ranging between 2.9 and 6.2. FE models predicted high shear stress concentration at the end of CRPs in all beams strengthened with full-length or spliced CRPs. For the beams that were strengthened with spliced CRPs and had CFRP U-shaped fabrics over CRP ends, FE analysis shows that

the fabric anchorage to be effective in shifting the location of maximum shear stress from the panel's end to inside the strengthening length.

5.2 Introduction

With the development of powerful computer platforms, numerical models have become widely available and useful in simulating the behavior of structural members under various loading, geometrical, and material configurations. Numerical models can be used as an alternative method when the geometry, loading configuration, or material behavior of a member are too complex to be solved by closed-form analytical models. Also, numerical tools can supplement experimental testing and assist in exploring effects of various parameters, left out in the experimental program, due to time, apparatus or cost limitations. Several methods, namely finite element (FE), finite difference, boundary element, are available. The FE method is the most widely practiced method (Lu et al 2005, Park et al 2007, Teng and Zhang 2014).

When performing a FE modeling of FRP bonded concrete members, there are several approaches followed by researchers, depending on the degree of accuracy required, time restrictions, FE software robustness, computer capability, etc. For starter, the model can be three-dimensional or two-dimensional (Omran and El-Hacha 2012). The material properties of the constituents can be simplified, assuming linear models, or advanced nonlinear relations can be implemented (Kheyroddin and Naderpour 2008). Some researchers model the internal steel reinforcement as smeared layer inside the concrete elements (Supoviriyakit et al 2004), while others use link or truss elements to realistically model the reinforcement (Ross et al 1999). The concrete-FRP interface can be

simplistically assumed to have perfect bond criteria, applicable in cases where the failure mode is not due to debonding at the interface (Pendhari et al 2006); while contact elements with proper shear stress-slip relation and normal (peeling) stress values, ought to be prescribed to accurately predict the interface debonding (Ferretti and Savoia 2003).

5.3 Experimental Program

Nine RC beams were tested in the experimental program, including: (1) one control (or un-strengthened) beam; (2) one beam strengthened with a continuous (full-length) CRP-070; (3) one beam strengthened with a spliced CRP-070 [two CRP-070 made continuous at mid-span by 150 mm (6 in) overlap]; (4) one beam strengthened with two spliced CRP-070 and anchored at panel's ends with U-shaped CFRP fabrics; (5) one beam strengthened with a continuous CRP-195; (6) one beam strengthened with two spliced CRP-195 [two CRP-195 made continuous at mid-span by 150 mm (6 in) overlap]; (7) one beam strengthened with two spliced CRP-195 and anchored at panel's ends with U-shaped CFRP fabrics; (8) one beam strengthened with a continuous CFRP laminate; and (9) one beam strengthened with spliced CFRP laminate system. The strengthening length for all CFRP strengthened beams is 2286 mm (90 in.). CFRP laminate and CRP-070 have an equal cross-sectional area (A_f) of 64 mm^2 ($100 \times 10^{-3} \text{ in}^2$), while for CRP-195, A_f is 173 mm^2 ($268 \times 10^{-3} \text{ in}^2$). Both CRP-070 and CRP-195 were set to have a width, w_f , that covers the entire beam's underside. While CRP-070 and CFRP laminate had an equal cross-sectional area to compare the performance of the two strengthening systems, CRP-195 was included in the program to investigate its performance when it's used to strengthen a concrete member.

The beams were tested until failure in a static, four-point bending configuration. Figures 5.1 and 5.2 describe the details of tested specimens. High strength concrete was used in fabrication of the RC beams. For each individual beam, three accompanying concrete cylinders [with dimensions of 150 mm (6 in.) for diameter, and 300 mm (12 in.) for length] were cast and tested on the same day of beam testing. The average compressive strength of the nine specimens is 64.7 MPa (9384 psi). The concrete modulus, E_c , was determined by attaching strain gages onto several concrete cylinders and plotting the stress-strain curve while the specimens were in compression, following ASTM C469/C469M-10 (2010) standards. The modulus was found to be 4.068×10^4 MPa (5.90×10^6 psi).

. Grade 60 steel rebars were used for both the longitudinal (tensile and compressive) and shear reinforcements. The mechanical properties of the steel were verified by performing tensile tests on several specimens, prepared from the actual rebars used in the experimental program, according to ASTM A370-09 standards. CFRP rods were used to generate the CRP-070 and CRP-195. The manufacturer's [Diversified Structural Composites (2015)] guaranteed tensile modulus of elasticity is 134 GPa (19,500 ksi) and the tensile strength is 2,340 MPa (320 ksi). CFRP laminates were normal modulus Sika CarboDur S1012 and had a tensile strength of 2800 MPa (406 ksi) and a modulus of elasticity of 160 GPa (23200 ksi), according to the manufacturer's specifications [Sika CarboDur plates, (2011)].

CFRP fabrics were SikaWrap Hex 103C type and had a tensile strength of 960 MPa (139 ksi) and a modulus of elasticity of 73 GPa (10600 ksi) [SikaWrap Hex 103C, (2014)]. Two types of adhesive were used in the experiment: (1) Sikadur 30 (epoxy adhesive), which was used as the adhesive for bonding CRP and CFRP laminates to the beam's bottom face, and (2) Sikadur 300 (impregnating resin), used to impregnate and bond CFRP fabric to the

beam's side face and to the bottom of CRP. The material properties for Sikadur 30 are: 24.8 MPa (3.6 ksi) for tensile strength and 4482 MPa (650 ksi) for modulus of elasticity [Sikadur 30 (2014)], and for Sikadur 300: 55 MPa (8 ksi) for tensile strength and 1724 MPa (250 ksi) for modulus of elasticity [Sikadur 300 (2014)].

5.4 FE Analysis

Commercial software ANSYS V 14.5 (ANSYS 2012) is adopted in this study to perform the 3D finite element modeling of RC beams strengthened in flexure with CRP'S and CFRP laminates.

5.4.1 Modeling of Materials

5.4.1.1 Concrete Material modeling

A nonlinear stress-strain model, proposed by Kent and Park 1971, is used to simulate the concrete's uniaxial compressive behavior. The model was selected due its capability of including the effects of reinforcement confinement, on the concrete compressive behavior. The model consists of two parts: a non-linear ascending curve, and a linear descending portion, figure 5.3 (a). The first part, which is identical for confined and un-confined concrete, describes the stress-strain behavior for stresses up to the maximum compressive stress (f'_c), at accompanying strain of 0.002. The descending linear portion continues until concrete crushing, which is assumed to occur at 20% of f'_c (Kent and Park 1971). The mathematical expression for the model is as follows:

First part,

$$f_c = f'_c \left[2 \cdot \frac{\varepsilon_c}{\varepsilon_0} - \left(\frac{\varepsilon_c}{\varepsilon_0} \right)^2 \right] \quad \text{for } 0 < \varepsilon_c < \varepsilon_0 \quad (5.1)$$

Second part,

$$f_c = f'_c [1 - Z \cdot (\varepsilon_c - \varepsilon_0)] \quad \text{for } \varepsilon_0 < \varepsilon_c \quad (5.2)$$

Where f_c is compressive stress in MPa (psi), at any strain (ε_c). ε_0 is the strain at the maximum compressive stress, f'_c , ($\varepsilon_0 = 0.002$).

Z represents the slope of the descending line, and is given by:

$$Z = \frac{0.5}{\varepsilon_{50h} + \varepsilon_{50u} - \varepsilon_0} \quad (5.3)$$

$$\varepsilon_{50h} = \left(\frac{3}{4} \right) \frac{2(b'' + d'')A_s}{b'' \times d'' \times s} \sqrt{\frac{b''}{s}} \quad (5.4)$$

$$\varepsilon_{50u} = \frac{30 + 0.002 \times f'_c}{f'_c - 1000} \quad (5.5)$$

Where ε_{50u} is strain at 50% f'_c for un-confined concrete. ε_{50h} is the strain increment due to the effects of confinement for confined concrete, also at 50% f'_c . b'' is width of the confined concrete core, measured to the outside of shear reinforcement, and d'' is height of the confined concrete core, measured to the outside of shear reinforcement. s is the center to center stirrup spacing, and A_s is the stirrup cross-sectional rebar area.

According to the beam shear reinforcement lay-out, shown in figure 5.1 (a) and 5.2 (a), the concrete beam inside core was divided into three regions: (1) at constant moment, where no shear stirrups were provided, (2) at locations with shear stirrups spaced at 75 mm (3 in.), and (3) at locations with shear stirrups spaced at 150 mm (6 in.). For the first region,

a non-confined concrete stress-strain model is used, while for the second and third regions, a confined concrete stress-strain model, using the respective stirrups spacing, is assigned to each region. The nonlinear stress-strain model was incorporated into ANSYS by using a multilinear curve idealization. Fifteen stress/strain points were used to sufficiently represent the model.

Figure 5.3 (b) shows the concrete tensile stress-strain model used in this study. Under uniaxial tensile stress-strain loading, the response is assumed to be linear elastic. Cracks are assumed to form when the concrete tensile strength, f_t , is reached. The tension-stiffening phenomenon, which refers to the capability of cracked concrete to carry some tensile stresses at locations between adjacent cracks, due to the bond between reinforcement and concrete, is considered in the model. After cracking, the stress is assumed to drop abruptly to $0.6f_t$ and then drops gradually to zero.

A failure criteria is needed to define the failure type of concrete; either in cracking (for regions under tensile stresses) or crushing (for regions under compressive stresses). ANSYS uses the failure criteria proposed by Willam and Warnke 1975. Other inputs required for modeling concrete material are: poisson's ratio (ν), and shear coefficient for open and closed crack (β). Poisson's ratio, (ν), was assumed as 0.2 (Kachlakev et al 2001), while the shear coefficient, β , varies from 0.0 to 1.0, and depends on the crack face conditions. A value of 0.3 was used in this study based on recommendations of other researchers (Kachlakev et al 2001, Wolanski 2004).

5.4.1.2 Steel Reinforcement

The steel reinforcement (both longitudinal rebars and shear stirrups) were assumed to have an elastic-perfectly plastic stress-strain response, identical in tension and compression, see figure 5.4. A poisson's ratio of 0.3 was assigned to the material (Obaidat 2010).

5.4.1.3 CFRP Material (Rods, Laminates, and Fabrics), and Adhesives

An isotropic linear elastic behavior is assigned for CFRP components (rods, laminates, and fabrics) and for adhesives, see figure 5.5. A failure criteria is defined for each component. The linear response is assumed to continue until the tensile strength is reached, and beyond that a complete tensile failure is assumed. The material properties that define the response [tensile strength (σ_{fu}), tensile modulus (E_f), and ultimate strain (ε_{fu})], are described in the experimental program (section 5.2). A poisson's ratio of 0.3 was assigned for CFRP components and of 0.35 for adhesives (Demakos et al 2013).

5.4.2 Geometrical Representation

Since the tested RC beams have inherent discontinuities in the out-of-plan direction, such as the presence of steel reinforcements, and CFRP rods, three dimensional models are needed to accurately capture the behavior of tested beams (especially the overlap region of spliced CRP's). A half-model of the actual specimen was used to reduce modeling and computational time and computer space by benefiting from symmetry of geometry, material, and loading conditions. The half model, rather than a quarter one, is needed because: (1) spliced CRP's are not symmetrical in the length direction (one CRP has extra rod), and, therefore, (2) a unified model for all specimens is needed, to allow for justifiable comparisons between specimens strengthened with different materials.

5.4.3 Element Types

Solid 65: Concrete volume was modeled using 8-node, brick element (solid 65). The element has three degrees of freedom at each node, translations in the global x , y , and z directions, and it is capable of representing concrete's inherent nonlinear properties such as cracking in three orthogonal directions, crushing, creep, and plastic deformations (ANSYS 2012).

Solid 185: CFRP laminates, CFRP fabrics, adhesives, and the steel plates that are placed between concrete and loading apparatus or supports were modeled using 8-node brick element (solid 185). The element also has eight nodes with three degrees of freedom at each node, translations in the global x , y , and z directions, and is capable of considering nonlinear properties such as multi-linear material model, plasticity, stress stiffening, and large deformations (ANSYS 2012).

REINF264: For CFRP rods and steel reinforcement, a discrete representation is followed to accurately capture the behavior of CFRP rods, especially at overlap regions. A reinforcing element, REINF 264, is used to model the rods. The element is recommended for modeling reinforcing fibers, having random orientations and only uniaxial stiffness. The element has two nodes, with three degrees of freedom at each node, translations in the global x , y , and z directions, and is capable of plasticity, creep, and large deformations. REINF264 is assigned to a base (solid) element, such as (Solid 65, and solid185), and it interacts with the base element via the global nodes of the base element. The inputs for REINF264 element are: orientation, location relative to the base element, cross-sectional area, and material model. A perfect bond assumption, at the interface between concrete base elements (Solid 65) and steel reinforcing elements, and also at the interface between

adhesive base elements (Solid 185) and CFRP rod reinforcing elements, was adopted, since in the experiment, debonding has never been observed at those interfaces.

5.4.4 Loading Scheme and Boundary conditions

The boundary conditions (B.C's) of the tested beams are simple-supports. The half-beam FE model was also constructed with similar conditions. A pin-type B.C's was assigned to the left support, and a roller-type B.C's was assigned to the right support. For nodes located along the plane of symmetry (at beam's mid-width), displacement in the direction perpendicular to the plane was assigned a zero value. The tested beams were loaded in a four-point bending and a displacement-controlled approach is adopted. The load was applied as non-zero displacement constraints at the respective loading positions, rather than applying forces.

The reactions of nodes located along the roller and pin supports were collected to form the total reaction, which is equal to the applied load. The displacement-control loading approach is adopted due to its capability to track drops in load that occur due to local damage such as debonding, or concrete cracking and crushing. Within the force-controlled loading, it is not possible to capture the drops in load because in nonlinear solution algorithms, such as in ANSYS, the force is applied in an incremental manner. The B.C's and non-zero displacement constraints were applied as a line load to all nodes in the width direction, at respective loading or support positions. Figure 5.6 illustrates the boundary conditions and loading scheme of the FE model.

5.4.5 FE Meshing

Along the length of the beam, a refined mesh, consisting 6.25 mm (0.25 in.) long elements, is used at locations where stress concentrations are expected, i.e. [at rods' overlap region (finger joint mid-span), at curtailments of CRPs and CFRP main or splice laminate (figure 5.7)] . At other locations along the length, the element size is doubled to 12.5 mm (0.5 in.), as shown in figure 5.7. Along the width and height of the beam, the element size is 12.5 mm (0.5 in.), as shown in figure 5.7. For adhesives, CFRP main and splice laminates, and CFRP fabric, one element is used through the thickness. Steel plates were divided into four elements through the thickness [figure5.7 (d)], each element is 3 mm (0.125 in.) thick. .

5.4.6 Nonlinear Solution

The Full Newton-Raphson method is adopted to solve the set of nonlinear equations, with a sufficiently large number of solution sub-steps during the loading process to capture the different stages of the behavior, such as cracking, yielding, and failure. The automatic time stepping, which regulates the sub-step size according to the convergence of the solution, is activated to help reduce computational time. For Solid 65 element, 185 brick element, a 2 x 2 x 2 set of Gaussian integration points is used. A convergence tolerance of 5% is assumed for the displacement degree of freedom.

5.4.7 Modeling of Debonding

Modeling of the debonding phenomenon in adhered materials requires appropriate knowledge of the behavior of each bonded component as well as the interaction between the bonded parts. In the experimental program, four tested beams failed by debonding: two of the beams were strengthened with spliced and anchored CRP's and the other two beams were strengthened with CFRP laminates (full-length laminate and spliced laminate system).

For the beams strengthened with spliced and anchored CRP's, debonding occurred along the adhesive-concrete interface. The debonding initiated from loading locations and progressed toward the panel's end. Part of the fabric wrap debonded from the beam's side face due to debonding of CRP and its movement away from the beam. The other part of the fabric, which is placed outside the strengthening length, remained attached to the beam. For the beam strengthened with a full-length CFRP laminate, the laminate debonded from the beam at the laminate adhesive interface. The debonding initiated from one of the laminate ends and moved towards the mid-span. The adhesive, between the laminate and the beam, remained attached to the beam. For the beam strengthened with a spliced CFRP laminate system, the splice debonded from the main laminate system [figure 4.12 (b)]. Debonding started at the splice ends and progressed towards mid-span. The main laminates remained attached to the beam.

Debonding of the above specimens is included in the developed FE models by using the interface element INTER 205 and cohesive zone material CZM. INTER 205 is a 3-D linear interface element used to model debonding at the surface between the linear 3D elements, such as Solid 65 and Solid 185 (ANSYS 2012). INTER 205 has eight nodes and each node

has three degrees of freedom (translations in x, y, and z) as shown in figure 5. 12. The debonding process is defined by the relative movement between the 205 nodes. Figure 5.13 presents the shows FE models of the debonded interfaces.

A cohesive zone material (CZM) model is required for INTER 205 element to define the traction-separation [(normal or shear stress)-(normal jump or tangential slip)] behavior along the interface. A bilinear CZM model, available in ANSYS, is used in this study. The model consists of a linear elastic portion until a maximum normal (peeling) or shear stress is reached, and a softening line, that ends at the maximum normal jump or tangential slip. Figure 5.14 shows a typical bilinear CZM model, in which six parameters are needed to define the model. For debonding induced by normal stresses, the parameters are: σ_{\max} (maximum normal stress), u_n^* (normal jump accompanying σ_{\max}), and u_n^c (normal jump at completion of debonding). While for debonding caused by shear stresses, the parameters are: τ_{\max} (maximum stress stress), δ_t^* (tangential slip accompanying τ_{\max}), and δ_t^c (tangential slip at completion of debonding).

5.4.7.1 CZM Model for Debonding of CRP

A mixed-mode CZM model (including both, normal debonding and shear debonding) is used to model the debonding of CRP at the beam's bottom. The reason for using the mixed mode CZM model for this interface is because debonding of CRP, in the experiment, was by intermediate crack induced debonding (ICID). The failure initiates at locations of flexural or flexural-shear cracks (e.g. at loading points) as a result of the relative vertical displacement at the tip of the crack, causing high concentration of normal and shear stresses, and advances toward other locations (Teng et al 2003). The bilinear bond-slip

model, proposed by Lu et al 2005, and used widely in analytical and numerical investigations of FRP bonded concrete members, is used to determine the shear-debonding parameters (τ_{\max} , δ_t^* , and δ_t^c), as such:

$$\tau_{\max} = 1.1\beta_w f_t \quad (5.6)$$

$$\delta_t^* = 0.0195\beta_w f_t \quad (5.7)$$

Where τ_{\max} (in MPa) and δ_t^* (in mm) are governed by the concrete tensile strength f_t (MPa), and width ratio (β_w). β_w is given as:

$$\beta_w = \sqrt{\frac{2.25 - (w_f / b_c)}{1.25 + (w_f / b_c)}} \quad (5.8)$$

w_f is the width of CRP in mm, and b_c is width of concrete member, in mm. f_t is estimated in this study from the concrete compressive strength, f_c' (ACI 318-11, 2011).

$$f_t = 0.56\sqrt{f_c'} \quad [\text{SI units (MPa), ACI-11}] \quad (5.9)$$

$$\delta_t^c = \frac{2G_f}{\tau_{\max}}, \text{ mm} \quad (5.10)$$

Where G_f is the fracture energy per unit bond area required for complete debonding, and it is equal to the area under the bond-slip curve, G_f is given by:

$$G_f = 0.308\beta_w^2 \sqrt{f_t} \quad (5.11)$$

The normal debonding parameters (σ_{\max} , u_n^* , and u_n^c) are determined, following suggestions by Wittman 2002 and Holmer 2010. σ_{\max} is limited to the concrete tensile strength (f_t), while u_n^c is assumed to be equal to 0.06 mm, and u_n^* equal to 0.024 mm.

The following energy criterion in ANSYS is used to define the contribution of shear and normal debonding to the mixed-mode debonding (ANSYS 2012):

$$\left(\frac{\int \sigma du_n}{G_{cn}} \right) + \left(\frac{\int \tau d\delta_t}{G_{ct}} \right) = 1 \quad (5.12)$$

Where G_{cn} and G_{ct} are the total fracture energies for normal and shear fractures, and are calculated as the area under respective CZM models.

5.4.7.2 CZM Model for Debonding of CFRP fabric and laminates

For debonding of the CFRP fabric from the beam's side, the full-length CFRP laminate from beam's bottom, and the CFRP splice laminate from the laminate system, a shear debonding CZM model, with only τ_{\max} , δ_t^* , and δ_t^c parameters, is used to define the debonding process. Table 5.1 lists the values used for the above parameters, for each debonding interface. The slips (δ_t^* and δ_t^c) were obtained from Lu et al's 2005 model (equations 5.7 and 5.10). The maximum shear stress, τ_{\max} , of the CFRP fabric was determined from the manufacturer's specifications (Sika 2014). For debonding of the full-length and spliced laminates, and since the debonding was at laminate/adhesive interface, equation 5.6 of Lu et al's model (2005) could not be used to determine τ_{\max} since it was derived for debonding at concrete/adhesive interface. Alternatively, τ_{\max} was determined from correlation analyses between the FE and experimental results.

5.5 Results and Discussions

5.5.1 Load-Deflection Response

Figures 5.15 to 5.17 show the experimental and FE load vs mid-span deflection response for the control beam, the beams strengthened with CRP-70, and the beams strengthened with CFRP laminate. For beams strengthened with CRP-195, the experimental and FE load-deflection comparisons are presented in appendix C (figure C.1). In general, there is a good agreement between FE and experimental results, and the FE load-deflection curves seem to correctly follow the experimental trends. It should be mentioned that for some specimens, and after cracking stage, the FE load-deflection curve is stiffer than the experimental one. This difference in stiffness can be attributed to many factors, some belong to the experiment, and others to limitations within the FE model. For example, micro-cracks caused by shrinkage and slippage at steel/concrete interface or at other interfaces might be present in the experiments, but not accounted for in the FE model. The FE model has some limitations regarding element type and size, material models, etc. Furthermore, due to implementing a displacement-controlled loading scheme, the FE response was capable of capturing the drops in load that were seen in some specimens due to debonding or concrete crushing failures (figures 5.15 to 5.17 and figure C.1). Most FE studies that utilize ANSYS software fail to present the load drops because the force-controlled loading scheme is used rather than displacement-controlled scheme (Omran and El-Hacha 2012). Table 5.2 lists loads and mid-span deflections at cracking, yielding and failure stages, obtained from the experiment and FE analysis. As the table shows, the FE models predicted well the loads and deflections at the three main stages.

5.5.2 Simulation of Concrete Cover Separation

Four specimens, strengthened with full-length and spliced CRP-070 or CRP-195 failed by concrete cover separation (CCS). The failure occurred near one of the panels' ends and was characterized by the separation of the concrete cover from the beam's section, along the level of internal steel reinforcement. Several theoretical studies concerned with determining the ultimate load when CCS is predominant, assume that the failure initiates when the tensile stress in concrete section near the end of the strengthening plate and along the level of internal reinforcement, exceeds the concrete tensile strength (Zhang et al 1995, Raouf and Hassanen 2000, Al-Mahmoud et al 2010).

In this study, a section of concrete (bound by the beam's bottom face and tensile reinforcement), at CRP cut-off location, was isolated from the FE model, and used to perform a post processing analysis, figure 5.18. A stress failure criterion, similar to what Al-Mahmood et al 2010 and Radfar et al 2012 used in their analysis, is followed. At each load step, normal stresses at the above mentioned section were observed and compared to the concrete tensile strength, and when the maximum tensile stress exceeds the tensile strength, CCS failure is assumed to initiate and the accompanying load step is considered to be the ultimate load. In agreement with theoretical studies, the FE distribution of normal stresses in the section shows that the maximum tensile stress is registered at CRP end, along the tensile steel reinforcement level (figure 5.18). Furthermore, the failure loads obtained from the post processing analysis, and given in table 5.2, are in a good agreement with the experimental loads.

5.5.3 Simulation of Debonding and Concrete Crushing Failures

Figures 5.19 through 5.23 show, respectively, the FE simulation of failures for (1) control (un-strengthened) beam, (2) beam strengthened with spliced and anchored CRP-070, (3) beam strengthened with spliced and anchored CRP-195, (4) beam strengthened with full-length CFRP laminate, and (5) beam strengthened with spliced CFRP laminate system. As can be seen in those figures, cohesive zone material (CZM) models, along the respective debonding interfaces, were able to accurately capture the debonding failure for CRPs, CFRP laminates, and CFRP fabrics.

For specimens that experienced concrete crushing at mid-span region, the FE models were able to predict the failure mode. FE predictions show that concrete compressive stresses at the beam's top face, at mid-span, exceeded the concrete compressive strength (f'_c). Furthermore, and at mid-span, concrete strains (both compressive and tensile) are very large and thus indicate that there is excessive deformations and loss of section integrity due to steel yielding and concrete crushing (i.e. plastic hinge formation at mid-span section).

5.5.4 Load versus Strain in CFRP at Mid-Span

Experimental and FE load versus strain in CFRP material, at mid-span, are plotted in figure 5.24 for specimens strengthened with CRP-070 and in figure 5.25 for specimens strengthened with CFRP laminate. For specimens strengthened with CRP-195, the plots are given in appendix C (figure C.2). The load vs strain variations from the FE models seem to match the experimental results. The only exception is, in the specimen strengthened with full-length CRP-070 (beam CS70) in which, around the load at yielding of tension steel, the experimental strain readings decreased suddenly [figure 5.25 (a)]. This

strain decrease could be a result of strain gage malfunction or cracks in the adhesive at locations near the strain gages.

In specimens that experienced debonding failures (beams SSW70, CSSC2, SSSC2, and SSW195), the load-strain curve encounters load reversal (drop in load and strain) when debonding occurs. This is due to the loss of the composite action between the bonded reinforcement and the beam. In turn, this leads to (1) reduction in load due to the loss of the force contributed by CFRP reinforcement, and (2) release of strain in CFRP, since it's no longer connected to the beam. The FE post-debonding load-strain curve was capable of predicting this behavior and agreed well with the experimental trend.

It should be mentioned that in specimens that failed in concrete cover separation (CCS), as in beams CS70, SS70, CS195, and SS195, the reversal in load-strain curve is not captured by the FE models. This is a result of not explicitly including CCS in the simulations; rather, the failure load was estimated by post-processing analyses and failure criteria. It is possible to capture the reversal in the load-strain curve for beams that failed by CCS by modeling the interface between concrete cover and the rest of the beam as a cohesive zone material (CZM). Such models require the identification of the interface path (location and length) and CZM properties such as, interface shear stress, interface normal stress, slips, interface fracture energy, etc. The analytical procedure followed in section 5.5.2 provided sufficient predictions for the scope of this chapter, while FE modeling of the CCS failure as debonding surface (interface elements and CZM) will be highly recommended for future investigations.

5.5.5 Strain Profile along CRP and CFRP Laminate Length

Experimental and FE strain profiles along the length of the CFRP material, for several load levels up to 18 kN (4 kip), are presented in figure 5.26 for CRP-070 strengthened beams and in figure 5.27 for CFRP laminate strengthened beams. For CRP-195 strengthened beams, the strain profile plots are given in appendix C (figure C.3). The FE predicted strains along the CFRP length are seen to roughly agree with the experimental strain readings, although discrepancies exist between the two, at some locations within the CFRP length. These discrepancies are expected, considering the nonlinear nature of CFRP bonded RC beams, where concrete cracks, local debonding and interfacial slip at interior regions, among other factors, could have direct effects on the experimental strain measurements. In addition, the FE model contains some limitations, such as mesh size, and perfect-bond assumption at interfaces that didn't develop visible debonding failure (e.g. steel rebar/concrete interface).

5.5.6 Load versus Concrete Strain at Mid-Span

In the experiments, the concrete surface strains (i.e. compressive strain at top face and tensile strain at bottom face) were not measured at mid-span. It was assumed that any strain gage at these locations would give erroneous results as the load approaches the load at failure because of concrete cracking and crushing. Therefore, the validated FE models were used to extract these strains, and provide an insight on the behavior of concrete in compression and in tension, when different CFRP reinforcements are used as strengthening reinforcement (e.g. full-length CRP-070, two spliced CRP-070, etc.). Figure 5.28 plots the FE predicted load versus concrete surface strains at the top and bottom faces at mid-span,

for all modeled specimens. The figure shows that the compressive strains in specimens that failed by concrete crushing failure (control beam, beams strengthened with CFRP laminates) reached values between 0.004-0.005. Those values exceed the maximum compressive strain of 0.003, adopted in (ACI 318-14) code. For the same specimens, and considering the tensile strains, figure 5.28 shows that, after steel yielding (for the control beam) and steel yielding followed by debonding of the laminate (for the laminate strengthened beams), the load vs. tensile strain curve displayed a plateau. This plateau, indicates ductile response of the member and provides an ample warning against imminent failure.

On the other hand, the tensile and compressive strains in CRP-070 and CRP-195 strengthened beams increase with load after yielding of tension tensile steel until failure. When comparing CRP-070 (full-length or two spliced) with respective CFRP laminate, (CRP-070 and laminate have equal cross-sectional area), beams bonded to CRP-070 reached higher ultimate loads, but CFRP laminate bonded beams displayed larger ductility.

5.5.7 Tensile Stress Distribution in CRP and CFRP laminate

Since the specimens are tested under four-point loading, the maximum tensile stress in the strengthening CFRP reinforcement, is expected to appear in constant-moment region (between load points). Figure 5.29 shows, at a load level of 18 kN (4 kip), the tensile stress in the constant moment region for the full-length CFRP laminate, the full-length CRP-070, and the two spliced CRP-070. The tensile stresses in the constant moment region of the full-length and two spliced CRP-195 are shown in figure 5.30. Furthermore, figures C.4 to C.10 in appendix C present the tensile stresses of each CFRP reinforcement for the

following load stages: (1) immediately after cracking, (2) before steel yielding, (3) after steel yielding, and (4) at maximum load.

Figure 5.29 shows that, at $P = 18$ kN (4 kip), the maximum stress in the full-length CFRP laminate, full-length CRP-070, and two the spliced CRP-070, are of comparable magnitude. Also at $P = 18$ kN, the full-length and two spliced CRP-195, have comparable maximum tensile stress, as can be seen in figure 5.30. These above observations are also true at other load levels, as can be seen in figures C.4 to C.10 in Appendix C. The maximum tensile stress of the two spliced CRPs (i.e. CRP-070 or CRP-195) occurs just a few millimeters outside the rod overlap region, as shown in figures 5.29 and 5.30. The stress inside the overlap region is fairly uniform, and the magnitude of the average stress inside the overlap is almost half that of the maximum stress.

As the beam is subjected to four point loading, it is anticipated that the tensile stress profile be uniform within constant moment region. For the full-length CFRP laminate and CRPs, and considering the highly non-linear nature of RC members, the stresses are seen to be fairly uniform, except for segments adjacent to the load points. For spliced CRPs, the tensile stress profile within the constant moment region can no longer be expected to be uniform due to the overlapping and the fact that one panel has an extra rod.

5.5.8 Maximum Tensile Stress in CRP and CFRP laminate

The tensile stresses of each CFRP strengthening reinforcement, at maximum load, was extracted from FE results and are presented in table 5.3. Table 5.3 also shows the stress ratio for each reinforcement which is defined as the reinforcement's maximum tensile stress divided by the material's guaranteed tensile strength, as obtained from the

manufacturer. The FE predictions for the maximum stress ratio are summarized in the following paragraphs:

1- The stress ratio is 58% for full-length CRP-070, 53% for two-spliced CRP-070, 25% for full-length CFRP laminate, and 22% for spliced CFRP laminate system.

2- The stress ratio is 19% for the full-length CRP-195 and 22% for the two-spliced CRP-195. These values are less than half the stress ratios for the two spliced CRP-070. All four beams strengthened with full-length and spliced CRP-070 and CRP-195 failed at comparable loads by concrete cover separation. Consequently, the stress ratio in CRP-195 is expected to be lower than that in CRP-070, because CRP-195 cross-sectional area is 2.73 times the area of CRP-070.

3-The beam strengthened with two spliced CRP-070 anchored with CFRP fabrics achieved the largest stress ratio of 74%.

5.5.9 Interfacial Shear Stress distribution along CFRP Length

Generally, in experimental tests, the interfacial stress distribution of CFRP/concrete interface is indirectly determined from strain data measurement at the surface of the CFRP, by employing force equilibrium principles and simplistic relations for material properties. When reliable, validated FE models are available, the shear stress profile can directly and accurately be drawn. Interfacial shear stress distribution along CFRP length for beams strengthened with CRP-070 and CFRP laminate, obtained from FE analysis, at maximum load, are plotted in figures 5.31 to 5.33. For CRP-195, the interfacial shear stress distribution is plotted in figure C.11 (of appendix C).

For the full-length and spliced CRP-070 and CRP-195, the maximum shear stress occurs at CRP's end [figures 5.31, and C.11 (a, b)]. Figure 5.32, and C.11 (c) show that, when CFRP fabrics are attached at CRP ends, the maximum shear location is not at the CRP end but inside the strengthening length [225 mm (9 in.) from CRP's end] and at load points. For the full-length CFRP laminate, the maximum shear stress is roughly located 125 mm (5 in.) away from the laminate ends (figure 5.32).

In the beam strengthened with the spliced laminate system, the FE predicted shear stress distribution is presented in figure 5.33 for two interfaces, (1) CFRP main laminate/concrete interface, and (2) main laminate/splice interface. For the first interface, the maximum shear stress occurs at mid-span (the butt-joint between main laminates). For the second interface, although the maximum shear stress also exists at mid-span, but debonding initiated from splice ends and propagated toward mid-span, as can be seen in figure 5.33 (b). The FE predicted maximum interfacial shear and normal tensile (peeling) stresses for each CFRP reinforcement are presented in table 5.4. The locations of the maximum interfacial stresses along the strengthening length are listed in table 5.5.

5.6 Conclusions

A comprehensive 3D nonlinear finite element (FE) model was developed in this chapter to simulate the behavior of RC beams strengthened in flexure with CRPs and CFRP laminates. The model accounts for concrete nonlinear behavior in tension and compression, confinement effects on concrete compressive stress-strain relation, concrete cracking, and concrete crushing. The debonding failure of various reinforcement and interfaces was accounted for in the FE model by using cohesive zone material (CZM)

models as well as interface elements. The following conclusions can be outlined, based on the findings of this study:

(1) There is a good agreement between the FE and experimental results when comparing the load vs. mid-span deflection response, load vs. strain in CFRP at mid-span, and strain profile along CFRP length.

(2) Concrete cover separation failure was accurately predicted in the FE analysis by using post-processing analysis, along with tensile stress failure criteria for concrete.

(3) At failure, the FE results indicated that the CRP-070 is stressed to 58% and 53% of the guaranteed strength for the full-length panel and the two spliced panels, respectively. The CFRP laminate is stressed to 25% and 22% of the guaranteed strength for full-length laminate and the spliced laminate system, respectively.

(4) At all load levels, the maximum tensile stress in the full-length CFRP laminate, full-length CRP-070, and the two spliced CRP-070 are all of comparable magnitudes. For example, at a load of 18 kN (4 kip) in figure 5.29, the maximum tensile stress was 373.74 MPa (54.20 ksi) in the full-length CFRP laminate, 359.00 MPa (52.07 ksi) in the full-length CRP-070, and 390.80 MPa (56.68 ksi) in the spliced CRP-070. Also, the full-length and spliced CRP-195, have a comparable maximum tensile stresses at same load levels, figure 5.30.

(5) The maximum tensile stress of two spliced CRPs (i.e. CRP-070 or CRP-195) occurs at 12.5 mm (0.5 in.), outside the rod overlap region (figure 5.29 (c) and, and figure 5.30 (b, c). The stress inside the overlap region is fairly uniform, and the magnitude of the average stress inside the overlap is almost half the maximum stress.

(6) The FE models predicted a high shear stress concentration at the end of the CRPs in all beams strengthened with full-length or spliced CRPs. The fabric anchorage seems to be effective in shifting the location of maximum shear stress from the panel's end to inside the strengthening length [225 mm (9 in.) from CRP's end toward the center of the beam] and at load points [figure 5.31 (c)].

Table 5.1 Numerical parameters for CZM model of CFRP fabric and laminates.

Debonded region	τ_{\max} (MPa)	δ_t^c (mm)	δ_t^* (mm)
CFRP fabric from beam's side face	1.4 ^(a)	0.3 ^(b)	0.06 ^(b)
Full-length CFRP laminate from beam's bottom, at laminate-adhesive interface	1.75 ^(c)	0.3 ^(b)	0.06 ^(b)
CFRP splice laminate from the laminate system, at splice-adhesive interface.	3.75 ^(c)	0.3 ^(b)	0.06 ^(b)

^(a) Given by manufacturer, (Sika 2014).

^(b) Calculated from Lu et al 2005 model, equations 5.6 to 5.11

^(c) Determined from correlation analyses between FE models and the experiment. It should be noticed that for debonding of full-length laminate, and debonding of splice laminate and because the debonding was at laminate/adhesive interface, equation 5.6 of Lu et al 2005 model could not be used to determine τ_{\max} , since the model was derived for debonding at concrete/adhesive interface.

Table 5.2 (a) Comparisons between FE and experimental results at cracking, yielding, and maximum load stages, SI.

Beam code	Cracking				Yielding				Maximum			
	P_{test} (kN)	P_{FE} (kN)	Δ_{test} (mm)	Δ_{FE} (mm)	P_{test} (kN)	P_{FE} (kN)	Δ_{test} (mm)	Δ_{FE} (mm)	P_{test} (kN)	P_{FE} (kN)	Δ_{test} (mm)	Δ_{FE} (mm)
CB2	5.21	5.03	1.5	1	13.48	13.35	18.25	16	18.38	17.31	88.75	79
CS70	7.92	5.97	2.75	1.175	20.73	21.31	19.5	18.5	38.97	40.68	56.75	52.25
SS70	7.43	6.5	2	1.25	24.69	22.47	21.75	18	37.95	39.54	46	43
SSW70	7.52	7.12	2.5	3.25	28.03	23.09	26.5	18	47.42	45.37	70.5	58.5
CSSC2	6.99	6.9	2.5	1.25	18.46	22.16	15.75	16.75	27.36	26.69	26	23.25
SSSC2	8.01	7.74	2	2.75	19.49	23.36	13.75	16.25	24.25	24.56	19.5	18
CS195	7.43	5.34	2.25	1	30.25	— ⁽¹⁾	18.25	— ⁽¹⁾	37.41	35.08	24.25	21
SS195	7.21	5.39	2.25	1	— ⁽¹⁾	36.00	— ⁽¹⁾	20.75	35.81	36.84	23.5	20.5
SSW195	7.92	7.3	2.5	2.25	45.51	39.15	29.75	21.75	54.18	59.21	39	42.75

⁽¹⁾ Value is not observed in the analysis.

Table 5.2 (b) Comparisons between F.E and experimental results at cracking, yielding, and maximum load stages, US.

Beam code	Cracking				Yielding				Maximum			
	P_{test} (kip)	P_{FE} (kip)	Δ_{test} (in.)	Δ_{FE} (in.)	P_{test} (kip)	P_{FE} (kip)	Δ_{test} (in.)	Δ_{FE} (in.)	P_{test} (kip)	P_{FE} (kip)	Δ_{test} (in.)	Δ_{FE} (in.)
CB2	1.17	1.13	0.07	0.04	3.03	3.00	0.73	0.64	4.13	3.89	5.11	3.16
CS70	1.78	1.34	0.11	0.05	4.66	4.79	0.78	0.74	8.76	9.14	2.27	2.09
SS70	1.67	1.46	0.08	0.05	5.55	5.05	0.87	0.72	8.53	8.88	1.84	1.72
SSW70	1.69	1.6	0.10	0.13	6.30	5.19	1.06	0.72	10.66	10.2	2.82	2.34
CSSC2	1.57	1.55	0.10	0.05	4.15	4.98	0.63	0.67	6.15	6	3.93	0.93
SSSC2	1.80	1.74	0.08	0.11	4.38	5.25	0.55	0.65	5.45	5.52	3.54	0.72
CS195	1.67	1.2	0.09	0.04	6.80	— ⁽¹⁾	0.73	— ⁽¹⁾	8.41	7.88	0.97	0.84
SS195	1.62	1.21	0.09	0.04	— ⁽¹⁾	8.09	— ⁽¹⁾	0.83	8.05	8.28	0.94	0.82
SSW195	1.78	1.64	0.10	0.09	10.23	8.8	1.19	0.87	12.18	13.31	1.57	1.71

⁽¹⁾ Value is not observed in the analysis.

Table 5.3 Stress at maximum, and stress ratio for CFRP strengthening reinforcements, obtained from the FE simulations.

Beam code.	Strengthening reinforcement	Tensile stress at maximum load		Stress ratio ⁽³⁾ %
		MPa	ksi	
CS70	Full-length CRP-070 ⁽¹⁾	1282	186	58
SS70	Two spliced CRP-070 ⁽¹⁾	1172	170	53
SSW70	Two spliced CRP-070 ⁽¹⁾ , anchored with CFRP fabric	1641	238	74
CS195	Full-length CRP-195 ⁽²⁾	427	62	19
SS195	Two spliced CRP-195 ⁽²⁾	496	72	22
SSW195	Two spliced CRP-195 ⁽²⁾ , anchored with CFRP fabric	958	139	43
CSSC2	Full-length CFRP laminate ⁽¹⁾	689	100	25
SSSC2	Spliced CFRP laminate system ⁽¹⁾	620	90	22

⁽¹⁾ CRP-070 and CFRP laminate have an equal CFRP area of 64 mm² (100 x 10⁻³ in²).

⁽²⁾ CRP-195 has a CFRP area of 173 mm² (268 x 10⁻³ in²).

⁽³⁾ Stress ratio is calculated by dividing the tensile stress at maximum load for each reinforcement by its guaranteed tensile strength. The guaranteed tensile strength, obtained from the manufacturer, for CFRP rods is 2340 MPa (320 ksi), and for CFRP laminate is 2800 MPa (406 ksi).

Table 5.4 FE predicted interfacial shear and peeling stresses, at maximum load.

Beam code	Strengthening material	Maximum load		Interfacial shear stress		Interfacial peeling stress	
		kN	kip	MPa	ksi	MPa	ksi
CS70	Full-length CRP-070 ⁽¹⁾	40.7	9.1	9.47	1.37	1.6	0.22
SS70	Two spliced CRP-070 ⁽¹⁾	39.5	8.9	13.00	1.90	3.15	0.46
SSW70	Two spliced CRP-070 ⁽¹⁾ , with fabric anchorage	45.4	10.2	6.17	0.89	2.68	0.39
CS195	Full-length CRP-195	35.0	7.9	11.36	1.65	0.92	0.133
SS195	Two spliced CRP-195	36.8	8.3	9.11	1.32	1.83	0.27
SSW195	Two spliced CRP-195, with fabric anchorage	59.2	13.3	5.82	0.84	1.20	0.17
CSSC2	Full-length CFRP laminates ⁽¹⁾	26.7	6.0	4.44	0.64	2.00	0.29
SSSC2⁽²⁾	Spliced CFRP laminate system ⁽¹⁾	24.0	5.5	14.7	2.14	3.6	0.52
SSSC2⁽³⁾	=	=	=	3.93	0.57	0.48	0.07

⁽¹⁾ CFRP laminate and CRP-070 are of equal cross-sectional area [64 mm² (100 x 10⁻³ in²)].

⁽²⁾ Results are for the interface between CFRP main laminate and concrete (interface 1).

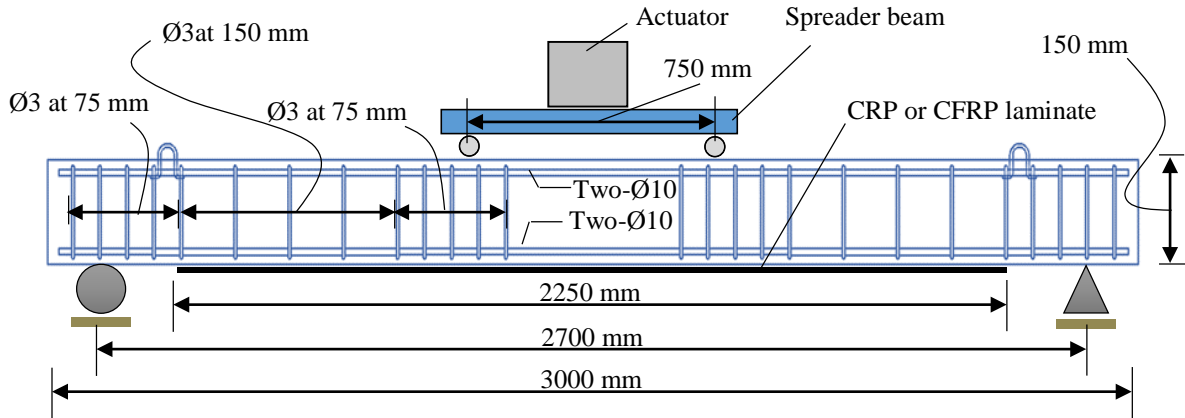
⁽³⁾ Results are for the interface between CFRP main laminate and splice (interface 2).

Table 5.5 FE predicted locations of maximum shear and peeling stresses.

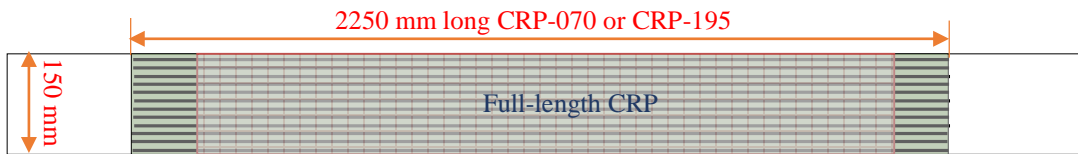
Beam code	Location of maximum shear stress	Location of maximum peeling stress
CS70	Panel ends	150 mm (6 in.) from Panel ends
SS70	Panel ends	Edge of rods overlap [75 mm (3 in.) from mid-span]
SSW70	At fabric termination [75 mm (3 in.) from Panel ends]	Edge of rods overlap [75 mm (3 in.) from mid-span]
CS195	Panel ends	425 mm (17 in.) from Panel ends
SS195	Panel ends	Edge of rods overlap [75 mm (3 in.) from mid-span]
SSW195	At fabric termination [75 mm (3 in.) from Panel ends]	Edge of rods overlap [75 mm (3 in.) from mid-span]
CSSC2	125 mm (5 in.) from laminate ends	Near load points
SSSC2 ⁽¹⁾	At mid-span (butt joint)	Laminate ends
SSSC2 ⁽²⁾	=	Near load points

⁽¹⁾ Results are for the interface between CFRP main laminate and concrete (interface 1).

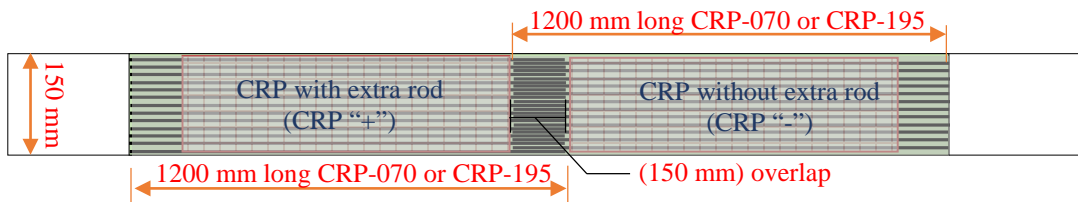
⁽²⁾ Results are for the interface between CFRP main laminate and splice (interface 2).



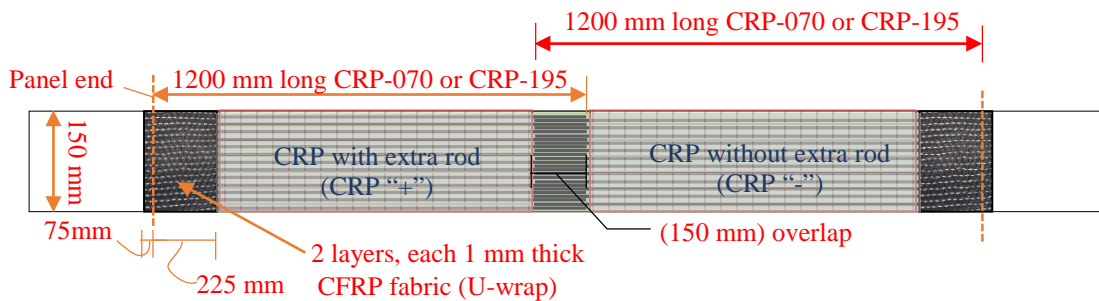
(c) RC beam details



(b) Bottom face of RC beam strengthened with full-length CRP (CRP-070, CRP-195)



(c) Bottom face of RC beam strengthened with spliced CRP (CRP-070, CRP-195)



(d) Bottom face of RC beam strengthened with spliced CRP (CRP-070, CRP-195) and anchored at panel's ends with CFRP fabrics

Figure 5.1 (a) Geometry of experimental RC beams, CRP strengthening technique.

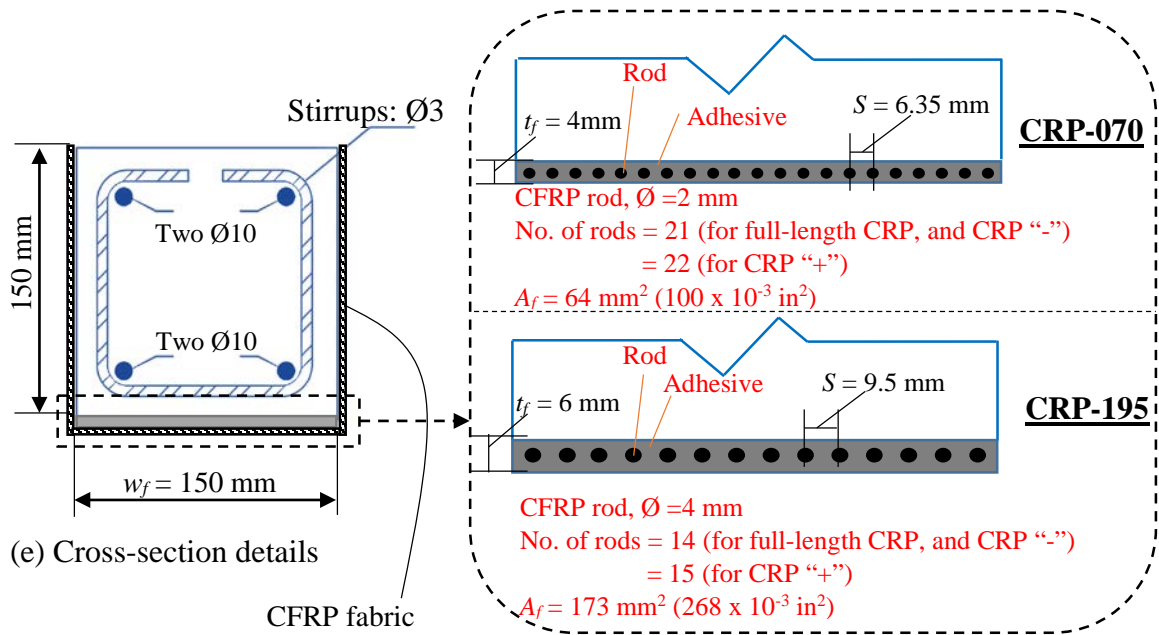


Figure 5.1 (a) (continued) Geometry of experimental RC beams, CRP strengthening technique, dimensions in mm.

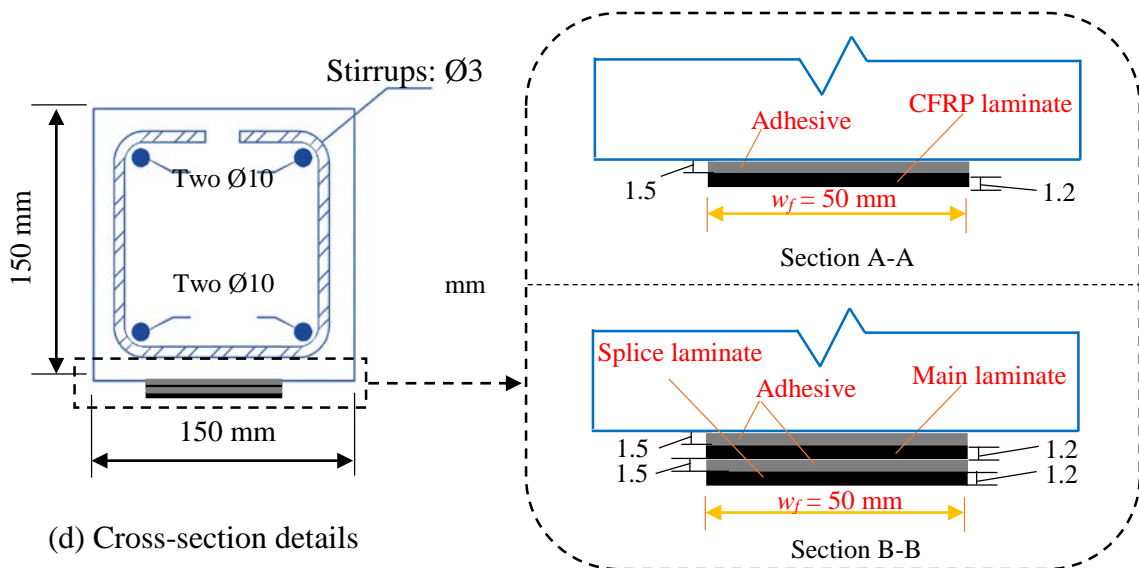
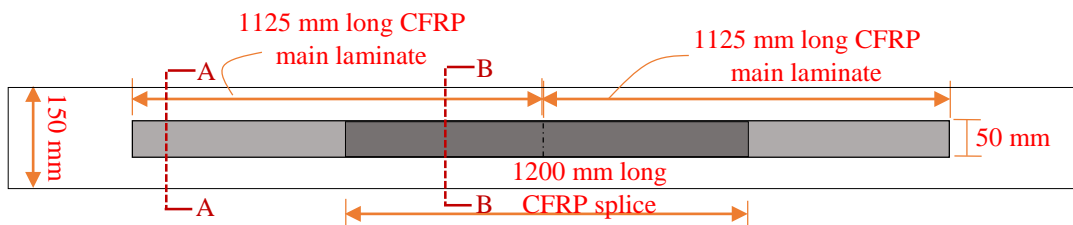
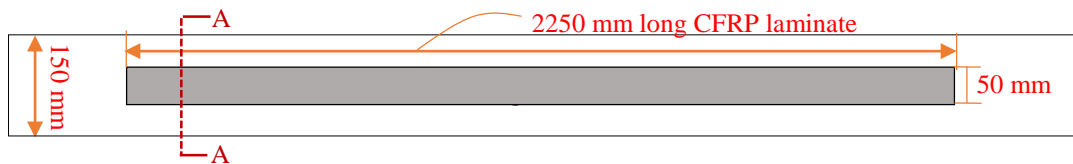
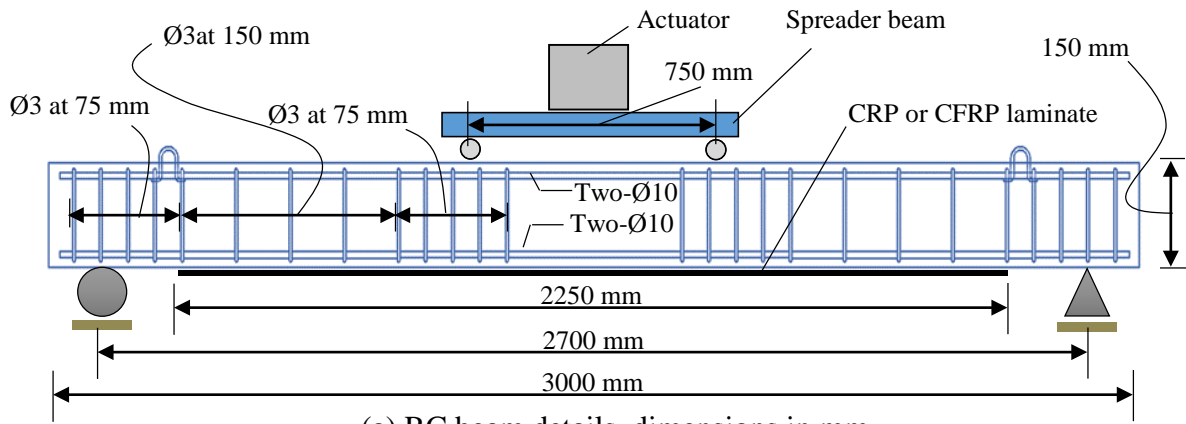
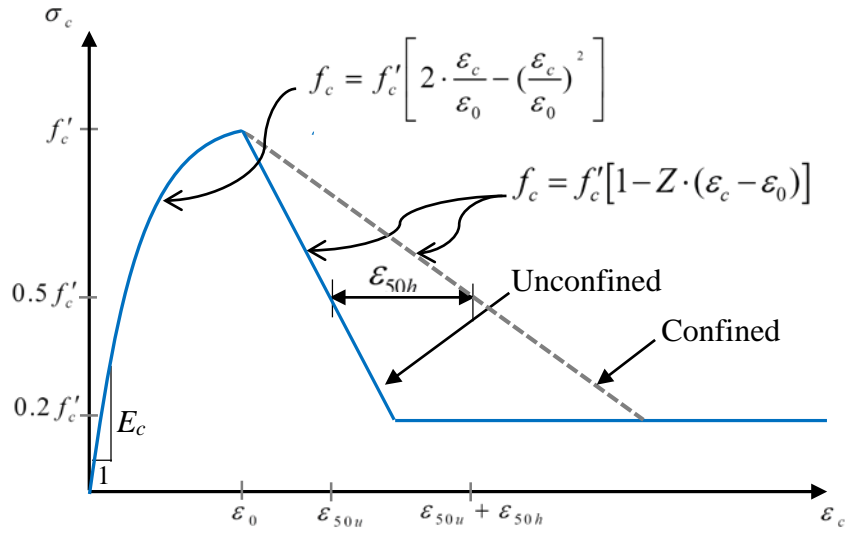
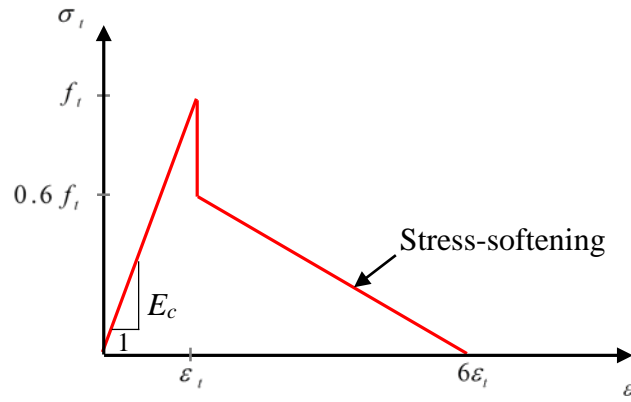


Figure 5.2 Geometry of experimental RC beams, CFRP laminate strengthening technique, dimensions in mm.



(a) Compressive stress-strain curve



(b) Tensile stress-strain curve

Figure 5.3 concrete constitutive material models.

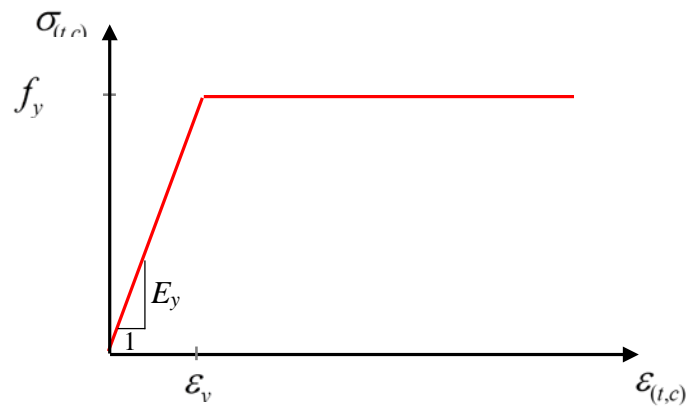


Figure 5.4 Steel constitutive material model.

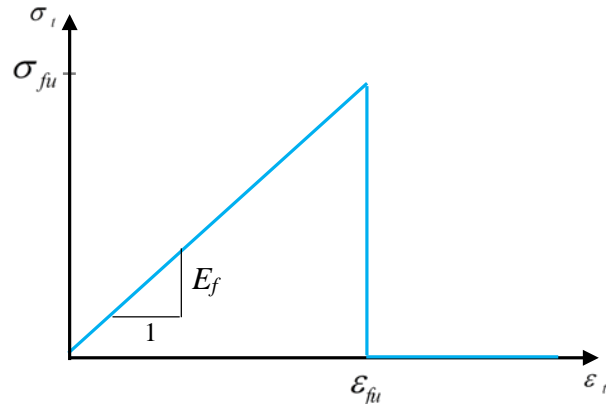


Figure 5.5 Uniaxial stress-strain response of CFRP components and adhesives.

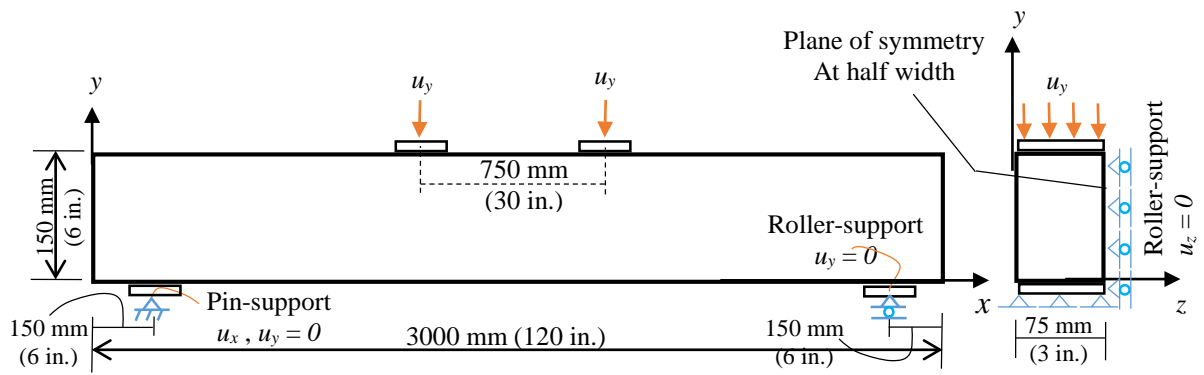
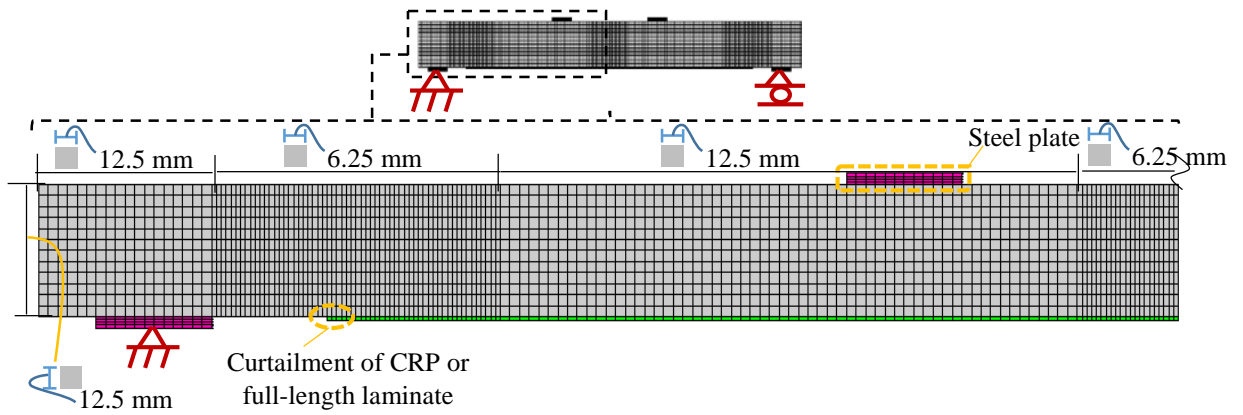
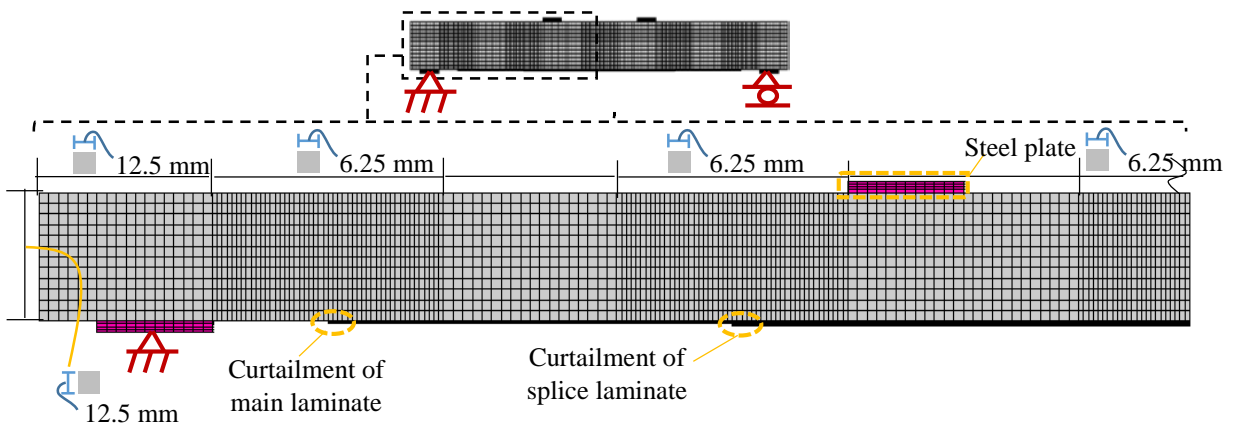


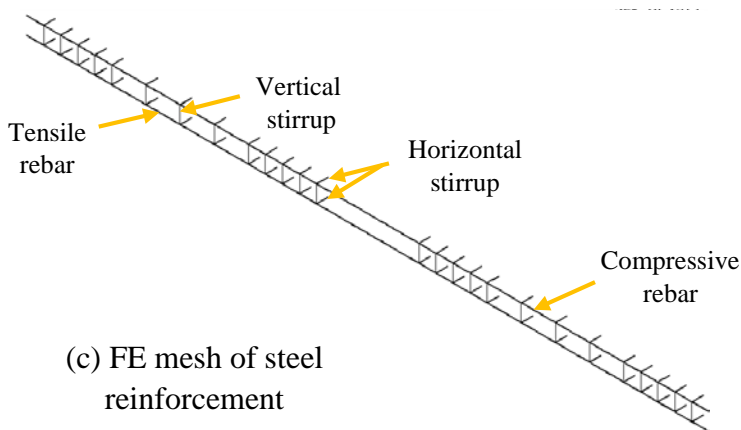
Figure 5.6 Boundary conditions and loading scheme of FE models.



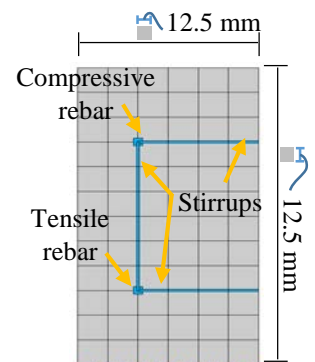
(a) FE mesh for (1) control beam, (2) strengthened with CRP's, (3) strengthened with full-length CFRP laminate



(b) FE mesh for RC beam strengthened with spliced CFRP laminate

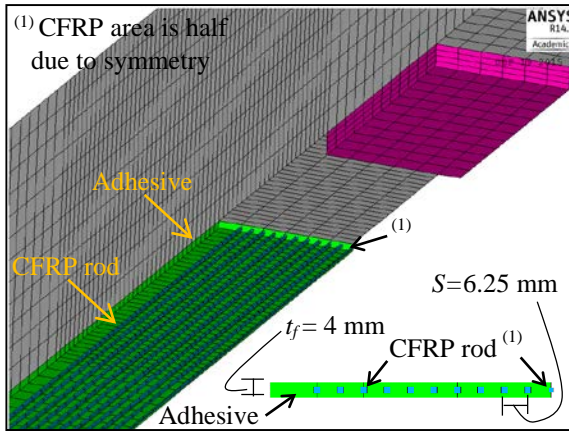
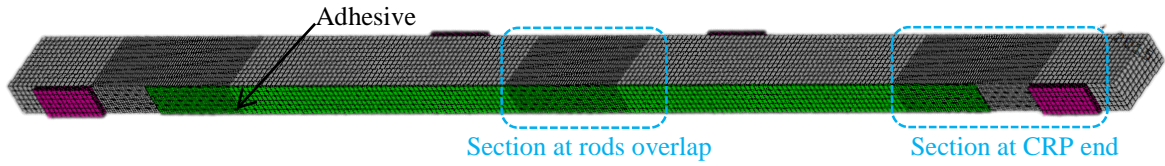


(c) FE mesh of steel reinforcement

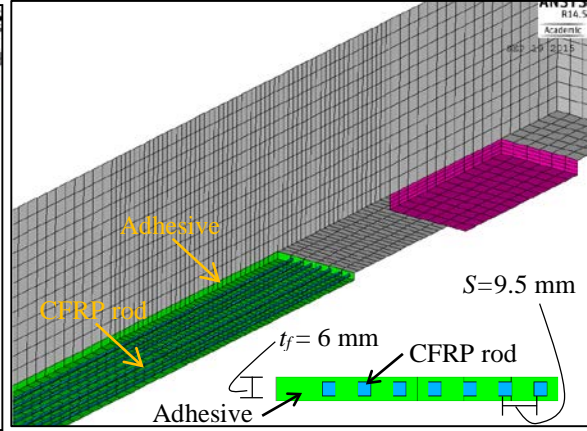


(d) Cross-section of the model

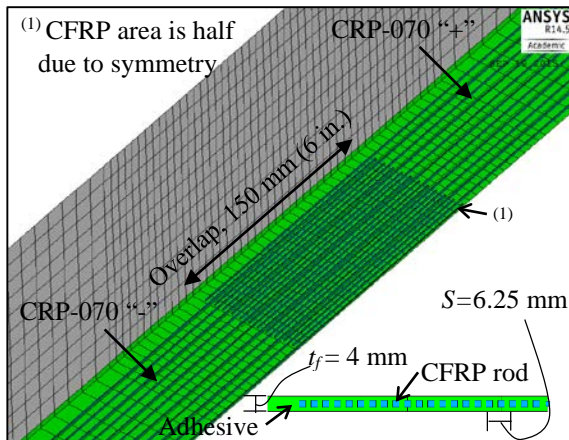
Figure 5.7 FE mesh of RC beams strengthened with CRPs or CFRP laminates.



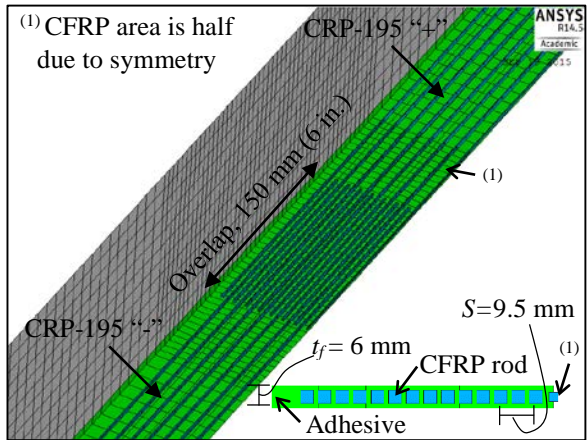
(a) FE model of CFRP rods at CRP end for beams strengthened with full-length CRP-070



(b) FE model of CFRP rods at CRP end for beams strengthened with full-length CRP-195



(c) FE model of CFRP rods at overlap for beams strengthened with spliced CRP-070



(d) FE model of CFRP rods at overlap for beams strengthened with full-length CRP-070

Figure 5.8 FE mesh of RC beams strengthened with CRPs, showing FE model of CFRP rods at overlap and CRP end locations.

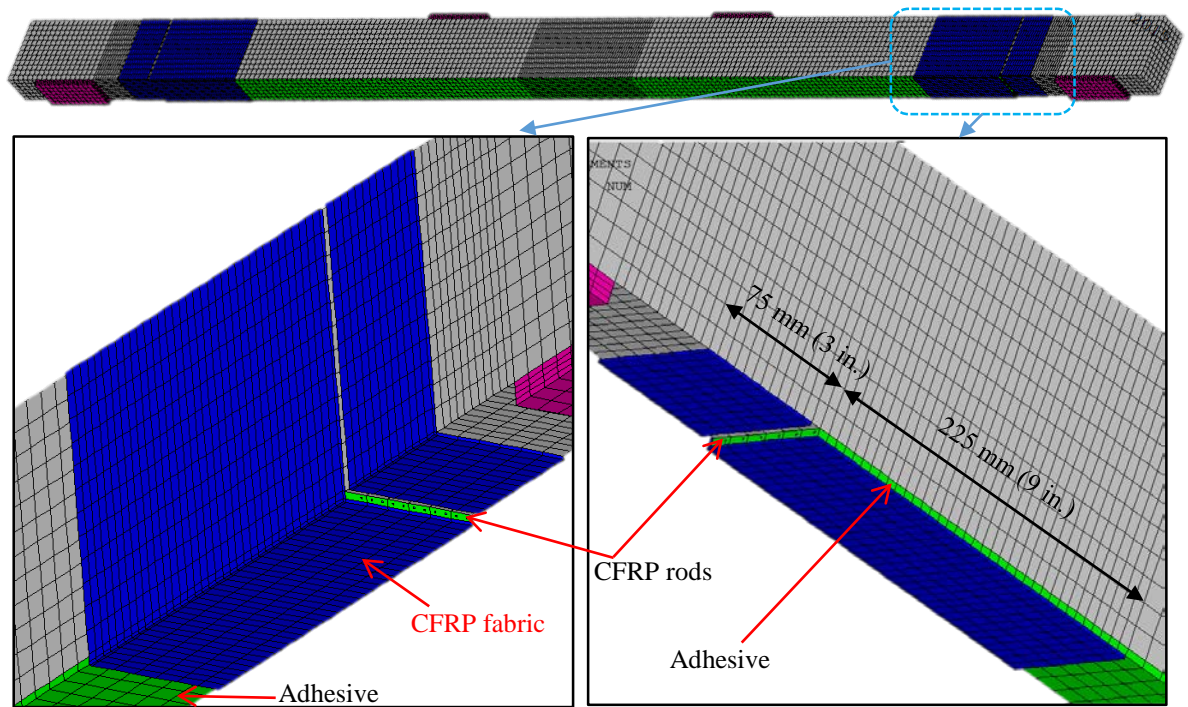


Figure 5.9 FE mesh of RC beams strengthened with spliced CRPs, and anchored at CRP ends with CFRP fabrics.

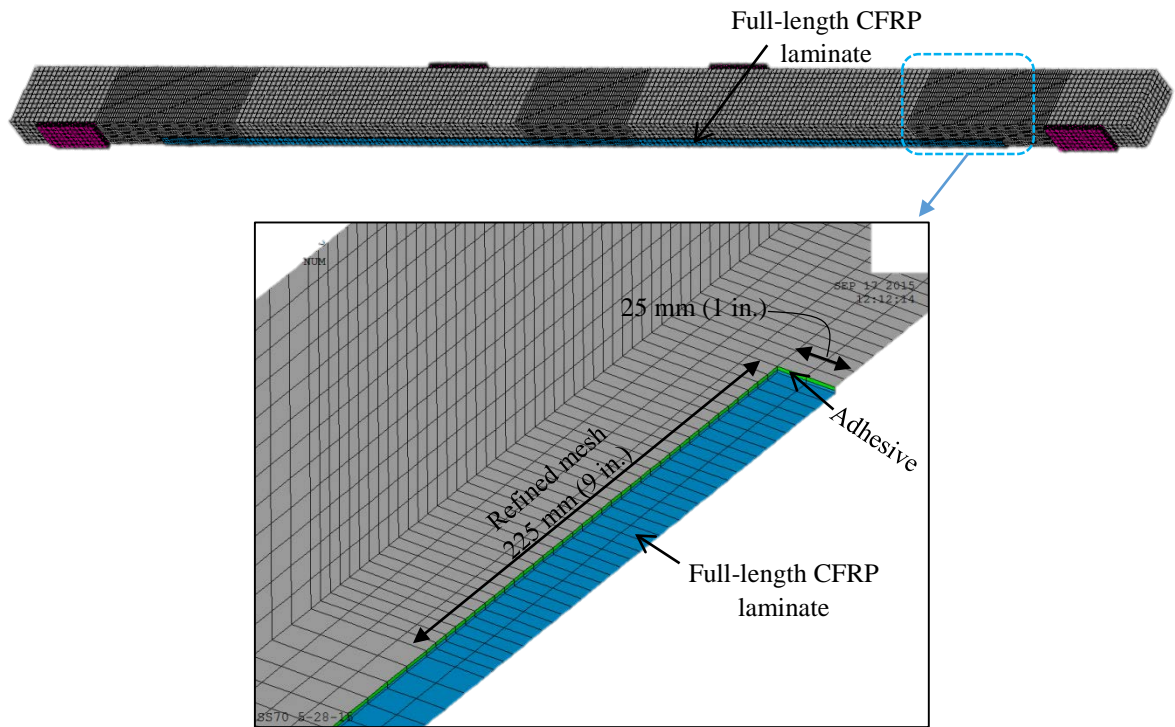


Figure 5.10 FE mesh of RC beams strengthened with full-length CFRP laminate.

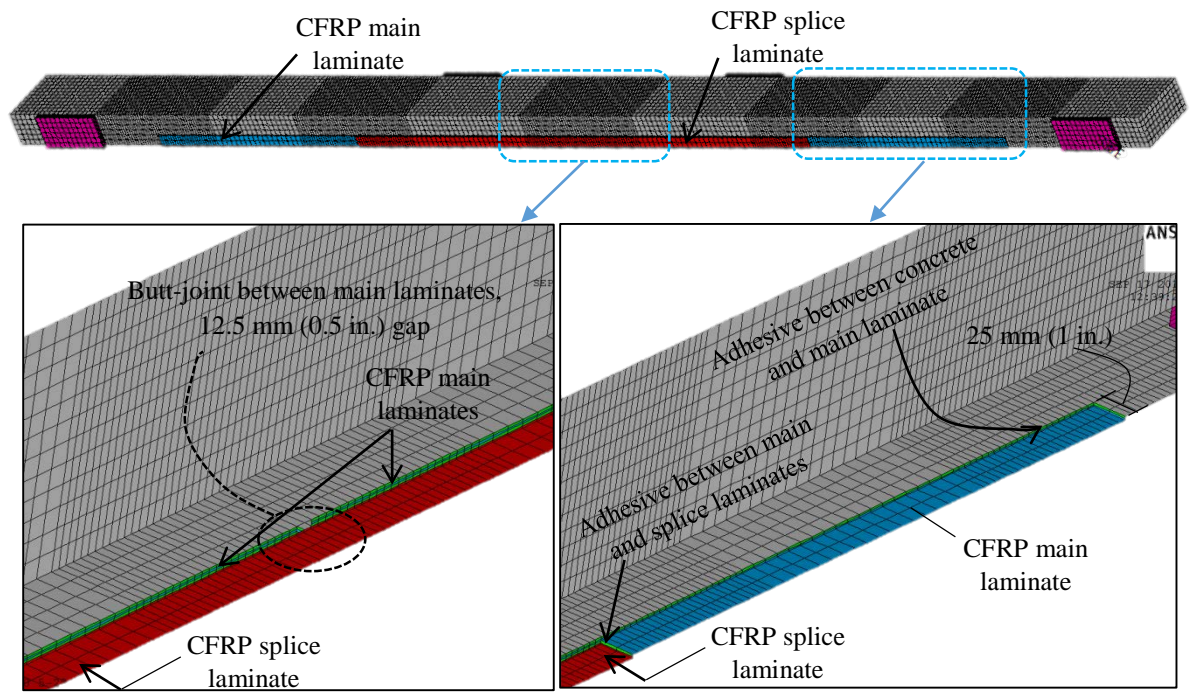


Figure 5.11 FE mesh of RC beams strengthened with spliced CFRP laminate system.

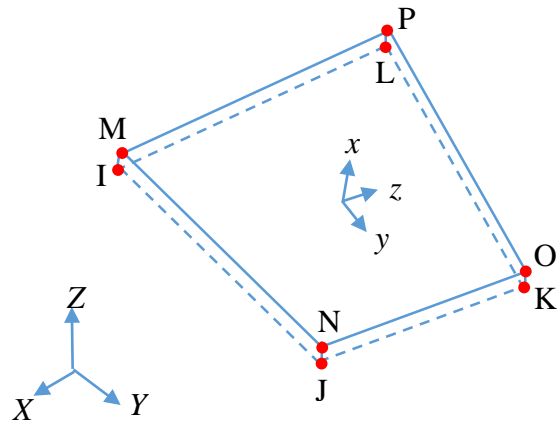
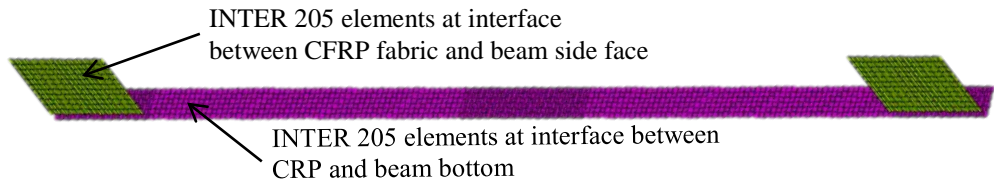
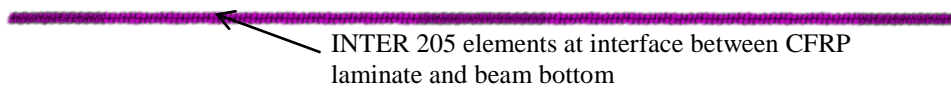


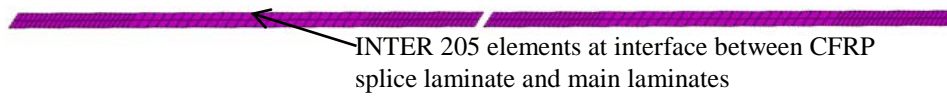
Figure 5.12 Geometry of INTER 205 element (after ANSYS 2012).



(a) Beams strengthened with spliced CRPs and anchored with CFRP fabrics



(b) Beam strengthened with full-length CFRP laminate



(c) Beam strengthened with full-length CFRP laminate

Figure 5.13 FE simulation of debonding at various interfaces by INTER 205 element.

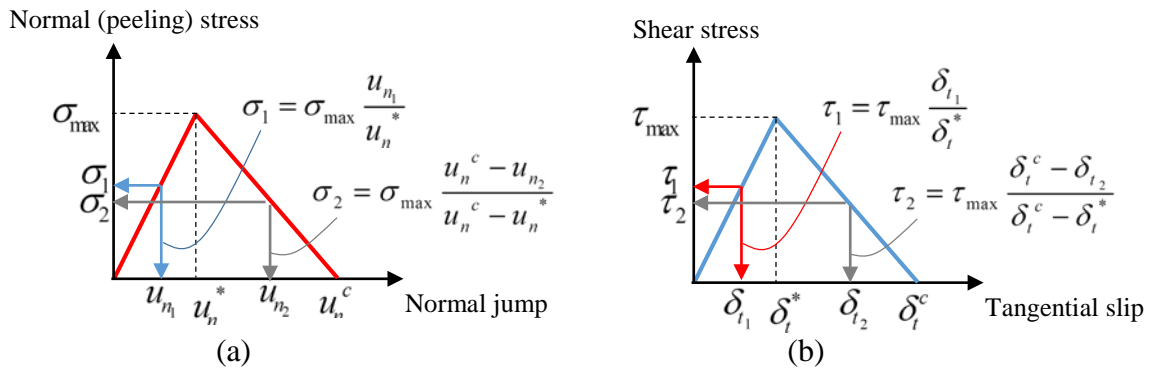


Figure 5.14 Bilinear CZM model (a) normal (peeling) debonding, (b) shear debonding.

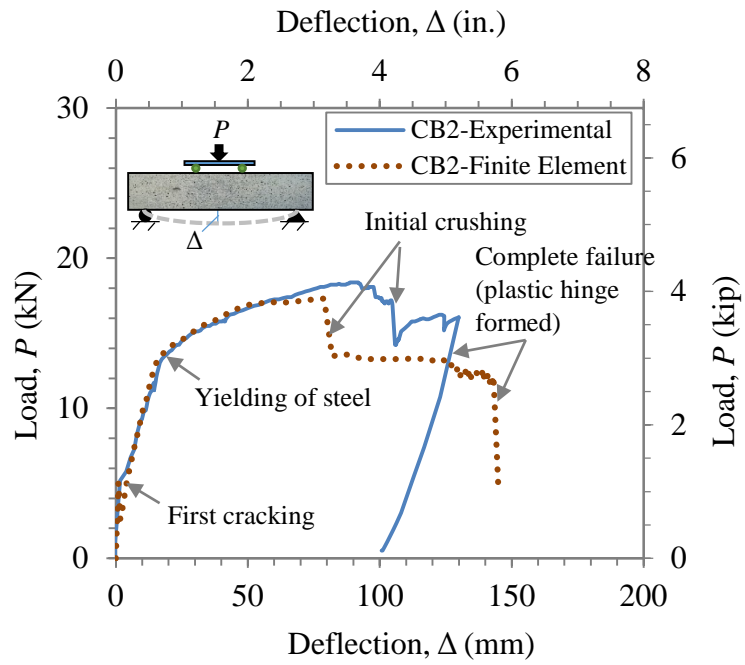
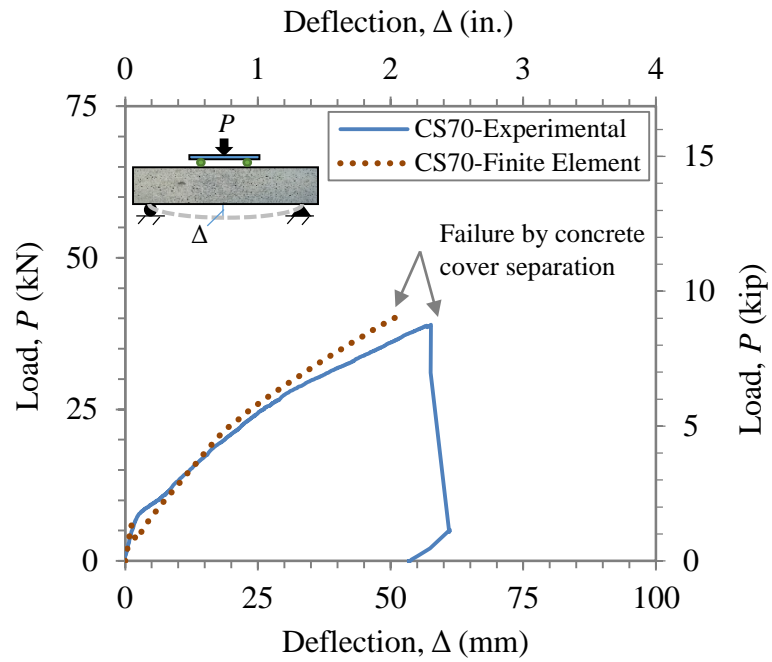
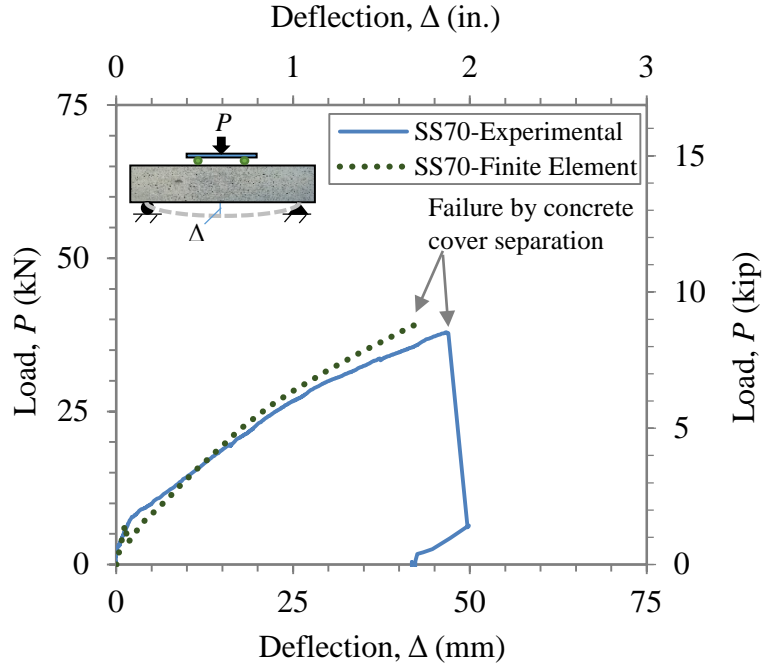


Figure 5.15 Load-mid span deflection comparisons, between experiment and FE, for Control beam (specimen CB2).

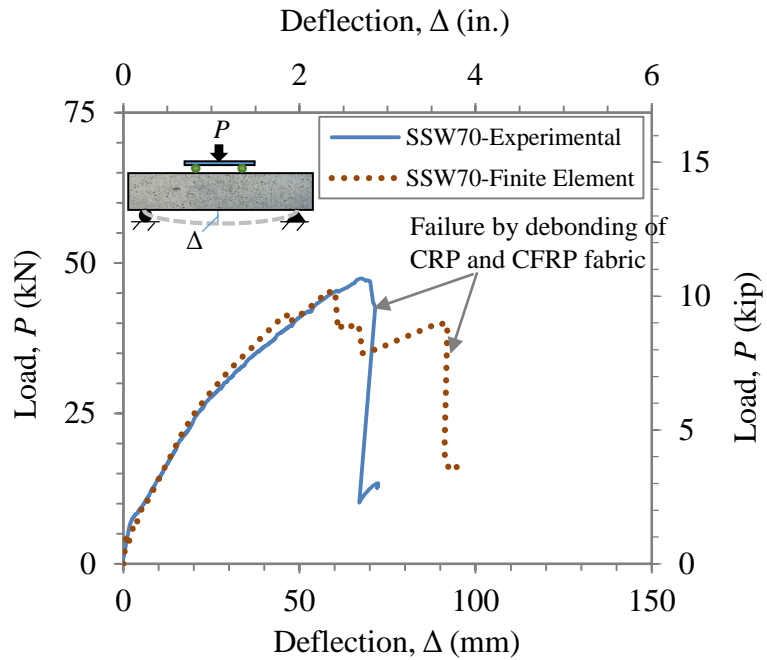


(a) Strengthened with full-length CRP-070 (specimen CS70)

Figure 5.16 Load-mid span deflection comparisons, between experiment and FE, for beams strengthened with CRP-070.

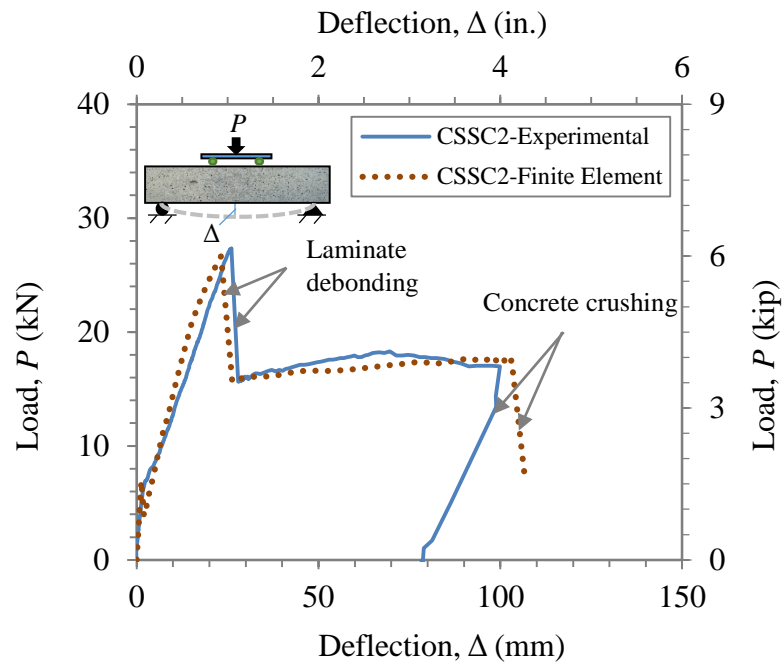


(b) Strengthened with two spliced CRP-070 (specimen SS70)

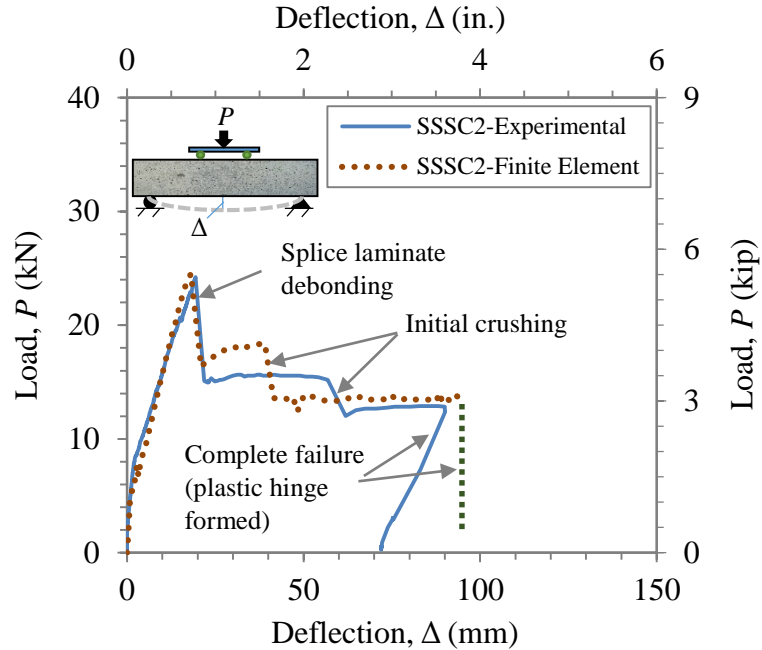


(c) Strengthened with two spliced CRP-070, anchored with fabric (specimen SSW70)

Figure 5.16 (continued) Load-mid span deflection comparisons, between experiment and FE, for beams strengthened with CRP-070.



(a) Strengthened with full-length CFRP laminate (specimen CSSC2)



(b) Strengthened with spliced CFRP laminate system (specimen SSSC2)

Figure 5.17 Load-mid span deflection comparisons, between experiment and FE, for beams strengthened with CFRP laminates.

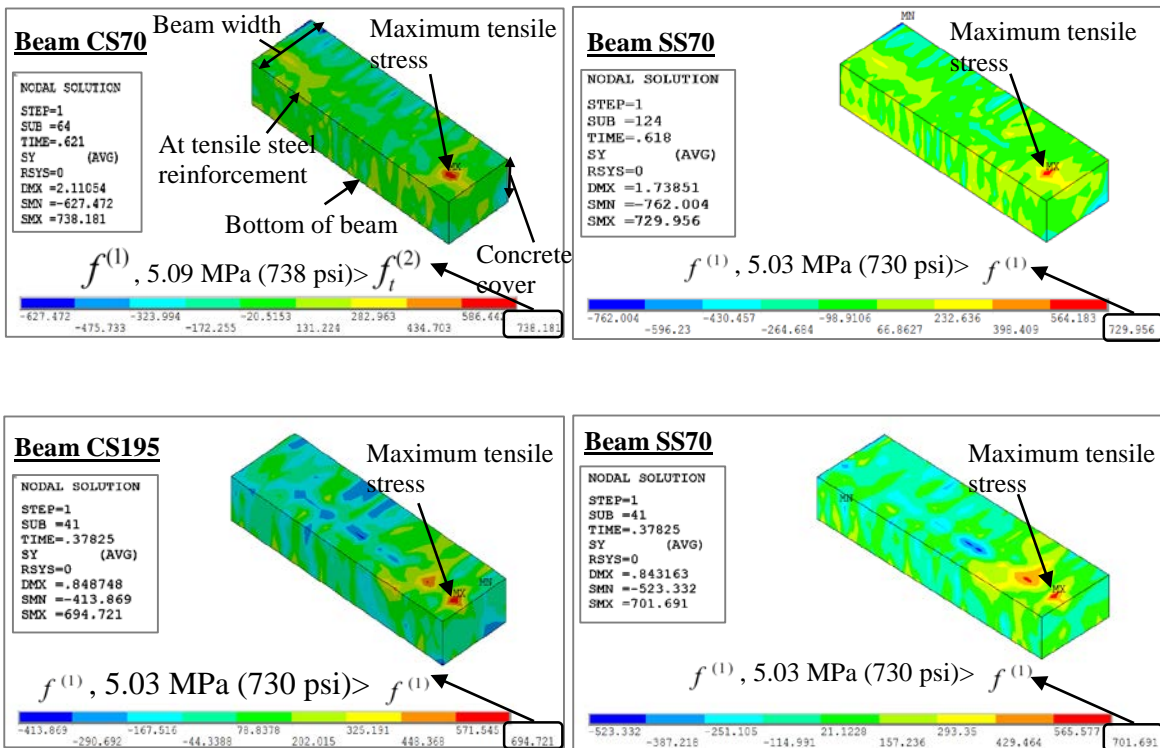
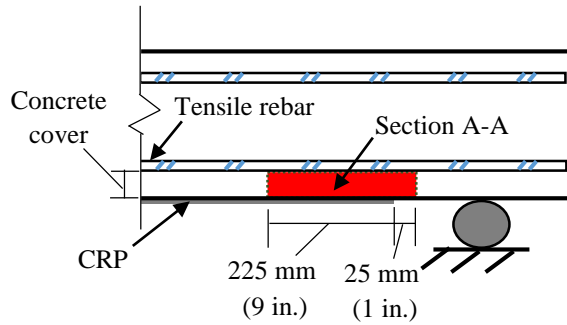
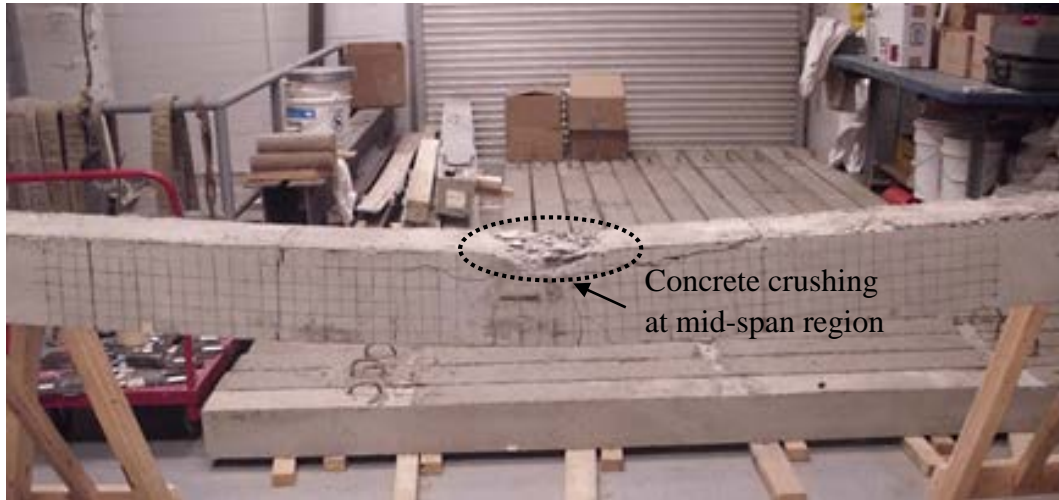
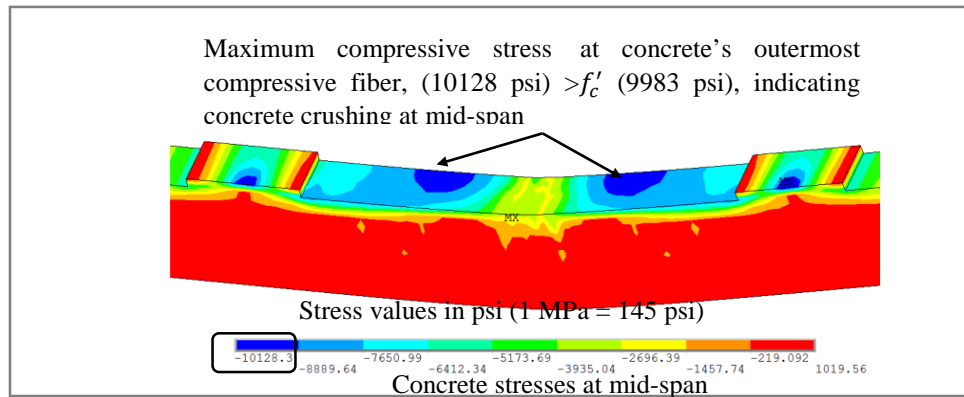


Figure 5.18 Normal stress distribution of section A-A.

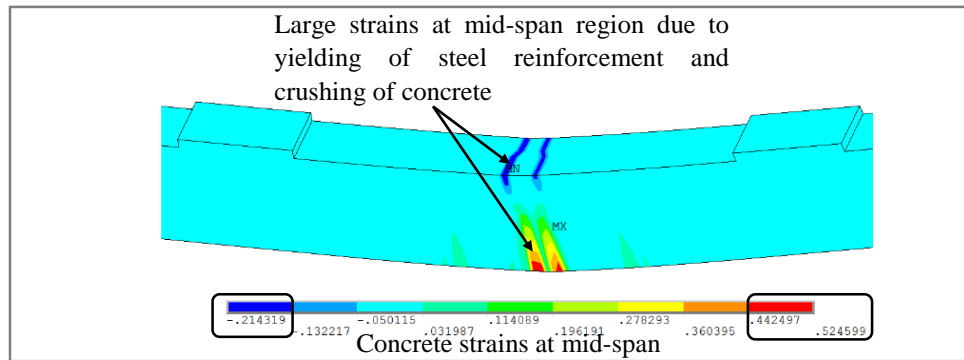
- (1) Maximum normal tensile stress in concrete, of the concrete section near CRP end, from post processing of FE results.
- (2) Concrete tensile strength, calculated from ACI-11 and given by $[f_t = 0.56 \sqrt{f'_c}]$, where f'_c is concrete compressive strength, (f_t and f'_c) are in MPa units].



(a) Experimental specimen



(d) FE model showing large compressive concrete stresses at mid-span



(c) FE model showing large strains at mid-span

Figure 5.19 FE simulation of concrete crushing failure of control beam (beam CB2).

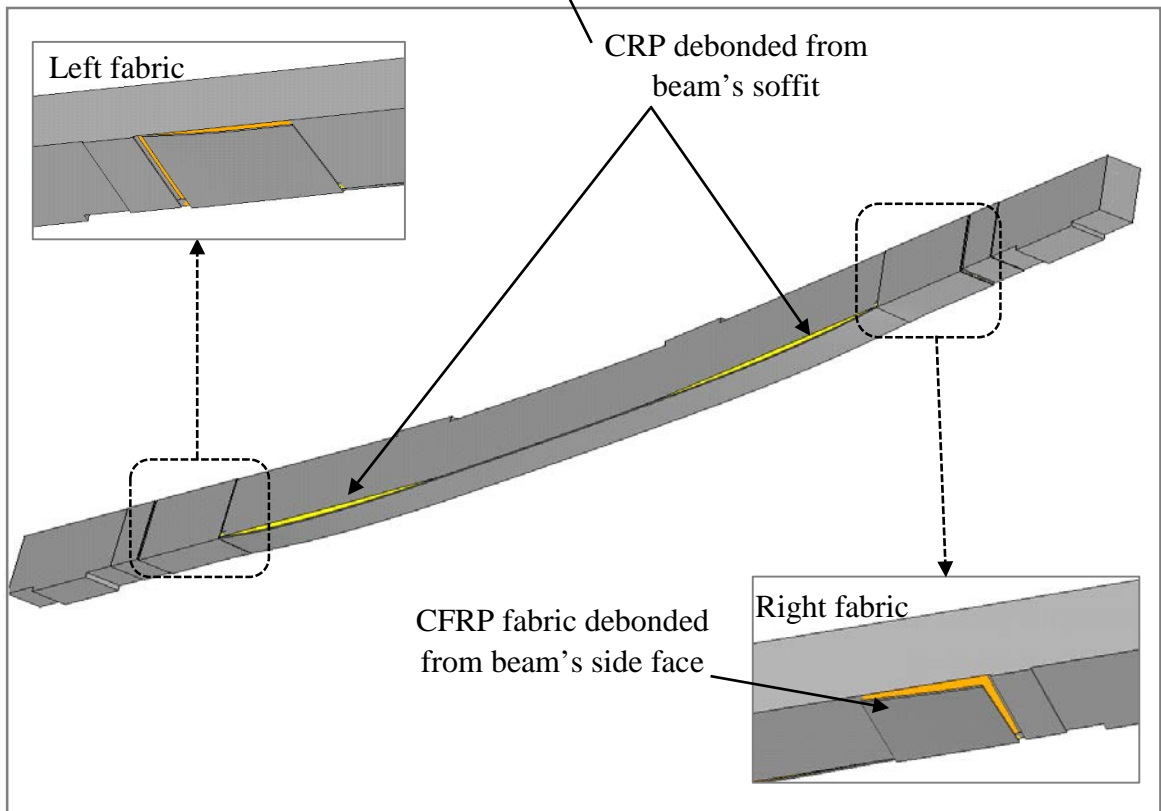


Figure 5.20 FE simulation for debonding of the beam strengthened with two spliced CRP-070, and anchored with CFRP fabric (beam SSW70).

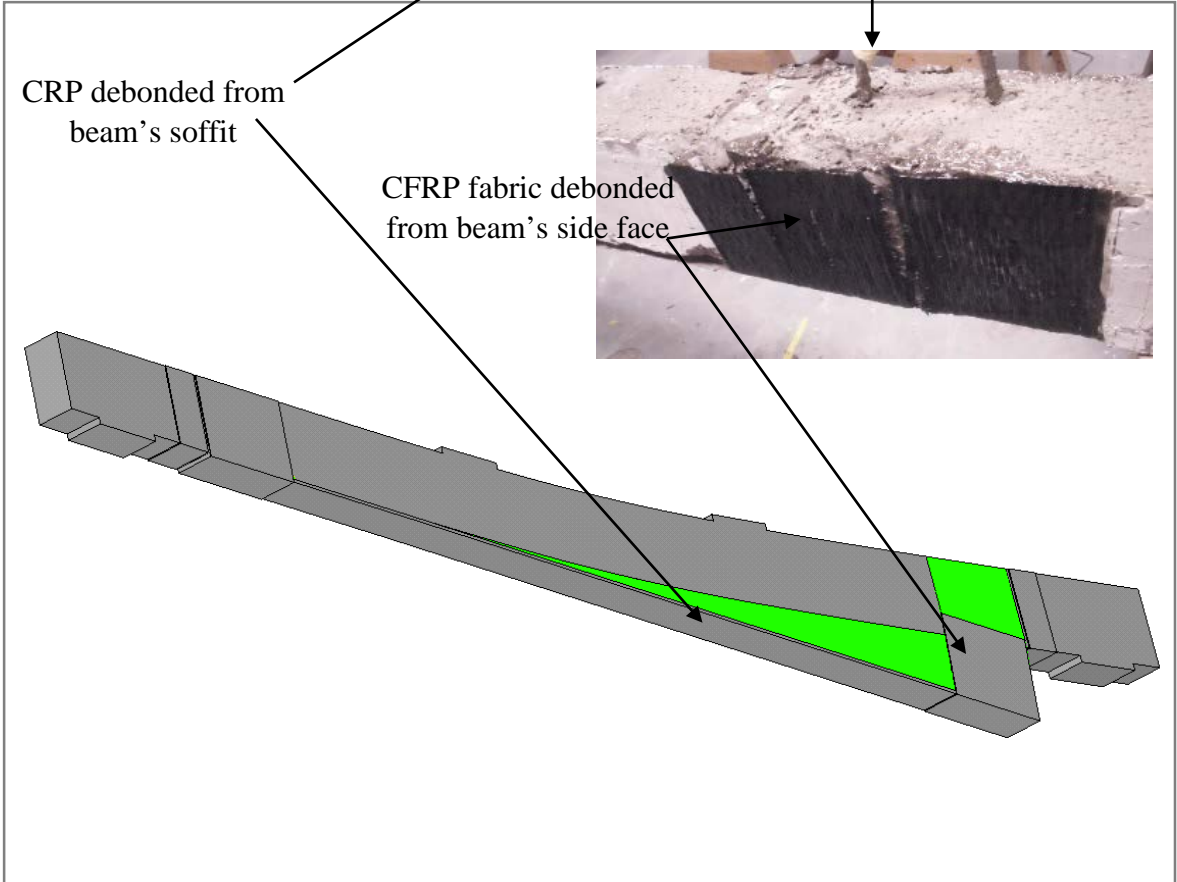
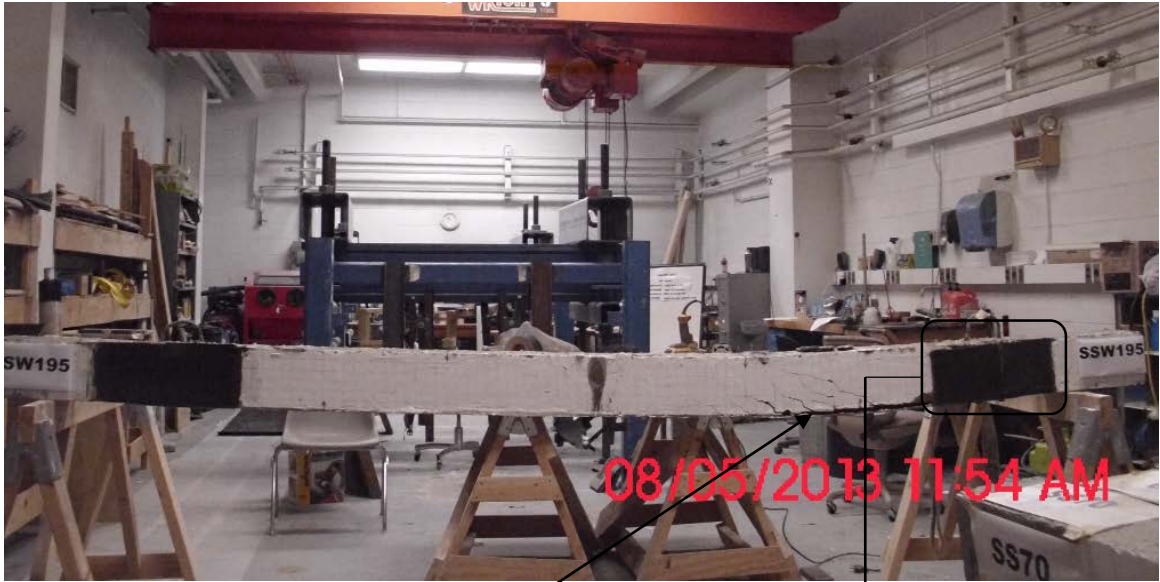


Figure 5.21 FE simulation for debonding of the beam strengthened with two spliced CRP-195, and anchored with CFRP fabric (beam SSW195).

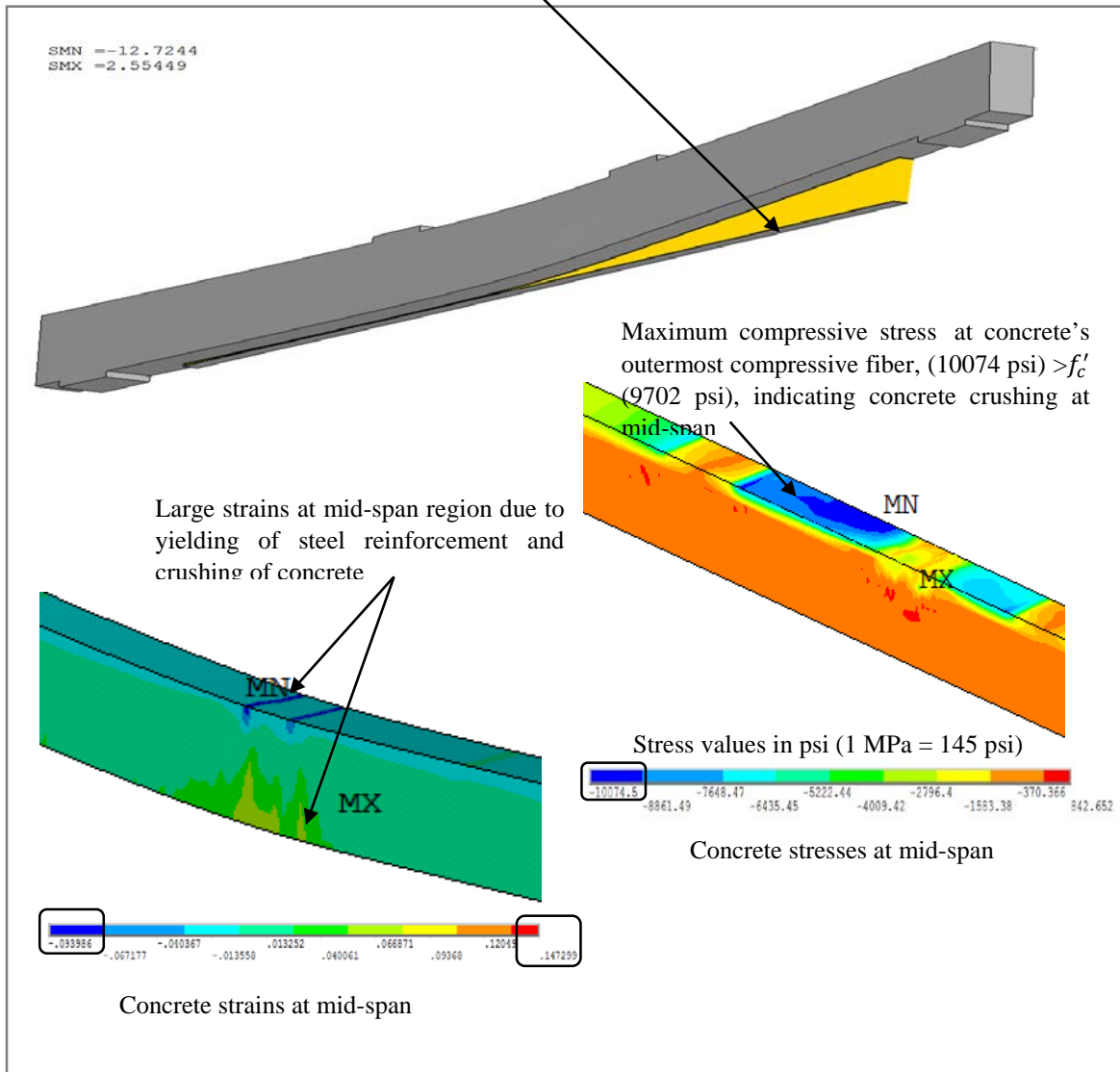
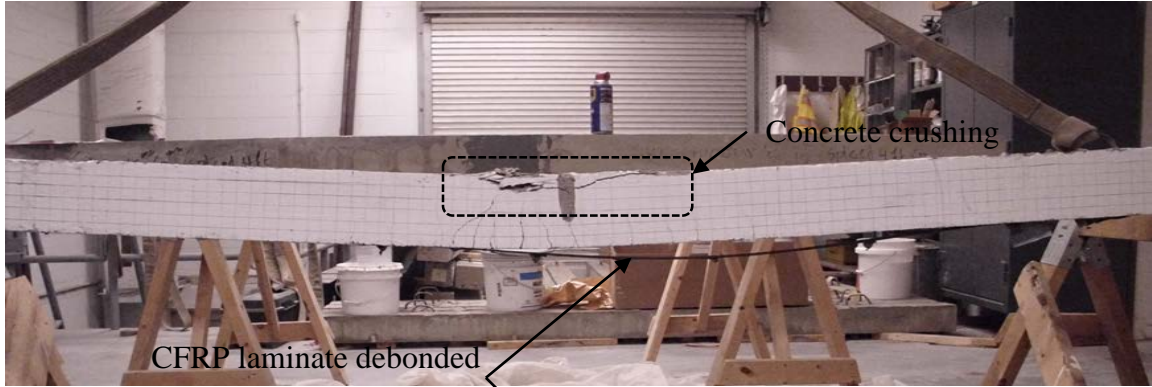


Figure 5.22 FE simulation for debonding and concrete crushing failures of the beam strengthened with full-length CFRP laminate (beam CSSC2).

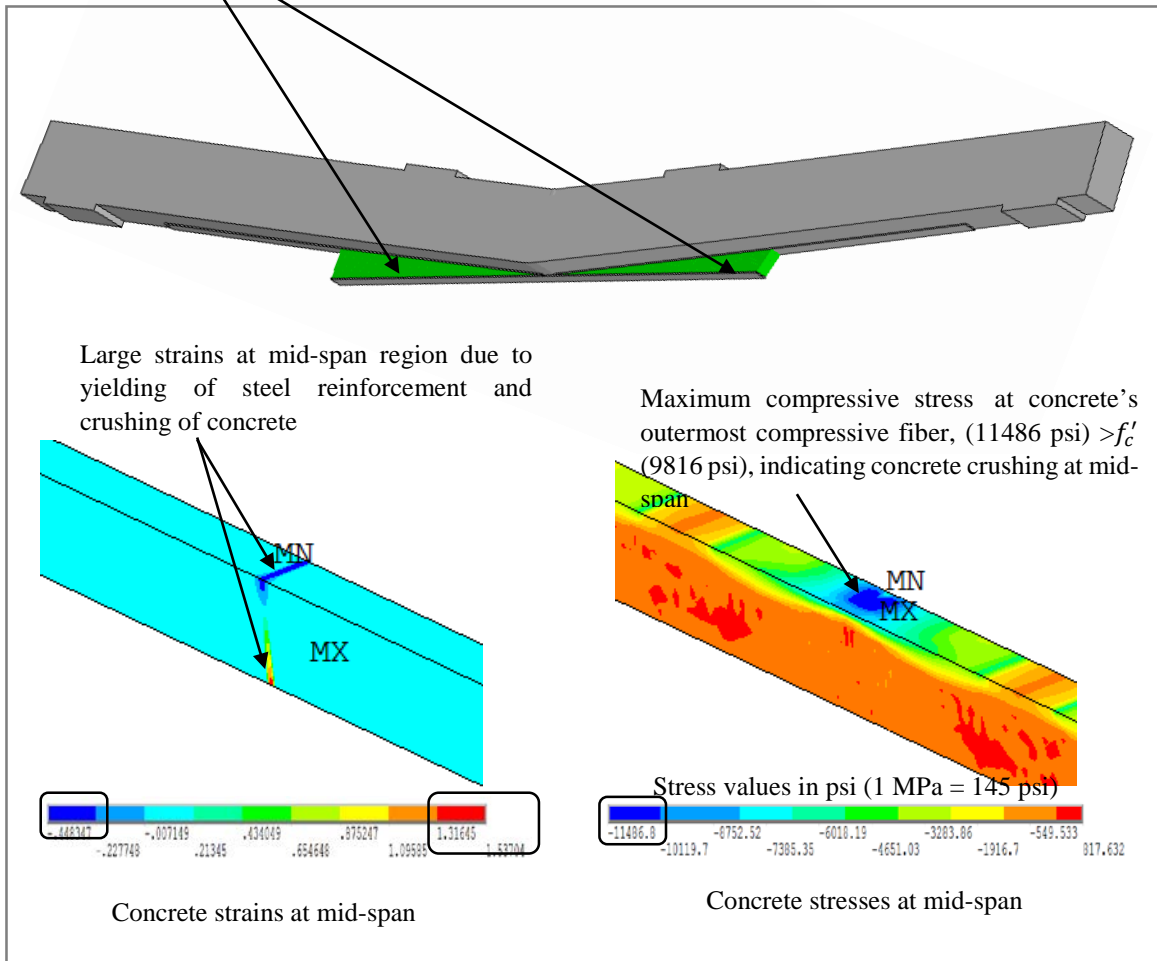
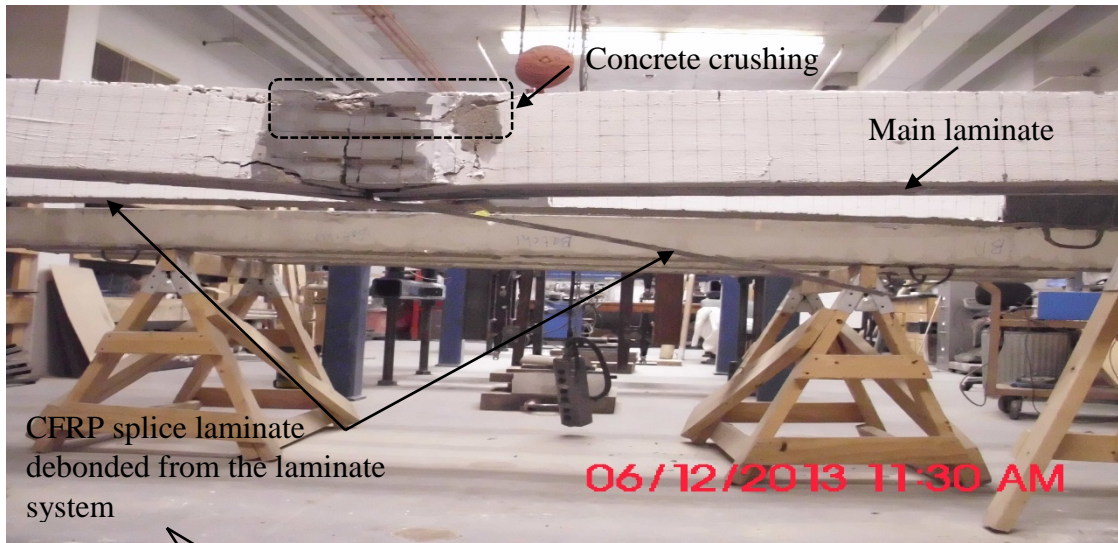
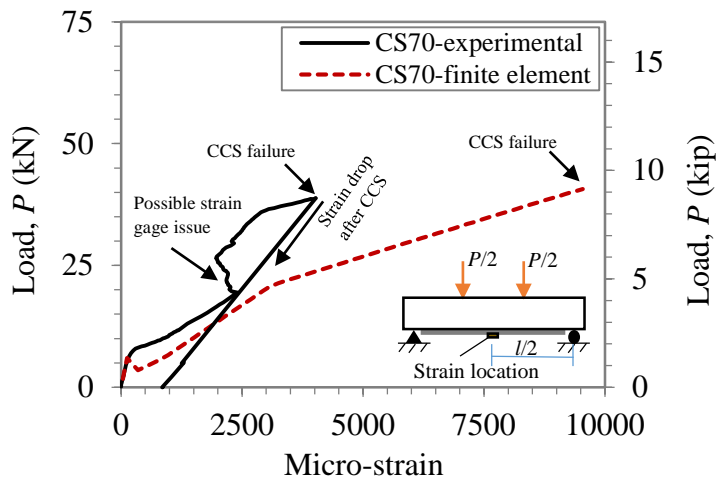
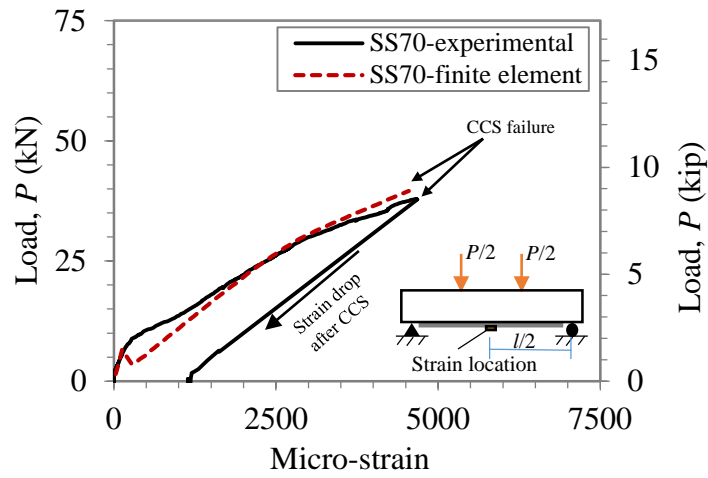


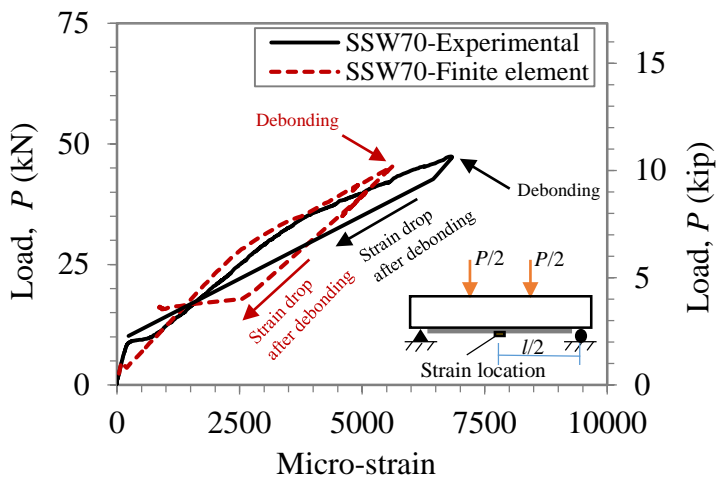
Figure 5.23 FE simulation for debonding and concrete crushing failures of beam strengthened with spliced CFRP laminate system (beam SSSC2).



(a) Beam strengthened with full-length CRP-070 (beam CS70)

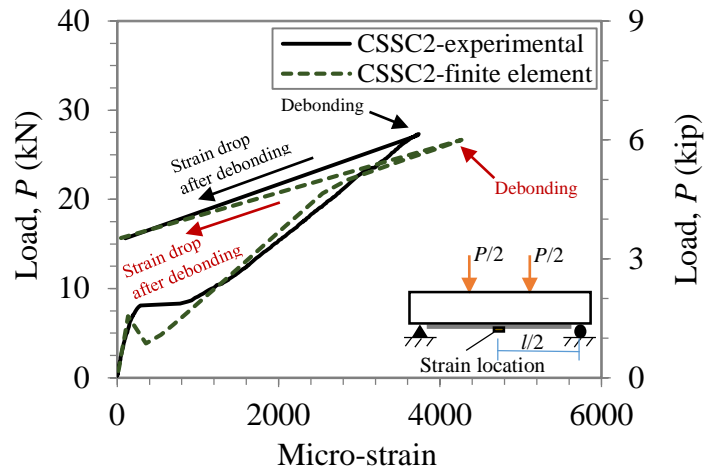


(b) Beam strengthened with two-spliced CRP-070 (beam SS70)

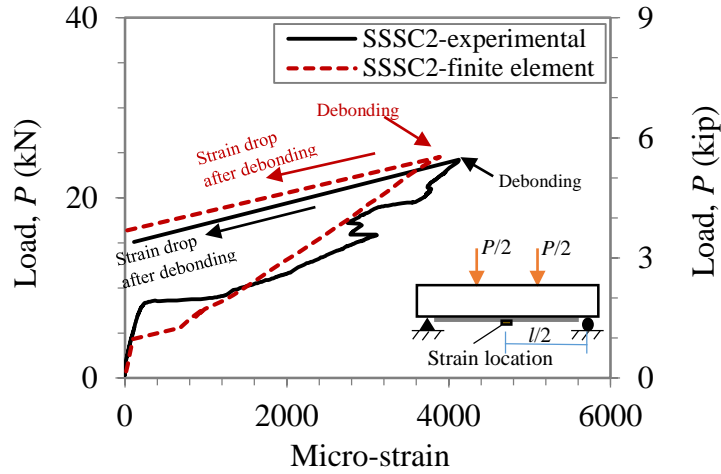


(c) Beam strengthened with two-spliced CRP-070, anchored with fabric (beam SSW70)

Figure 5.24 Load vs. strain in CRP-070, at mid-span.

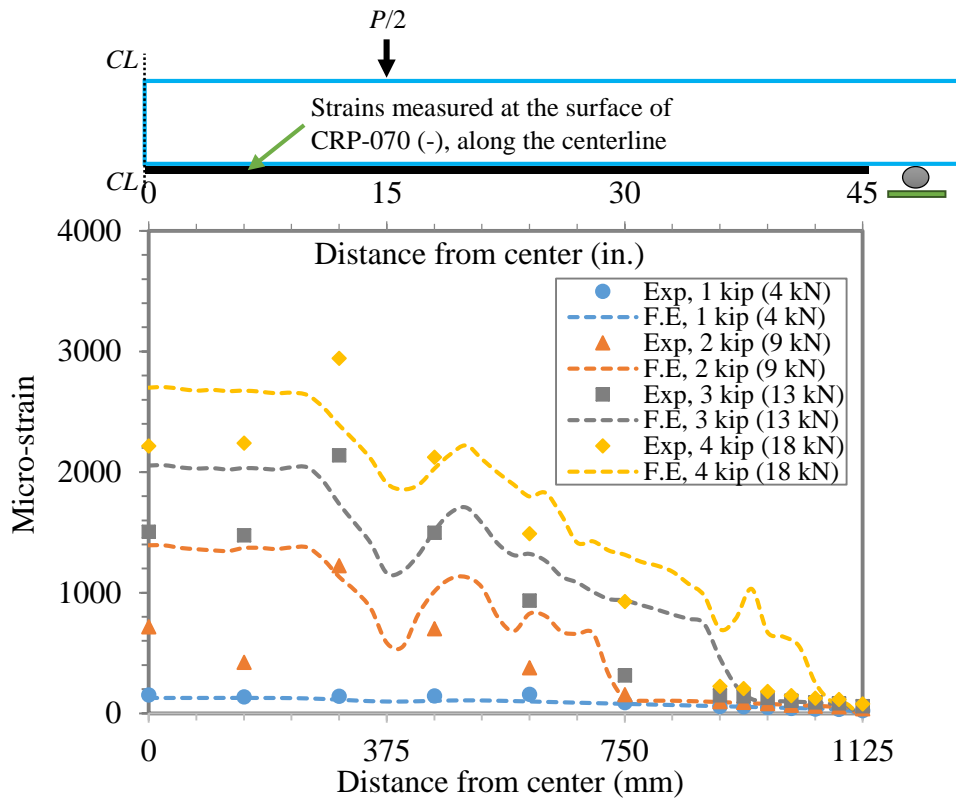


(a) Beam strengthened with full-length CFRP laminate (beam CSSC2)

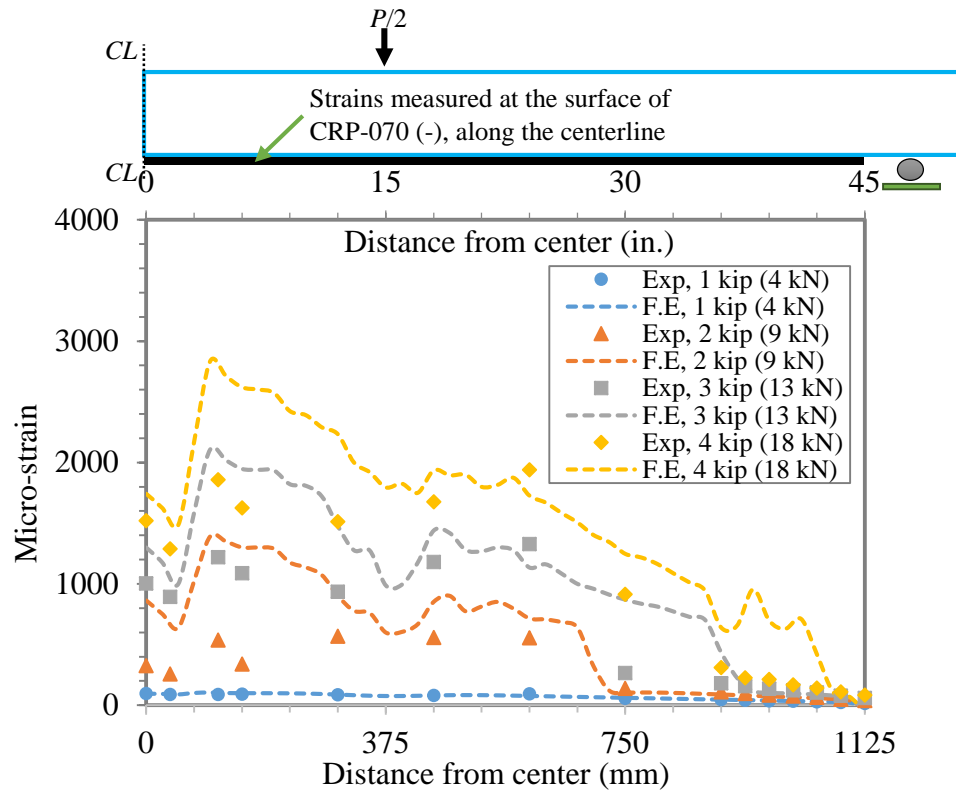


(b) Beam strengthened with spliced CFRP laminate system (beam SSSC2)

Figure 5.25 Load vs. strain in CRP-070, at mid-span.

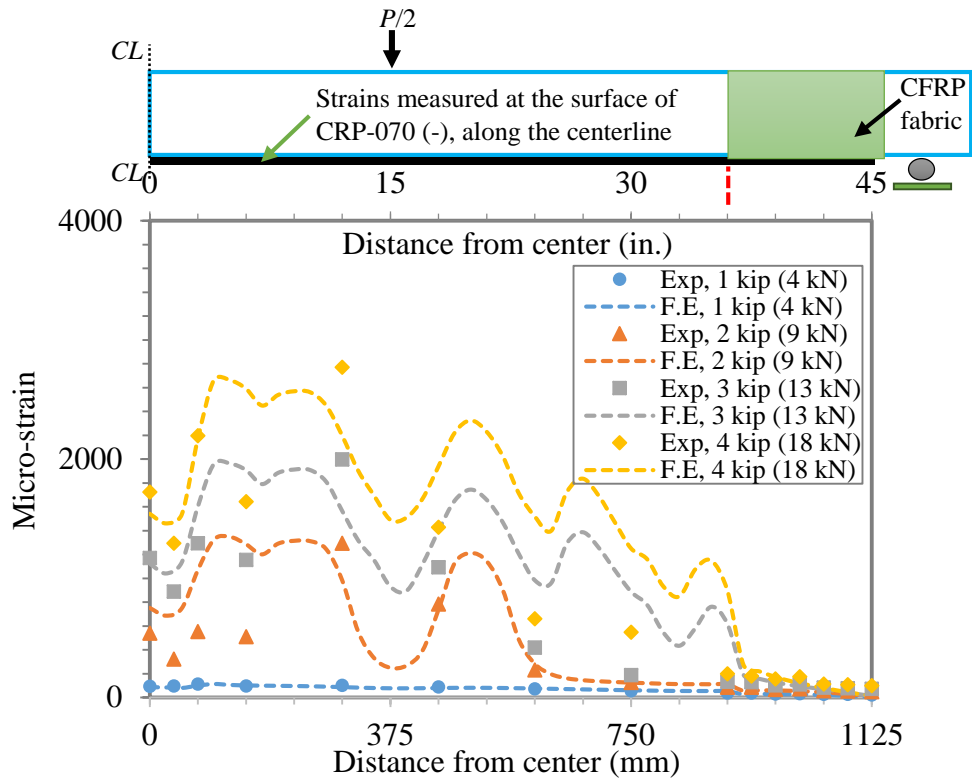


(a) Beam strengthened with full-length CRP-070 (beam CS70)

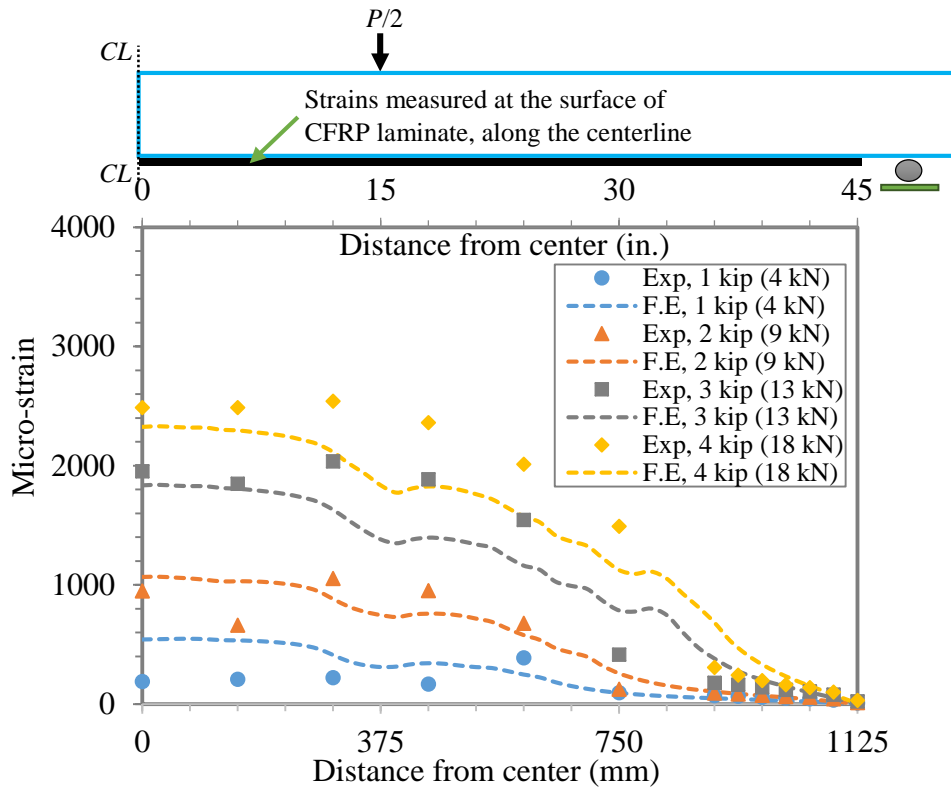


(b) Beam strengthened with two-spliced CRP-070 (beam SS70)

Figure 5.26 Strain distribution along CRP-070 surface, for loads up to 18 kN.

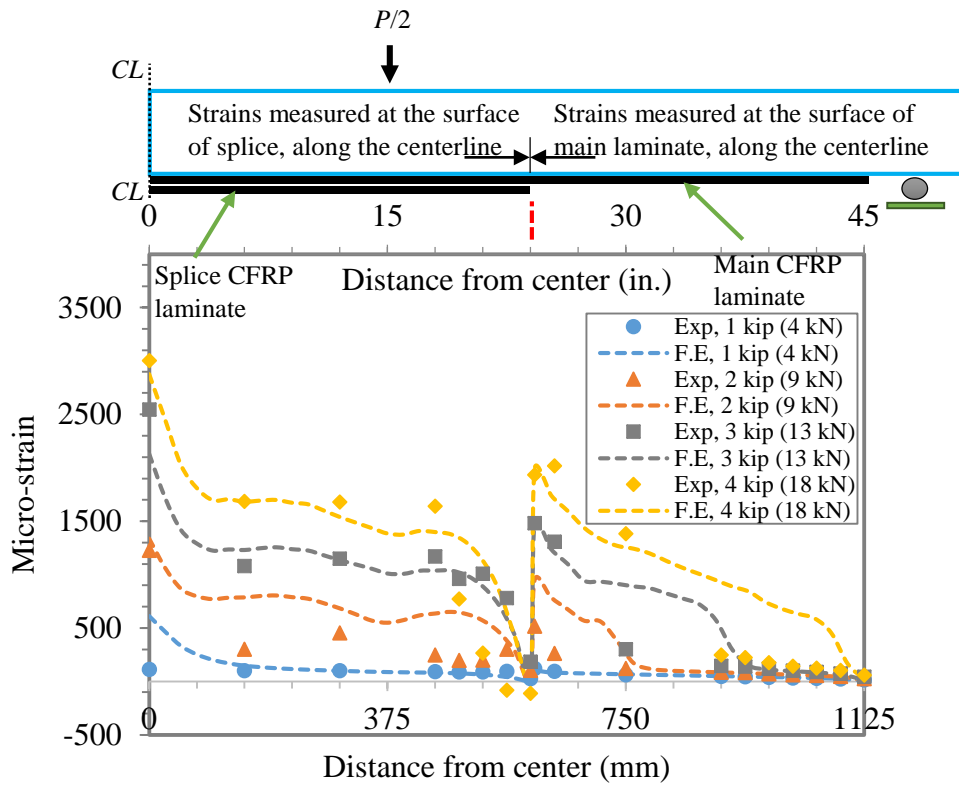


(c) Beam strengthened with two-spliced CRP-070, anchored with fabric (beam SSW70)
Figure 5.26 (cont.) Strain distribution along CRP-070 surface, for loads up to 18 kN.



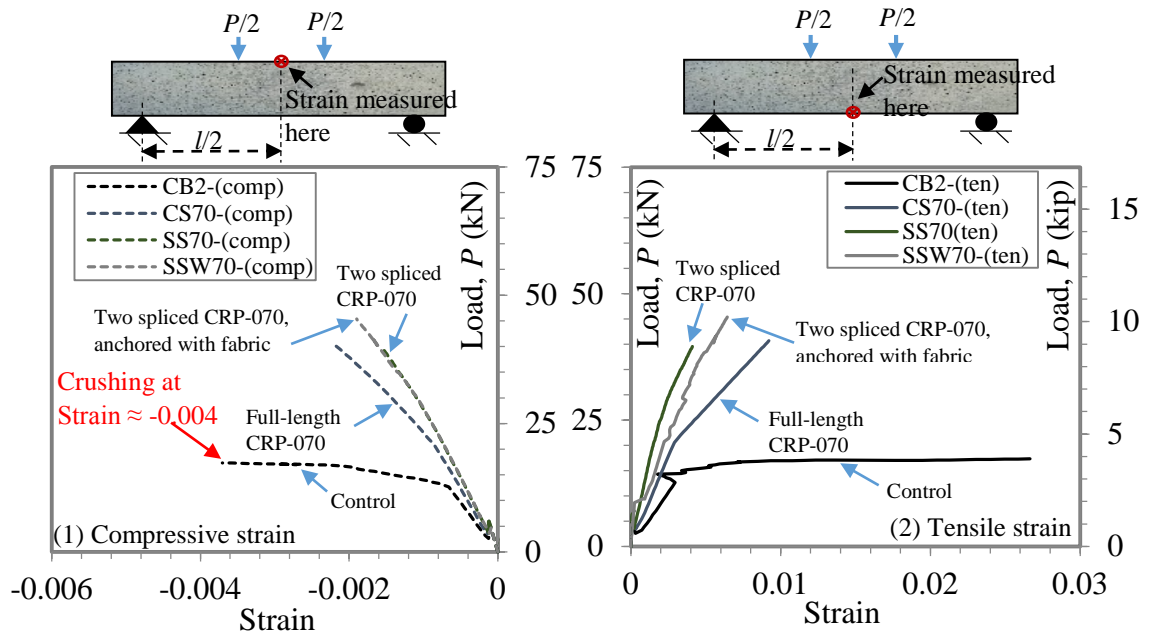
(a) Beam strengthened with full-length CFRP laminate (beam CSSC2)

Figure 5.27 Strain distribution along CFRP laminate surface, for loads up to 18 kN.



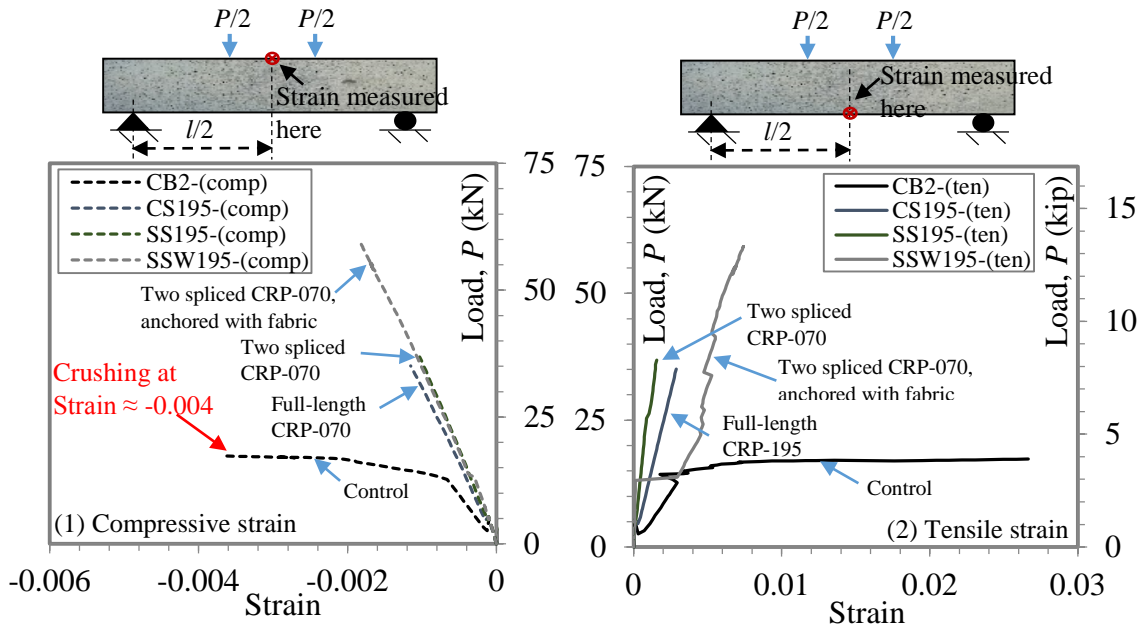
(b) Beam strengthened with spliced CFRP laminate system (beam SSSC2)

Figure 5.27 (cont.) Strain distribution along CFRP laminate surface, for loads up to 18 kN.

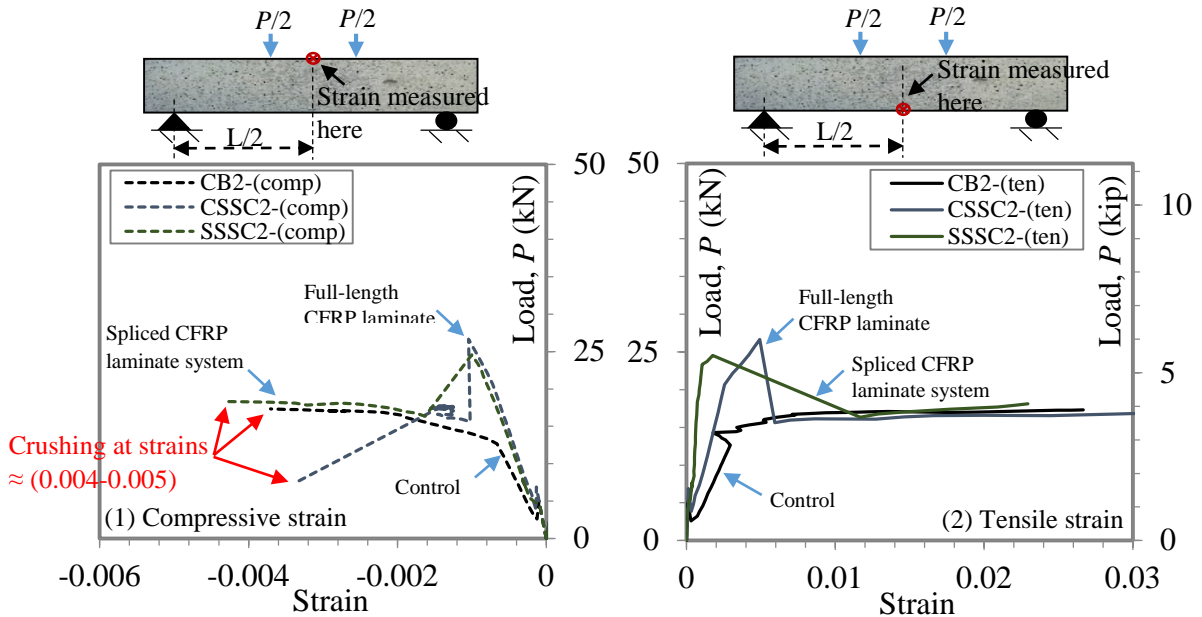


(a) Comparisons of beams strengthened with CRP-070

Figure 5.28 Load vs. strain at concrete's outermost compressive and tensile surfaces.

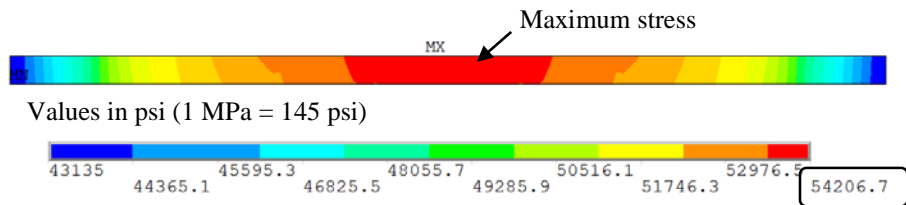


(b) Comparisons of beams strengthened with CRP-195

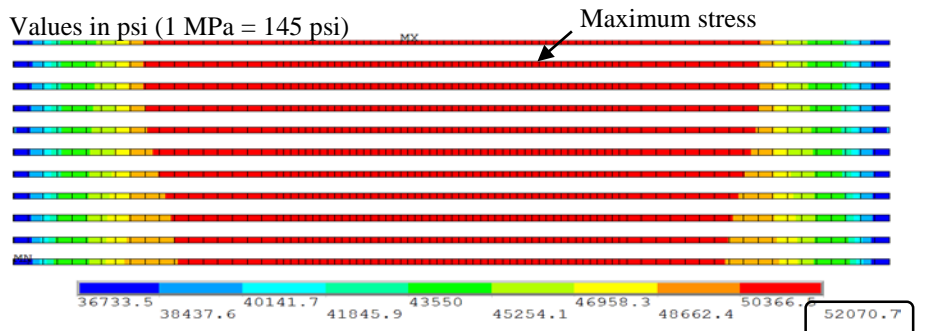


(c) Comparisons of beams strengthened with CFRP laminate

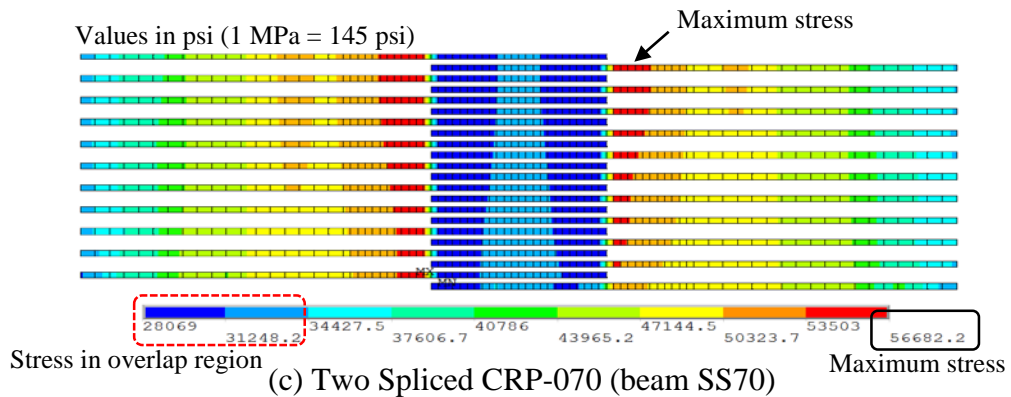
Figure 5.28 (continued) Load vs. strain at concrete's outermost compressive and tensile surfaces.



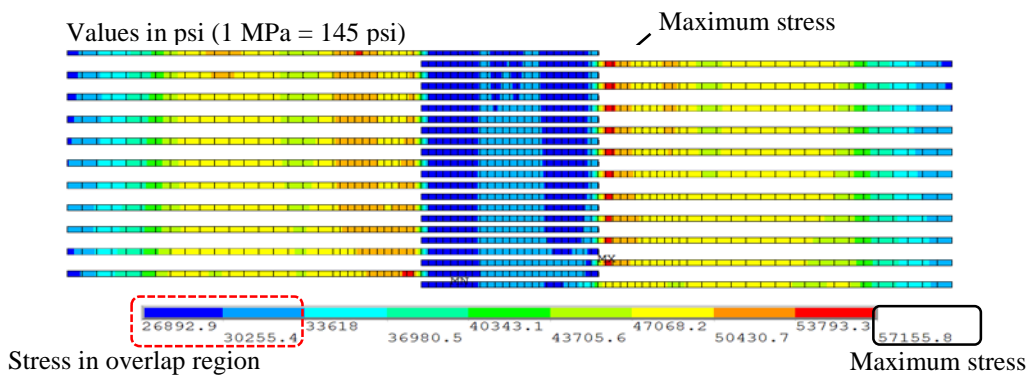
(a) Full-length CFRP laminate, (beam CSSC2)



(b) Full-length CRP-070, (beam CS70)



(c) Two Spliced CRP-070 (beam SS70)



(d) Two Spliced CRP-070 (beam SSW70, with fabric anchorage)

Figure 5.29 Tensile stress distribution in CRP-070 and CFRP laminate, at constant moment region, $P = 18$ kN (4 kip).

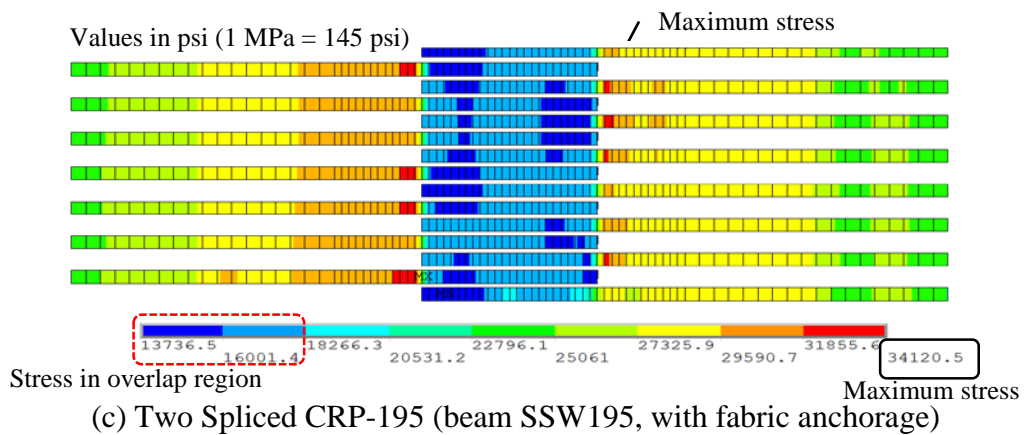
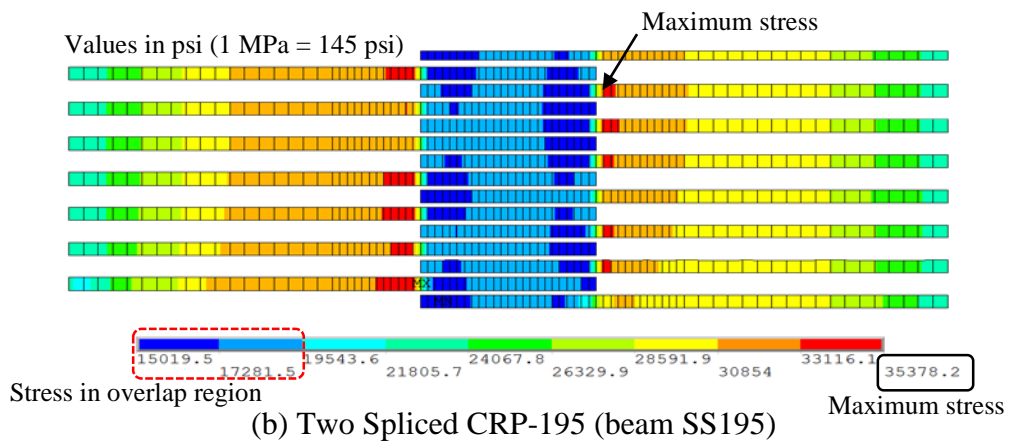
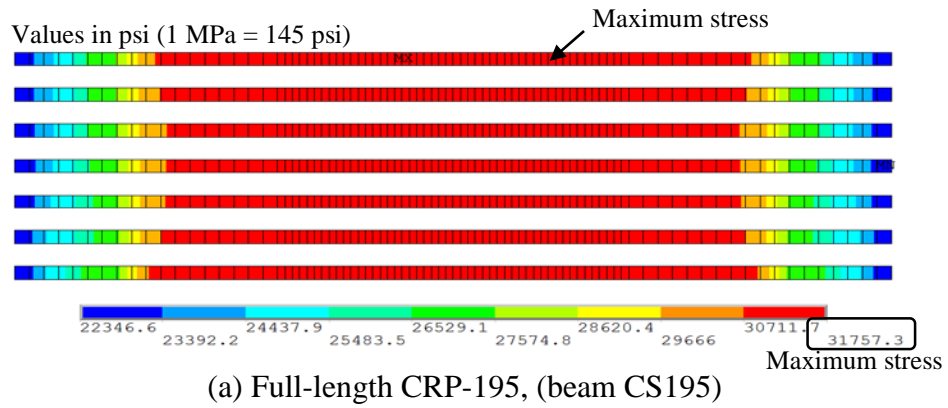
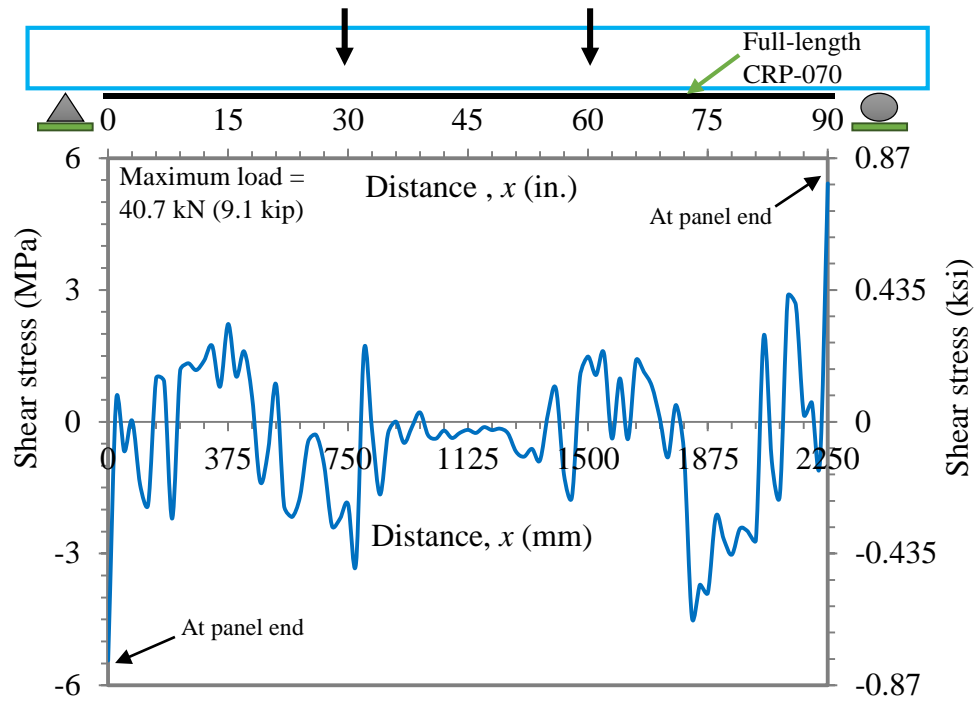
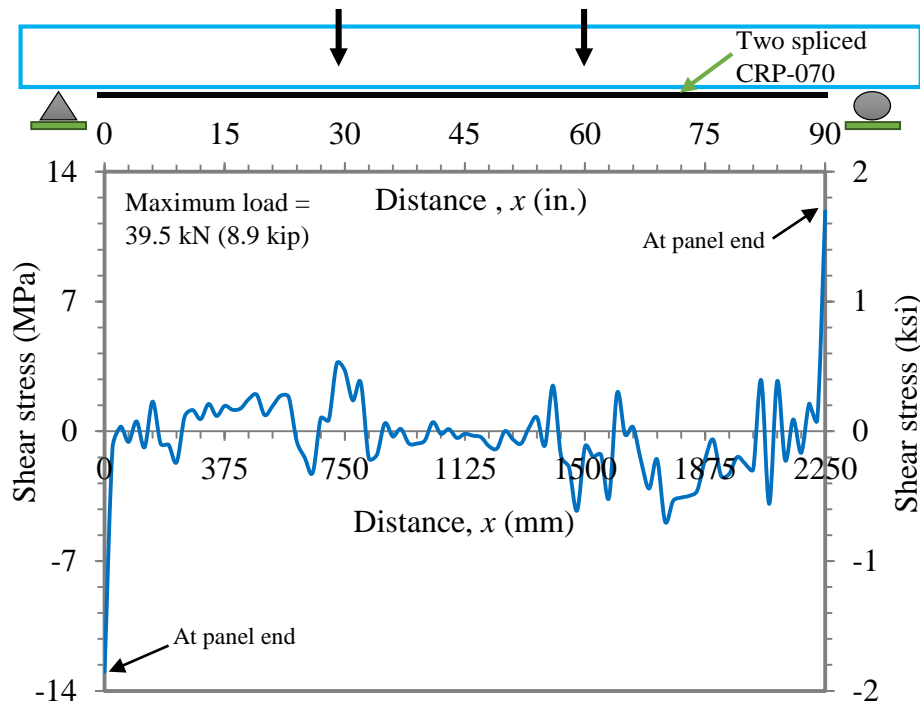


Figure 5.30 Tensile stress distribution in CRP-195, at constant moment region, $P = 18$ kN (4 kip).

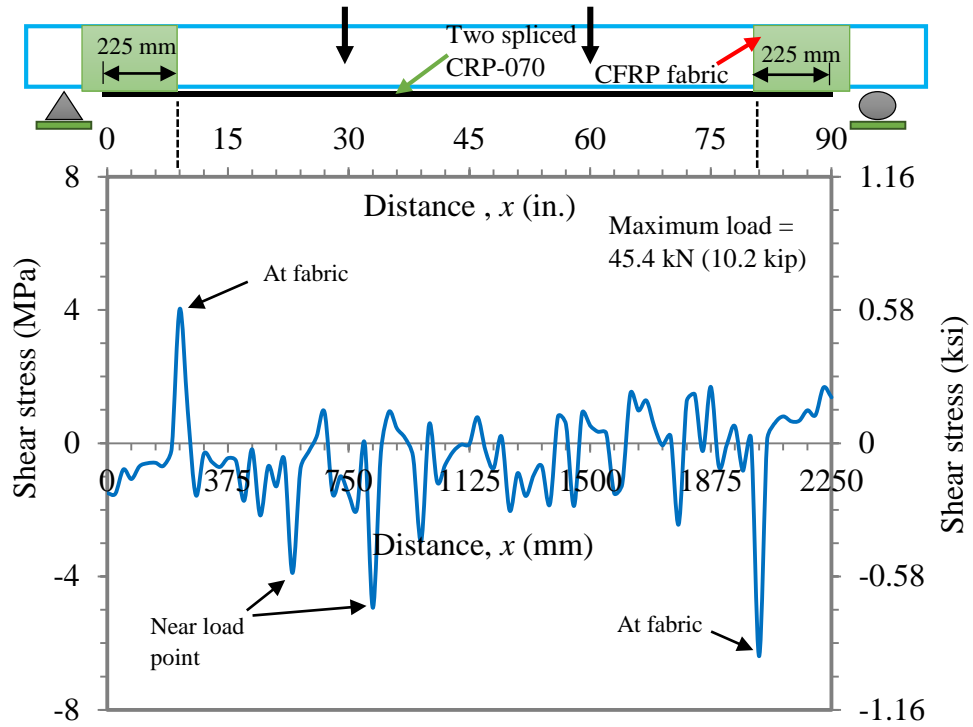


(a) Full-length CRP-070 (beam CS70)



(b) Two spliced CRP-070 (beam SS70)

Figure 5.31 FE shear distribution along CRP/concrete interface, for CRP-070, at maximum load.



(c) Two spliced CRP-070, anchored with CFRP fabric (beam SSW70)

Figure 5.31 (continued) FE shear distribution along CRP/concrete interface, for CRP-070, at maximum load.

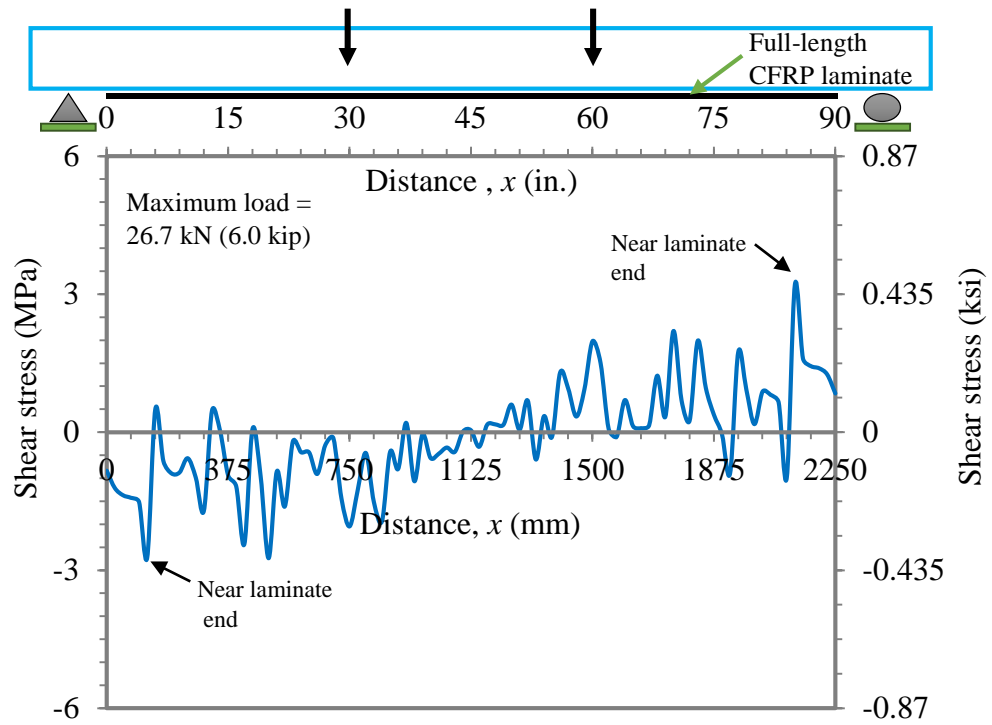
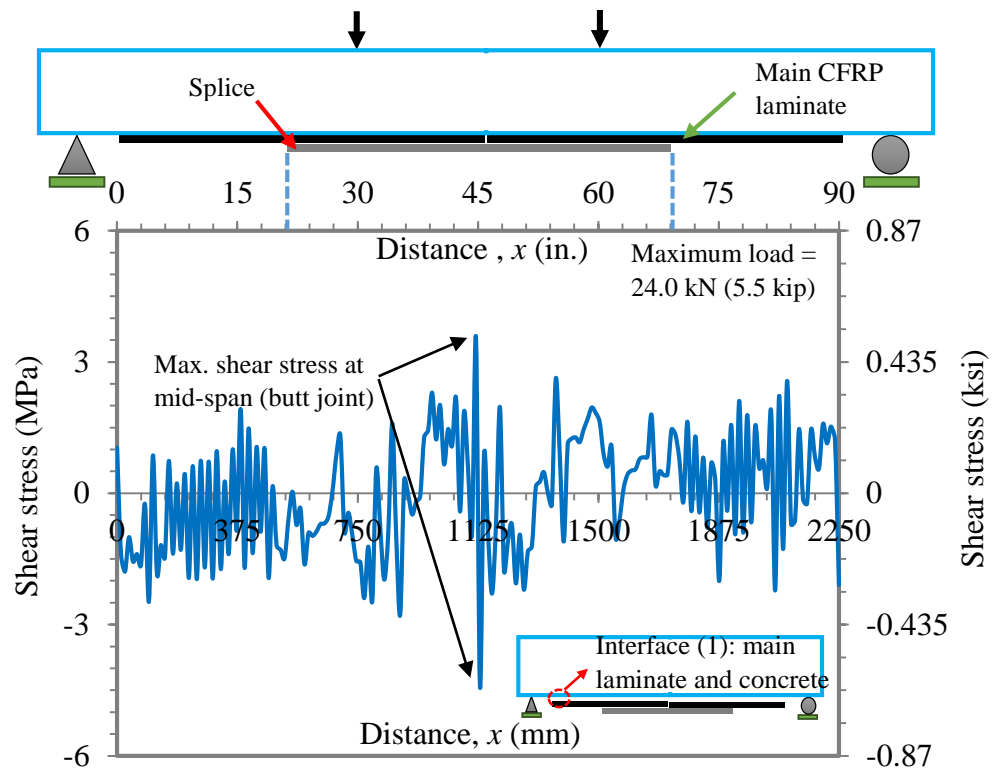
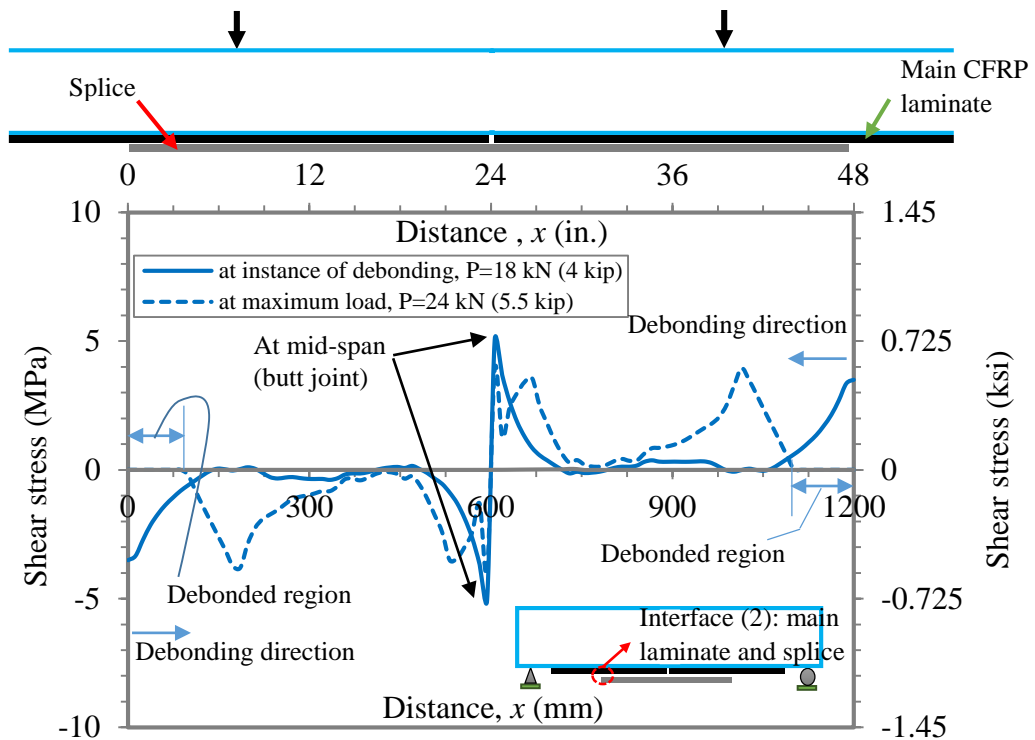


Figure 5.32 FE shear stress distribution along laminate/concrete interface, for CFRP full-length laminate (beam CSSC2), at maximum load.



(a) Shear stress profile at interface (1) between main laminate and concrete



(b) Shear stress profile at interface (2) between main laminate and splice

Figure 5.33 FE shear stress distribution along laminate/concrete interface, for spliced CFRP laminate system (beam SSSC2), at maximum load.

CHAPTER 6: ANALYTICAL INVESTIGATION OF CFRP ROD PANELS BONDED TO CONCRETE MEMBERS

6.1 Synopsis

In this chapter, the behavior of RC members strengthened with CFRP rod panels (CRPs) is investigated using analytical approaches. First, the bond behavior and development length of the double-lap shear specimens tested in the experimental program were analyzed using a simple shear-lag approach. This model is applicable for moderate loads in the linear elastic range of the behavior. Analytical terms for shear stress, slip, and strain along the length of CRPs were developed. The model findings were compared with the experimental results for strain distributions along the CRP length of several specimens, and it was found that the model compares well with the experiment. The approximate development length predicted from the analytical model for CRP-070 and CRP-195 was 100 mm (4 in.). The panel width was found to have negligible effects on transfer length of CRP-070 and CRP-195. Second, since four RC beams strengthened with CRPs (full-length or spliced) failed by concrete cover separation (CCS), two analytical models were developed. One is based on the concrete tooth concept and the other on the shear capacity concept. Analytical terms for the ultimate load for CRP strengthened RC beams when CCS is predominant are presented. Comparisons of ultimate loads from the analytical models and the experiments showed the validity of the analytical models.

6.2 Introduction

Laboratory and field testing programs can initially be utilized to validate the merit of new materials, and techniques, and to provide baseline for detailed studies. However, those programs, due to monetary, space, and time restraints, cover only some aspects of the tested concept or system. Analytical tools are great supplements to experimental studies, and can serve in examining more parameters and cases if they are calibrated with experimental findings. The analytical studies concerning the behaviour of FRP bonded concrete elements can be categorized into three groups. The first group is based on analyzing stresses, strains, and failure loads of a member, applying static concepts of deformation compatibility and force equilibrium, in conjunction with appropriate material stress-strain curves, failure modes and strain limits, (Wei et al 1991, Alagusundaramoorthy et al 2003, Brena et al. 2003, Daugevicius et al 2012). ACI 440.2R-08 provides in depth procedure on how to estimate the strength of FRP plated concrete members.

The second and third groups are the empirical models and fracture mechanics models, respectively. Empirical models, derived from regression and curve fitting analyses of experimental data, and fracture mechanics models, are intended to model the member's local behaviour, such as bond-slip relation, failure strains and causes, and load-causing debonding. A number of bond strength models for FRP-concrete joint are available in the literature (Maeda et al 1997, Hiroyuki and Wu 1997, Bizindavyi and Neale 1999, Chen and Teng 2001, Ben Oueddou et al 2009, Fawzia et al 2010).

6.3 Analysis of Double-Lap Shear Tests

An analytical model (model no.1) for predicting the strain, shear stress, and slip distribution along the bonded CRP-concrete joint, based on a simple shear-lag approach and applicable only in the linear elastic range of the behavior, is developed in this section. Figure 6.1 (a) shows the double-lap shear test specimen and the bonded CRP of length l_b on one side. A finite segment of the CRP of length dx is presented in figure 6.1 (b). Assuming a linear elastic behavior for both the CFRP rods and the adhesive, and a uniform shear stress distribution along the finite segment of length of dx , the equilibrium of forces acting on the segment in figure 6.1 (b) yields:

$$dF_x - \tau_x [s(x)] \cdot dx \cdot w_f = 0 \quad (6.1)$$

Where F_x = CRP tensile force, τ_x = shear stress at a distance x from the end of the CRP [figure 6.1 (a)], $s(x)$ = slip at a distance x , and w_f = bond (or panel) width.

The tensile force contributed by the adhesive layer, $dF_x(adhesive)$, is derived by assuming a linear stress-strain relationship for the adhesive. The contribution of the adhesive is limited to strain levels below the strain at failure of the adhesive as specified by the manufacturer [Sikadur 30 (2014)].

$$dF_x = dF_x(rod) + dF_x(adhesive) \quad (6.2-a)$$

$$dF_x = d\varepsilon_f(x) \cdot [E_f \cdot A_f] + d\varepsilon_a(x) \cdot [E_a \cdot \{(w_f \cdot t_a) - A_f\}] \quad (6.2-b)$$

Where, ε_f = strain in CFRP rods at a distance x , ε_a = strain in the adhesive at a distance x , E_f = CFRP rod modulus of elasticity, A_f = total cross-sectional area of CFRP rods (equal

to the number of rods multiplied by the area of one rod), E_a = adhesive modulus of elasticity, and t_a = thickness of adhesive layer.

The experimental observations indicated that failure resulted from debonding at the concrete-epoxy interface (concrete shear-off), while no debonding or any signs of distress were observed at the rod-adhesive interface. Strain compatibility is employed in the following derivation and, since the distance between surface of the adhesive and center of

$$d\varepsilon_f(x) = d\varepsilon_a(x) \quad (6.3)$$

$$dF_x = d\varepsilon_f(x) \cdot \left[\{E_f \cdot A_f\} + \{E_a \cdot \langle (w_f \cdot t_a) - A_f \rangle\} \right] \quad (6.4-a)$$

$$dF_x = d\varepsilon_f(x) \cdot a \quad (6.4-b)$$

where;

$$a = \left[(E_f \cdot A_f) + \{E_a \cdot \langle (w_f \cdot t_a) - A_f \rangle\} \right], \quad (6.5)$$

Rearranging equation. (6.1) leads to

$$\frac{d\varepsilon_f(x)}{dx} - \frac{w_f}{a} \cdot \tau_x(s(x)) \quad (6.6)$$

Recalling the definition of slip as the relative displacement between the reinforcement and a parent material (De Lorenzis and Nanni 2002), and recalling that

$$\varepsilon_f(x) = \frac{du_f}{dx} \quad \text{and} \quad \varepsilon_c(x) = \frac{du_c}{dx}, \quad (6.7)$$

Where u_f and u_c are the displacements of CRP and of concrete, respectively:

$$\frac{ds(x)}{dx} = \varepsilon_f(x) - \varepsilon_c(x) \approx \varepsilon_f(x) \quad (6.8)$$

Where the concrete strain, ε_c is assumed to be negligible when compared to the strain in CRP, ε_f , in pull-out tests (Bizindavyi and Neale 1999, De Lorenzis and Nanni 2002). The governing differential equation for the shear stress-slip relation of bonded CRP-concrete joint is derived by substituting equation (6.8) into equation (6.6):

$$\frac{d^2s(x)}{dx^2} - \frac{w_f}{a} \cdot \tau_x [s(x)] = 0 \quad (6.9)$$

At moderate load levels, a linear bond stress-slip model can be adopted (De Lorenzis et al 2001):

$$\tau_x = k \cdot s(x) \quad (6.10)$$

Solving equation (6.9), with τ_x given by equation (6.10), yields the following solution:

$$s(x) = c_1 \cdot \sinh(\omega \cdot x) + c_2 \cdot \cosh(\omega \cdot x) \quad (6.11)$$

$$\varepsilon_f(x) = \omega \cdot c_1 \cdot \cosh(\omega \cdot x) + \omega \cdot c_2 \cdot \sinh(\omega \cdot x) \quad (6.12)$$

Where

$$\omega = \sqrt{\frac{k \cdot w_f}{a}} \quad (6.13)$$

c_1 and c_2 are constants to be determined from the boundary conditions at $x = 0$ and $x = l_b$ (figure 6.1). At $x = 0$, which corresponds to the free end of the bonded panel, the strain is

negligible. At $x = l_b$, located at the gap between the two concrete blocks, the strain is maximum. The boundary conditions are as follows:

$$\varepsilon(x=0) \approx 0 \quad (6.14-a)$$

$$\varepsilon(x=l_b) = \varepsilon_f(x=l_b) = \varepsilon_a(x=l_b) \neq 0 \quad (6.15-a)$$

$$\varepsilon_f(x=l_b) = \frac{P_{CRP}}{E_f \cdot A_f}, \quad \varepsilon_a(x=l_b) = \frac{P_a}{E_a \cdot \langle (w_f \cdot t_a) - A_f \rangle} \quad (6.15-b)$$

$$\frac{P_{CRP}}{E_f \cdot A_f} = \frac{P_a}{E_a \cdot \langle (w_f \cdot t_a) - A_f \rangle} \quad (6.15-c)$$

and

$$P = P_{CRP} + P_a \quad (6.16)$$

Where P = total force applied at $x = l_b$, P_{CRP} = force carried by CFRP rods at $x = l_b$, and P_a = force carried by adhesive at $x = l_b$.

Solving for P_a in equation 6.16 and substituting in equation 6.15-c leads to

$$P_{CRP} = \frac{P}{\left[1 + \frac{E_a \cdot \langle (w_f \cdot t_a) - A_f \rangle}{E_f \cdot A_f} \right]} \quad (6.17)$$

$$\varepsilon(x=l_b) = \frac{P_{CRP}}{E_f \cdot A_f} \quad (6.18)$$

Solving for c_1 and c_2 from equations 6.11 and 6.12, and applying the boundary conditions

identified in equations (6.14-a) and (6.18), equations 6.11, 6.12. and 6.10, respectively, can be expressed as follows:

$$s(x) = \frac{\varepsilon(x=l_b)}{\omega \cdot \sinh(\omega \cdot l_b)} \cdot \cosh(\omega \cdot x) \quad (6.19)$$

$$\varepsilon(x) = \frac{\varepsilon(x=l_b)}{\sinh(\omega \cdot l_b)} \cdot \sinh(\omega \cdot x) \quad (6.20)$$

$$\tau_x = k \cdot \frac{\varepsilon(x=l_b)}{\omega \cdot \sinh(\omega \cdot l_b)} \cdot \cosh(\omega \cdot x) \quad (6.21)$$

6.3.1 Slip Modulus, k

The above analytical model has successfully been adapted for externally bonded FRP plates and fabrics where the slip modulus, k , is generally estimated as the ratio of the adhesive shear modulus to its thickness. In the case of bonded CRPs, this approach has no rational justification since the adhesive would have discontinuities in its thickness due to the presence of embedded rods. An empirical approach, suggested by De Lorenzis and Nanni (2002), and used in a similar context by the authors, for bonded (NSM) FRP rods, has been adopted to evaluate the slip modulus of bonded CRPs. This was achieved by best fitting the analytical strain distribution given by equation (6.20) and the experimental strain data obtained in the double-lap shear tests.

6.3.2 Model Verification

Experimental and analytical strain distributions along the bond length of CRP, at moderate load levels, are shown in figure 6.2. The comparisons are available for double-lap shear concrete specimens bonded to CRP-070 and CRP-195. In the experimental double-lap shear tests in chapter 3, specimens with short bond lengths displayed non-linear strain distributions that don't comply with the fundamental assumptions of the shear-lag theoretical model. Consequently, only experimental specimens with sufficiently long bond lengths, 150 mm (6 in.) and 175 mm (7 in.), were used to validate the analytical model. Following the method described in 6.2.1 for estimating the slip modulus, the modulus was estimated to be 375 MPa/mm (1360 ksi/in.) for CRP-070 [fabricated with 2 mm (0.078 in.) diameter rods, spaced at 6.35 mm (0.25 in.)] and 800 MPa/mm (2900 ksi/in.) for CRP-195 [fabricated with 4 mm (0.156 in.) diameter rods, spaced at 9.5 mm (0.375 in.)].

As can be seen from figure 6.2, strain profiles at moderate loads, from model no.1 (based on shear-lag approach) and the experiment, correlate reasonably well. The only discrepancy between experimental and model predictions was seen with specimen III-4-9-19-150 [figure 6.2 (d)], for which experimental strains at $x_l = 0$, for all load levels, were very low compared to the analytical values and the expected trend. This difference may be due to inaccurate initial readings in the strain gages, cracking in concrete block or adhesive layer, or limitations of the theoretical model.

6.3.3 Parametric Study

Model no.1 was further used to perform a parametric study investigating variables expected to have an impact on the behavior and efficiency of CRPs bonded to concrete, namely development length and effects of CRP width. The study was limited to those variables due to the lack of sufficient data regarding the slip modulus, k . Other influential variables, such as rod spacing, adhesive thickness, and FRP stiffness, can be further investigated provided that experimental testing or theoretical basis are available for characterizing the slip modulus.

6.3.3.1 Development Length

Model no.1 was used to approximate the development length, l_d , for CRP-070 and CRP-195. Equation 6.20 along with equations 6.17 and 6.18 were used to construct the strain distribution along bond length, l_b , for double-lap shear specimens bonded to CRPs with varied bond lengths. l_b was varied from 25 mm (1 in.) to 200 mm (8 in.). Other variables were kept constant, and as follows: (1) bond width, $w_f = 50$ mm (2 in.) for CRP-070 and $w_f = 19$ mm (0.76 in.) for CRP-195; (2) rod spacing, $S = 6.35$ mm (0.25 in.) for CRP-070 and $S = 9.5$ mm (0.375 in.) for CRP-195; and (3) number of rods is 16 for CRP-070 and 4 for CRP-195.

For each bond length, and considering a load level of 11.11 kN (2.5 kip), the strain profile along the bond length was constructed from equation 6.20 along with equations 6.17 and 6.18. The transfer length, which is the distance from the gap between concrete blocks, or $x = l_b$ in figure 6.1, of the joint to the point where the exponential strain profile approaches zero ($x = 0$ in figure 6.1), was recorded. Figure 6.3 (a, b) presents the variation of transfer

length with bond length for CRP-070 and CRP-195, respectively. From the transfer length vs. bond length curve, the analytical development length can be inferred. The development length is estimated to be 100 mm (4 in.) for both panels. In the experimental double-lap shear tests, the development length was 100 mm (4 in.) for CRP-70, and 125 mm (5 in.) for CRP-195.

6.3.3.2 CRP Width Effects

The effects of varying the bond width or CRP/concrete width ratio (w_f/b_c) were evaluated using model no.1, [w_f and b_c are shown in figure 6.1 (a)]. Equation 6.20 along with equations 6.17 and 6.18 were used to construct the strain distribution along the bond length for the double-lap shear specimens bonded to CRPs and with varied CRP widths. For CRP-070, the bond width was increased from 25 mm (1 in.) to 100 mm (4 in.) or the (w_f/b_c) ratio, was varied from 0.25 to 1.0. For CRP-195, the width was increased from 19 mm (0.76 in.) to 95 mm (3.8 in.) or the (w_f/b_c) ratio, was varied from 0.19 to 0.95.

The rod spacing was kept constant, 6.35 mm (0.25 in.) for CRP-070 and 9.5 mm (0.375 in.) for CRP-195, while the number of rods was increased depending on the width of the CRP. A bond length of 150 mm (6 in.) was used for all specimens. For each bond width, and considering a load level of 11.11 kN (2.5 kip), the strain distribution along bond length was constructed and the transfer length was estimated. Figure 6.4 (a, b) presents the variation of transfer length with the panel width, for CRP-070 and CRP1-95, respectively. As can be seen from the figure, the transfer length did not vary when CRP width increased. This observation aligns with the previous findings of experimental tests where the bond

width was found to have negligible effects on the bond strength and ultimate load capacity of CRPs bonded to concrete double-lap shear specimens (chapter 3, section 3.4.6).

6.4 Analysis of concrete Cover Separation

Four beams that were strengthened with CRPs, both full-length panels and spliced ones failed due to concrete cover separation (CCS), as discussed in Chapter 4. The failure occurred near the cut-off location of CRP and was characterized by the separation of the concrete cover from the beam's section, along the level of tensile steel reinforcement. This section analytically investigates the causes and theories behind CCS, and also predicts the ultimate load carrying capacity of CRP strengthened RC beams when CCS is predominant.

6.4.1 Analytical models

Existing studies concerning the development of analytical models to predict concrete cover separation and the ultimate load capacity of strengthened RC beams when CCS failure is predominant are generally classified into three categories (Zhang et al 2012). In the first category are models that concentrate on the derivation of interfacial normal and shear stresses at the plate ends at the instance of cover separation, based on linear elastic bending theory (Zhang et al 2012). Shear capacity based models constitute the second category and are based on comparing the shear force at the plate ends with concrete shear strength with or without stirrup contribution. Models in the third category are called “concrete tooth” models and are based on comparing tensile stresses at the plate ends, along the level of internal steel, with concrete tensile strength. In this chapter, two analytical models for predicting the CCS failure in CRP bonded RC beams were derived and presented. The first

analytical model (model no.2) is based on the concrete shear capacity, while the second model (model no.3) is based on the concrete tooth concept.

6.4.1.1 Shear Capacity Based Models

Oehlers (1992) introduced the first shear capacity model to predict plate end debonding failures for steel plated RC beams. If the plate is terminated at or very close to supports, it was suggested that debonding occurs when the shear force at the plate end (loads before steel plate is bonded are considered) reaches the concrete shear capacity. In this model, experimental results have indicated that shear stirrups do not have an impact on the debonding load and only concrete shear strength needs to be considered. In general, when both the shear force and bending moment are large at the plate end, a debonding formula, that considers the interaction between shear and flexural peeling, is usually adopted based on empirical fitting of test results.

Most of shear capacity models for RC beams bonded to FRPs originated from Oehlers' model for beams attached to steel plates. A study by Smith and Teng (2002a) has shown that Oehlers' model can be used directly and successfully for the case of FRP plated beams when geometrical and material properties are modified to consider FRP characteristics. Most of the recent shear capacity models for FRP bonded RC beams have included the influence of different factors such as internal shear stirrups, shear force induced by FRP plates, and non-linear terms instead of linear ones used for the interaction formula between shear force and bending moment (Gao et al 2005, Yao and Teng 2007b).

6.4.1.2 Concrete Tooth Models

The first introduction of a concrete tooth model was given in Zhang et al (1995) and was utilized for RC beams bonded to steel plates. Concrete tooth models were developed and intended to rely only on theoretical analyses without the need for correlation factors or empirical equations used in other approaches. The main concept behind the model is, when the loading is applied, flexural cracks will develop on the tension face of the concrete member and, when the loading is increased, new cracks will develop between the former ones until they are stabilized in size and spacing. At this stage, the concrete cover between longitudinal steel rebars and the member's outermost tensile face resembles a comb-like structure (see figure 6.5).

When the loading is further increased, the individual concrete teeth between adjacent cracks deform like a cantilever beam under the influence of horizontal shear stresses at their ends. Peeling off occurs when these shear stresses generate tensile stresses at the root of the tooth (i.e. at the level of steel rebar) that exceed the tensile strength of the concrete. Since the model depends mainly on the flexural crack spacing, and because crack spacing can be expected to vary between minimum and maximum spacing, lower and upper bound equations for the ultimate load values are introduced. The corresponding lower and upper bounds of the ultimate peeling moment are determined using conventional section analysis and bending theory assumptions.

6. 4.2 Application of Analytical Models to RC Beams Strengthened with CRPs

6.4.2.1 Analytical model No. 2

The first analytical model for predicting CCS (model no.2), carried out in this chapter to simulate the ultimate capacity of CRP strengthened RC beams that fail by CCS, is based on the concrete tooth concept. The model presented here was originally obtained from Al-Mahmoud et al (2010) model, which was used to determine the failure load of NSM-FRP rod strengthened RC beams. The Al-Mahmoud et al model is also an extension of previous concrete tooth models that were used in the case of externally bonded steel or FRP plates [Zhang et al (1995), Raof and Hassanen (2000)].

CRP rod panels are geometrically different from both externally bonded plates and NSM technique, consequently, modifications are needed to make the model applicable in the case of CRP bonded beams. The criteria in the following calculations is that all concrete teeth formed inside the region between CRP and tensile steel reinforcement fail simultaneously, and therefore only the first tooth that is formed at the panel's end is required to obtain the solution. This approach has been used for predicting CCS in RC members bonded to NSM FRP rods [Al-Mahmoud et al (2010)], FRP laminates [Raof and Hassanen (2000)], and steel plates [Zhang et al (1995)].

Pivotal to the calculations is the measurement or estimation of the crack spacing, S_{cr} . In this study, S_{cr} was directly measured from the failed experimental beams. As stated previously, the concrete tooth formed at the panel's end behaves like a cantilever beam and the forces acting on that cantilever are: (1) the tensile stress in the CRP rods at distance equal to S_{cr} from the panel's end, and (2) the resisting moment at the cantilever tip (i.e.

beneath the internal reinforcement). Figure 6.6 shows the first concrete tooth and the forces acting on it. The classic bending theory is used to solve the cantilever model. At point A in figure 6.6, the tensile stress is given by:

$$\sigma_A = \frac{M_A \cdot \frac{S_{cr}}{2}}{I_{tooth}} \quad 6.22$$

$$I_{tooth} = \frac{b \cdot S_{cr}^3}{12} \quad 6.23$$

The moment at the tooth tip is:

$$M_A = \sigma_f \cdot A_f \cdot h' \quad 6.24$$

Substituting equation 6.24 into equation 6.22, leads to

$$\sigma_A = \frac{6 \cdot A_f \cdot h'}{b \cdot S_{cr}^2} \cdot \sigma_f \quad 6.25$$

Where, σ_A = tensile stress at point A, M_A = bending moment of the tooth structure, I_{tooth} = moment of inertia of the tooth, S_{cr} = crack width, b = beam width, σ_f = tensile stress of CRP at distance of S_{cr} from panel's end, A_f = total area of CFRP rods, and h' = depth from the level of internal steel to the tensile face of the concrete.

σ_f can be determined using the bending theory for the whole beam and considering the applied loads (i.e. four-point bending test beams in this dissertation) as shown in figure 6.7.

The other assumptions are: (1) near the panel's end, all materials are within their linear-elastic range, and (2) concrete is cracked.

$$\sigma_f = n_f \frac{d_f - c}{I_{tr,cr}} M_{B-B} \quad 6.26$$

$$n_f = \frac{E_f}{E_c} \quad 6.27$$

where, M_{B-B} = bending moment of the beam at section (B-B) in [figure 6.7 (b, c)] = distance from extreme compressive fiber of concrete to neutral axis, d_f = distance from concrete extreme compressive fiber to the center of CFRP rods, $n_f = E_f/E_c$ = FRP rods modular ratio, E_f = modulus of elasticity of CFRP rods, E_c = modulus of elasticity of concrete, $I_{tr,cr}$ = cracked and transformed moment of inertia of the beam. $I_{tr,cr}$ and c can be calculated, assuming a cracked beam section with tensile steel reinforcement and FRP rods transformed into equivalent concrete areas, see figure 6.7 (c).

Other variables shown in figure 6.7 (c) are: A_s = area of tensile steel reinforcement, A_s' = area of compressive steel reinforcement, and n = steel modular ratio, $n = (E_s/E_c)$, E_s = modulus of elasticity of steel.

Substituting equation 6.26 in equation 6.25, σ_A can be expressed as

$$\sigma_A = \frac{6 \cdot A_f \cdot n_f \cdot h' \cdot (d_f - c)}{b \cdot S_{cr}^2 \cdot I_{tr,cr}} \cdot M_{B-B} \quad 6.28$$

Assuming that failure initiates when $\sigma_A = f_t$ (concrete tensile strength), M_{B-B} , at the instance of cover separation, can be calculated from equation 6.28. f_t is estimated in the current chapter from the concrete compressive strength, f_c' , following ACI 318-14 (2014)

$$f_t = 0.56 \cdot \sqrt{f_c'} \quad \text{SI units (MPa), ACI-14M} \quad 6.29$$

The ultimate load, P , can now be estimated from summing moments at section (B-B) of the beam segment shown in figure 6.7 (b)

$$P = \frac{2 \cdot M_{B-B}}{(S_{cr} + x_0)} \quad 6.30$$

M_{B-B} can be determined easily from equation 6.28 and substituted in 6.30. Finally, the ultimate load of RC beams strengthened with CRPs that fail by concrete cover separation, CCS, is:

$$P = \frac{f_{ct} \cdot b \cdot S_{cr}^2 \cdot I_{tr,cr}}{6 \cdot A_f \cdot n_f \cdot h' \cdot (d_f - c) \cdot (S_{cr} + x_0)} \quad 6.31$$

6.4.2.2 Analytical model No. 3

The second analytical model (model no.3), for simulation of CCS failure in CRP strengthened RC beams, is based on the shear capacity models and is adapted from Smith and Teng (2003) with proper modifications to suit the model for the case of externally bonded CRPs. The original Smith and Teng model is given as follows:

$$\frac{M_{db,end}}{M_{db,f}} + 0.4 \times \frac{V_{db,end}}{V_{db,s}} = 1 \quad \text{if } V_{db,end} \geq 0.67 \times V_{db,s} \quad 6.32$$

$$M_{db,end} = M_{db,f} \quad \text{if } V_{db,end} < 0.67 \times V_{db,s} \quad 6.33$$

$$M_{db,f} = \frac{E_c \cdot I_{tr,cr} \cdot f_{ct}}{0.90 \cdot E_f \cdot t_f} \quad 6.34$$

$$V_{db,s} = V_c = \left[1.4 - \frac{d}{2000} \right] \cdot b \cdot d \cdot (\rho_s \cdot f_c')^{1/3} \quad 6.35 (a)$$

$$\left[1.4 - \frac{d}{2000}\right] \geq 1.1 \quad 6.35 \text{ (b)}$$

$$\rho_s = \frac{A_s}{b \cdot d} \quad 6.36$$

where, $M_{db,end}$ = bending moment at CRP's end at the instance of CCS initiation, $V_{db,end}$ = shear force at CRP's end at the instance of CCS initiation, $M_{db,f}$ = flexural moment capacity at CRP's end derived by considering pure flexural failure when the CRP is terminated at regions of large moments and negligible shear forces, $V_{db,s}$ = concrete shear capacity at CRP's end, d = distance from outermost compressive concrete fiber to center of tensile steel reinforcement. Other variables have been defined in analytical model No.1.

$M_{db,f}$, given by equation 6.34, was proposed by Oehlers (1992) based on the calibration of the test results for steel plates bonded to concrete, and was later used for FRP plates by Smith and Teng (2003) who accounted for the geometric and material properties for FRP instead of steel. $V_{db,s}$, the concrete shear capacity at CRP's end, can be estimated from the ACI code or any other code of practice. In this study, $V_{db,s}$, presented in equation 6.35, as given by Oehlers (1992) and Smith and Teng (2003), is the concrete shear strength taken from the Australian code (AS 3600 1988).

Equation 6.34 needs to be modified to suit the case of CRPs, since t_f , thickness of FRP or steel plates, is not directly applicable for the case of CRPs. In this chapter, an equivalent plate thickness, t_f , is proposed by assuming an equivalent plate having a CFRP area (A_f) and width (w_f) equal to those of CRP [figure 6.8 (a)]

$$t_f = \frac{A_f}{w_f}, \quad 6.37$$

where, A_f and w_f are the total rod area and bond width of CRP.

$V_{db,end}$ and $M_{db,end}$ are calculated from the equilibrium of forces of the beam, using the boundary conditions and loading configurations for the tested beams (i.e. simple-supports and four-point loading), and ignoring the weight of the beam, figure 6.8 (b). The load at failure, P , at the instance of concrete cover separation, is calculated from equation 6.32 or 6.33. It should be noted that all equations in the analytical model no.2 are in the SI unit system.

$$M_{db,end} = \frac{P}{2} \cdot x_0 \quad 6.38$$

$$V_{db,end} = \frac{P}{2} \quad 6.39$$

6.4.3 Results of analytical models no.2, and no.3

Ultimate loads of the tested beams that failed by CCS, predicted using the two analytical models (models no.2, and no.3), and are given in table 6.1. The corresponding graphical representations of the analytical/experimental failure load ratios are also shown in figure 6.9. It should be noted that in both analytical models, f'_c , the specified 28-day, compressive concrete strength is used, while in the experimental program, the compressive strength was evaluated at the time of testing. Therefore, a correction formula to relate the “at-testing”

strength to the 28-day specified strength was needed. The formula used in the PCI Bridge Design Manual of 2010 is adopted in this chapter:

$$(f'_c)_t = \frac{t}{A + (B \cdot t)} \times (f'_c)_{28} \quad 6.40$$

where, $(f'_c)_t$ and $(f'_c)_{28}$ compressive strengths at-testing and at 28 days, respectively, t is time in days, and A and B are constants.

Both models presented a very good correlation with the experimental failure loads. The maximum difference between prediction and experimental loads is 4.5%, and 13.5 % for models no.2 and no.3, respectively. Model no.2 presented the best agreement with the experimental results, possibly because the model was derived from purely theoretical analysis of the cracked concrete cover without any use of correlation factors, and in the current investigation, the flexural cracks spacing was obtained from direct measurements of the cracks seen in the tested beams.

As can be seen in table 6.1, and previously mentioned in chapter 4, and 5, the four beams failed at comparable experimental loads, regardless that CS195 and SS195 beams were strengthened with CRP-195, while CS70 and SS70 beams were strengthened with CRP-070 (A_f for CRP-195 is 2.7 times that of CRP-070). As it was discussed earlier, concrete strength, f'_c has the largest effects on the ultimate load when CCS takes place. Both models used concrete strength as failure criteria, and therefore were able to predict well this trend. During the analysis, using model no. 3, it was noticed that when the bending moment at the panel's end is removed from equation 6.32, while keeping only the shear force at the panel's end as the failure criteria, the model presents a better agreement with the experimental results. Figure 6.10 shows the trend for analytical/experimental load ratio

when neglecting the bending moment. Oehlers (1992), and Smith and Teng (2003), argued that when the FRP composite is terminated close to the supports, or when the composite is terminated in regions where shear forces are high and bending moments are very low, the bending moment can be neglected in the interaction equation. In this experiment, CRPs were terminated 225 mm (9 in.) from the supports. Therefore, equation 6.32 can be adjusted to arrive at a new analytical model, as given by the following:

$$0.4 \times \frac{V_{db,end}}{V_{db,s}} = 1 \quad 6.41$$

Substituting equations 6.35 (a) and 6.39 in 6.35, the failure load can be written as:

$$P = 5 \times V_{db,s} = 5 \times \left[1.4 - \frac{d}{2000} \right] \cdot b \cdot d \cdot (\rho_s \cdot f'_c)^{1/3} \quad 6.42$$

It should be noted that equation 6.42 is only applicable for the beams tested in this experiment, and only for the case of simply supported beams loaded in four-point bending.

Additional studies are needed before making any generalizations.

6.5 Conclusions

In this chapter, several aspects of the bond and flexural characteristics of bonded CRP and concrete were analytically examined in two studies. Three analytical models are presented.

The first, or model no.1, is an analytical model to predict the shear stress, slip between CRP reinforcement and concrete, and strain along the length of CRP, at moderate load levels. The model results were calibrated with double-lap concrete specimens bonded to CRP-070 and CRP-195 that were tested in chapter 3. The model was used to perform a

parametric study, examining the development length and bond width of CRPs. The model predicted the development length to be 100 mm (4 in.) for both CRP-070 and CRP-195, while the bond width was found to have minor effects on the transfer length of the above panels.

Model no.2 and model no.3 are analytical models used to predict the ultimate load of RC beams strengthened with CRPS, when the strengthened beam fails by CCS. Model no.2 is derived from the “concrete tooth concept”, while model no.3 is based on “concrete shear capacity concept”. Both models were calibrated with the experiments of chapter 4 (four-point bending tests on RC beams strengthened with CRPs), and it was found that the maximum difference between the analytical and experimental loads is 4.5% and 13.5 % for model no.2 and no.3, respectively. The two analytical models were derived based on the observed failure mode of the tested RC beams that were strengthened with full-length or spliced CRPs, and are only applicable when the failure mode is CCS. In case the strengthened member fails by debonding of CRP reinforcement, CRP rupture, concrete crushing, etc., other analytical models, incorporating the properties of aforementioned failure mechanisms should be derived.

Table 6.1. (a) Results of analytical investigation of CCS, SI system.

Beam code	f'_c (MPa)	S_{cr} (mm)	P_{exp} (kN)	Model no.2		Model no.3	
				$P_{m.2}$ (kN)	$P_{m.2}/P_{exp}$	$P_{m.3}$ (kN)	$P_{m.3}/P_{exp}$
CS70	59.20	59.37	38.90	38.33	0.985	36.00	0.925
SS70	55.84	60.00	37.94	37.22	0.981	35.27	0.930
CS195	50.33	84.10	37.49	36.92	0.984	32.43	0.865
SS195	51.34	84.40	35.71	37.32	1.045	32.86	0.920

Where: f'_c specified, 28-day concrete compressive strength, P_{exp} experimental failure load, $P_{m.2}$, $P_{m.3}$ predicted failure load, from model no.2 and no.3, respectively, and S_{cr} flexural crack spacing, measured from experiment.

Table 6.1. (b) Results of analytical investigation of CCS, US customary system.

Beam code	f'_c (ksi)	S_{cr} (in.)	P_{exp} (kip)	Model no.2		Model no.3	
				$P_{m.2}$ (kip)	$P_{m.2}/P_{exp}$	$P_{m.3}$ (kip)	$P_{m.3}/P_{exp}$
CS70	8.58	2.37	8.74	8.62	0.985	8.09	0.925
SS70	8.09	2.40	8.53	8.36	0.981	7.93	0.930
CS195	7.30	3.36	8.43	8.30	0.984	7.29	0.865
SS195	7.44	3.37	8.03	8.39	1.045	7.38	0.920

Where: f'_c specified, 28-day concrete compressive strength, P_{exp} experimental failure load, $P_{m.2}$, $P_{m.3}$ predicted failure load, from model no.2 and no.3, respectively, and S_{cr} flexural crack spacing, measured from experiment.

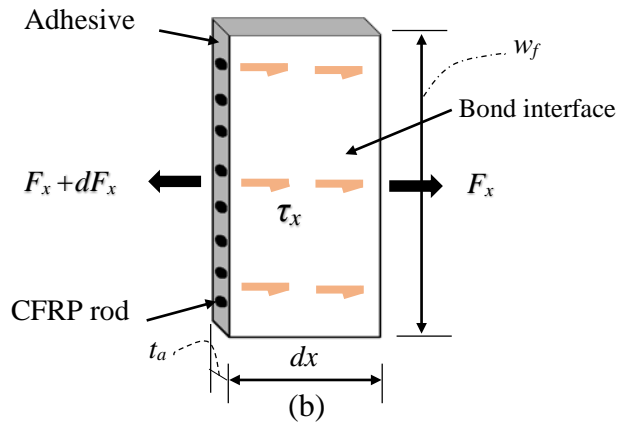
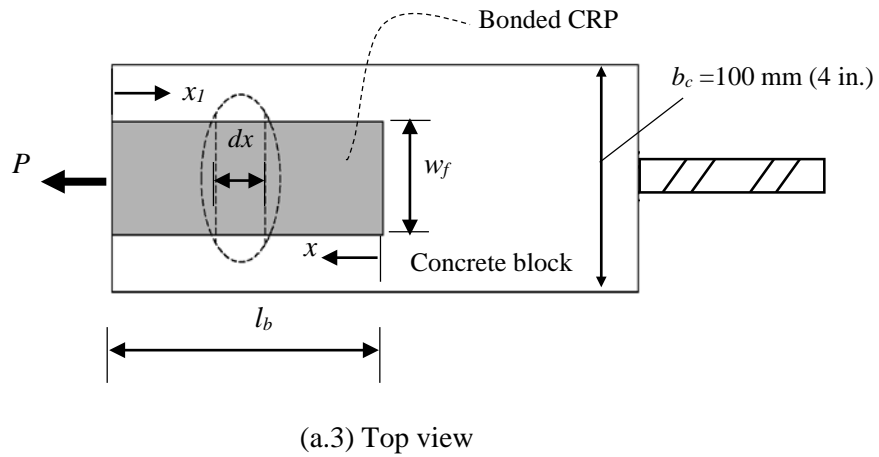
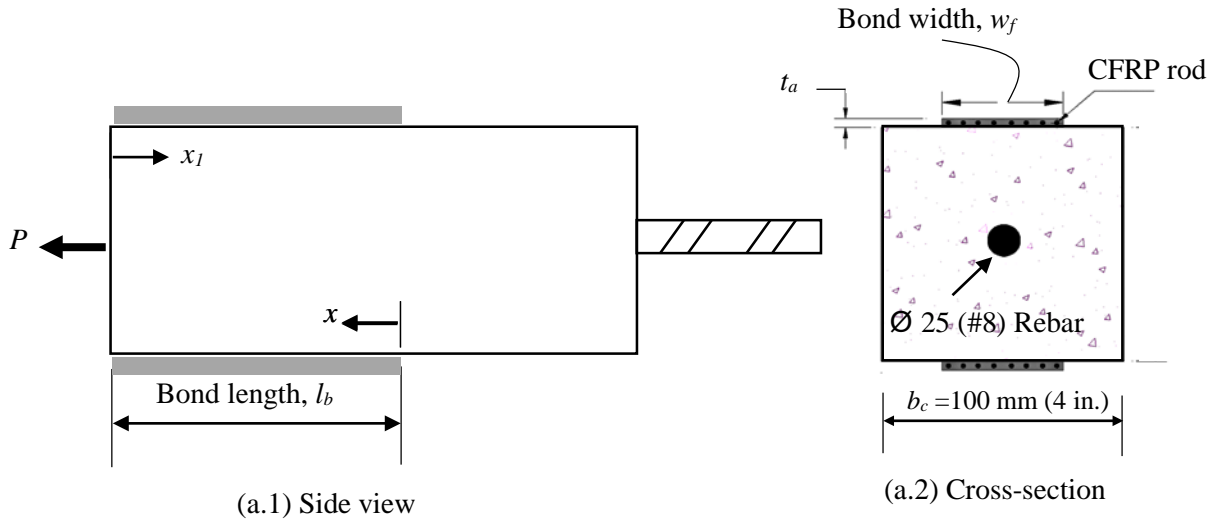
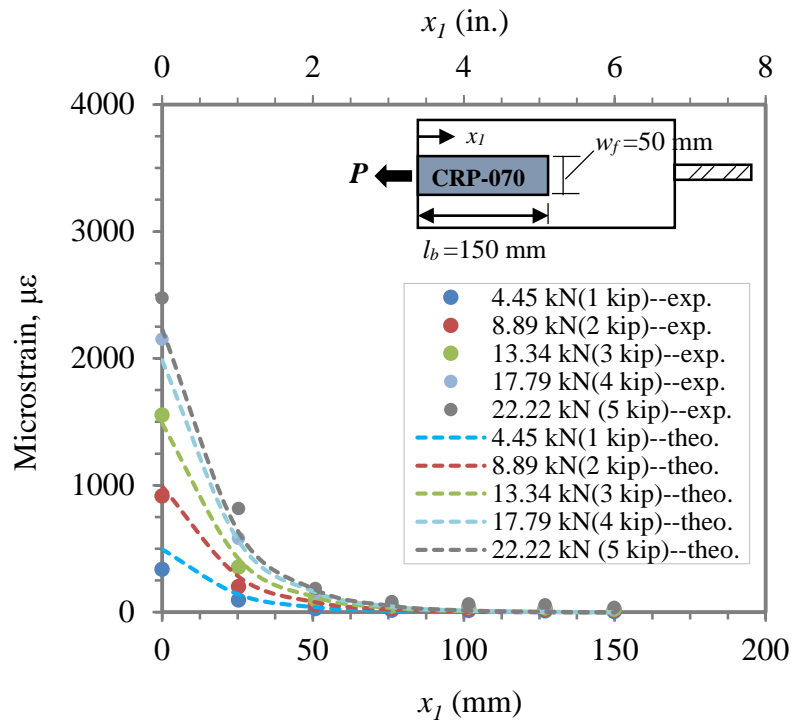
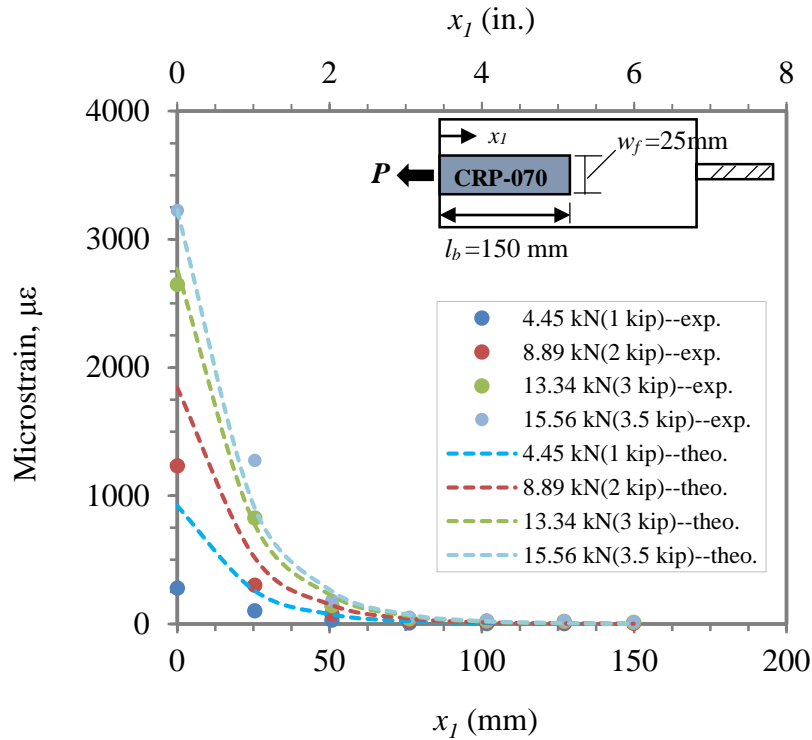


Fig. 6.1. (a) Concrete block bonded to CRP, (b) finite segment of bonded CRP, showing the bond interface and acting forces.

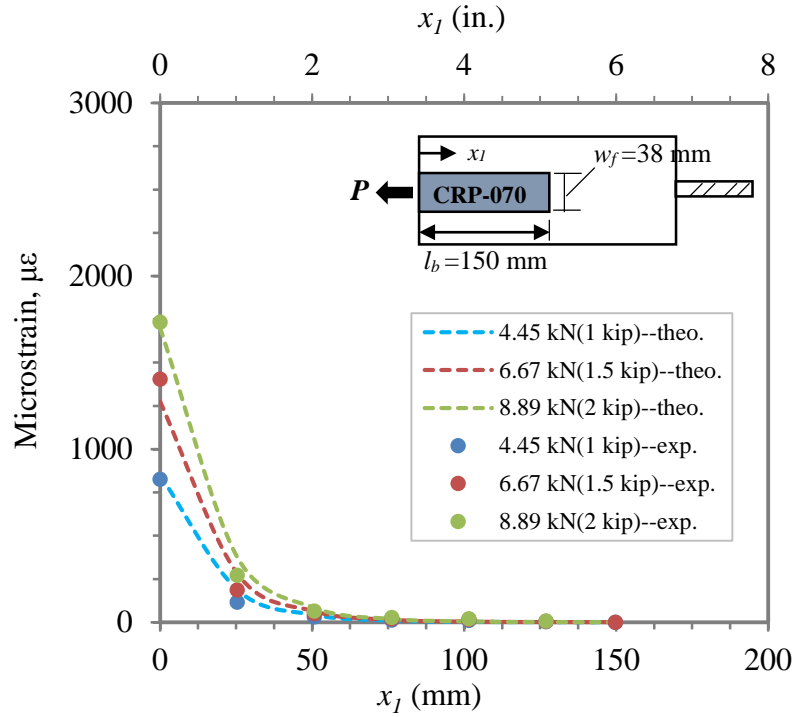


(a) Specimen (I-2-6-50-150)

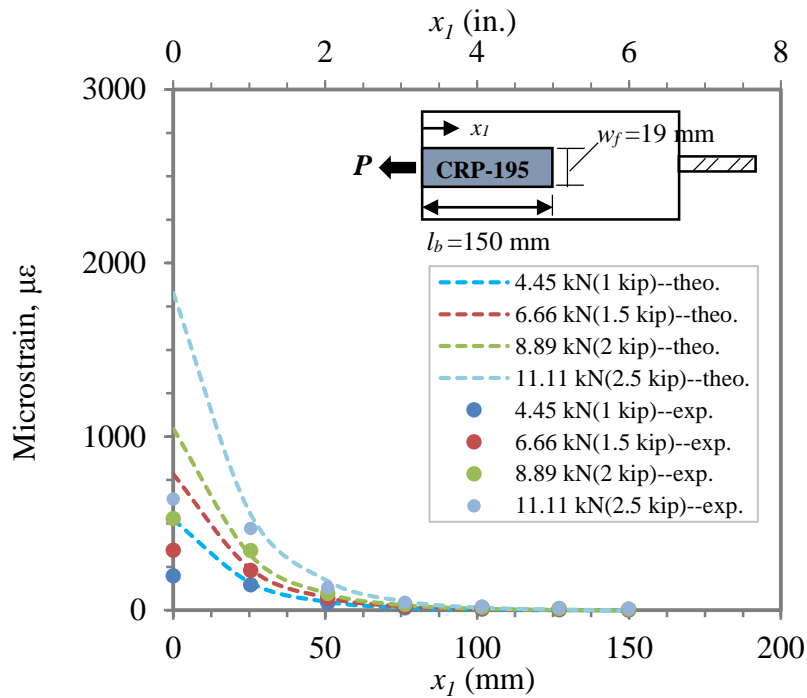


(b) Specimen (II-2-6-25-150)

Fig. 6.2. Experimental and analytical (model no.1) strain-displacement comparisons for double-lap shear tests.

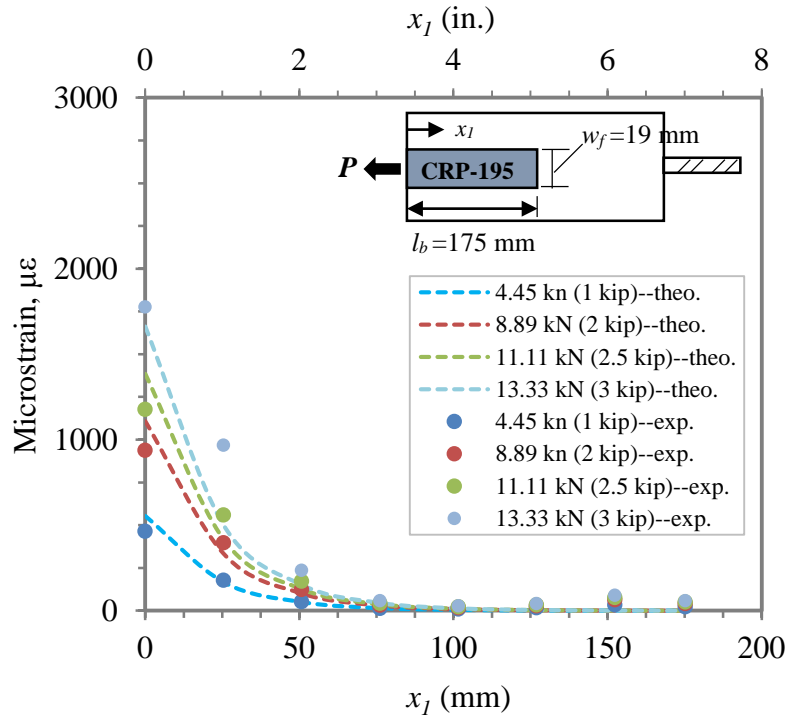


(c) Specimen (II-2-9-37-150)



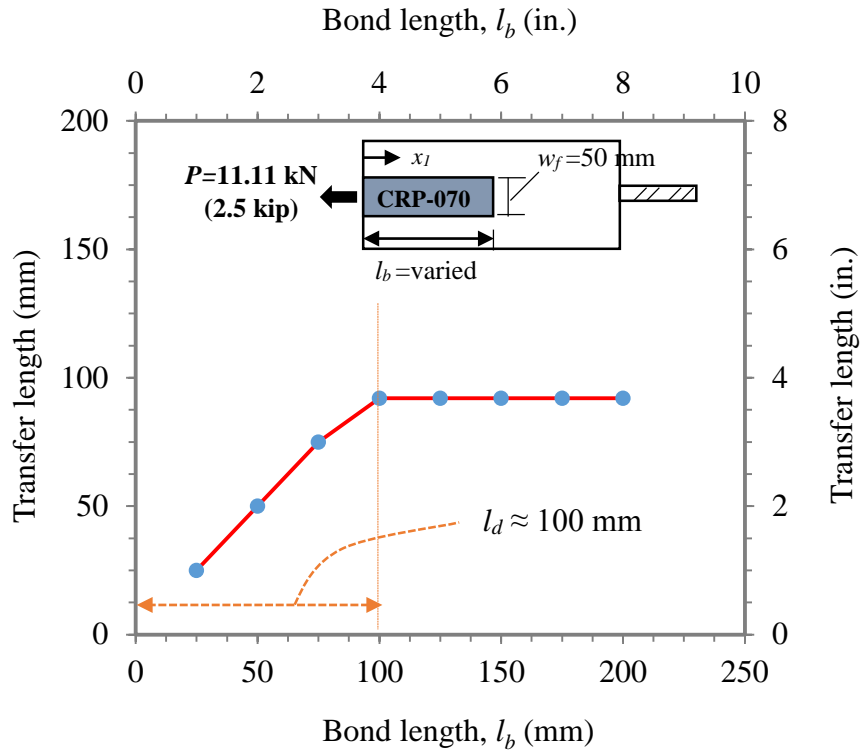
(d) Specimen (III-4-9-19-150)

Fig. 6.2. (continued) Experimental and analytical (model no.1) strain-displacement comparisons for double-lap shear tests.

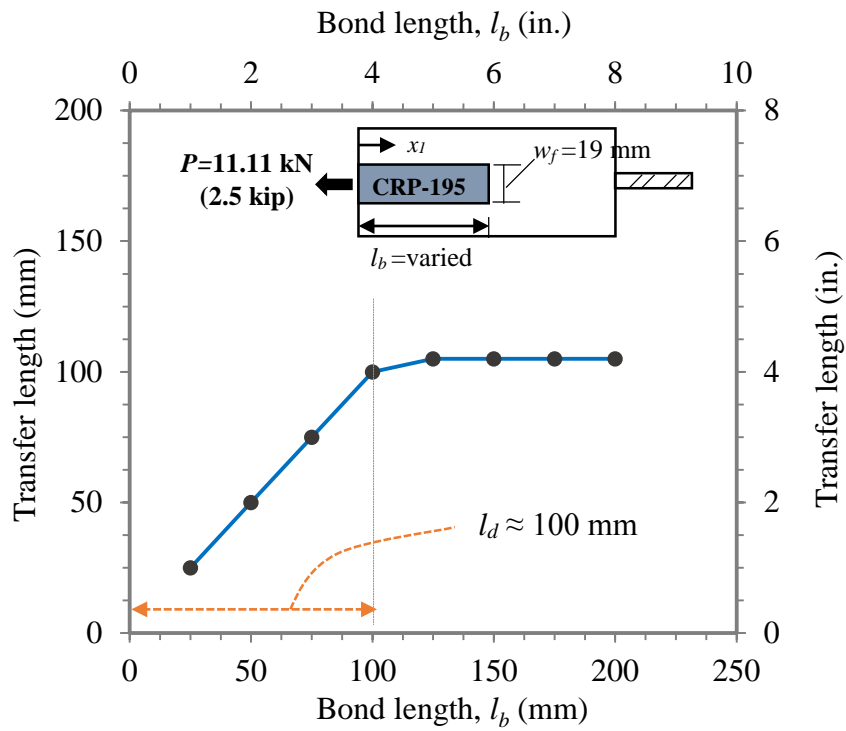


(d) Specimen (III-4-9-19-175B)

Fig. 6.2. (continued) Experimental and analytical (model no.1) strain-displacement comparisons for double-lap shear tests.

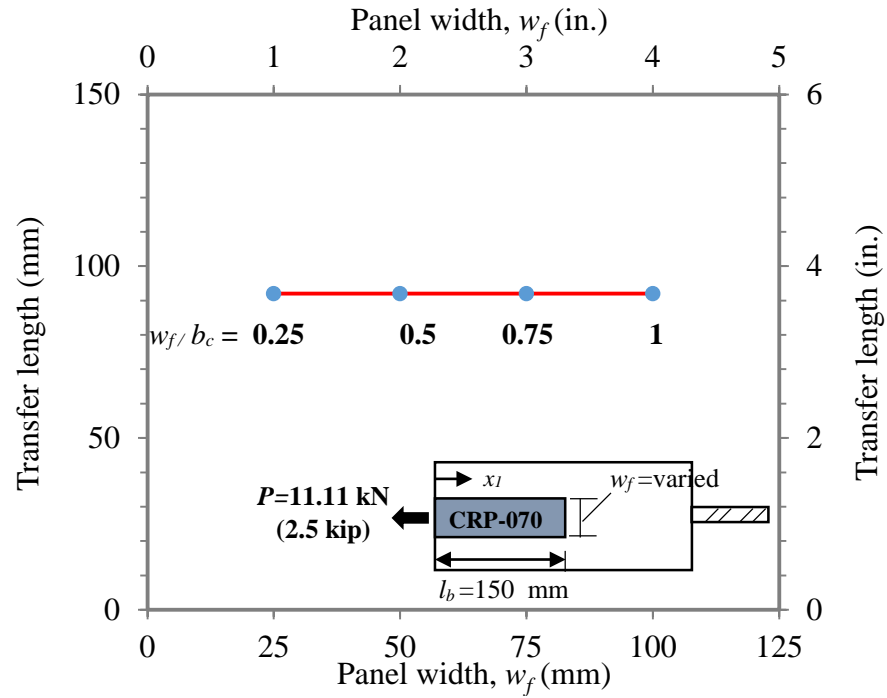


(a) CRP-070

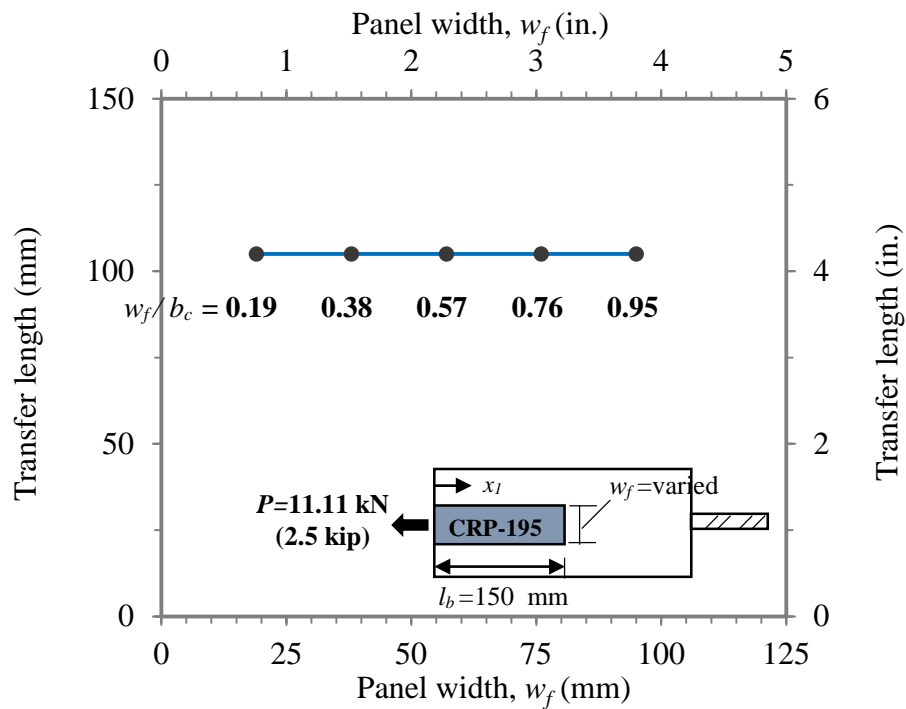


(b) CRP-195

Fig. 6.3. Transfer length vs. bond length relation, obtained from model no.1.



(a) CRP-070



(a) CRP-195

Fig. 6.4. Transfer length vs CRP width relation, obtained from model no.1.

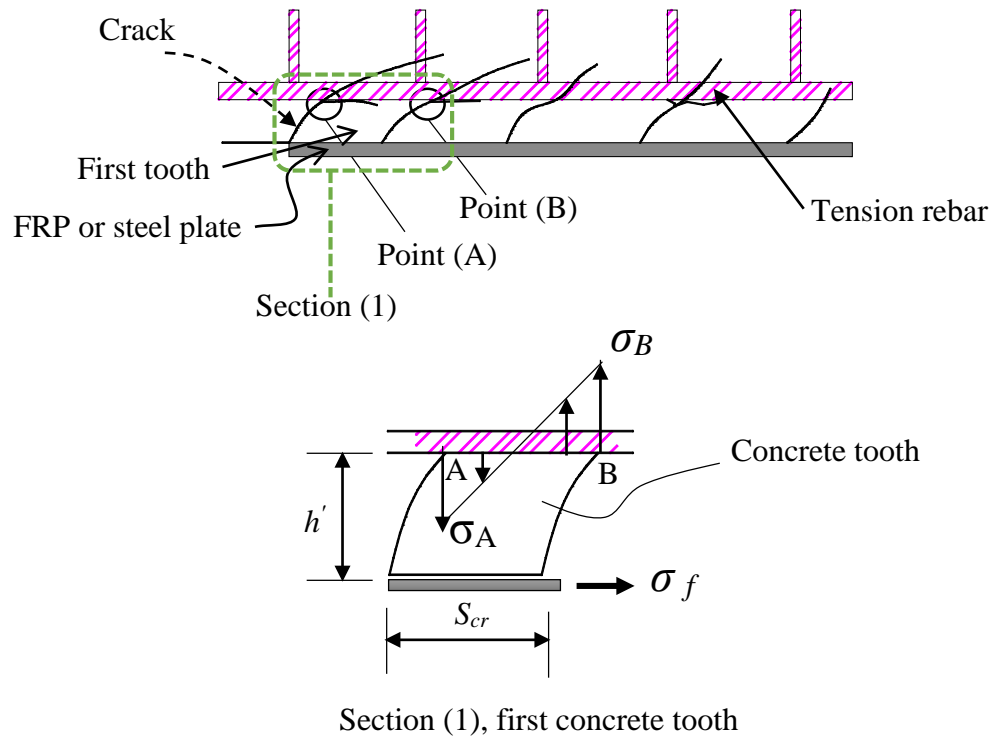


Fig. 6.5. Concept of concrete tooth models (after Zhang et al 1995).

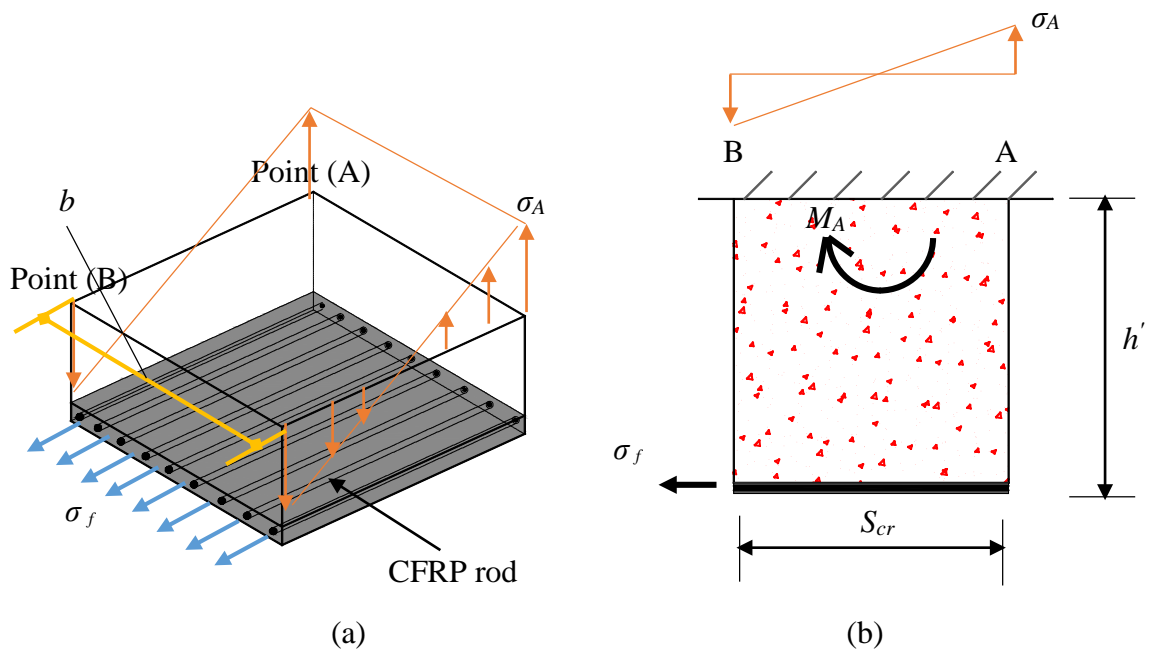
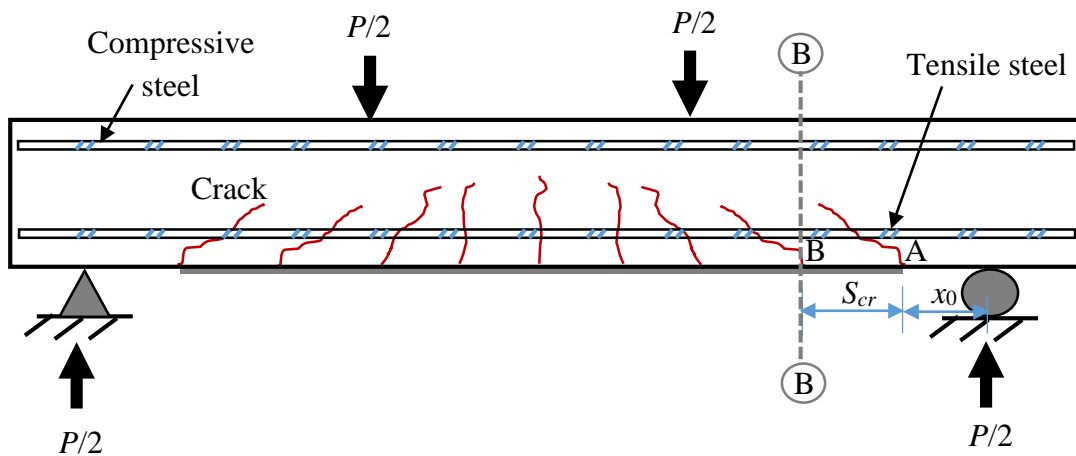
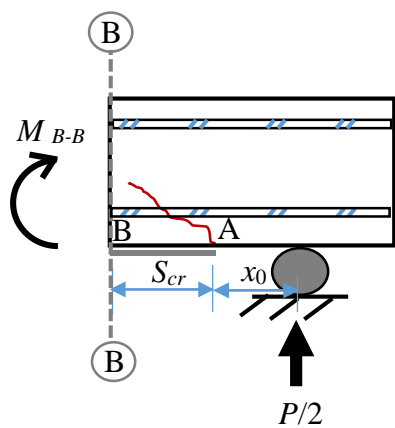


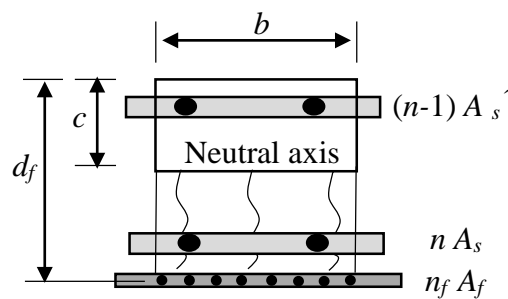
Fig. 6.6. First concrete tooth with proper forces, (a) three-dimensional section, (b) two-dimensional section.



(a) Side view of CRP strengthened beam with applied loads



(b) Section (B-B)



(c) Transformed and cracked beam cross-section

Fig. 6.7. CRP strengthened RC beam, calculations of bending moment (M_{B-B}).

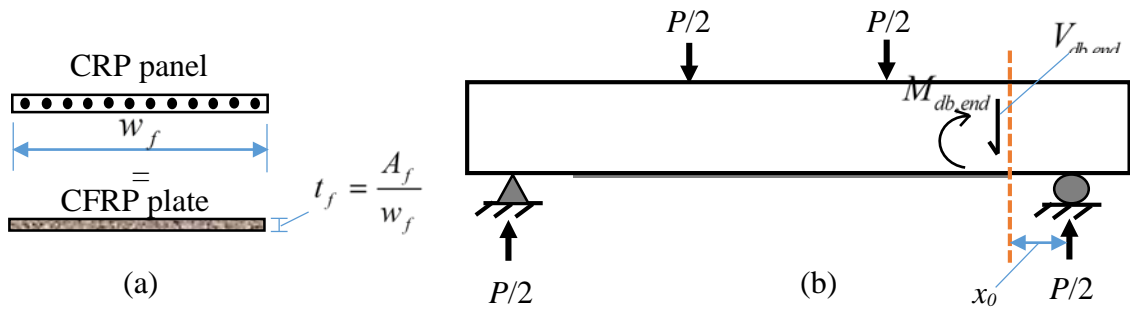


Fig. 6.8. (a) Equivalent plate concept, (b) tested beam, showing shear force and bending moment at panel's end and applied loads.

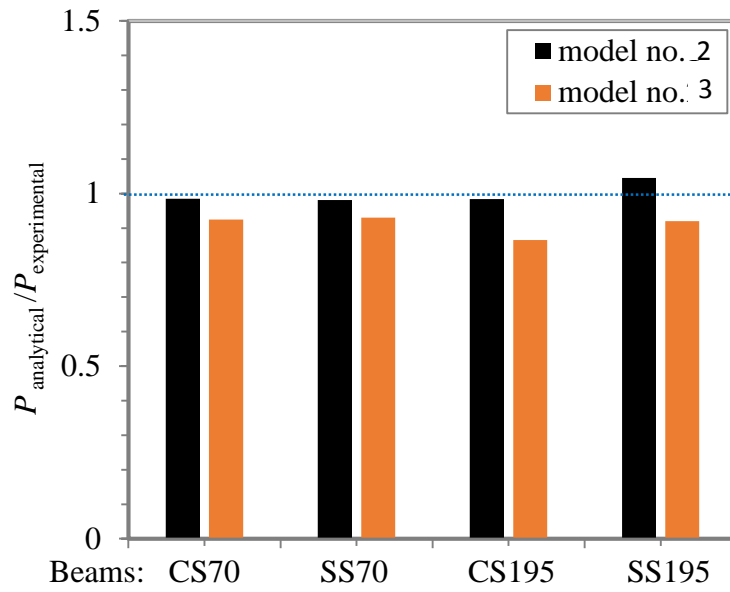


Fig. 6.9. Analytical/experimental failure load ratios for analytical models no.2, 3.

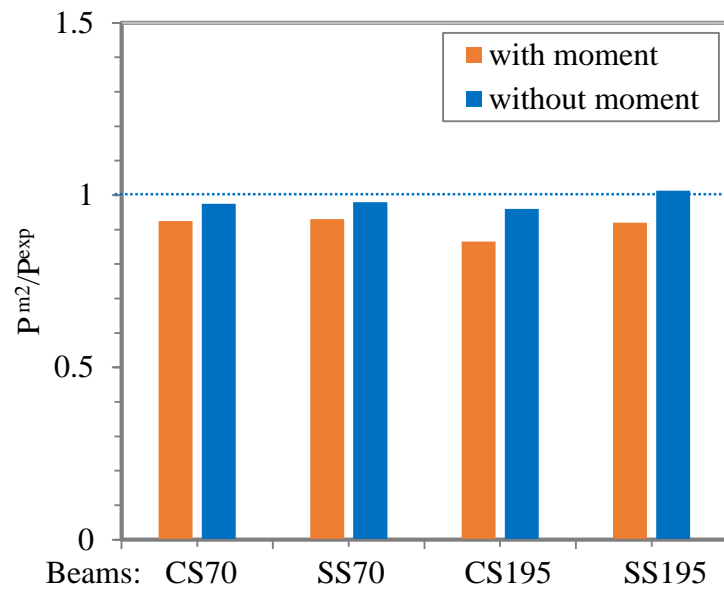


Fig. 6.10. Prediction of model no.3, as a percentage of experimental load, with and without bending moment.

CHAPTER 7: CONCLUSIONS AND RECOMMENDATIONS

7.1 Summary and Conclusions

This doctoral dissertation examined the bond and flexural characteristics of spliced CFRP rod panels (CRPs) when used for strengthening and repair of concrete structures. The bond performance of CRPs was investigated by conducting 25 double-lap shear tests on concrete blocks adhered to small-scale CRPs. The effectiveness of CRPs, as a flexural reinforcement to strengthen or repair concrete members, was investigated in four-point bending tests on nine RC beams that were: (1) un-strengthened, (2) strengthened with spliced CRPs, (3) strengthened with full-length CRPs, and (4) strengthened with full-length and spliced CFRP laminates. Three-dimensional (3D) finite element models were developed to examine the behavior of the experimental RC beam tests in order to extract essential data that could not be deduced from the experiments alone, and to examine the state of deformation, and stress of the CFRP rods. Additionally, analytical models were also developed to provide closed-form solutions to aspects of the bond and flexural response of concrete members bonded to CRPs.

7.1.1 Conclusions of Chapter 3 (Double-Lap Shear Tests)

Chapter 3 presented 25 double-lap shear experiments to estimate the development length, bond strength, and other properties related to the bond between the CRP and concrete substrate. Two CRPs were evaluated in this study, namely: CRP-070 [fabricated with 2 mm (0.078 in.) diameter CFRP rods, spaced at 6.35 mm (0.25 in.)], and CRP-195 [fabricated with 4 mm (0.156 in.) diameter CFRP rods, spaced at 9.5 mm (0.375 in.)]. Several bond lengths, ranging from 25 mm (1 in.) to 175 mm (7 in.) were tested in order to

estimate the bond properties of CRP-070 and CRP-195. Three bond widths, 25 mm (1 in.), 37.5 mm (1.5 in.), and 50 mm (2 in.), were included to quantify the effects of bond width. The effects of rod spacing were also preliminarily scrutinized, by testing three spacing: 6.35 mm (0.25 in.), 9.50 mm (0.375 in.), and 12.5 mm (0.5 in.). Based on the results of testing program, the following conclusions can be drawn:

1. Testing revealed three types of failure modes: concrete shear-off, concrete block failure by diagonal cracking, and rod peel-off. Most specimens of CRP-070, and CRP-195 failed by debonding at the concrete-adhesive interface through concrete shear-off beneath the adhesive layer. A thin concrete layer was attached to the debonded CRP after failure, having an average thickness of 1- 6 mm (0.04-0.24 in.).
2. The development length was found to be 100 mm (4 in.) for CRP-070 and 125 mm (5 in.) for CRP-195.
3. The bond strength for one-unit (e.g. one meter) wide CRP was determined to be 563 kN/m (38.5 kip/ft.) for CRP-070 and 712 kN/m (48.8 kip/ft.) for CRP-195. The average bond strength of the adhesive is estimated to be 5.5 MPa (0.85 ksi).
4. Strain variations along the CRP bond length for various load levels up to failure, were produced from strain gages mounted on the surface of CRPs. The strain variations were then used to establish the shear stress-slip relation for CRP-070 and CRP-195. Shear stress-slip relation is extremely useful when the behavior of CRP-concrete joint is studied by analytical or numerical solutions.
5. The bond width was found to have negligible effects on the bond behavior of CRP-070.

7.1.2 Conclusions of Chapter 4 (Four-Point Bending Beam Tests)

In chapter 4, the effectiveness of using spliced CRPs in strengthening/repair RC members was evaluated by conducting four-point flexural tests on nine RC beam specimens. The testing program consists of: (1) control (un-strengthened) beam; (2) two beams strengthened with a continuous (full-length) CRPs; (3) two beams strengthened with two spliced CRPs; (4) two beams strengthened with two spliced CRPs, and anchored at ends with U-shaped CFRP fabrics; (5) one beam strengthened with a continuous CFRP laminate; and (7) one beam strengthened with spliced CFRP laminate system. In (2), (3), and (4), one specimen was bonded to CRP-070 (fabricated with rods of $\text{Ø}=2$ mm, spaced at 6.35 mm), and the other bonded to CRP-195 (fabricated with rods of $\text{Ø}=4$ mm, spaced at 9.5 mm). The CFRP area (A_f) of CRP-070 and CFRP laminate are equal, 64 mm^2 ($100 \times 10^{-3} \text{ in.}^2$), while A_f of CRP-195 is 173 mm^2 ($268 \times 10^{-3} \text{ in.}^2$). The following paragraphs conclude the results of the tests:

1. The following are the maximum loads at failure for the strengthened beams and the corresponding percentage increase in load capacity, relative to the control beam: 38.98 kN (8.76 k) or 112% increase for the full-length CRP-070; 37.94 kN (8.53 k) or 106% increase for the spliced CRP-070; 47.43 kN (10.66 k) or 158% increase for the spliced/anchored CRP-070; 27.3 kN (6.15 k) or 49% increase for the full-length laminate; and 24.2 kN (5.45 k) or 31.8% increase for the spliced laminate.
2. Comparing CRPs with CFRP laminates, both full-length and spliced counterparts, it was found that CRPs achieved larger capacity increase. This is due to the different type of failure experienced in the CRP technique. CFRP laminates failed pre-maturely by

- debonding at laminate or splice ends, while debonding was not observed with CRP-070.
3. The maximum loads and percentage increase in load capacity for beams strengthened with CRP-195 are as follows: 37.42 kN (8.41 k) or 104% increase for the full-length CRP-195; 35.80 kN (8.05 k) or 95% increase for the spliced CRP-195; 54.17 kN (12.18 k) or 195% increase for the spliced and anchored CRP-195.
 4. Beams strengthened with full-length or spliced CRP-070 and CRP-195, failed at similar maximum loads; despite that the CFRP area, A_f , of CRP-195 is 2.7 times that of CRP-070. A_f was not effective in enhancing the flexural capacity due to the nature of failure in full-length or spliced CRP strengthened beams. Since the failure mode is initiated at concrete cover (concrete cover separation, CCS).
 5. CFRP end anchorage was very effective in preventing CCS failure and further increasing the load capacity of beams strengthened with spliced CRPs.
 6. The proposed 150 mm (6 in.) overlap seems to be sufficient in transferring forces between spliced panels and maintaining composite action throughout loading stages. Notably, specimens strengthened with spliced CRPs or full-length CRPs, both failed at comparable maximum loads and identical failure modes. No signs of debonding or distress were seen at the rod overlap region in all of the four beams strengthened with spliced CRPs. In contrast, spliced CFRP laminates debonded from the laminate system.
 7. The control beam failed in the conventional way of under-reinforced concrete members, by yielding of tensile steel reinforcement, followed by crushing of compressive concrete in the mid-span region. Beams strengthened with full-length and spliced CRPs failed by CCS at one of the panel ends. Beams strengthened with spliced

- and anchored CRPs failed by intermediate crack-induced debonding (ICID). While beams strengthened with CFRP laminate, both spliced and full-length, failed by laminate or splice end debonding.
8. On average, the first concrete crack was visibly observed at loads of: 8.9 kN (2 kip) for the control beam, 15.7 kN (3.5 kip) for beams strengthened with CRP-070, 23.7 kN (5.3 kip) for beams strengthened with CRP-195, and 13.3 kN (3 kip) for beams strengthened with CFRP laminate. For the control beam and beams bonded to CFRP laminate, cracks were located at both inside and outside the constant moment region. Whereas, for CRP strengthened beams, except in the SS70 beam, cracks were limited to within constant moment region.
 9. The measured post-yielding neutral axis (N.A) is approximately 37.5 mm (1.5 in.) for CRP-070 strengthened beams, 50 mm (2 in.) for CRP-195 strengthened beams, and 40 mm (1.6 in.) for CFRP laminate strengthened beams.
 10. The maximum adhesive shear stress, τ_a , for beams bonded to full-length or spliced CRPs is roughly 3 MPa (0.445 ksi), which is less than the adhesive average bond stress of 5.50 MPa (0.80 ksi), previously estimated from double-lap shear tests.
 11. The two beams strengthened with spliced and anchored CRPs, which failed by ICID, showed large strain values near the loading-point, along with a maximum shear stress of 5-7.5 MPa (0.72-1.09 ksi). This shear stress range exceeds the average bond stress and strain limit set forth by ACI 440.2R-08 (2008), indicating that debonding might have initiated near load-point.
 12. For the beam bonded to full-length CFRP laminate, the debonding process started approximately at a load level of 0.75, $[(P/P_{max})]$, where P is current load, and P_{max} is

maximum load)], with a maximum stress of 4.25 MPa (0.62 ksi). This registered at roughly 150 mm (6 in.) from the laminate end.

13. For the beam strengthened with a spliced CFRP laminate system, the debonding process started approximately at a load level of 0.375, with a maximum stress of 2 MPa (0.29 ksi). This registered at spliced ends, with debonding then propagated toward the mid-span region.

7.1.3 Conclusions of Chapter 5 (Finite Element Analysis)

In chapter 5, a comprehensive 3D nonlinear finite element (FE) model was developed to simulate the behavior of RC beams strengthened in flexure with CRPs and CFRP laminate. The developed F.E model accounts for: concrete nonlinear behavior in tension and compression, confinement effects on concrete compressive stress-strain relation, concrete cracking, and crushing. The debonding failure of various reinforcement at several interfaces, was accounted for in the FE model by using cohesive zone material (CZM) and interface elements. The following conclusions can be outlined, based on the findings of this study;

1. There is a good agreement between FE predictions and experimental results when comparing the load vs. mid-span deflection response, load vs. strain in CFRP at mid-span, and strain profile along CFRP length. Furthermore, due to implementing a displacement-controlled loading scheme, the FE response was reasonably able to capture the drops in load that were seen in some specimens due to debonding or concrete crushing failures.

2. The model accurately predicted the debonding failure of (1) CRP and CFRP laminate from a beam's tension face, (2) CFRP fabric from the beam's side, and (3) CFRP splice from the laminate system.
3. Concrete cover separation failure was predicted in the FE analysis by using post-processing analysis, along with tensile stress failure criteria for concrete. The failure criteria is employed for a concrete section near the termination of CRP, at the level of tension steel reinforcement. The assumed analysis methodology appeared to give a reliable prediction, since the failure load obtained from the analysis is in good agreement with the experimental failure load, with the difference between FE and experimental maximum loads range between 2.87% and 6.22%.
4. At failure, the FE results indicated that the CRP-070 is stressed to 58% and 53% of the guaranteed strength for the full-length panel and the two spliced panels, respectively. The CFRP laminate is stressed to 25% and 22% of the guaranteed strength for full-length laminate and the spliced laminate system, respectively.
5. FE predicted that the concrete's maximum compressive strain, at mid-span, ranged between (0.004-0.005), for beams that experienced concrete crushing failure (control beam, and beams strengthened with CFRP laminate). Those values exceed the maximum compressive strain of 0.003, adopted in (ACI 318-14) code. The model predictions of the concrete maximum compressive strains (of the CRP strengthened beams) were less than the ACI's 0.003 strain limit.
6. At all load levels, the maximum tensile stress in the full-length CFRP laminate, full-length CRP-070, and the two spliced CRP-070 are all of comparable magnitudes. Also,

the full-length and spliced CRP-195, have a comparable maximum tensile stresses at same load levels.

7. The maximum tensile stress of two spliced CRPs (i.e. CRP-070 or CRP-195) occurs at 12.5 mm (0.5 in.), outside the rod overlap region. The stress inside the overlap region is fairly uniform, and the magnitude of the average stress inside the overlap is almost half the maximum stress.
8. The FE models predicted a high shear stress concentration at the end of the CRPs in all beams strengthened with full-length or spliced CRPs. The fabric anchorage seems to be effective in shifting the location of maximum shear stress from the panel's end to inside the strengthening length [225 mm (9 in.) from CRP's end toward the center of the beam] and at load points.

7.1.4 Conclusions of Chapter 6 (Analytical Models)

Chapter 6 analytically examined aspects of the bond and flexural properties of CRPs when adhered to concrete substrate. Given in this chapter, were two studies. In the first study, an analytical model (model no.1), based on the simple shear lag approach, and was applicable only for moderate loads within the linear elastic range, was derived to characterize the outcomes of double-lap shear tests. Analytical terms were presented for CRP strains, adhesive shear stress, and slip between CRP and concrete. The second study investigated concrete cover separation (CCS) failure, observed in the experimental RC beam testing, in which four specimens strengthened with full-length or spliced CRPs, failed by CCS. Two analytical models, one based on concrete tooth concept (model no.2) and the other on concrete shear capacity (model no.3), were derived for estimating the ultimate load of CRP

strengthened RC beams when CCS is predominant. The following, are concluded remarks of the chapter:

- 1- Comparisons of tensile strains, along the entire CRP bond length, in double-lap shear tests, showed a good correlation between analytical model no.1 and the experiment.
- 2- The approximate development length predicted from model no.1, for both CRP-070 and CRP-195, was 100 mm (4 in.).
- 3- The panel width was found to have negligible effects on transfer length of CRP-070 and CRP-195, as examined by model no.1.
- 4- The ultimate loads obtained from analytical models no.2 and no.3, were compared with failure loads of the experimental beams. It was found that both models presented a very good match with the experiment. The maximum difference in analytical and experimental load ratio, is 4.5%, and 13.5 % for model no.2 and no.3, respectively.
- 5- Model no. 3 was further reviewed and was found that when the term containing bending moment at CRP ends is removed from the model, a better match with experimental results can be obtained. Therefore, a modified model, that neglects the bending moment at ends, is given. The modified equation is only applicable for the beams tested in this experiment, as more data is needed before making any generalizations.

7.2 Study Limitations and Future Recommendations

The current research examined both the bond and flexural properties of spliced CRPs when used as an external reinforcement to strengthen or repair concrete members. Double-lap shear tests, four-point bending tests, F.E models, and analytical tools were carried out to evaluate the effectiveness of the overlap rod joint in maintaining composite action between

neighboring panels and transferring forces from one panel to another. However, the current study only investigated some areas concerning the performance of spliced CRPs as an external reinforcement for concrete members. Due to inevitable limitations on time, funds, laboratory space or apparatus, not all areas of investigation were included. However, some of those areas, which can deepen the understanding of the CRP behavior and its interaction with the structural member, were identified and listed as follows for investigative studies in the future:

1. The double-lap shear tests included only few samples that examined preliminarily the effects of bond width and rod spacing. Further tests, are needed to determine the effects of bond width and rod spacing.
2. The double-lap shear tests did not take into account the effects of concrete surface preparation methods, CRP axial stiffness, and adhesive properties. These factors, among others, are expected to have an impact on the bond between CRP and concrete substrate and need further examination.
3. The bond properties of CRPs were determined from pure shear tests. In practice, CRPs are used at locations where both shear forces and bending moments are present, therefore in those circumstances, beam tests could better evaluate the bond characteristics of CRPs.
4. Small-scale beam tests were used in the current investigation. Larger scale (field size) specimens can be tested experimentally or studied by reliable finite element models to assess the behavior of CRPs when used in actual rehabilitation practices. Furthermore, field testing on bridge or other typical structures, can provide essential data on the

- efficiency of CRP strengthening systems by evaluating: time of CRP application, labor, and cost, in addition to measurements of structural properties before and after retrofit.
5. In the four-point beam tests, CRP width, w_f , was set equal to the beam's width, b_c , (or width ratio, $w_f/b_c = 1$). Further experimental or F.E studies should cover a wide range of ratios in order to study the effects of (w_f/b_c) . Extensive research has been dedicated to study the effects of (w_f/b_c) for externally bonded FRP laminates and fabrics, and has concluded that pre-mature debonding failures are likely with small width ratios.
 6. The beams were made of high-strength concrete [$f'_c = 62$ MPa (9 ksi)]. A wider range of concrete strengths, varying from normal to high strength, need to be tested in order to cover the effects of concrete strength.
 7. The testing was limited to simply supported, rectangular beams, under four-point bending. Other geometrical shapes, such as flanged sections and slabs, and other support conditions and loading types can be investigated experimentally, analytically, or numerically.
 8. As in most retrofit projects, the concrete member is generally retrofitted after being in service for a considerable time. Therefore, the effects of pre-loading (pre-cracking) and effects of concrete damage can be examined to determine their influence on the behavior of CRP retrofitted RC members.
 9. The study was limited to static loading. Cyclic and fatigue loads can be further investigated for CRP adhered structures.
 10. The effects of long-term behavior and environmental effects such as concrete creep, freezing-thawing cycles, and effects of temperature need to be further studied.

11. Other structural substrates such as steel, timber and masonry can be investigated to evaluate the applicability of CRP system for those important materials.

7.2.1 Effects of Rod Spacing

The double-lap testing program included three specimens that were intended to preliminarily examine the effects of varying rod spacing, S . The specimens utilize CRP-070, and all have the following: bond length, $l_b = 150$ mm (6 in.), four rods with diameter, $\varnothing = 2$ mm (0.078 in.), in each double-lap shear side. The varied parameter was S , and three values were investigated: 6.35 mm (0.25 in.), 9.5 mm (0.38 in.), and 12.5 mm (0.50 in.). The bond width, w_f is a function of the rod spacing and number of rods, and therefore w_f was altered once S was varied. However, the double-lap testing studied the effects of w_f on CRP bond behavior, and it was found that w_f had negligible effects.

The failure load for the specimen with $S = 6.35$ mm was 31.84 kN (7.16 kip), while it was 47.195 kN (10.61 kip) for specimen with $S = 9.5$ mm and 49.322 kN for specimen with $S = 12.5$ mm. Furthermore, the failure mode was altered when S was increased. For specimen with $S = 6.35$ mm, the failure mode was concrete shear-off, (see figure 7.1), while for specimens with $S = 9.5$, and 12.5 mm, the failure mode was rod peel-off from the embedding adhesive, combined with cracks and fracture of the adhesive at locations near the gap between the two concrete blocks, (see figure 7.2). Figure 7.3 shows the stress ratio, f_f , in CFRP rods for each one of the three tested specimens. f_f was derived by dividing the failure stress in the rods (calculated as the specimen's failure load divided by CRP area) by the guaranteed CFRP rod strength, 2,340 MPa [(320 ksi), Diversified Structural Composites (2016)]. As can be seen in the figure, the rods were able to carry 86% and

91% of the manufacturer guaranteed strength when the rod spacing was 9.5, and 12.5 mm, respectively; while for rod spacing of 6.35 mm the rods were only stressed to 58% of the guaranteed strength.

While the tested specimens were very limited [three spacings with only one specimen for each spacing], and that would prevent making any sound judgment regarding the exact effects of rod spacing, the specimens serve as incentive to study the effects of rod spacing in depth with larger scale in terms of spacing range and quality control. Using a large-yet-satisfactory rod spacing is extremely important, since FRP material is still expensive and any reduction in the material quantity while providing an adequate performance, would provide an economic solution.

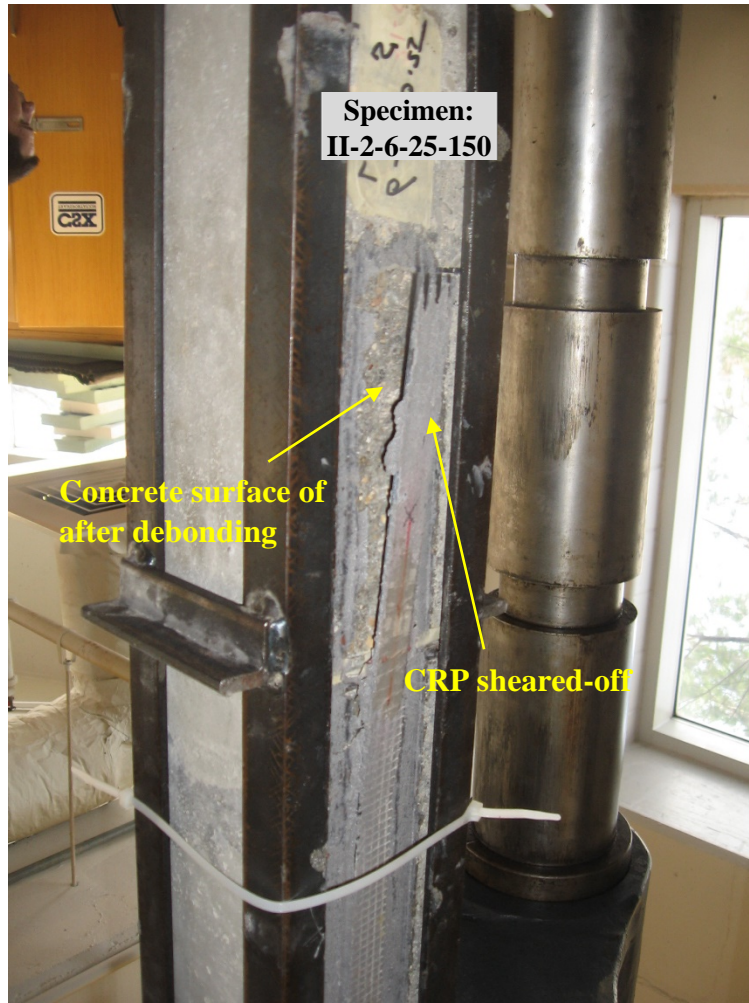
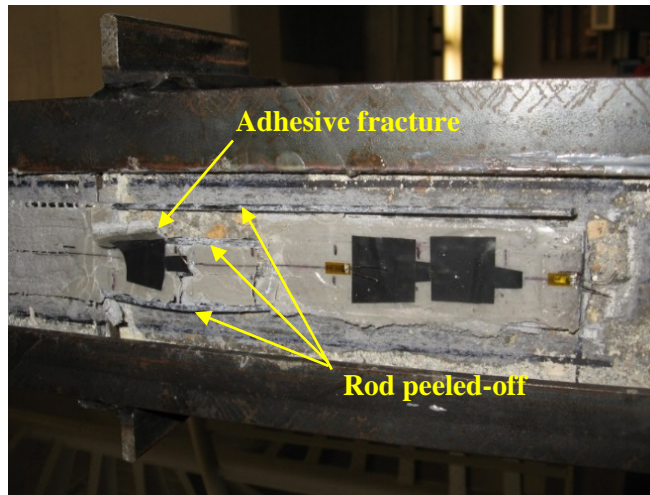
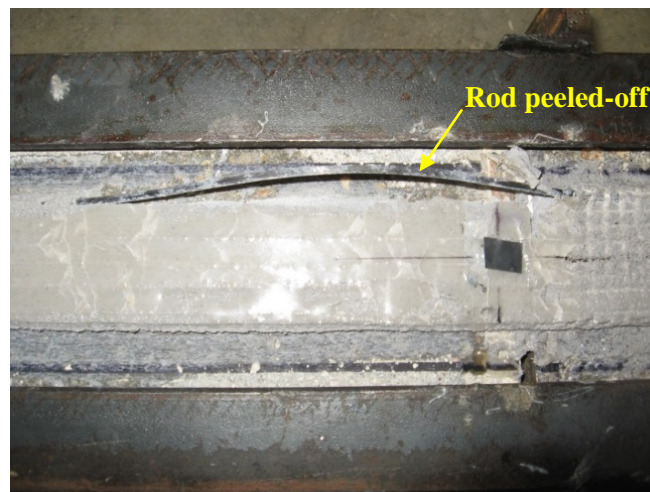


Fig. 7.1. Concrete shear-off failure in specimen with rod spacing, $S = 6.35$ mm (0.25 in.).



(b) Monitored side, specimen (II-2-9-37-150)



(b) Un-monitored side, specimen (II-2-9-37-150)

Fig. 7.2. Rod peel-off failure in a specimen with rod spacing, $S = 9.5$ mm (0.375 in.).

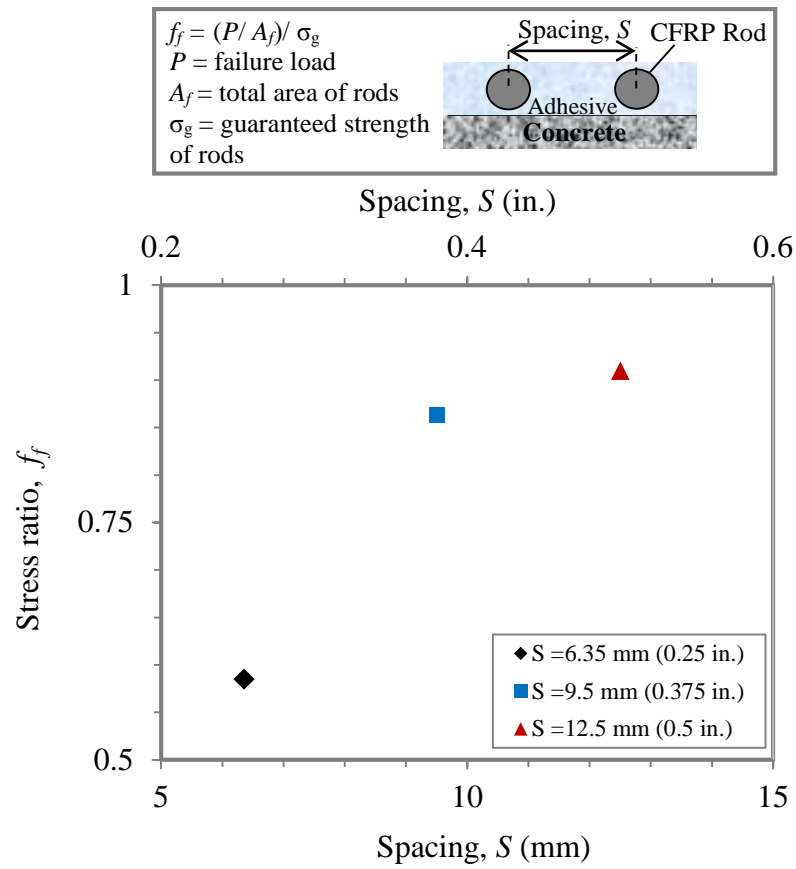


Fig. 7.3 Stress ratio in CFRP rods of specimens with different rod spacing.

**APPEDIX A: BOND STUDY ON CFRP ROD PANELS EXTERNALLY
ADHERED TO CONCRETE**

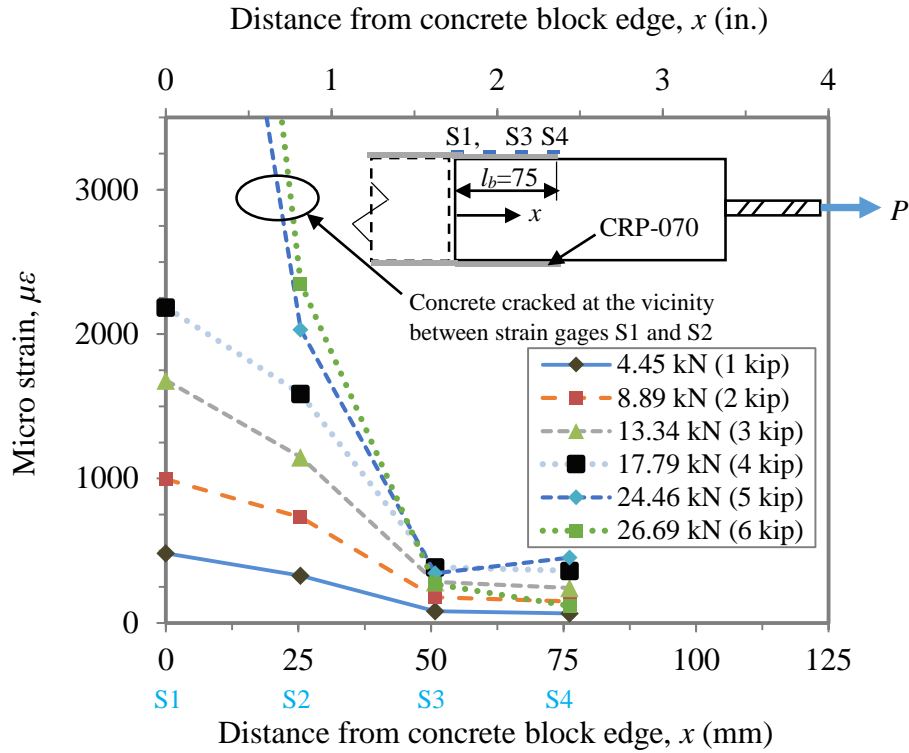


Figure. A. 1 Strain variation along bond length, for specimen (I-2-6-50-75).

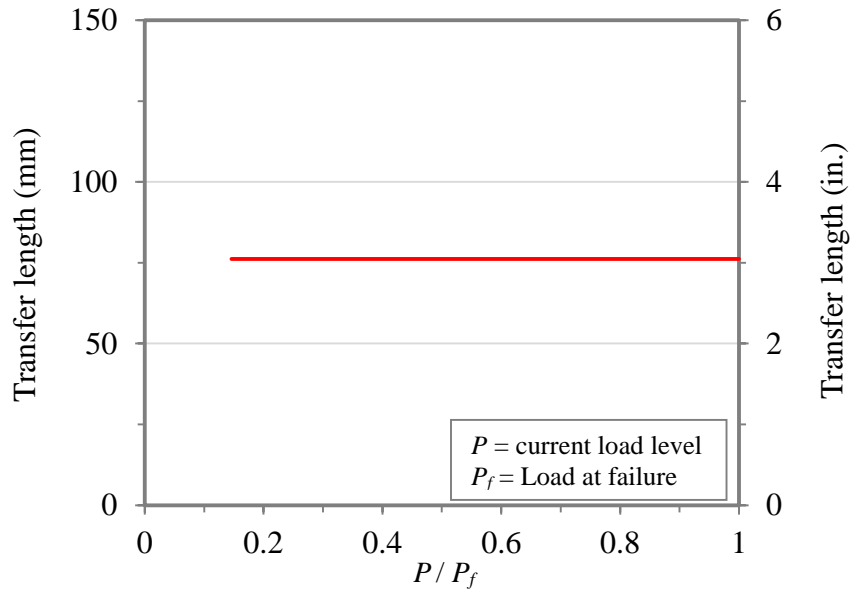


Figure. A. 2 Measured transfer length vs. relative load level, specimen (I-2-6-50-75).

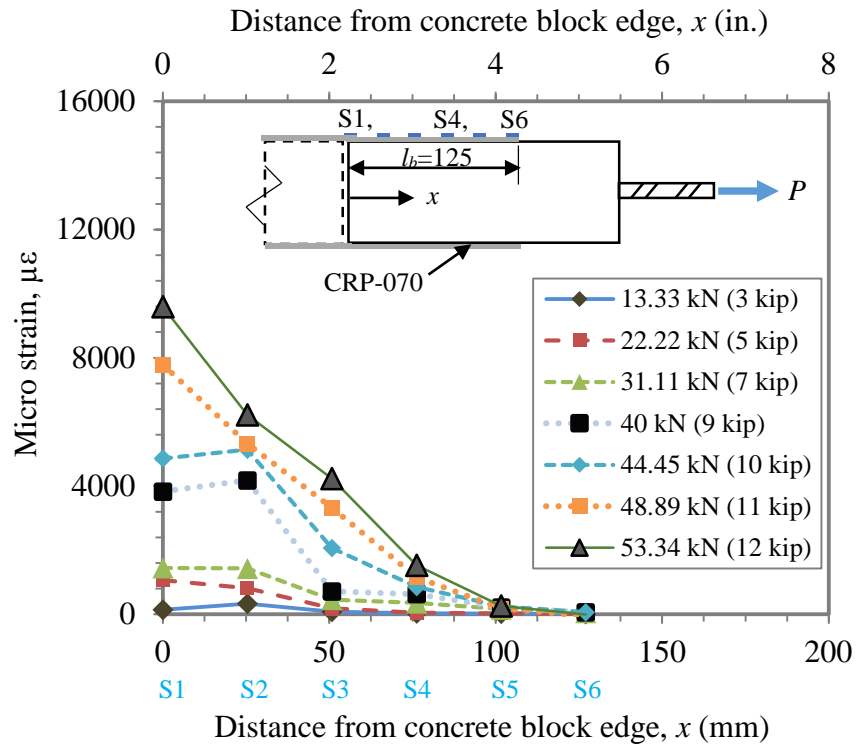


Figure. A. 3 Strain variation along bond length, for specimen (I-2-6-50-125).

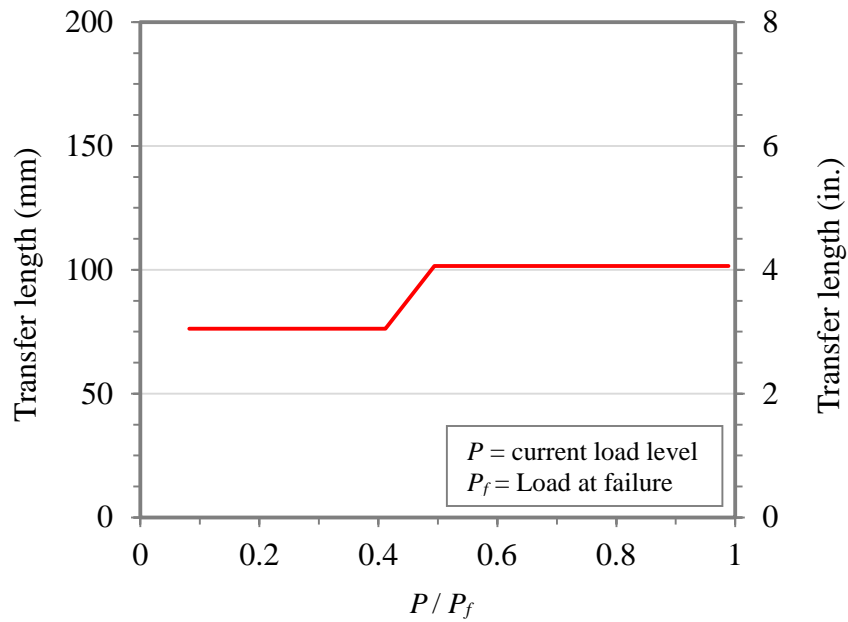


Figure. A. 4 Measured transfer length vs. relative load level, specimen (I-2-6-50-125).

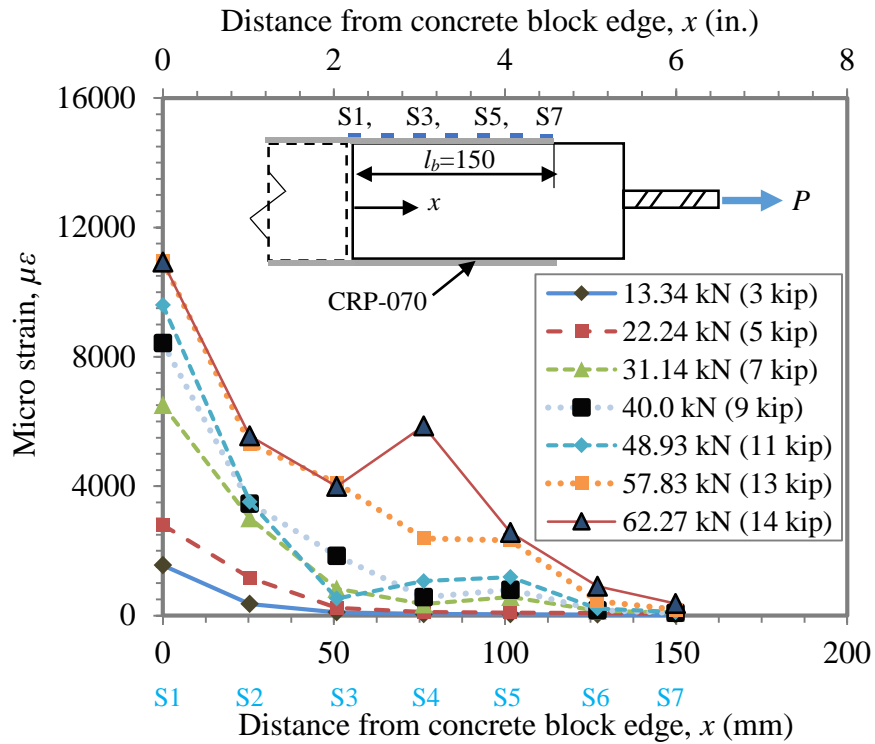


Figure. A. 5 Strain variation along bond length, for specimen (II-2-6-25-150).

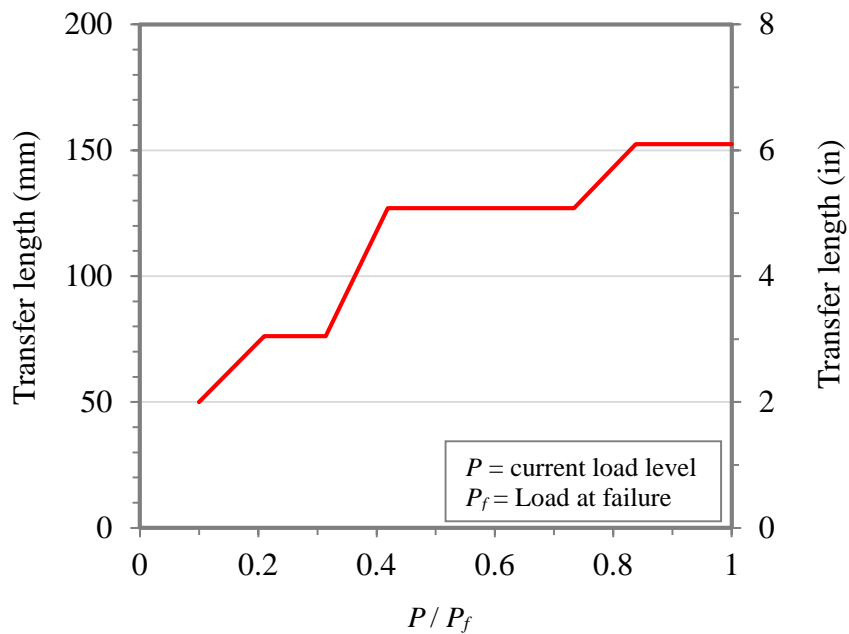


Figure. A. 6 Measured transfer length vs. relative load level, for specimen (II-2-6-25-150).

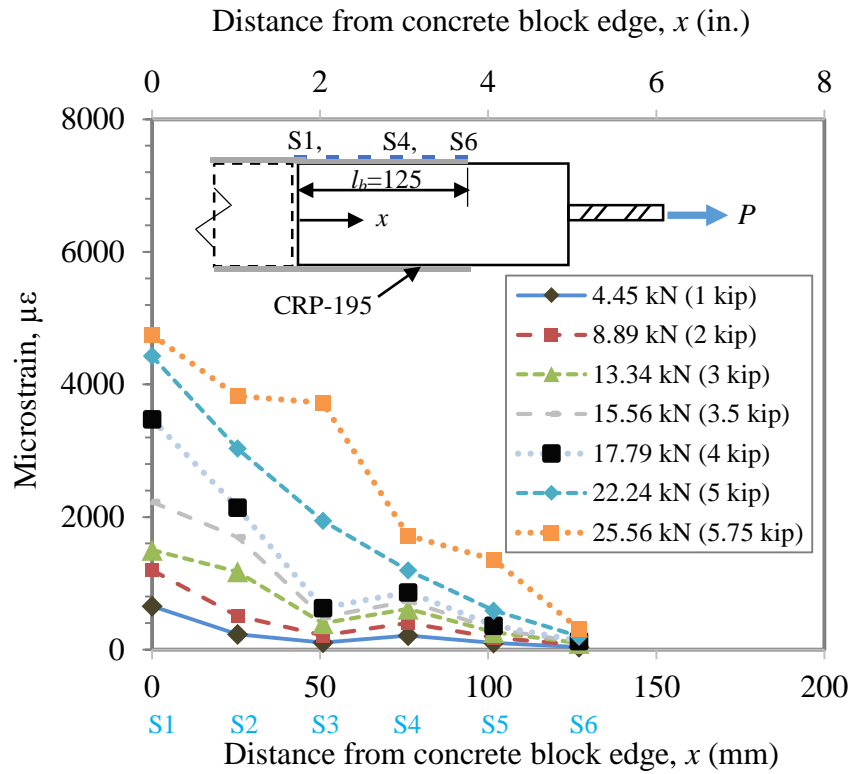


Figure. A. 7 Strain variation along bond length, for specimen (III-4-9-19-125).

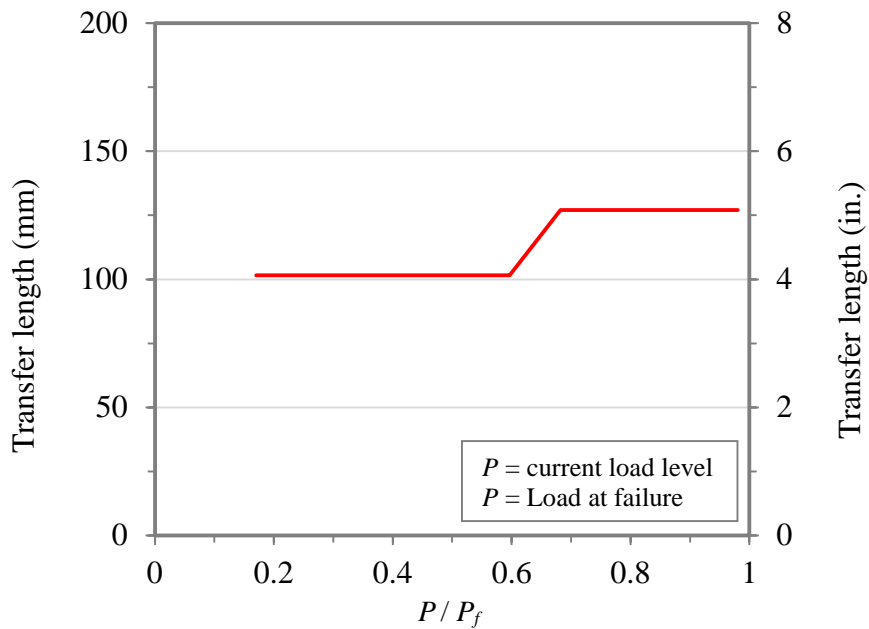


Figure. A. 8 Measured transfer length vs. relative load level, specimen (III-4-9-19-125).

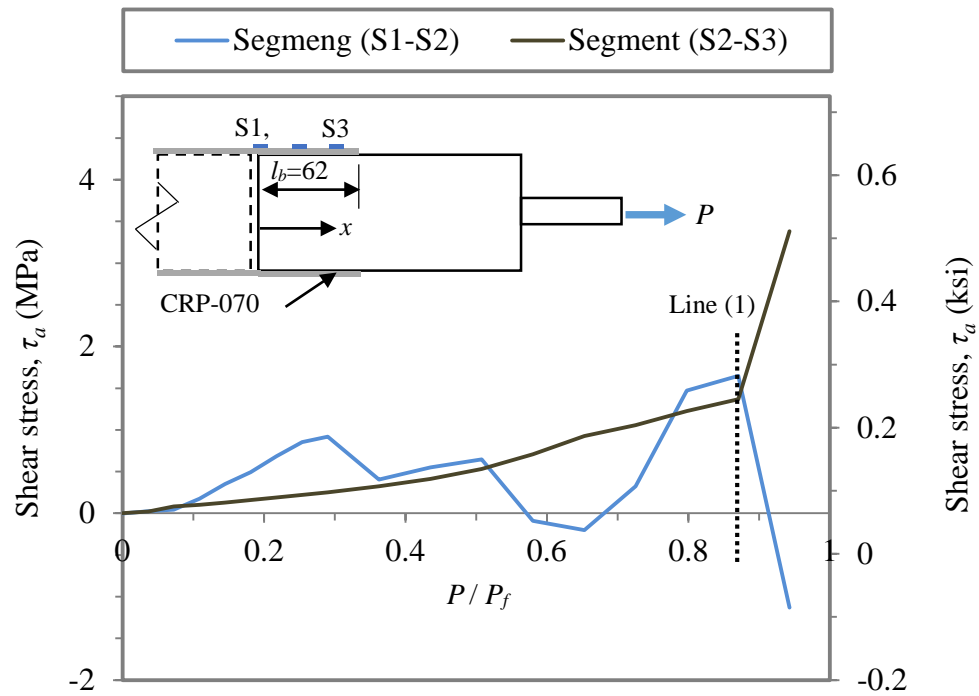


Figure. A. 9 Shear stress vs. relative load level for specimen (I-2-6-50-62.5).

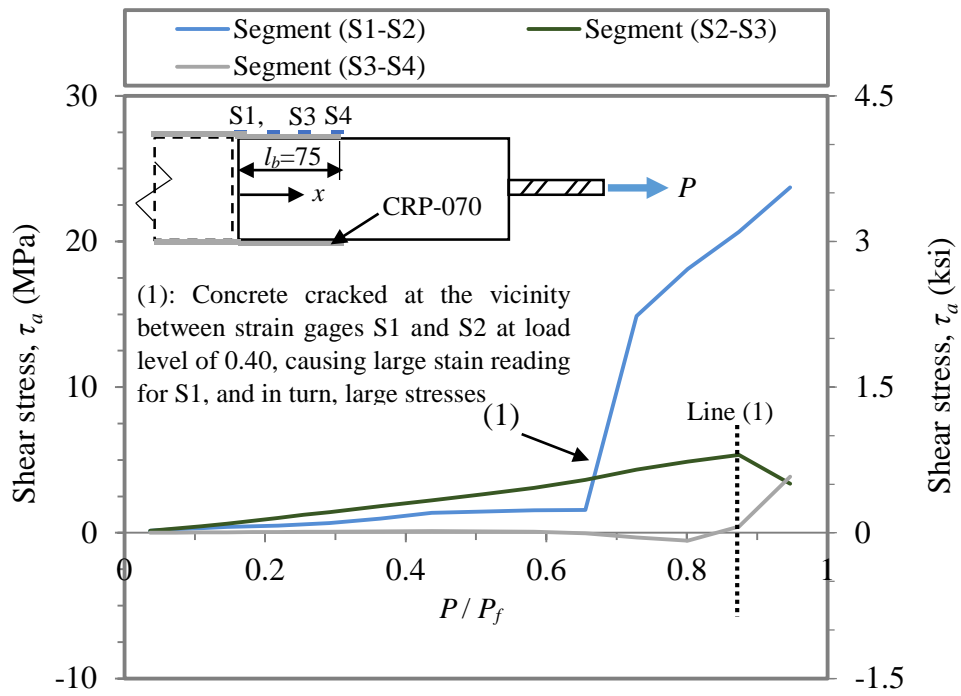


Figure. A. 10 Shear stress vs. relative load level for specimen (I-2-6-50-75).

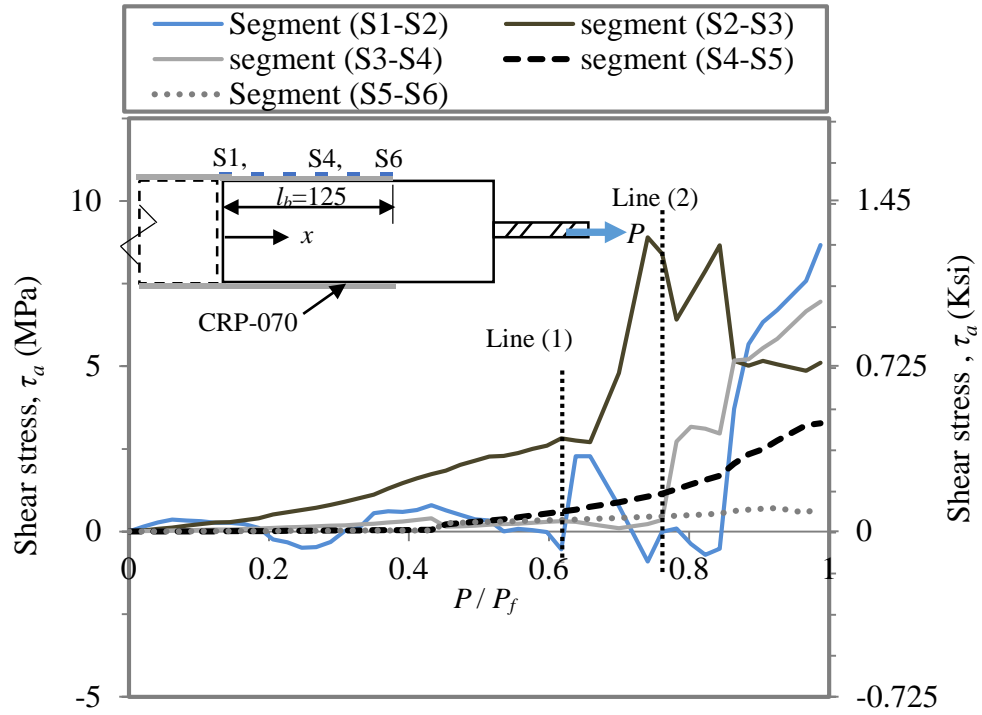


Figure. A. 11 Shear stress vs. relative load level for specimen (I-2-6-50-125).

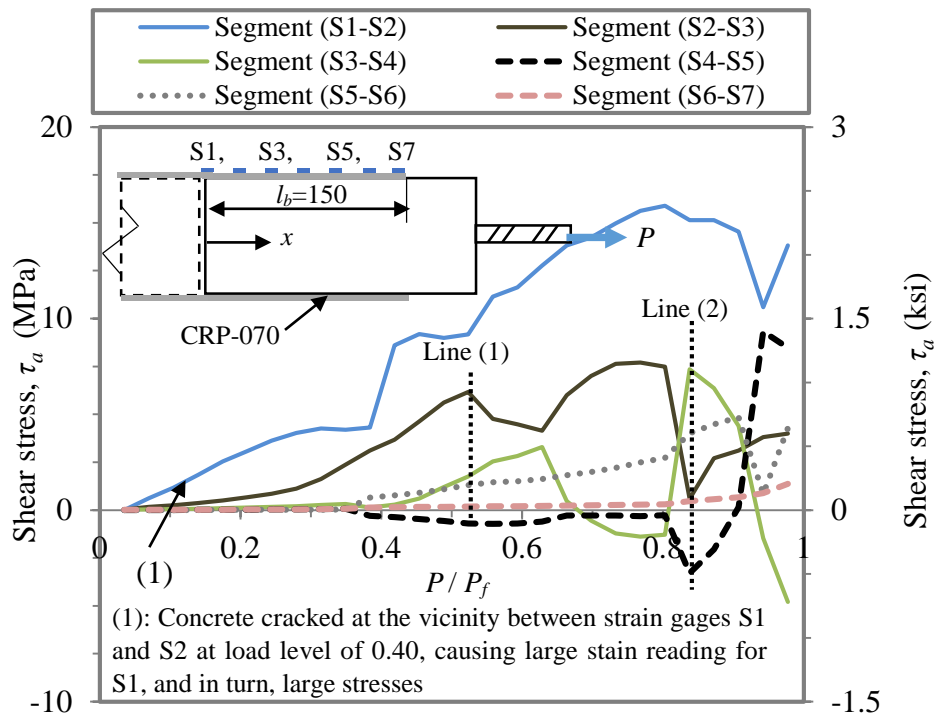


Figure. A. 12 Shear stress vs. relative load level for specimen (I-2-6-50-150).

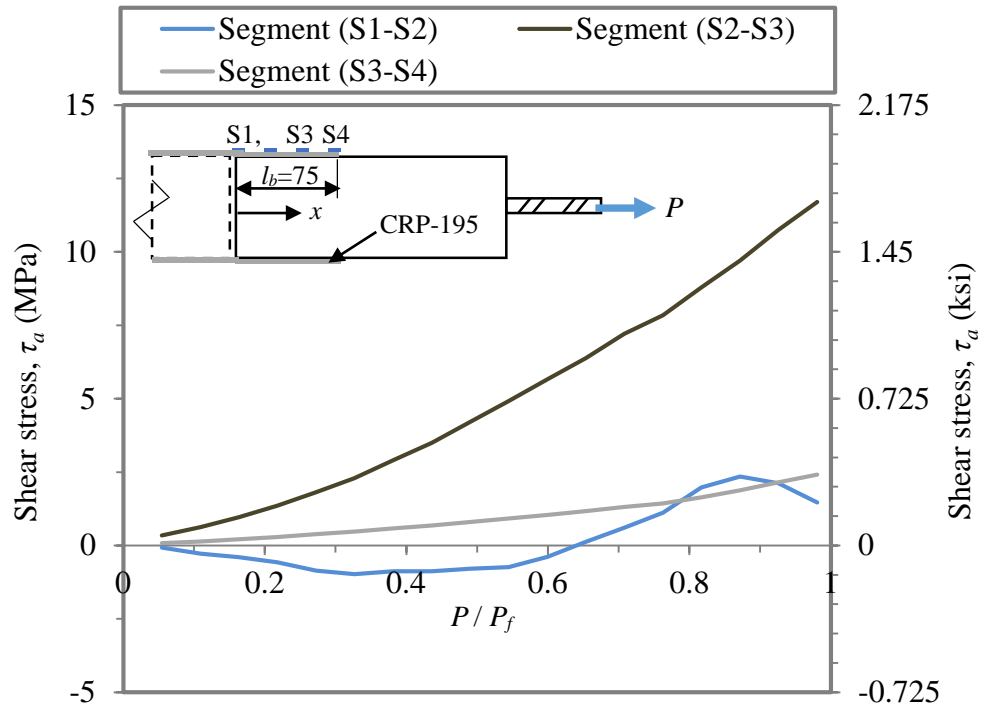


Figure. A. 13 Shear stress vs. relative load level for specimen (III-4-9-19-75).

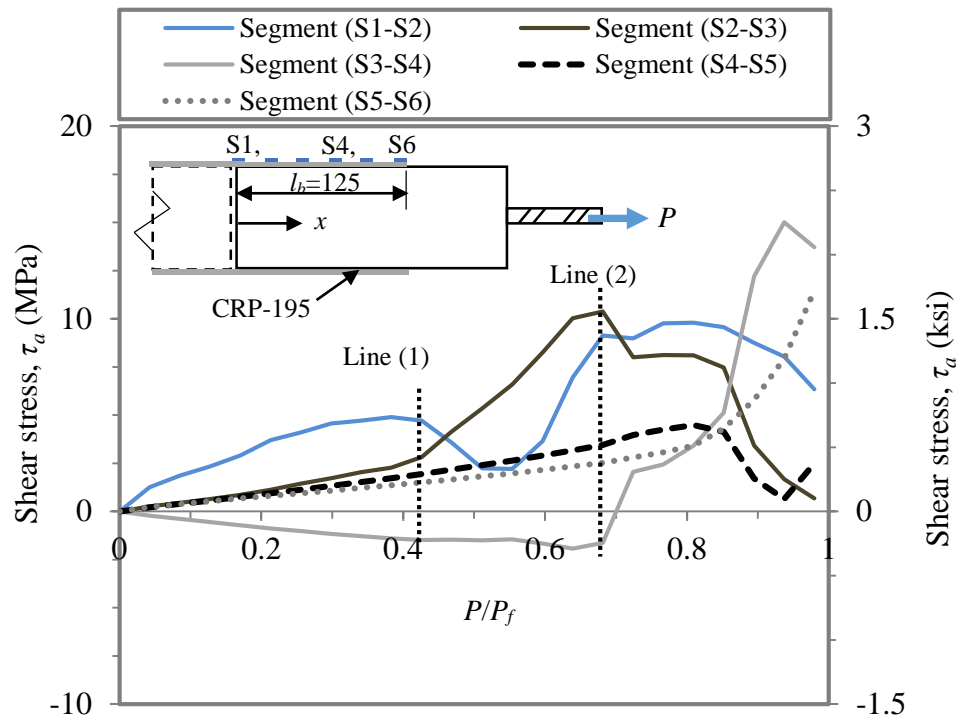
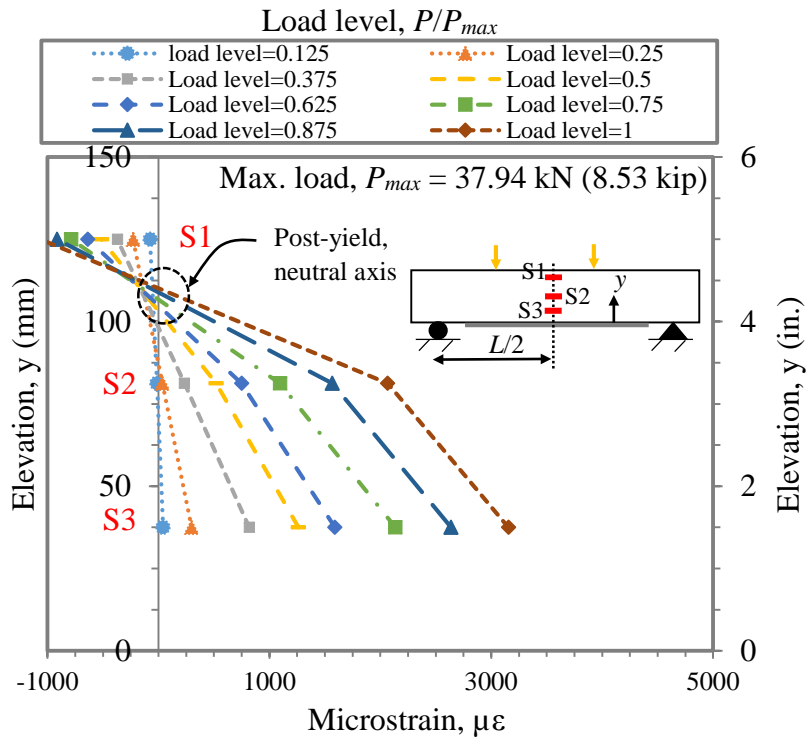
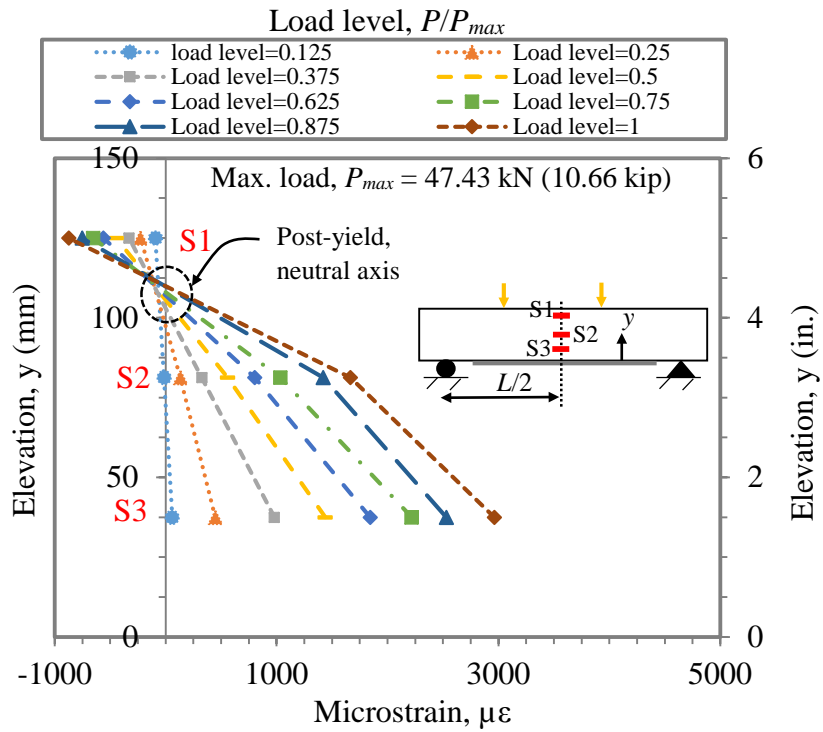


Figure. A. 14 Shear stress vs. relative load level for specimen (III-2-6-50-125).

**APPEDIX B: FLEXURAL STUDY ON RC BEAMS STRENGTHENED WITH
CFRP ROD PANELS AND CFRP LAMINATES**

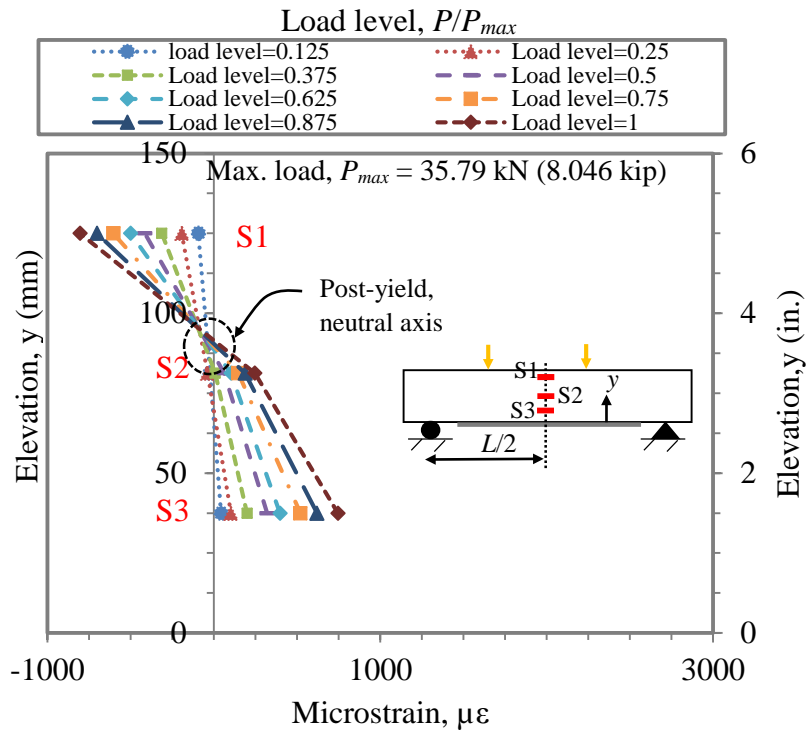


(a) SS70 beam (spliced CRP-070)

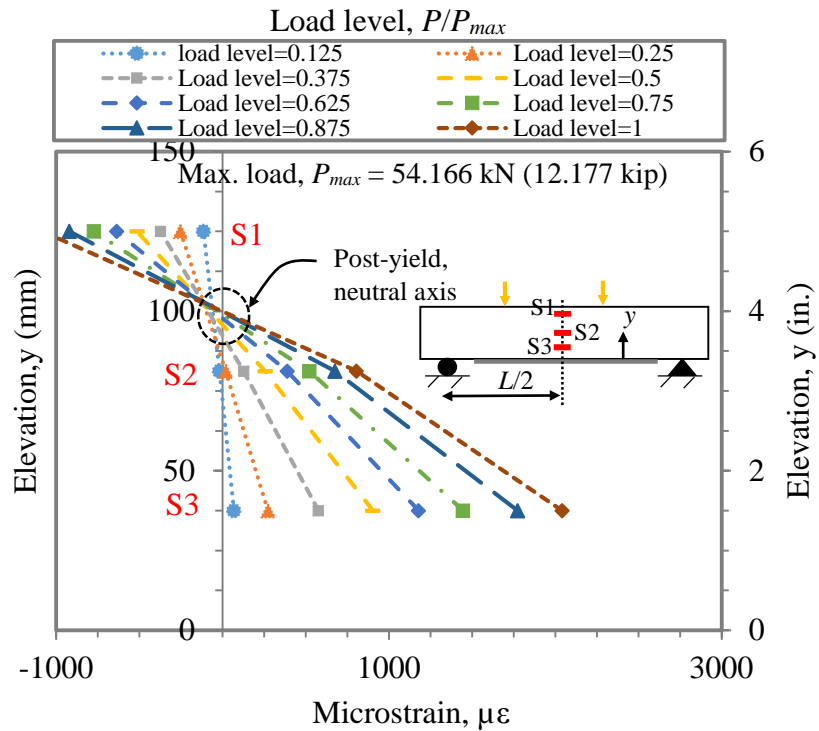


(b) SSW70 beam (spliced and anchored CRP-070)

Fig. B.1 Strain profile along depth, at mid-span, SS70 and SSW70 beams.



(a) SS195 beam (spliced CRP-195)



(b) SSW195 beam (spliced and anchored CRP-195)

Fig. B.2 Strain profile along depth, at mid-span, SS195 and SSW195 beams.

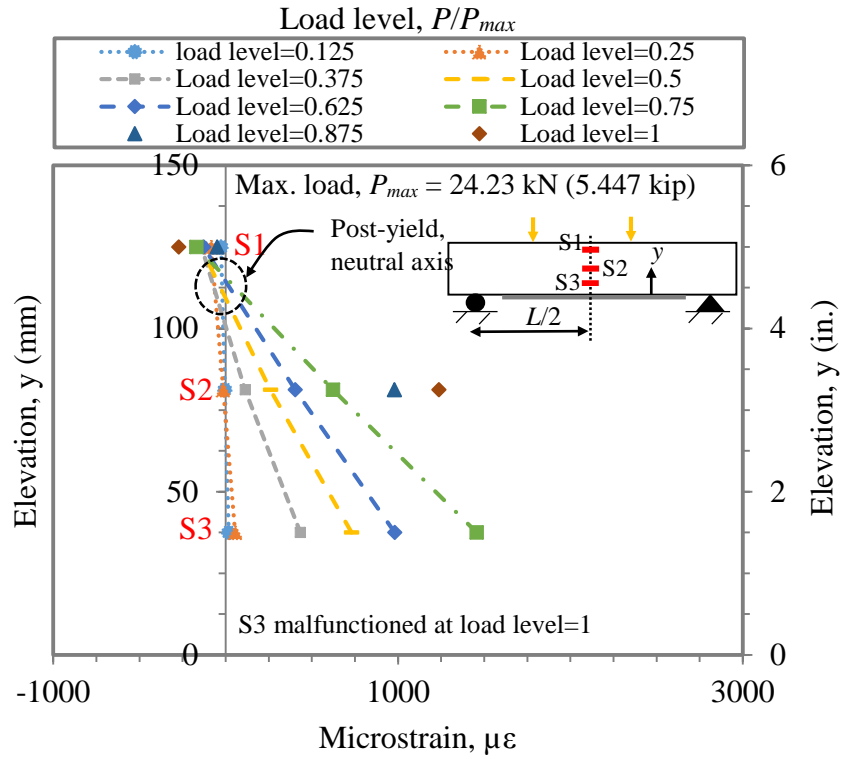
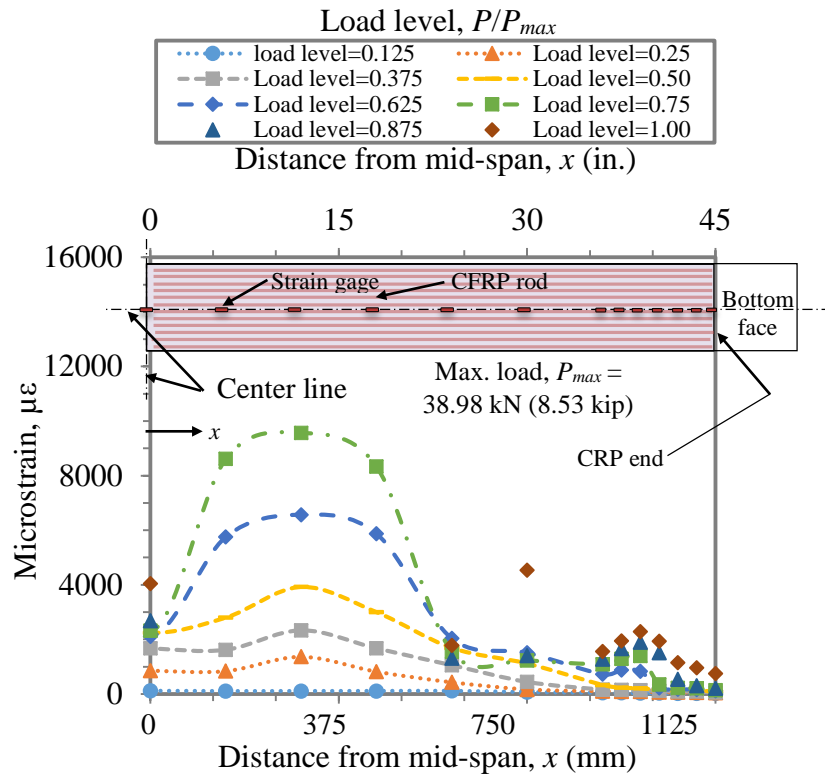
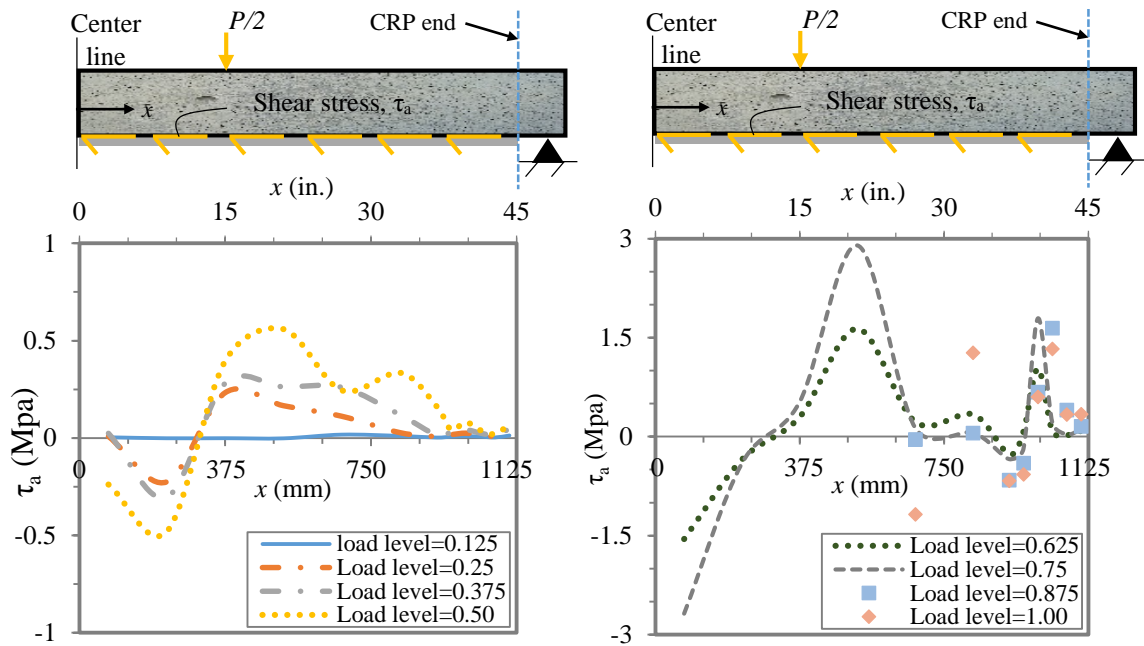


Fig. B.3 Strain profile along depth, at mid-span, SSSC2 beam.



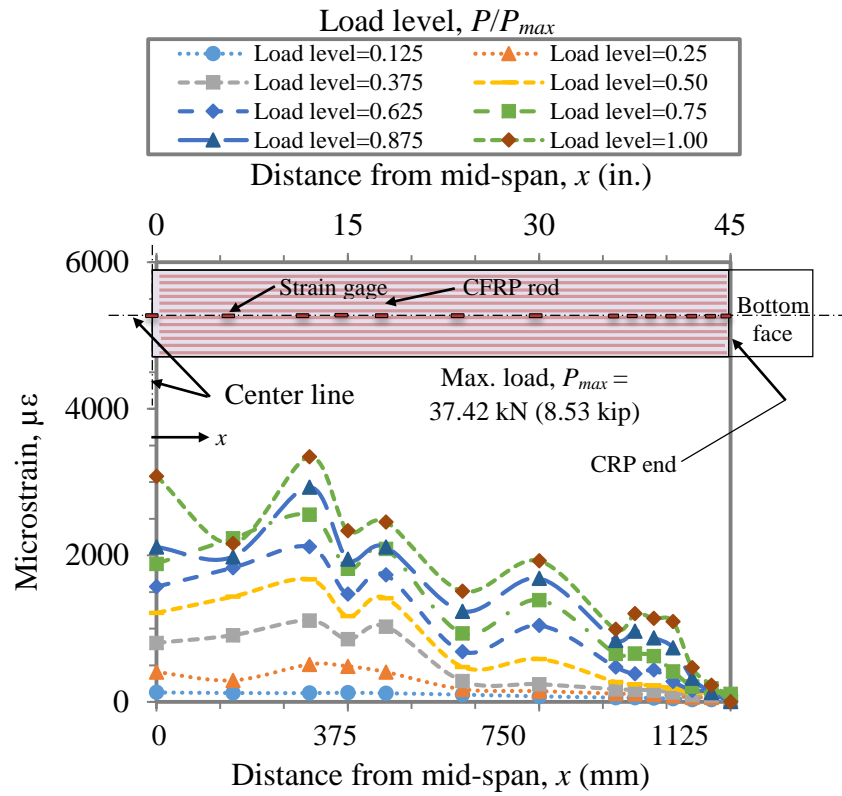
(a) Tensile strains



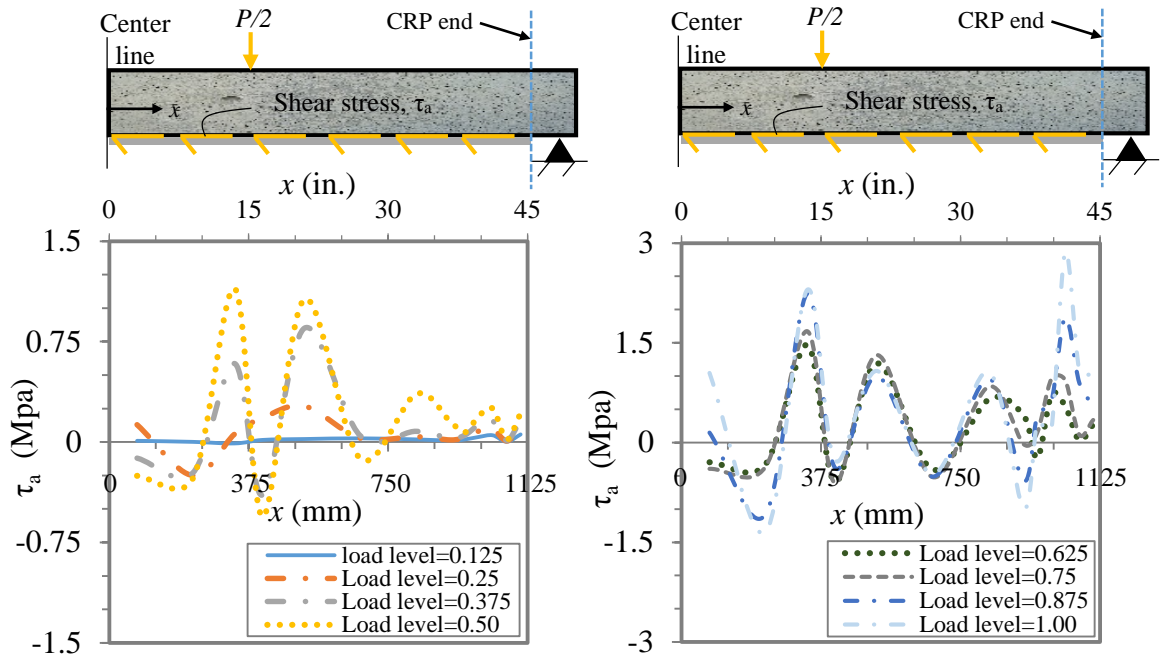
(b) Shear stresses

Fig. B.4 Tensile strain and shear stress distribution along CRP length, beam CS70 (full-length CRP-070).

Note: several strain gages malfunctioned at load levels of 0.875 and 1.00, therefore, for those load levels, strains and shear stresses were drawn as individual points instead of continuous curves.

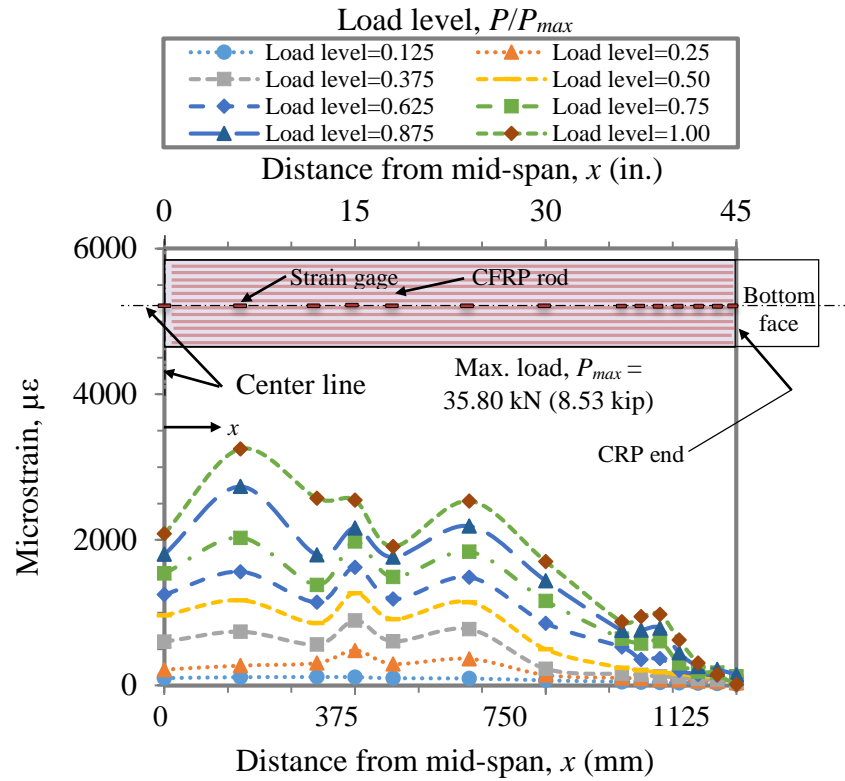


(a) Tensile strains

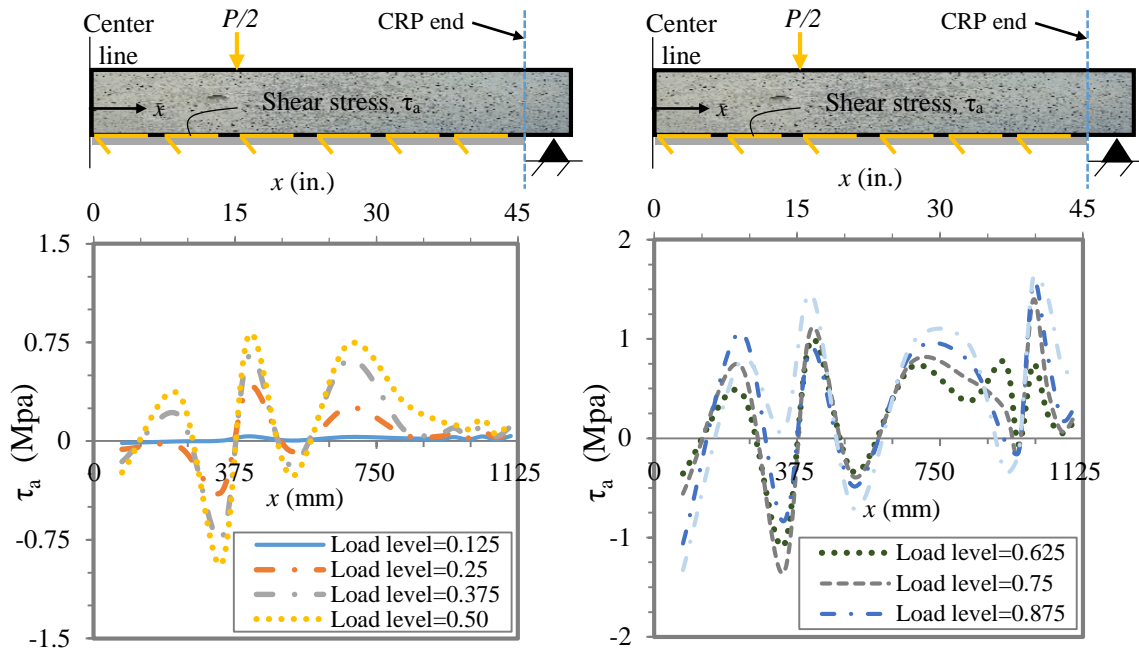


(b) Shear stresses

Fig. B.5 Tensile strain and shear stress distribution along CRP length, beam CS195 (spliced CRP-195).



(a) Tensile strains



(b) Shear stresses

Fig. B.6 Tensile strain and shear stress distribution along CRP length, beam SS195 (spliced CRP-195).

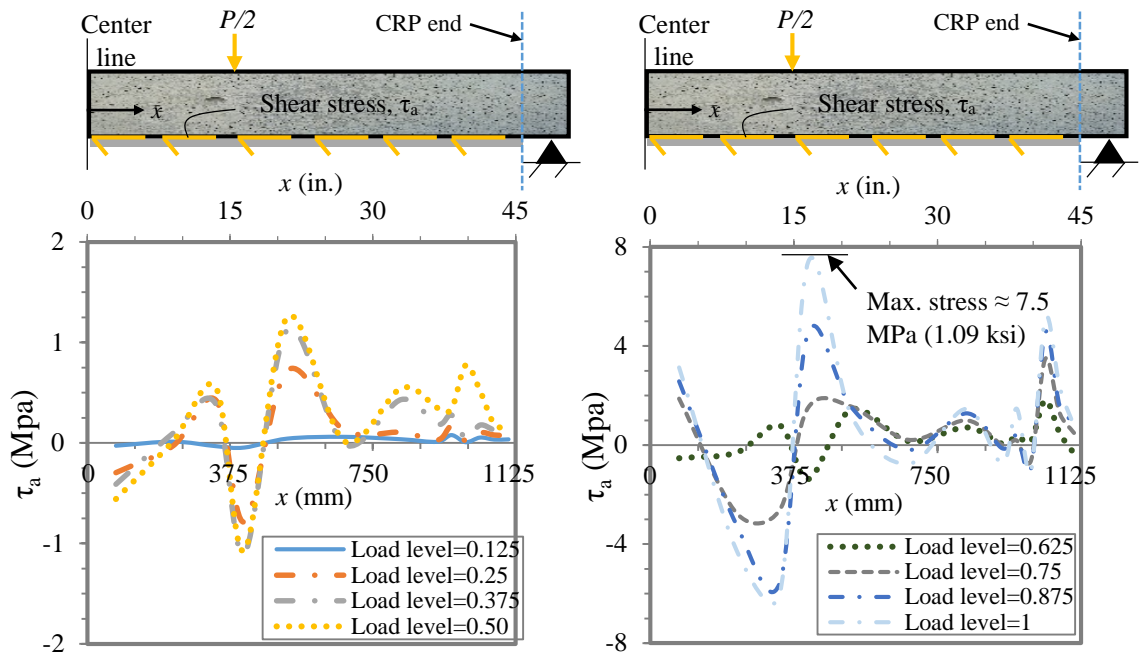
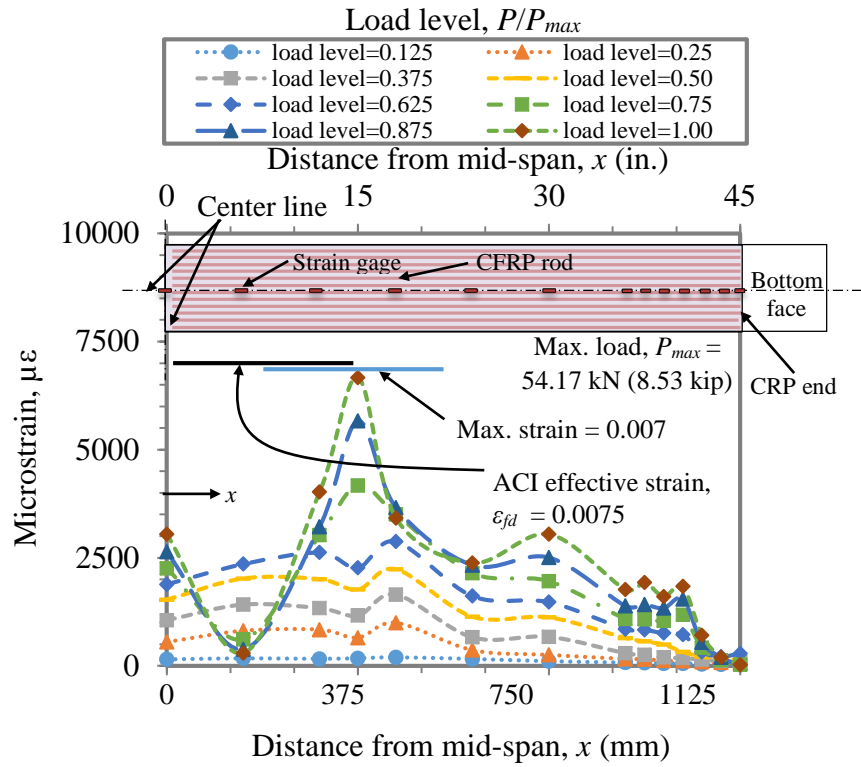
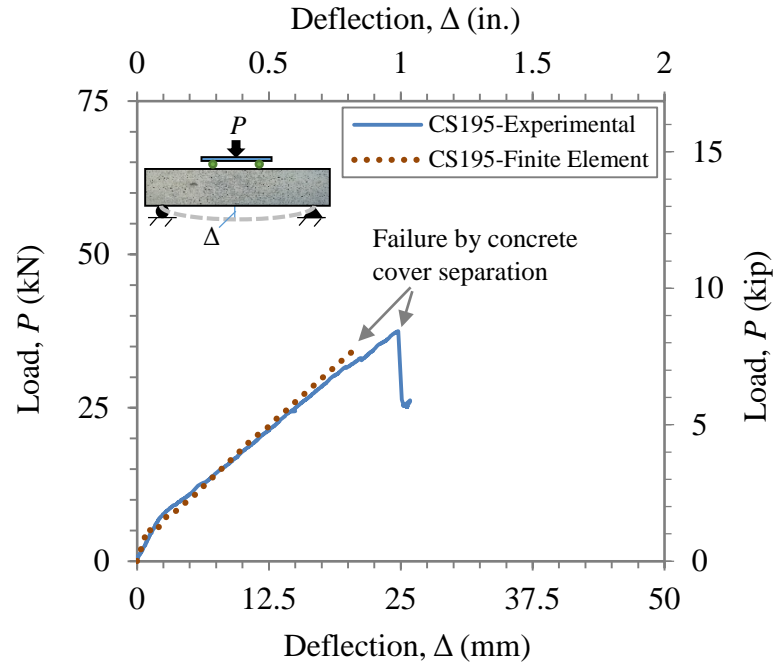
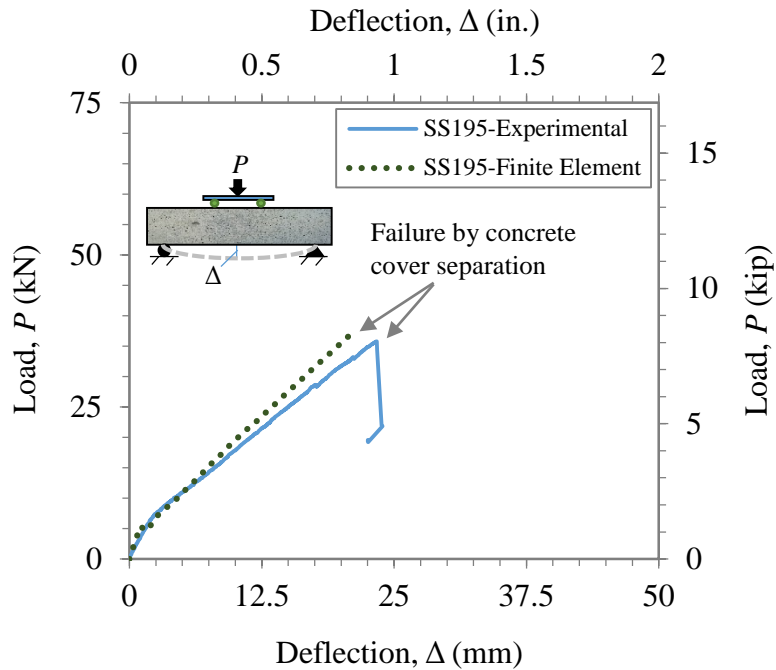


Fig. B.7 Tensile strain and shear stress distribution along CRP length, beam SSW195 (spliced and anchored CRP-195).

**APPEDIX C: FINTE ELEMENT ANALYSIS OF RC BEAMS BONDED TO
CFRP ROD PANELS (CRPS) and CFRP LAMINATES**

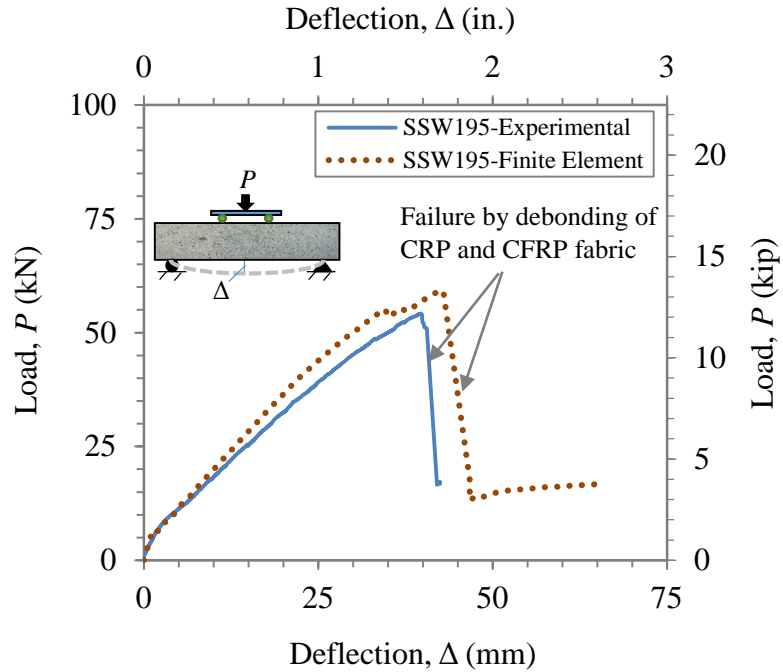


(a) Strengthened with full-length CRP-195 (specimen CS195)



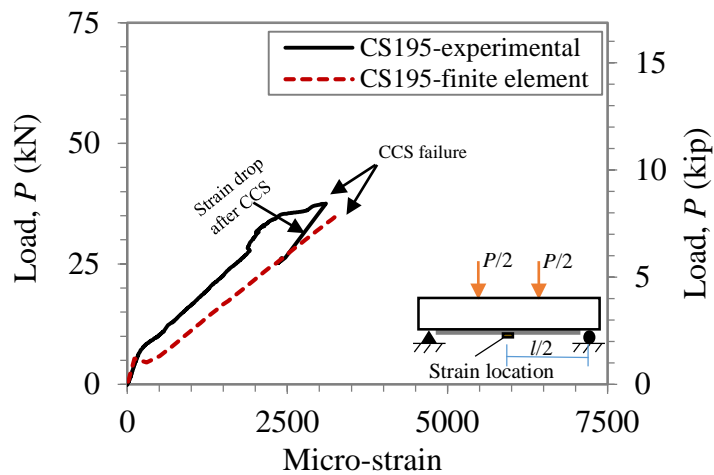
(b) Strengthened with two spliced CRP-195 (specimen SS195)

Figure C.1 Load-mid span deflection comparisons, between experiment and F.E, for beams strengthened with CRP-195.



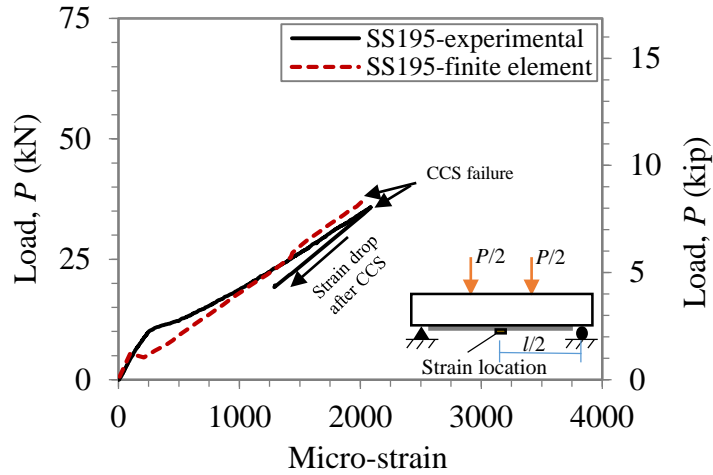
(c) Strengthened with two spliced CRP-195, anchored with fabric (specimen SSW195)

Figure C.1 (continued) Load-mid span deflection comparisons, between experiment and F.E, for beams strengthened with CRP-195.

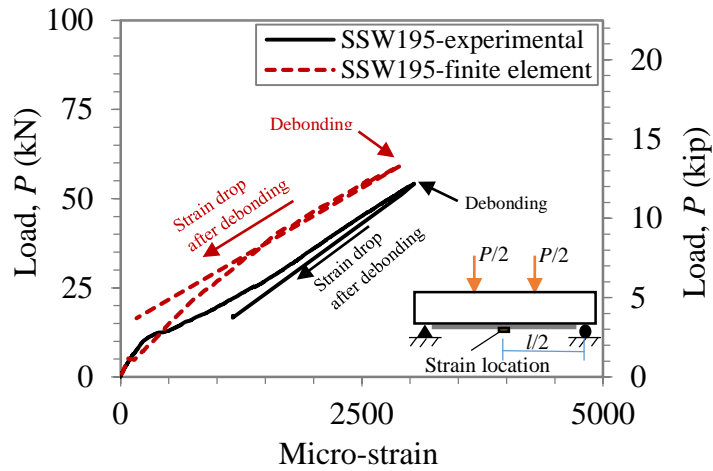


(a) Beam strengthened with full-length CRP-195 (beam CS195)

Figure C.2 Load vs. strain, at mid-span, of beams strengthened with CRP-195.

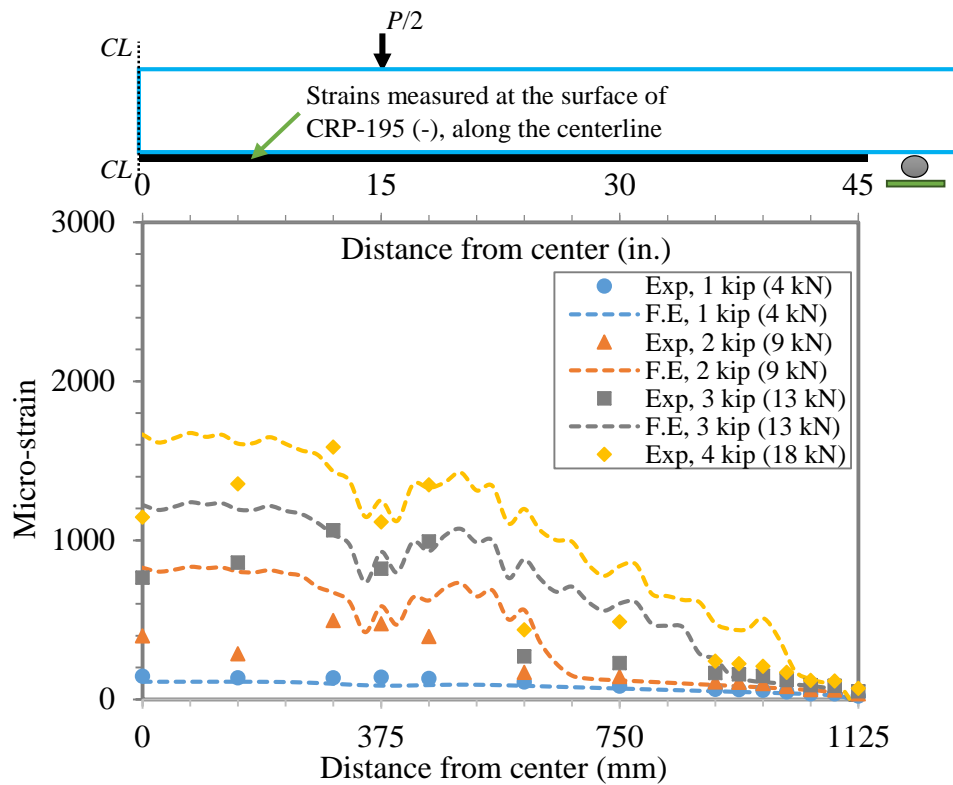


(b) Beam strengthened with two-spliced CRP-195 (beam SS195)

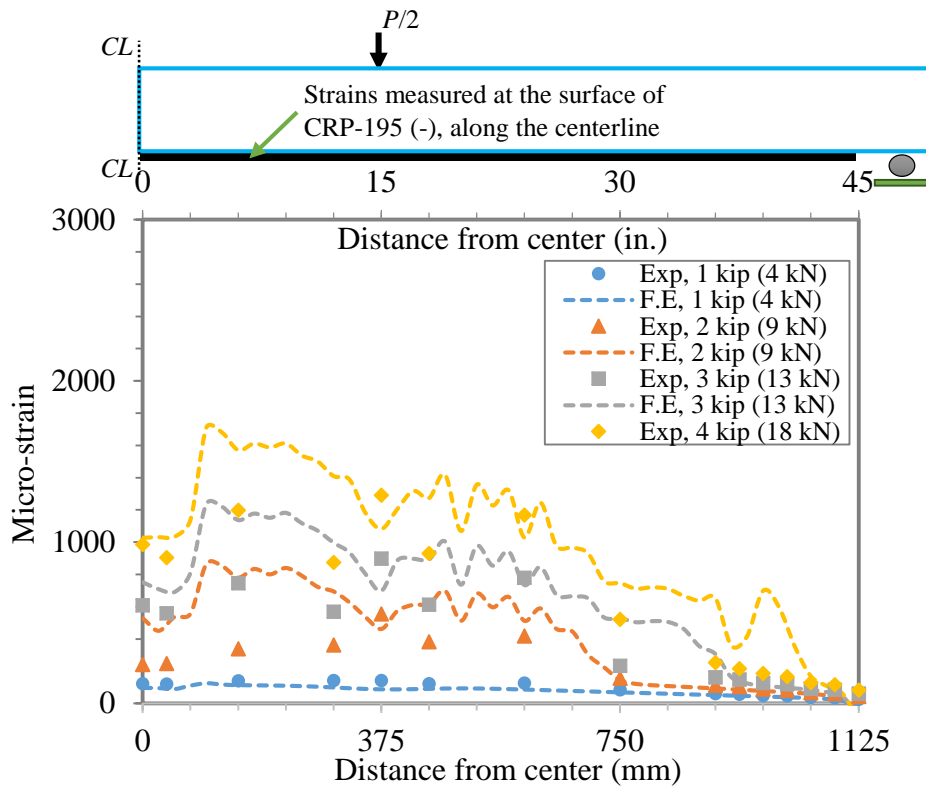


(c) Beam strengthened with two-spliced CRP-195, anchored with fabric (beam SSW195)

Figure C.2 (continued) Load vs. strain, at mid-span, of beams strengthened with CRP-195.

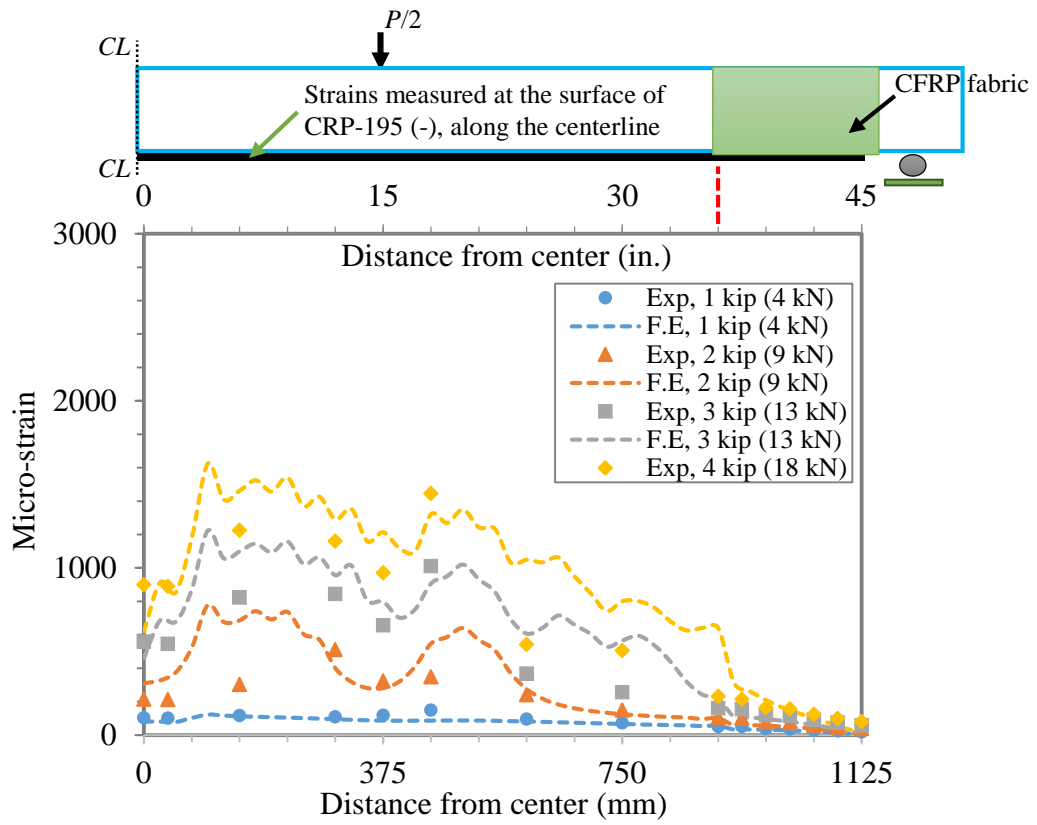


(a) Beam strengthened with full-length CRP-195 (beam CS195)



(b) Beam strengthened with two-spliced CRP-195 (beam SS195)

Figure C.3 Strain distribution along CRP-195 surface for loads up to 18 kN.



(c) Beam strengthened with two-spliced CRP-195, anchored with fabric (beam SSW195)
Figure C.3 (continued) Strain distribution along CRP-195 surface for loads up to 18 kN.

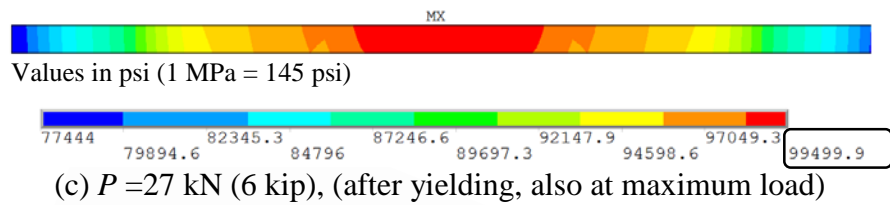
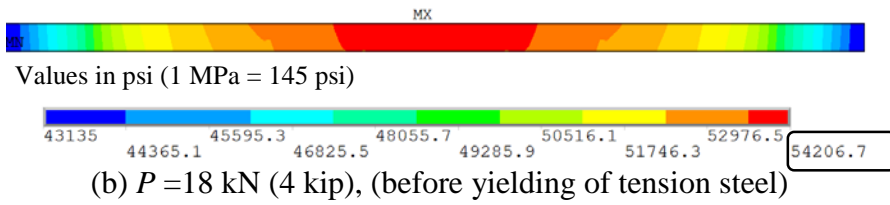
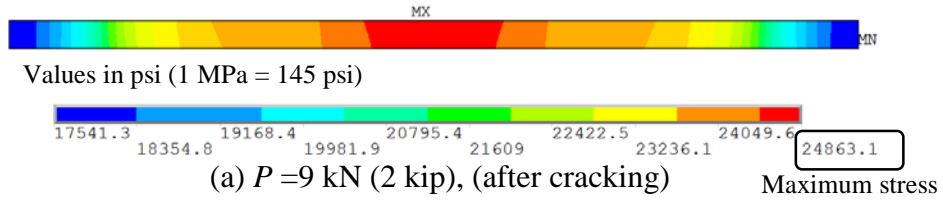


Figure C.4 Tensile stress distribution in full-length CFRP laminate [beam CSSC2], at constant moment region, for different load levels.

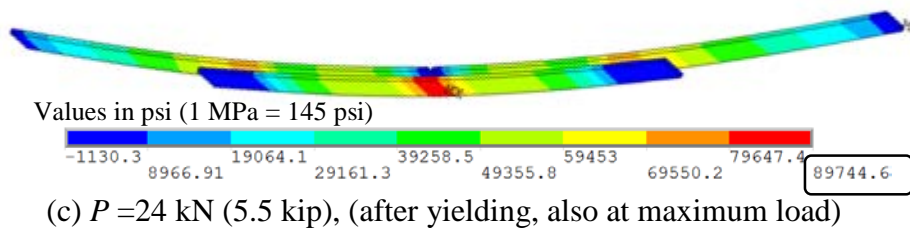
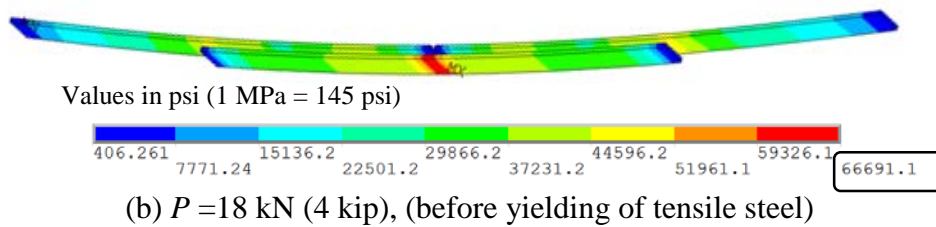
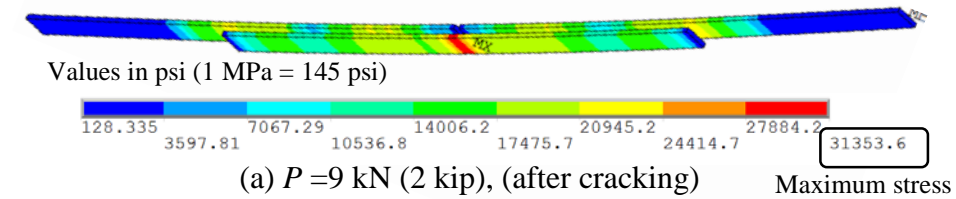


Figure C.5 Tensile stress distribution in spliced CFRP laminate system [beam SSSC2], at total length, for different load levels.

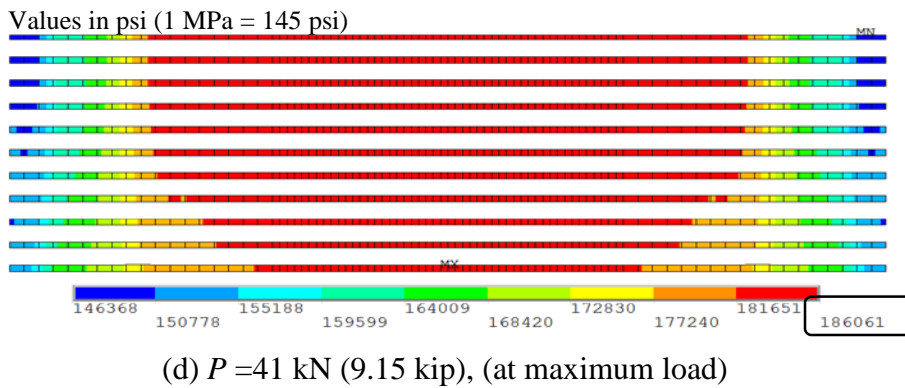
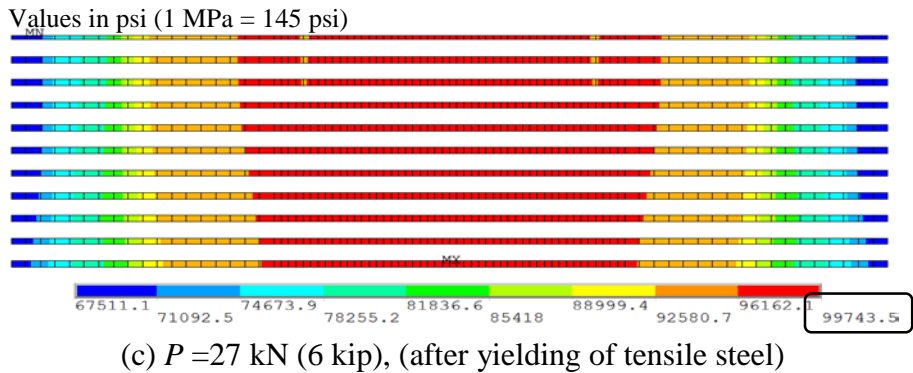
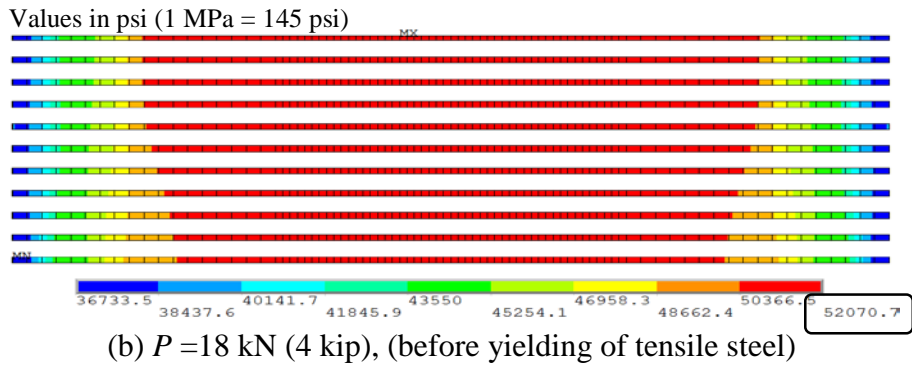
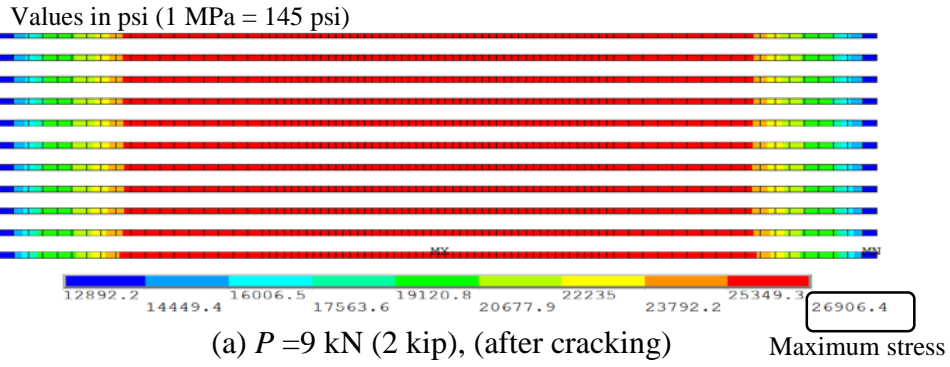


Figure C.6 Tensile stress distribution in full-length CRP-070 [beam CS70], at constant moment region, for different load levels.

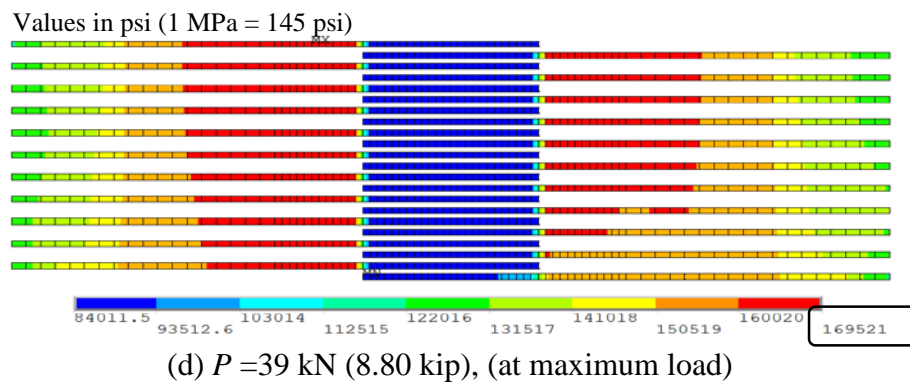
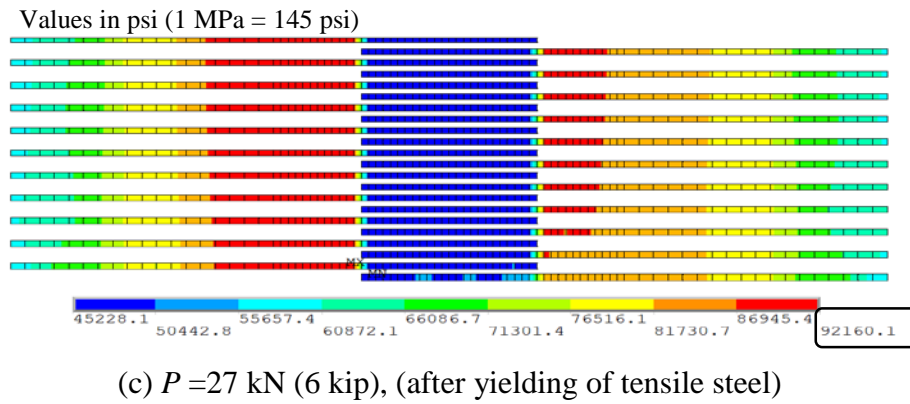
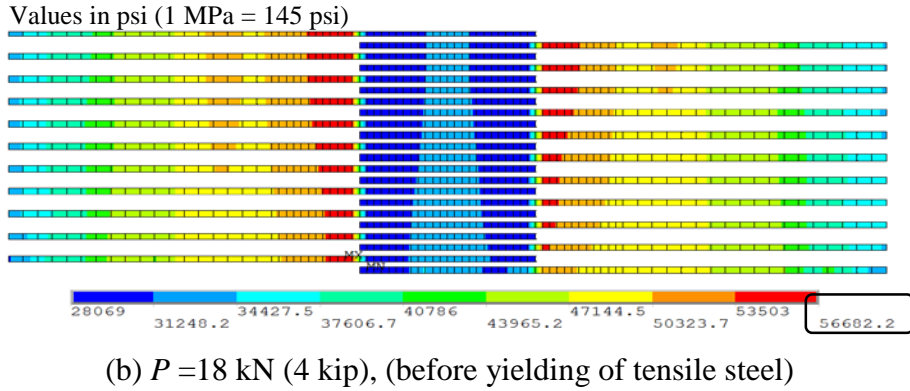
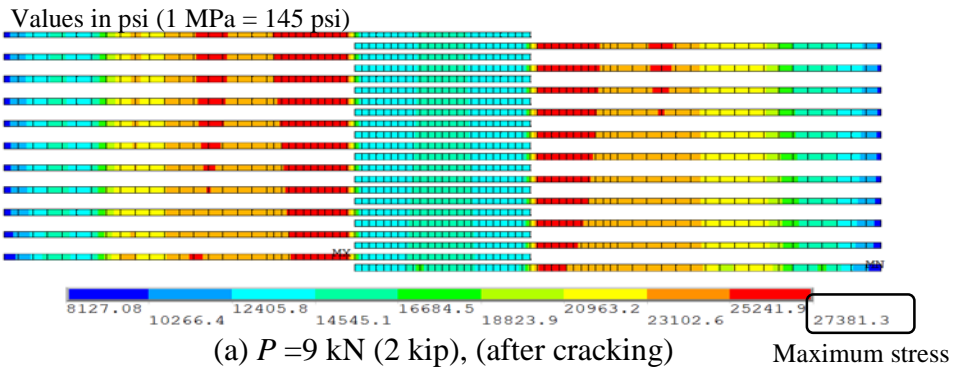


Figure C.7 Tensile stress distribution in spliced CRP-070 [beam SS70], at constant moment region, for different load levels.

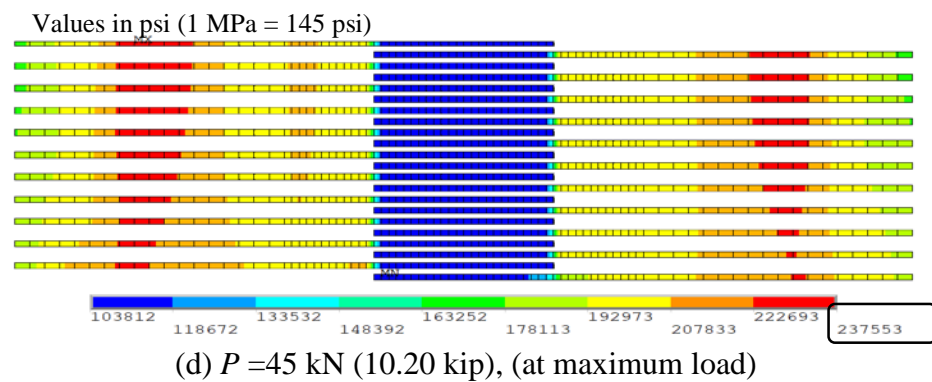
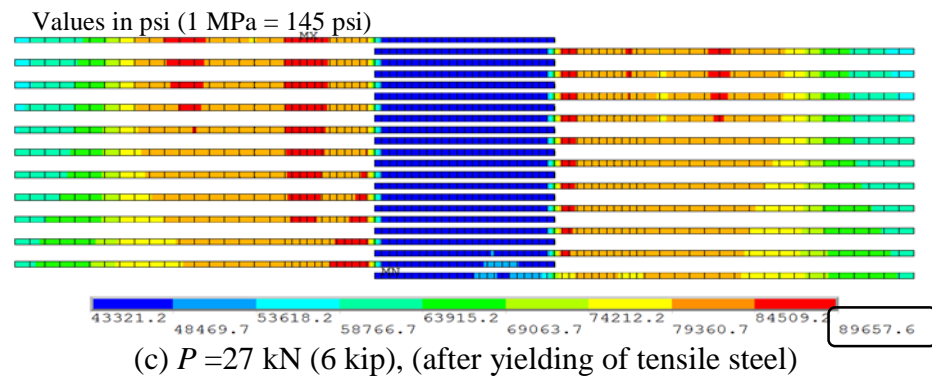
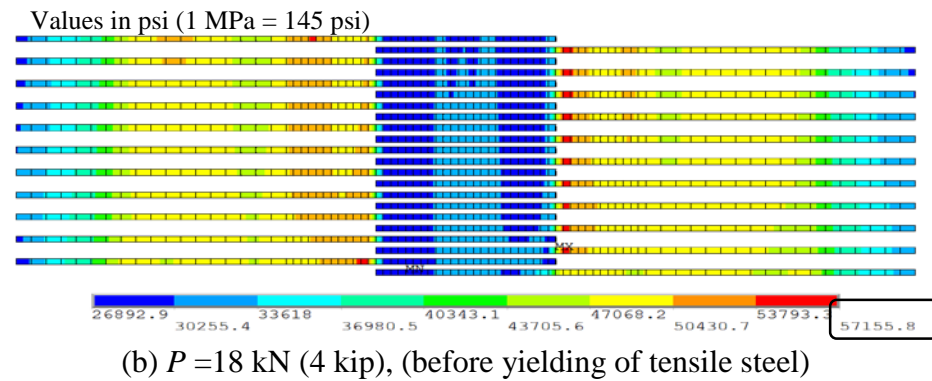
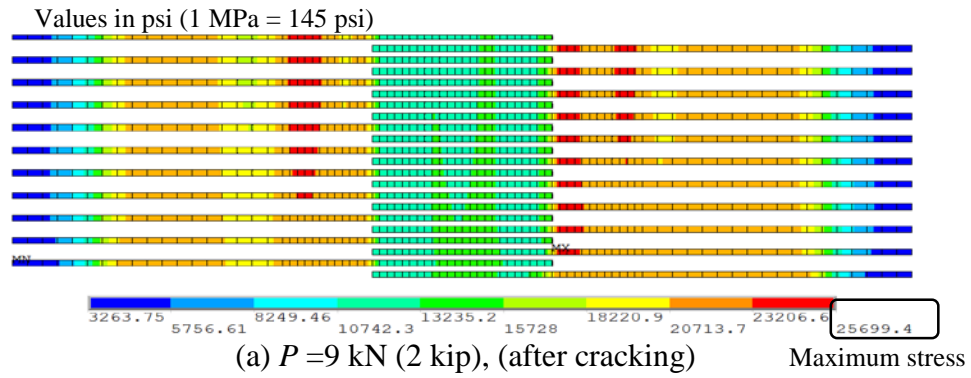


Figure C.8 Tensile stress distribution in spliced CRP-070 [beam SSW70, with fabric anchorage], at constant moment region, for different load levels.

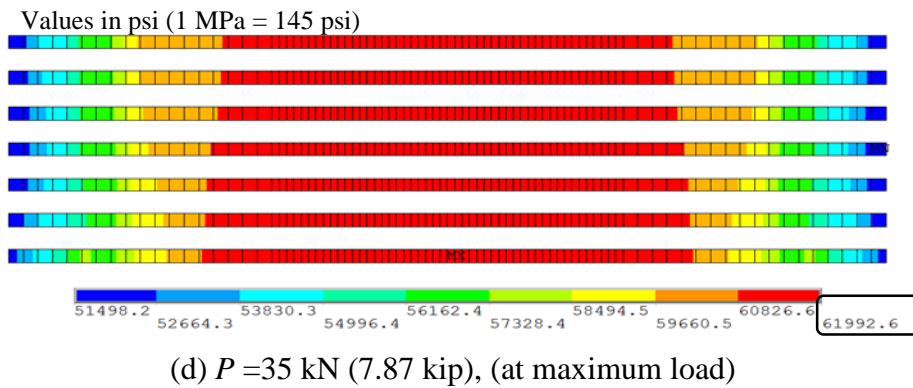
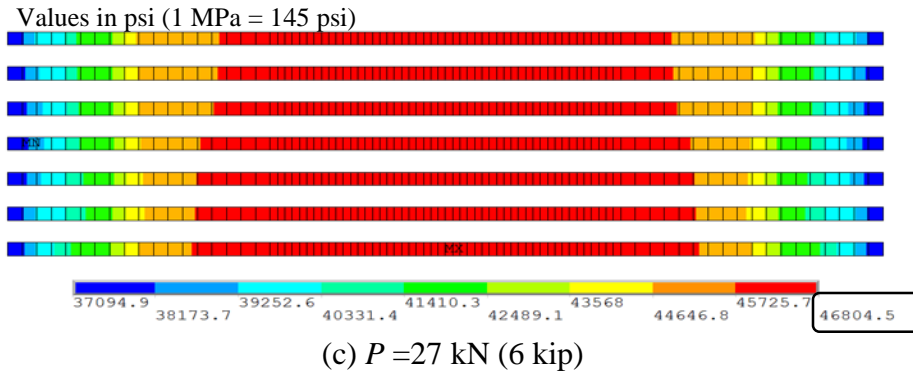
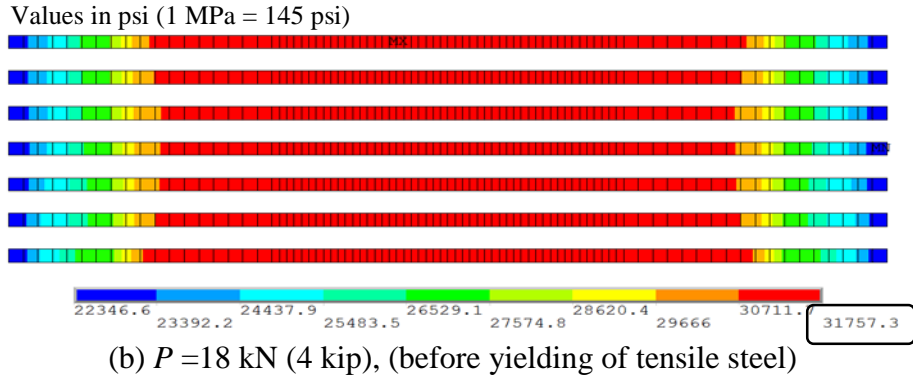
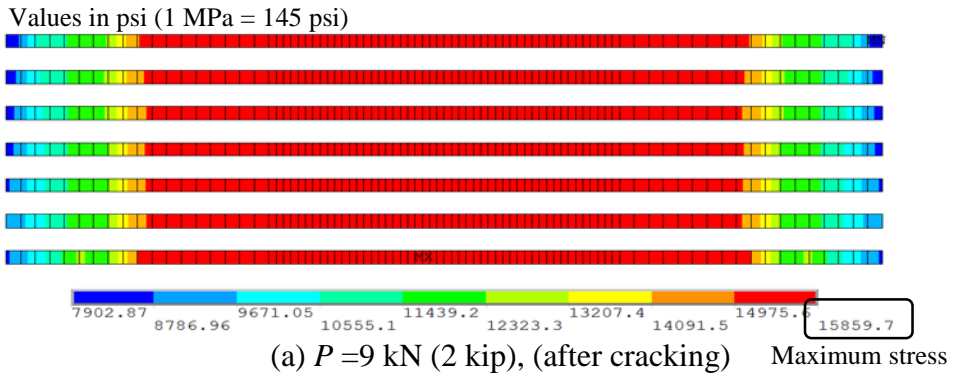


Figure C.9 Tensile stress distribution in full-length CRP-195 [beam CS195], at constant moment region, for different load levels.

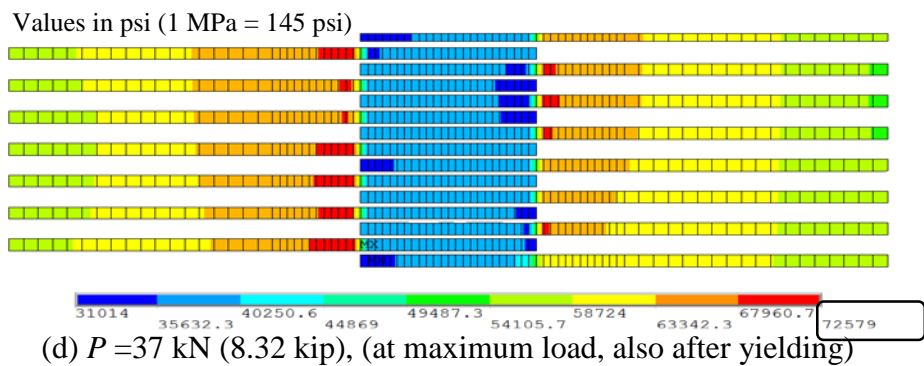
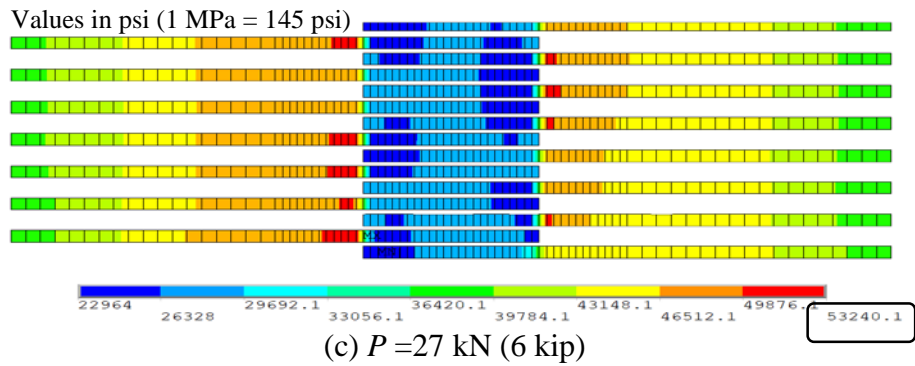
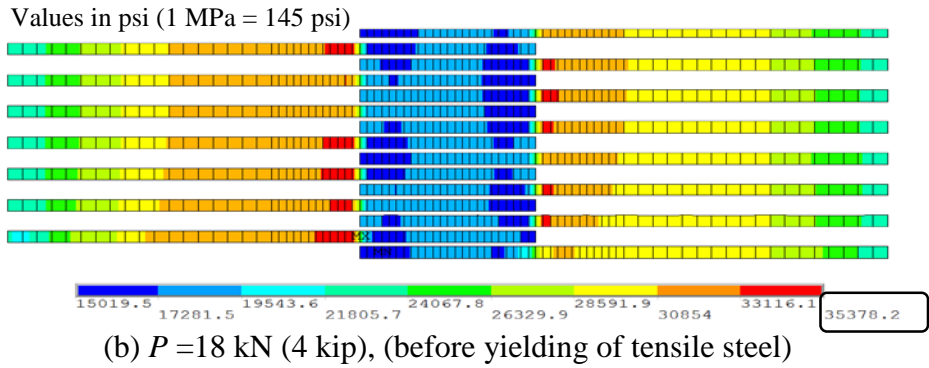
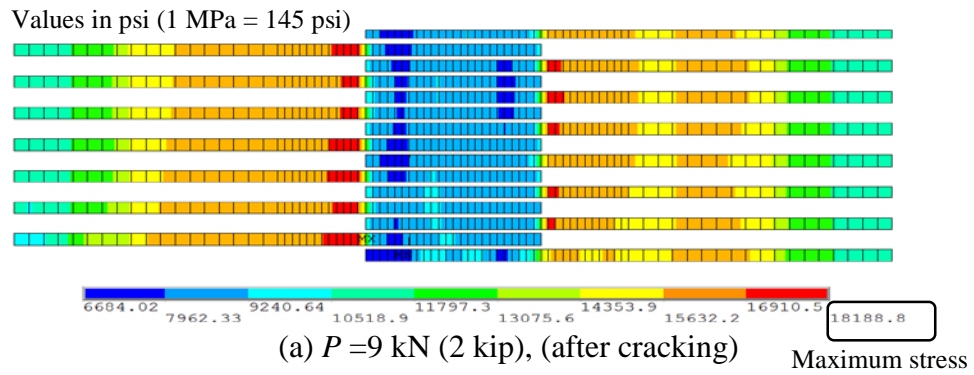


Figure C.10 Tensile stress distribution in spliced CRP-195 [beam SS195], at constant moment region, for different load levels.

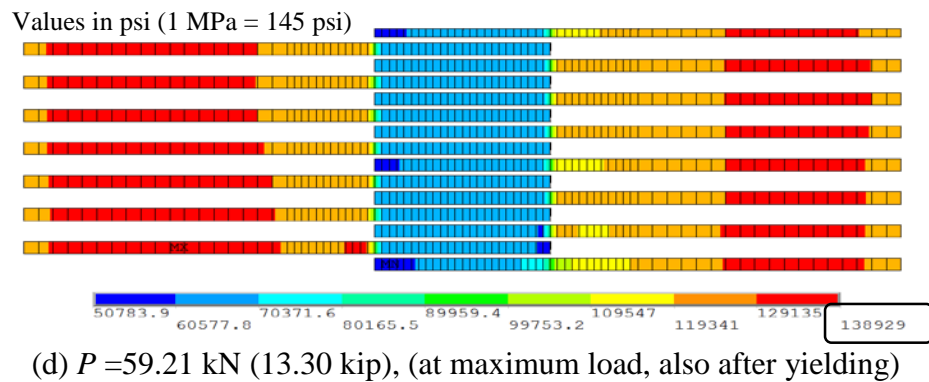
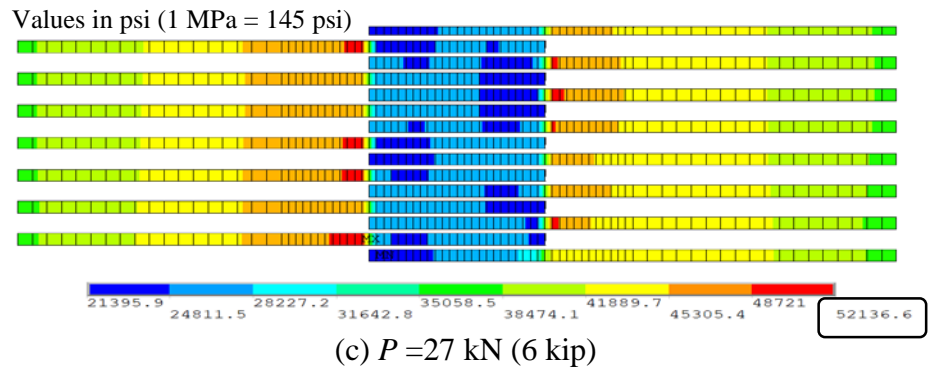
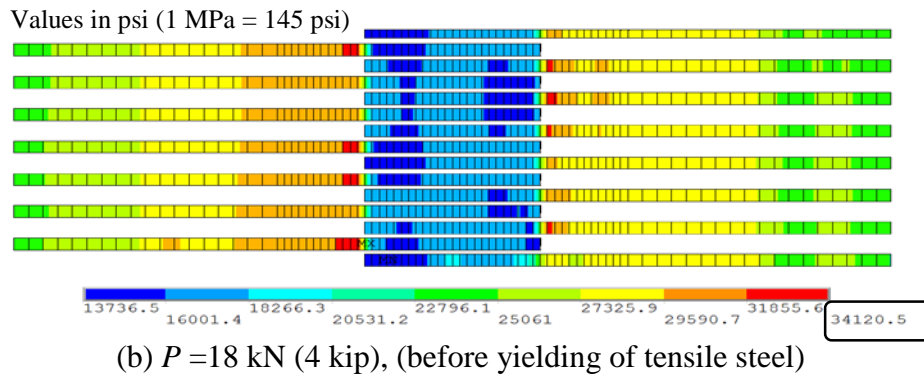
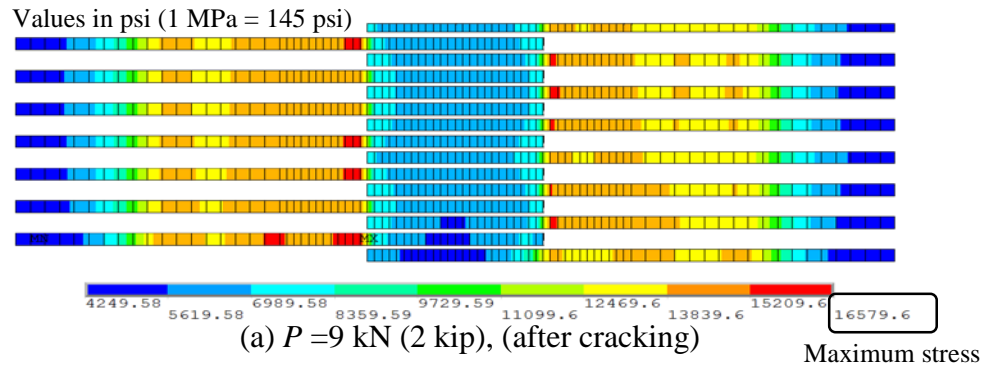
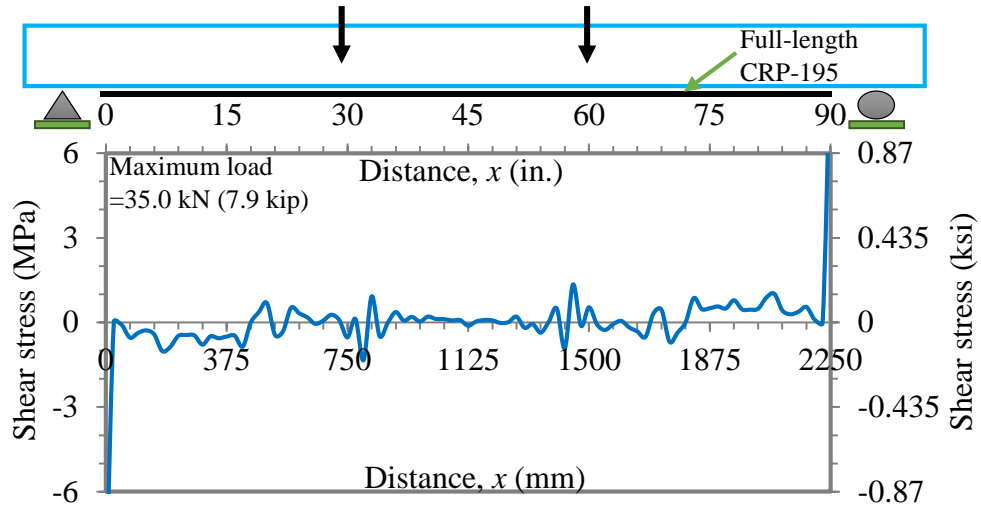
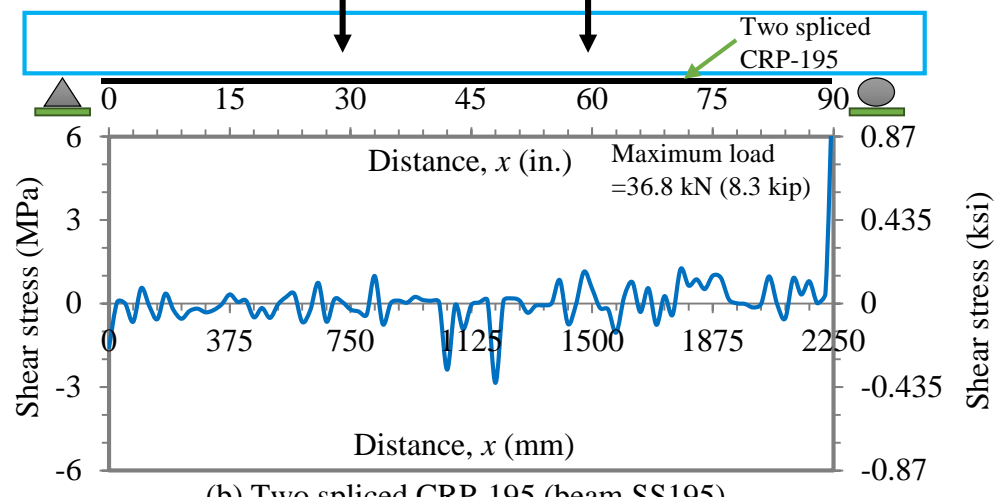


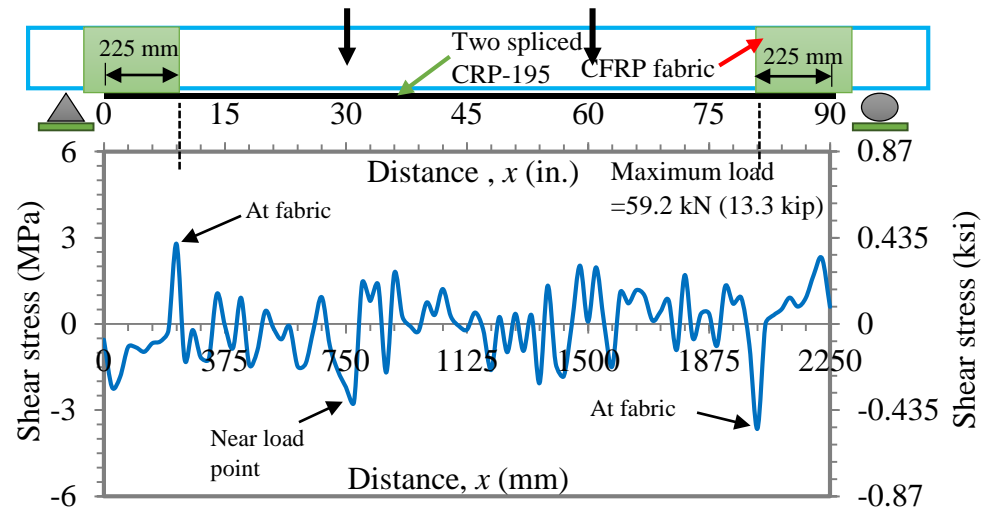
Figure C.11 Tensile stress distribution in spliced CRP-195 [beam SSW195, with fabric anchorage], at constant moment region, for different load levels.



(a) Full-length CRP-195 (beam CS195)



(b) Two spliced CRP-195 (beam SS195)



(c) Two spliced CRP-195, anchored with CFRP fabric (beam SSW195)

Figure C.12 F.E shear stress distribution along CRP/concrete interface, for CRP-195, at maximum load.

REFERENCES

- ACI 318-11 (2011). "Building Code Requirements for Reinforced Concrete," American Concrete Institute, ISO# 193382007E.
- ACI Committee 440 (2008), "Guide for the Design and Construction of Externally Bonded FRP Systems for Strengthening Concrete Structures", American Concrete Institute, Detroit.
- Adhikary, B. B. and H. Mutsuyoshi (2002). "Numerical simulation of steel-plate strengthened concrete beam by a nonlinear finite element method model." *Construction and Building Materials* 16(5): 291-301.
- Ahn, J. S., K. S. Woo, P. K. Basu and J. H. Park (2006). "p-Version nonlinear analysis of RC beams and slabs strengthened with externally bonded plates." *Finite Elements in Analysis and Design* 42(8-9): 726-739.
- Alaee, F. J. and B. L. Karihaloo (2003). "Retrofitting of Reinforced Concrete Beams with CARDIFRC." *Journal of Composites for Construction* 7(3): 174-186.
- Alagusundaramoorthy, P., Harik, I. E., and Choo, C., (2003). "Flexural Behavior of R/C Beams Strengthened with Carbon Fiber Reinforced Polymer Sheets or Fabric." *Journal of Composites for Construction* 7(4): 292-301.
- Alfarabi, S., Al-Sulaimani, G.J. and Ghaleb, B. N., (1994). "Strengthening of Initially Loaded Reinforced Concrete Beams using FRP Plates", *ACI Structural J.*, Vol. 91, No. 2, pp. 160-168, March 1994.
- Al-Jelawy, H. (2009). "Experimental and Numerical Investigation on Bond Durability of CFRP Strengthened Concrete Members Subjected to Environmental Exposure.", Master thesis, University of Central Florida, Orlando, Florida.
- Alkhadraji, T. (2004). "Structural Strengthening Using External Post-Tensioning Systems." *Structural Magazine*, <http://www.structural.net/article/structural-strengthening-using-external-post-tensioning-systems>
- Alkhadraji, T., and Thomas, J. (2009). "Structural Strengthening Using External Post-Tensioning Systems.", *Structural Magazine*, <http://www.structuremag.org/?p=5070>
- Allawi, A. (2006). "Nonlinear Analysis of Reinforced Concrete Beams Strengthened by CFRP in Torsion." Doctoral dissertation, Baghdad University, Iraq.
- Al-Mahmoud, F., A. Castel, R. Francois and C. Tourneur (2009). "Strengthening of RC Members with Near-Surface Mounted CFRP Rods." *Composite Structures* 91(2): 138-147.

- Al-Mahmoud, F., A. Castel, R. Francois and C. Tourneur (2010). "RC Beams Strengthened with NSM CFRP Rods and Modeling of Peeling-off Failure." *Composite Structures* 92(8): 1920-1930.
- Ambrisi, A., and Focacci, F. (2011). "Flexural Strengthening of RC Beams with Cement-Based Composites." *ASCE, Journal of Composites for Construction*, 2011.15:707-720.
- Andra, H. P., Sander, D., and Meier, M. (2001). "Prestressed CFRP Strips as Surface Tendons-Example of Coupling Joint Rehabilitation.", *Beton-und Stahlbetonbau*, V.96, no.12, pp. 737-747.
- ANSYS (2012). Release 14.5 Documentation for ANSYS. Version 14.5, ANSYS Inc., Canonsburg, PA, USA.
- Aram, M. R., C. Czaderski and M. Motavalli (2008). "Debonding Failure Modes of Flexural FRP-Strengthened RC Beams." *Composites Part B-Engineering* 39(5): 826-841.
- Arduini, M., and Nanni, A., (1997), "Behavior of Precracked RC Beams Strengthened with Carbon FRP Sheets", *ASCE Journal of Composites for Construction*, Vol. 1, No. 2, pp. 63-70.
- ASTM A370-09 (2009), Standard Test Methods and Definitions for Mechanical Testing of Steel Products, ASTM International, West Conshohocken, PA, 2009, www.astm.org.
- ASTM C31 / C31M-09 (2009), Standard Practice for Making and Curing Concrete Test Specimens in the Field, ASTM International, West Conshohocken, PA, 2009, www.astm.org.
- ASTM C39 / C39M-09 (2009), Standard Test Method for Compressive Strength of Cylindrical Concrete Specimens, ASTM International, West Conshohocken, PA, 2009, www.astm.org.
- ASTM C469 / C469M-11 (2011), Standard Test Method for Static Modulus of Elasticity and Poisson's Ratio of Concrete in Compression, ASTM International, West Conshohocken, PA, 2011, www.astm.org.
- ASTM C805-08 (2008). "Standard Test Method for Rebound Number of Hardened Concrete", ASTM International, West Conshohocken, PA, 2008.
- Attari, S. N. Amziane, M. Chemrouk, (2012), "Flexural strengthening of concrete beams using CFRP, GFRP and hybrid FRP sheets," *Construction and Building Materials*, Volume 37, December 2012, Pages 746-757, ISSN 0950-0618.

- BADAWI, M., (2007). "Monotonic and Fatigue Flexural Behavior of RC Beams Strengthened with Prestressed NSM CFRP Rods", PhD Thesis, University of Waterloo, Waterloo, Ontario, Canada 2007, 256 pp.
- Badawi, M., and soudki, K (2009). "Flexural strengthening of RC beams with prestressed NSM CFRP rods – Experimental and analytical investigation", *Construction and Building Materials*, Volume 23, Issue 10, October 2009, Pages 3292–3300.
- Bajpai, K., and Duthinh, D. (2003). "Bending Performance of Masonry Walls Strengthened with Near Surface Mounted FRP Bars," Noth American Masonry Conference, June 1-4, 2003, Clemson, South Carloina, USA.
- Barnes, R. A, Baglin, P. S, Mays, G. C, and Subedi, N. K. (2001). "External Steel Plate Systems for the Shear Strengthening of Reinforced Concrete Beams" *Engineering Structures* 23 (2001) 1162–1176.
- Ben Ouezdou, M., Belarbi, A., & Bae, S.-W. (2009). Effective Bond Length of FRP Sheets Externally Bonded to Concrete. *International Journal of Concrete Structures and Materials*, 3(2), 127–131.
- Berset, T. (2002). "Development of a Post-Tensioning System Using Unbonded CFRP Tendons." *Proceeding of the 4th International PhD Symposium in Civil engineering*, Munich, Germany, pp. 32-37.
- Bizindavyi, L., and Neale, K. W. (1999). "Transfer Lengths and Bond Strengths for Composites Bonded to Concrete." *J. Compos. for Constr., ASCE*, 3(4), 153–160.
- Blanksvard, T., B. Taljsten and A. Carolin (2009). "Shear Strengthening of Concrete Structures with the Use of Mineral-Based Composites." *Journal of Composites for Construction* 13(1): 25-34.
- Bonacci, J. F. and M. Maalej (2001). "Behavioral Trends of RC Beams Strengthened with Externally Bonded FRP." *Journal of Composites for Construction* 5(2): 102-113.
- Brena, S., Wood, S., and Kerger, M., (2003). "Full-Scale Tests of Bridge Components Strengthened Using Carbon Fiber-Reinforced Polymer Composites." *ACI Structural Journal*, Vol. 100, No. 6, pp. 775-784.
- Capozucca, R. (2014). "On the Strengthening of RC Beams with Near Surface Mounted GFRP Rods." *Composite Structures* 117: 143-155.
- Chajes M J, Karbhari V M, Mertz D R, Kaliakin V N and Faqiri A (1993). "Rehabilitation of Cracked Adjacent Concrete Box-Beam Bridges", *Proc Symp Practical Solutions for Bridge Strengthening and Rehabilitation*, NSF, Des Moines, Iowa, 1993, pp 265–274.

- Chajes M J, Thomson T A, Finch W W and Januszka T F (1994). 'Flexural Strengthening of Concrete Beams using Externally Bonded Composite Materials', *Construct Build Mater* 8(3) 191–201.
- Chansawat, K., T. Potisuk, T.H. Miller, S.C. Yim and D.I. Kachlakev, (2009). FE models of GFRP and CFRP strengthening of reinforced concrete beams. *Adv. Civil Eng.*, 2009: 13-13.
- Chen, J. F, and Teng, J. G. (2001). "Anchorage strength models for FRP and steel plates bonded to concrete." *Journal of Structural Engineering*, ASCE, 127(7), July 2001.
- Choi, H. T., West, J. S., and Soudki, K. A. (2011). "Effect of Partial Unbonding on Prestressed Near-Surface-Mounted CFRP-Strengthened Concrete T-Beams", ASCE, *Journal of Composites for Construction*, Vol. 15, No. 1, February 1, 2011, ASCE, ISSN 1090-0268/2011/1-93–102.
- Daugevicius, M., J. Valivonis and G. Marciukaitis (2012). "Deflection Analysis of Reinforced Concrete Beams Strengthened with Carbon Fibre Reinforced Polymer Under Long-Term Load Action." *Journal of Zhejiang University-Science A* 13(8): 571-583.
- Dawood, M., and Rizkalla, S. (2006). "Bond and Splice Behavior of High Modulus CFRP Materials Bonded to Steel Structures". Third International conference on FRP Composites in Civil Engineering (CICE 2006), December 13-15 2006, Miami, Florida, USA.
- Dawood, M., Guddati, M., and Rizkalla, S. (2007). "Bond Behavior of CFRP Strengthening System for Steel Structures". Asia-Pacific Conference on FRP in Structures (APFIS 2007).
- De Lorenzis, L. and Nanni, A. (2002). "Bond between Near-Surface Mounted Fiber-Reinforced Polymer Rods and Concrete in Structural Strengthening." *ACI Structural Journal*, Vol 99(2).
- De Lorenzis, L., M. Paggi, A. Carpinteri and G. Zavarise (2010). "Linear Elastic Fracture Mechanics Approach to Plate End Debonding in Rectilinear and Curved Plated Beams." *Advances in Structural Engineering* 13(5): 875-889.
- De Luca, A., F. Matta and A. Nanni (2010). "Behavior of Full-Scale Glass Fiber-Reinforced Polymer Reinforced Concrete Columns under Axial Load." *Aci Structural Journal* 107(5): 589-596.

- Demakos C. B, Repapis C. C, and Drivas D, (2013). "Investigation of structural response of reinforced concrete beams strengthened with anchored FRPs." *Open Construction and Building Technology Journal*, 2013; 7:146-57.
- Diversified Structural Composites (2016). "Specialty rods, tubes and shapes" < <http://www.diversified-composites.com/rdtbshp.php> >
- Ebead, U, and Marzouk, H. (2002). "Strengthening of Two-Way Slabs Subjected to Moment and Cyclic Loading." *ACI Structural Journal*, V. 99, No. 4, July-August 2002.
- Ebead, U. and H. Marzouk (2004). "Fiber-reinforced Polymer Strengthening of two-way Slabs." *Aci Structural Journal* 101(5): 650-659.
- Ehsani, M. R. and Saadatmanesh, H. (1996). "Repair and Strengthening of Earthquake-Damaged Concrete and Masonry Walls with Composite Fabrics," First International Conference on Fiber Composites in Infrastructures, ICCI'96, Tucson, Arizona, January 1996, pp. 1156-1167.
- El Maaddawy, T. and K. Soudki (2008). "Strengthening of Reinforced Concrete Slabs with Mechanically-Anchored Unbonded FRP System." *Construction and Building Materials* 22(4): 444-455.
- El-Hacha R. and Rizkalla S.H, (2004). "Near Surface Mounted FRP Reinforcements for Flexural Strengthening of Concrete Structures," *American Concrete Institute (ACI), Structural Journal*, Vol. 101, No. 5, pp. 717-726, 2004.
- El-Hacha, R., and Aly, M. (2013). "Anchorage System to Prestress FRP Laminates for Flexural Strengthening of Steel-Concrete Composite Girders." *Journal of Composites for Construction*, *Journal of Composites for Construction*, Vol. 17, No. 3, June 1, 2013.
- El-Hacha, R., Wight, R. G., and Green, M. F. (2003). "Innovative System for Prestressing Fiber-Reinforced Polymer Sheets." *ACI Struct. J.*, 100(3), 305–315.
- El-Maaddawy, T. and A. S. El-Dieb (2011). "Near-Surface-Mounted Composite System for Repair and Strengthening of Reinforced Concrete Columns Subjected to Axial Load and Biaxial Bending." *Journal of Composites for Construction* 15(4): 602-614.
- Elsayed, W. E., U. A. Ebead and K. W. Neale (2009). "Mechanically Fastened FRP-Strengthened Two-Way Concrete Slabs with and without Cutouts." *Journal of Composites for Construction* 13(3): 198-207.
- Enochsson, O., J. Lundqvist, B. Taljsten, P. Rusinowski and T. Olofsson (2007). "CFRP strengthened openings in two-way concrete slabs - An experimental and numerical study." *Construction and Building Materials* 21(4): 810-826.

- Esfahani M. R., Kianoush, M. R., and Tajari, A. R. (2007). "Flexural Behavior of Reinforced Concrete Beams Strengthened by CFRP Sheets", *Engineering Structures*, Volume 29, Issue 10, October 2007, Pages 2428–2444.
- Eshwar, N., T. J. Ibell and A. Nanni (2005). "Effectiveness of CFRP Strengthening on Curved Soffit RC Beams." *Advances in Structural Engineering* 8(1): 55-68.
- Federal Highway Administration (2010). "2010 Status of the Nation's Highway, Bridges, and Transit: Conditions and Performance", retrieved from Google on February 17, 2015. <http://www.fhwa.dot.gov/policy/2010cpr/chap11.htm#2>.
- Fawzia, S., Zhao, X. L., & Al-Mahaidi, R. (2010). Bond–Slip Models for Double Strap Joints Strengthened by CFRP. *Composite Structures*, 92(9), 2137-2145.
- Federal Highway Administration (2013). "Deficient Bridges by State and Highway System 2013", retrieved from Google on February 17, 2015. <http://www.fhwa.dot.gov/bridge/nbi/no10/defbr13.cfm>.
- Ferrier, E. and P. Hamelin (2002). "Long-time Concrete-composite Interface Characterization for Reliability Prediction of RC Beam Strengthened with FRP." *Materials and Structures* 35(253): 564-572.
- Ferretti, D. and M. Savoia (2003). "Non-linear Model for R/C Tensile Members Strengthened by FRP-Plates." *Engineering Fracture Mechanics* 70(7-8): 1069-1083.
- Florut, S. C., G. Sas, C. Popescu and V. Stoian (2014). "Tests on Reinforced Concrete Slabs with cut-out Openings Strengthened with Fibre-Reinforced Polymers." *Composites Part B-Engineering* 66: 484-493.
- Foret, G. and O. Limam (2008). "Experimental and Numerical Analysis of RC two-way Slabs Strengthened with NSM CFRP Rods." *Construction and Building Materials* 22(10): 2025-2030.
- Foster, P. B., Gergely, J., Young, D. T., McGinley, W. M, and Corzo, A. (2005). "FRP Repair Methods for FRP Repair Methods for Unreinforced Masonry Buildings Subject to Cyclic Loading." *ACI Special Publication* 230.
- Franca, P. M., (2007). "Reinforced Concrete Beams Strengthened with Prestressed CFRP Laminates." Doctoral dissertation, Lisbon Technical University, Portugal.
- Franca, P., and Costa, A. (2007). "Behaviour of Flexural Strengthened Beams with Prestressed CFRP Laminates." *Proceedings of 8th International Symposium on Fiber-Reinforced Polymer Reinforcement for Concrete Structures (FRPRCS-8)*.

- Gharachorlou, A. and A. A. Ramezaniapour (2010). "Resistance of Concrete Specimens Strengthened with Frp Sheets to the Penetration of Chloride Ions." *Arabian Journal for Science and Engineering* 35(1B): 141-154.
- Guenaneche, B., A. Tounsi and E. A. Bedia (2014). "Effect of shear deformation on interfacial stress analysis in plated beams under arbitrary loading." *International Journal of Adhesion and Adhesives* 48: 1-13.
- Guo, Y. Y., and Chai, Z. L (2014). "Flexural Behavior of Stone Slabs Reinforced with Prestressed NSM CFRP Bars." *J. Compos. Constr.*, 18(4), 04014004.
- Hajihashiemi, A., Mostofinejad, D., and Mojtaba, A. (2011). "Investigation of RC Beams Strengthened with Prestressed NSM CFRP Laminates", *ASCE, Journal of Composites for Construction*, Vol. 15, No. 6, December 1, 2011, ASCE, ISSN 1090-0268/2011/6-887-895.
- Hamid Y. Omran, and Raafat El-Hacha, (2012). "Nonlinear 3D finite element modeling of RC beams strengthened with prestressed NSM-CFRP strips", *Construction and Building Materials*, Volume 31, June 2012, Pages 74-85, ISSN 0950-0618.
- Harik, I., and Peiris, A. (2014). "Strengthening of Concrete Bridges using CFRP Rod Panels." *Proceeding, The 7th International Conference on FRP Composites in Civil Engineering, CICI 2014, Vancouver, Canada, August 20-22, 2014.*
- Hassan T. and Rizkalla S., (2003) "Investigation of Bond in Concrete Structures Strengthened with Near Surface Mounted Carbon Fiber Reinforced Polymer Strips," *American Society of Civil Engineers (ASCE), Journal of Composites for Construction*, Vol. 7, No. 3, pp. 248-257, 2003.
- Hiroyuki, Y. and Wu, Z. (1997). "Analysis of Debonding Fracture Properties of CFS Strengthened Member Subject to Tension." *Non-Metallic (FRP) Reinforcement for Concrete Structures, Proceedings of the 3rd International Symposium, Sapporo, Japan*, pp. 287-294.
- Hollaway, L. C., and Leeming, M. B. (2000), "Strengthening of Reinforced Concrete Structures using Externally Bonded FRP Composites in Structural and Civil Engineering.", Boca Raton FL, CRC Press LLC.
- Huang, Y., Wu, J., Yen, T., Hung, C, and Lin, Y. (2005). "Strengthening Reinforced Concrete Beams Using Prestressed Glass Fiber-Reinforced Polymer-Part I: Experimental Study." *Journal of Zhejiang University science (JZUS)*, pp. 166-174.
- Huang, Y., Yen, T., Wu, J., and Ong, C. (2000). "Strengthening Reinforced Concrete Beams Using Prestressed Glass Fiber-Reinforced Plastic." *Proceeding of the 4th International conference on Repair, Rehabilitation, and Maintenance of Concrete Structures, and Innovations in Design and Construction (ACI SP-193)*, pp 925-936.

- Hutchinson, R., Tadros, G., Kroman, J., and Rizkalla, S. (2003). Use of Externally Bonded FRP Systems for Rehabilitation of Bridges in Western Canada. ACI SP-215 (pp. 239-248). Farmington Hills: ACI.
- Hwan, B. O, Cho, J. Y., and Park, D. G. (2003). "Static and Fatigue Behavior of Reinforced Concrete Beams Strengthened with Steel Plates for Flexure" JOURNAL OF STRUCTURAL ENGINEERING ASCE / APRIL 2003 / 527.
- Japan Society of Civil Engineers, JSCE-E 545-200 (2000). "Test methods for direct pull-off strength of continuous fiber sheets with concrete." Japan Society of Civil Engineers, Tokyo, Japan.
- Jones, R., R.N. Swamy and A. Charif, (1988). "Plate Separation and Anchorage of Reinforced Concrete Beams Strengthened by Epoxy-Bonded Steel Plates". The Structural Engineering, 66(5): 85-94.
- Jones, R., Wamy. R. N, and Ang. T. H. (1982). "Under- and over-reinforced Concrete Beams with Glued Steel Plates." The International Journal of Cement Composites and Lightweight Concrete 4.
- Jumaat, M. Z., Alam, Md. A. (2008). "Strengthening of R.C. Beams Using Externally Bonded Plates and Anchorages." Australian Journal of Basic and Applied Sciences 3(3): 2207-2211.
- Kachlakev D., Miller T., and Yim S., (2001). "Finite Element Modeling of Reinforced Concrete Structures Strengthened with frp Laminates. " Oregon Dept. of Transp., USA, Res. Group, Final Report SPR, 316, May 2001.
- Kamel, A. M. S., Elwi, A. E., and Cheng, J. J. R. (2003). "Experimental and Numerical Analysis of FRP Sheets Bonded to Concrete." Structural Engineering Repor, No. 252, University of Alberta.
- Kamel, A. S., Elwi, A. A. and Cheng, R. J. (2004). "Experimental investigation on FRP sheets bonded to concrete." Emirates J. Eng. Res. 9, 71–76.
- Kasidit Chansawat, Tanarat Potisuk, Thomas H. Miller, Solomon C. Yim, and Damian I. Kachlakev, (2009) "FE Models of GFRP and CFRP Strengthening of Reinforced Concrete Beams," Advances in Civil Engineering, vol. 2009, Article ID 152196, 13 pages, 2009. doi:10.1155/2009/152196.
- Kent, D. C, and Park, R. (1971). "Flexural members with confined concrete." Journal of Structures. Div., ASCE, 97(7), 1969-1990.
- Kesavan, K., K. Ravisankar, R. Senthil and A. K. F. Ahmed (2013). "Experimental Studies on Performance of Reinforced Concrete Beam Strengthened with CFRP under Cyclic Loading using FBG Array." Measurement 46(10): 3855-3862.

- Kheyroddin, A. and H. Naderpour (2008). "Nonlinear Finite Element Analysis of Composite RC Shear Walls." *Iranian Journal of Science and Technology Transaction B-Engineering* 32(B2): 79-89.
- Kim, Y. J., Longwoth, J. M., Gordon, W. R., and Green, M. F. (2008). "Flexure of Two-Way Slabs Strengthened with Prestressed or Nonprestressed CFRP Sheets", *ASCE, Journal of Composites for Construction*, Vol. 12, No.4, August 1, 2008. ASCE, ISSN 1090-0268/2008/4-366-374.
- Kotynia, R., Krzysztof, L., and Staskiewicz, M. (2014). "Flexural Behavior of Preloaded RC Slabs Strengthened with Prestressed CFRP Laminates", *ASCE, Journal of Composites for Construction*, ISSN 1090-0268/A4013004 (11).
- Kotynia, R., Walendziak, R., Stoecklin, I., and Meier, U. (2011). "RC Slabs Strengthened with Prestressed and Gradually Anchored CFRP Strips under Monotonic and Cyclic Loading", *ASCE, Journal of Composites for Construction*, Vol. 15, No. 2, April 1, 2011, ASCE, ISSN 1090-0268/2011/2-168.
- Lamanna, A. J. (2002). "Flexural Strengthening of Reinforced concrete Beams with Mechanically Fastened Fiber Reinforced Polymer Strips." Doctoral dissertation, University of Wisconsin, Madison.
- Lamanna, A. J., Bank, L. C., and Borowicz, D. T. (2004). "Mechanically Fastened FRP Strengthening of Large Scale RC Bridge T Beams." *Adv. Struct. Eng.*, 7(6), 525-537.
- Lamanna, A. J., Bank, L. C., and Scott, D. W. (2001). "Flexural Strengthening of RC Beams Using Fasteners and FRP Strips," *ACI Structural Journal*, Vol. 98, No. 3, pp. 368-376, May-June 2001.
- Lee, H. K., G. Avila and C. Montanez (2005). "Numerical study on retrofit and strengthening performance of sprayed fiber reinforced polymer." *Engineering Structures* 27(10): 1476-1487.
- Lei, D., G. Chen, Y. Chen and Q. Ren (2012). "Experimental Research and Numerical Simulation of RC Beams Strengthened with Bonded Steel Plates." *Science China Technological Sciences* 55(12): 3270-3277.
- Lopez, M. M., A. E. Naaman, L. Pinkerton and R. D. Till (2003). "Behavior of RC Beams Strengthened with FRP Laminates and Tested under Cyclic Loading at Low Temperatures." *International Journal of Materials & Product Technology* 19(1-2): 108-117.
- Loreto, G., Leardini, L., Arboleda, D., and Nanni, A. (2014). "Performance of RC Slab-Type Elements Strengthened with Fabric-Reinforced Cementitious-Matrix Composites." *ASCE, Journal of Composites for Construction*, 2014.18.

- Lu, X. Z., L. P. Ye, J. G. Teng and J. J. Jiang (2005). "Meso-Scale Finite Element Model for FRP Sheets/Plates Bonded to Concrete." *Engineering Structures* 27(4): 564-575.
- Lu, X.Z., Teng, J.G., Ye, L.P., and Jiang, J.J. (2005b). "Bond-slip models for FRP sheets/plates bonded to concrete." *Engineering Structures*, Vol. 27, No. 6, pp. 920-937.
- Luke, P. S., Leeming, M. B., and Shwarski, A. J. (1998). "Robust results for Carbon Fibre," *Concrete Engineering International*, 2(2), 19-21.R.
- Lunn, D. S., and Rizkalla, S. H. (2011). "Strengthening of Infill Masonry Walls with FRP Materials." *Journal of Composites for Construction*, Vol. 15, No.2, April 1, 2011.
- MacDonald, M. D., and Calder, A. J. J. (1982), "Bonded Steel Plating for Strengthening Concrete Structures." *Int. J. Adhes.*, 2(2), 119-127.
- Macdonald, M.D. (1978). "The Flexural Behavior of Concrete Beams with Bonded External Reinforcement", TRRL Report SR 415 (Department of the Environment, Department of Transport), Crowthorne, 1978.
- Macdonald, M.D. (1982). "The Flexural Performance of 3.5 m Concrete Beams with Various Bonded External Reinforcements.", TRRL Report SR 728, (Department of the Environment, Department of Transport), Crowthorne, 1982.
- Maeda, T., Asano, Y., Sato, Y., Ueda, T., and Kakuta, Y. (1997). "A Study on Bond Mechanism of Carbon Fiber Sheet." *Non-Metallic (FRP) Reinforcement for Concrete Structures, Proc., 3rd Int. Symp.*, Vol. 1, 279–286.
- Mander, R.F. (1981). "Use of resins in road and bridge construction and repair", *International Journal of cement Composites and Lightweight Concrete*. Volume 3, No 1 (February 1981) pp 37-39.
- Martin, J. and Lamanna, A. (2008). "Performance of Mechanically Fastened FRP Strengthened Concrete Beams in Flexure." *J. Compos. Constr.*, 12(3), 257–265.
- Meier, U., (1987). "Bridge Repair with High Performance Composite Materials", *Material and Technik*, Vol. 15, 1987, pp. 125- 128.
- Meier, U., Deuring, M., Meier, H, and Schwengler, G. (1992). "Strengthening of Structures with CFRP Laminates", *Research and Applications in Switzerland*, Proceedings of the 1st International Conference on Advanced Composite Material in Bridges and Structures, Sherbrooke, Quebec, 1992, pp. 243-251.
- Micelli F, Nanni A. (2004). "Durability of FRP rods for concrete structures." *Constr Building Mater* 2004;18(7):491–503.

- Michels, J., Sena-Cruz, J., Czaderski, C., and Motavalli, M. (2013) "Structural Strengthening with Prestressed CFRP Strips with Gradient Anchorage", ASCE, Journal of Composites for Construction, Vol. 17, No. 5, October 1, 2013, ISSN 1090-0268.
- Miller, B. and Nanni, A., "Bond Between CFRP Sheets and Concrete," Proceedings, ASCE 5th Materials Congress, Cincinnati, OH, L.C. Bank, Editor, May 10-12, 1999, pp. 240-247.
- Monti, G., and Liotta, M. (2006). "Prestension of Externally Bonded FRP Sheets for Flexural Reinforcement of RC Beams: Methods and Design Equations" Proceedings of 2th fib International congress, ID 10-63.
- Myers, J. J., Belarbi, A., and El-Domiaty, K. A. (2004). "Blast Resistance of FRP Retrofitted Un-Reinforced Masonry (URM) Walls with and without Arching Action." The masonry society (TMS) Journal September 2004.
- Nanni, A. (2012). "A New Tool for Concrete and Masonry Repair." Concrete international, April 2012.
- Narayan, R. S, Jones, R, and Charif, A. (1996). "Contribution of Externally Bonded Steel Plate Reinforcement to the Shear Resistance of Reinforced Concrete Beams" ACI- SP Publication, No.165.
- Nordin, H., and Taljsten, B. (2006). "Concrete Beams Strengthened with Prestressed NSM CFRP." J. Compos. Constr., 10(1), 60–68.
- Norris, T., Saadatmanesh, H. and Ehsani, M. R. (1997). "Shear and Flexural Strengthening of RC Beams with Carbon Fibre Sheets. Journal of structural engineering, 1997; 123(7): 903-911.
- Nour, A., B. Massicotte, E. Yildiz and V. Koval (2007). "Finite Element Modeling of Concrete Structures Reinforced with Internal and External Fibre-Reinforced Polymers." Canadian Journal of Civil Engineering 34(3): 340-354.
- Obaidat, Y.T. (2010). "Structural Retrofitting of Reinforced Concrete Beams using Carbon Fiber Polymer." Licentiate dissertation, Structural Mechanics, Lund, Sweden, ISSN 0281-6679.
- Oehlers DJ. (1992). "Reinforced Concrete Beams with Plates Glued to their Soffits. J Struct Eng, ASCE 1992;118(8):2023–38.
- Ombres, L (2011). "Structural Performances of PBO FRCM-Strengthened RC Beams." Proceedings of the Institution of civil Engineers (ICE), Structures and Buildings, Volume 164, Issue 4.

- Ombres, L (2012). "Debonding Analysis of Reinforced Concrete Beams Strengthened with Fibre Reinforced Cementitious Mortar." *Engineering Fracture Mechanics* 81 (2012) 94–109.
- Omran, H. Y. and R. El-Hacha (2012). "Nonlinear 3D Finite Element Modeling of RC Beams Strengthened with Prestressed NSM-CFRP Strips." *Construction and Building Materials* 31: 74-85.
- Oral Buyukozturk, Oguz Gunes, Erdem Karaca, (2004), "Progress on understanding debonding problems in reinforced concrete and steel members strengthened using FRP composites," *Construction and Building Materials*, Volume 18, Issue 1, February 2004, Pages 9-19, ISSN 0950-0618.
- Park, J. G., K. M. Lee, H. M. Shin and Y. J. Park (2007). "Nonlinear Analysis of RC Beams Strengthened by Externally Bonded Plates." *Computers and Concrete* 4(2): 119-134.
- Peiris, N. A, (2011) "Steel Beams Strengthened with Ultra High Modulus CFRP Laminates," Doctoral dissertation, Paper 204.http://uknowledge.uky.edu/gradschool_diss/204, 2011.
- Pendhari, S. S., T. Kant and Y. M. Desai (2006). "Nonlinear analysis of reinforced concrete beams strengthened with polymer composites." *Structural Engineering and Mechanics* 24(1): 1-18.
- Peng, H., Zhang, J. F., Cai, C. S., and Liu, Y. (2014). "An Experimental Study on Reinforced Concrete Beams Strengthened with Prestressed Near Surface Mounted CFRP Strips", *Engineering Structures*, Volume 79, 15 November 2014, Pages 222–233.
- Plevris, N. and T. C. Triantafillou (1994). "Time-Dependent Behavior of Rc Members Strengthened with Frp Laminates." *Journal of Structural Engineering-Asce* 120(3): 1016-1042.
- Rabinovitch, O. (2014). "Dynamic Edge Debonding in FRP Strengthened Beams." *European Journal of Mechanics a-Solids* 47: 309-326.
- Radfar, S., Foret, G., Saeedi, N., and Sab, K. (2012). "Simulation of concrete cover separation failure in FRP plated RC beams." *Construction and Building Materials journal*, 37 (2012) 791-800.
- Raj, Rasheed. L. S, and Al-Azawi, T. K. (2013). "Experimental Analysis of Reinforced Concrete Slabs Strengthened with Steel Plates" *The Iraqi Journal for Mechanical and Material Engineering*, Vol.13, No.1, 2013.

- Raouf M, and Hassanen M.A.H. (2000). "Peeling failure of reinforced concrete beams with fibre reinforced plastic or steel plates glued to their soffits". Proceedings of the Institution of Civil Engineers: Structures and Buildings 2000; 140(8):291–305.
- Ren, W., L. Sneed, Y. Gai and X. Kang (2015). "Test Results and Nonlinear Analysis of RC T-beams Strengthened by Bonded Steel Plates." International Journal of Concrete Structures and Materials 9(2): 133-143.
- Ritchie, P. A., Thomas, D. A., Lu, L. W., and Connelly, G. M. (1991). "External reinforcement of concrete beams using fiber reinforced plastics." ACI Struct. J., 88(4), 490–500.
- Ross, C.A., Jerome, D.M., Tedesco, J.W., and Hughes, M.L.,(1999), "Strengthening of Reinforced Concrete Beams with Externally Bonded Composite Laminates", ACI Structural Journal, Vol. 96, No. 2, pp:212-220
- Saadatmanesh H and Ehsani M R (1991). "RC Beams Strengthened with GFRP Plates I: Experimental Study", J Struct Eng 117(11) 3417–3433.
- Sakar, G., and Tanaslan, h. M. (2014). "Prestressed CFRP Fabrics for Flexural Strengthening of Concrete Beams with an Easy Prestressing Technique", Mechanics of Composite Materials, Vol. 50, No. 4, September, 2014.
- Savoia, M., B. Ferracuti and C. Mazzotti (2005). "Creep Deformation of Fiber Reinforced Plastics-Plated Reinforced Concrete Tensile Members." Journal of Composites for Construction 9(1): 63-72.
- Schnerch, D. (2007). "Flexural Strengthening of Masonry Facades with Carbon Fiber reinforced Polymer (CFRP) Bars." 2007 Symposium on Building Envelope Technology.
- Sika carboDur plates (2011). Product data sheet, Sika services, Switzerland.
< <https://usa.sika.com/dms/...get/.../pds-cpd-SikaCarboDur-us.pdf> >
- Sikadur 30 (2014). Product data sheet, Sika services, Switzerland.
< <https://usa.sika.com/dms/...get/.../pds-cpd-Sikadur30-us.pdf> >
- Sikadur 300 (2014). Product data sheet, Sika services, Switzerland.
< <https://usa.sika.com/dms/...get/.../pds-cpd-Sikadur300-us.pdf> >
- SikaWrap Hex 103C (2014). Product data sheet, Sika services, Switzerland.
< <https://usa.sika.com/dms/.../pds-cpd-SikaWrap103C-us.pdf> >
- Si-Larbi, A., A. Agbossou, E. Ferrier and L. Michel (2012). "Strengthening RC beams with composite fiber cement plate reinforced by prestressed FRP rods: Experimental and numerical analysis." Composite Structures 94(3): 830-838.

- Sims, F. A. (1985). "Applications of Resins in Bridge and Structural Engineering", the international journal of cement composites and lightweight concrete, volume 7, November 4.
- Stallings, J. M., and Porter, N. M, (2003), "Experimental investigation of lap splices in externally bonded carbon fiber-reinforced plastic plates," ACI Structural Journal, 2003, 100 (1), 3-10.
- Stallings, J., Tedesco, J., El-Mihilmy, M., and McCauley, M. (2000). "Field Performance of FRP Bridge Repairs." J. Bridge Eng., 5(2), 107-113.
- Supaviriyakit, T., Pornpongsoj, P., and Pimanmas, A., "Finite-Element analysis of FRP-Strengthened RC Beams", Songkhanakar Journal of Science Technology, V. 26, N. 4, 2004, pp. 497-507.
- Swamy, R. N., Jones, R., and Charif, A., (1989). "The Effect of External Plate Reinforcement on the Strengthening of Structurally Damaged RC Beams", Ibid 67 (1989) 45-56.
- Taljsten, B. (1994). "Strengthening of Existing Concrete Structures with Epoxy Bonded Plates of Steel or Fibre reinforced Plastics." Doctoral dissertation, Division of Structural Engineering, Lulea University of Technology, November 1994.
- Taljsten, B., and Blanksvard, T. (2007). "Mineral-Based Bonding of Carbon FRP to Strengthen Concrete Structures." ASCE, Journal of Composites for Construction, 2007.11:120-128.
- Taljsten, B., Orosz, K., and Blanksvard, T. (2006). "Strengthening of Concrete Beams in Shear with Mineral Based Composites Laboratory Tests and Theory Third International Conference on FRP Composites in Civil Engineering (CICE 2006), December 13-15 2006, Miami, Florida, USA.
- Tedesco, J.W., and Stallings, J. M. (1998). "Rehabilitation of a reinforced concrete bridge using FRP laminates." Final Rep. 930-341, Auburn University Highway Research Center, Auburn, Ala.
- Tedesco, J.W., Stallings, J. M., El-Mihilmy, M., and McCauley, M. (1996). "Rehabilitation of a concrete bridge using FRP laminates." Materials for the New Millennium, Proceedings of the Fourth Materials Engineering Conference., Washington, DC, November 10-14, 1996, ASCE, New York, NY, 631-637.
- Teng, J. G, Smith., Yao, J. and Chen, j.F (2003). "Intermediate crack-induced debonding in beams and slabs", Construction and Building Materials, 17 (6-7), 447-462.

- Teng, X. D. and Y. X. Zhang (2014). "Nonlinear Finite Element Analyses of FRP-Strengthened Reinforced Concrete Slabs using a New Layered Composite Plate Element." *Composite Structures* 114: 20-29.
- Tinazzi, D., C. Modena, and A. Nanni, (2000). "Strengthening of Masonry Assemblages with FRP Rods and Laminates," *International Meeting on Composite Materials, PLAST 2000, Proceedings, Advancing with Composites 2000*, Ed. I.Crivelli-Visconti, Milan, Italy, May 9-11, 2000, pp. 411-418.
- Tommaso, A., and Focacci, F. (2008). "PBO-FRCM Composites to Strengthen R.C. Beams: Mechanics of Adhesion and Efficiency." *Fourth International Conference on FRP Composites in Civil Engineering (CICE2008)*, 22-24 July 2008, Zurich, Switzerland.
- Toutanji, H., Zhao, L., and Zhang, Y. (2006). "Flexural Behavior of Reinforced Concrete Beams Externally Strengthened with CFRP Sheets Bonded with an Inorganic Matrix." *Engineering structures*, pp.557-566.
- Triantafillou, T. and S. Matthys (2013). "Fibre-Reinforced Polymer Reinforcement enters fib Model Code 2010." *Structural Concrete* 14(4): 335-341.
- Triantafillou, T. C., Deskovic, N., and Dearing, M. (1992). "Strengthening of RC Beams with Epoxy-Bonded Fibre-Composite Materials," *Materials and Structural*, 25, 201-21.
- Tumialan, G., P.C. Huang, A. Nanni, and P. Silva, (2001). "Strengthening of Masonry Walls with Structural Repointing," *Non-Metallic Reinforcement for Concrete Structures - FRPRCS-5*, Cambridge, July 16-18, 2001.
- Van Gemert (1980). "Force Transfer in Epoxy Bonded Steel-Concrete Joints." *International Journal of Adhesion and Adhesives*, Vol 1 (Nr. 2) (Oct. 1980), pp. 67-72.
- Van Germert, D. and Maesschalck, R. (1983). "Structural Repair of a Reinforced Concrete Plate by Epoxy Bonded External Reinforcement", *the international journal of cement composites and lightweight concrete*, volume 5, November 4.
- Vasudevan, G. and S. Kothandaraman (2014). "Experimental investigation on the performance of RC beams strengthened with external bars at soffit." *Materials and Structures* 47(10): 1617-1631.
- Wight, R. G., Green, M. F., and Erki, M. A. (2001). "Prestressed FRP Sheets for Poststrengthening Reinforced Concrete Beams", *ASCE, Journal of Composites for Construction*, Vol. 5, No. 4, November 2001, pp. 214-220.

- William, K. J. and Warnke, E. P., (1975). "Constitutive Model for the Triaxial Behavior of Concrete," Proceedings, International Association for Bridge and Structural Engineering, Vol. 19, ISMES, Bergamo, Italy, pp. 174, 1975.
- Wipf T. J. Klaiber F. W., Dunker K. F. Methods of strengthening existing highway bridges. *Engineering Structures*, 26(5):553–565, 1987.
- Wolanski, A.J. (2004), "Flexural behavior of reinforced and prestressed concrete beams using finite element analysis", M.S.Thesis, Marquette University, Wisconsin.
- Wu, C. Q., D. J. Oehlers and I. Day (2009). "Layered Blast Capacity Analysis of FRP Retrofitted RC Member." *Advances in Structural Engineering* 12(3): 435-449.
- Wu, G., Shi, J., Jing, W., and Wu, Z. (2014). "Flexural Behavior of Concrete Beams Strengthened with New Prestressed Carbon-Basalt Hybrid Fiber Sheets", *ASCE, Journal of Composites for Construction*.
- Wu, Z., Yang, S., and Zheng, J. (2006). "An Analytical Prediction on RC Beams Retrofitted with Prestressed CFRP Plates or Sheets.", *Proceedings of the 2th fib International Congress*, ID 10-5.
- Yang, X., and Nanni, A, (2002) "Lap Splice Length and Fatigue Performance of Fiber-Reinforced Polymer Laminates," *ACI Materials Journal*, 2002, 99(4), 386-392.
- Zhang S, Raoof M, and Wood L.A. "Prediction of peeling failure of reinforced concrete beams with externally bonded steel plates". *Proceedings of the Institution of Civil Engineers: Structures and Buildings* 1995; 110(8):257–68.
- Zhang, J. W, Teng, J. G, Wong, Y. L., and lu, Z. T. (2001). "Behavior of Two-Way RC Slabs Externally Bonded with Steel Plate" *Journal of Structural engineering*, ACI, April 2001.

VITA

Name: Akram Rasheed Jawdhari

Place of Birth (City, State, country): Hilla, Babylon, Iraq

Education: B.S. (valedictorian) in Civil Engineering
University of Babylon, Hilla, Iraq
(Fall 2000-Spring 2005)

M.S. in Civil Engineering (Structures)
University of Babylon, Hilla, Iraq
(Fall 2005-Spring 2008)

Akram Rasheed Jawdhari

April 21, 2016